Solid Substrate Motility And Phototaxis Of The Alpha-Proteobacterium, *Rhodobacter capsulatus*

by

KRISTOPHER JOHN SHELSWELL

Honours B.Sc., University of Waterloo, 2002

A THESIS SUBMITTED IN PARTIAL FULFILLMENT OF THE REQUIREMENTS FOR THE DEGREE OF DOCTOR OF PHILOSOPHY

in

THE FACULTY OF GRADUATE STUDIES

(Microbiology and Immunology)

THE UNIVERSITY OF BRITISH COLUMBIA

(Vancouver)

February 2011

ABSTRACT

The work in this thesis reports the first discovery of flagellum-independent motility in *Rhodobacter capsulatus*, a purple photosynthetic bacterium. Furthermore, while aqueous swimming motility using a flagellum had been documented, the occurrence of movement over solid and semi-solid substrates had not been reported in *R. capsulatus*. This motility was found to be affected by the physical and chemical composition of the translocation surface. While motility was reduced under anaerobic (dark) conditions, it did not require oxygen. Cells appeared to respond to multiple stimuli, and were able to move both as coordinated masses and individual cells. Coordinated movements did not require any of the known cell-to-cell communication mechanisms. Movements were influenced by light such that cells usually moved toward a light source over a broad region of the visible spectrum, and this movement appeared to be a genuine phototaxis. A direct linkage between photoresponsive movement and photosynthesis was ruled out, because the photosynthetic reaction center was not required for movement toward white light. Photoresponsive movement occurred independently of the photoactive yellow protein, but appeared to require the bacteriochlorophyll and/or carotenoid pigments. Motility was mediated by flagellum-dependent and flagellum-independent contributions. Flagellum-dependent contributions were responsible for dispersive semi-random movements while flagellum-independent contributions resulted in linear, directed movements. Analysis of several strains indicated that flagellum-independent motility is widespread throughout *R. capsulatus*. This motility appears to be mediated by a gliding mechanism, perhaps involving the deposition of exopolysaccharide to achieve coordinated cell taxis.

TABLE OF CONTENTS

ABSTRACT ii

TABLE OF CONTENTS iii

LIST OF TABLES x

LIST OF FIGURES xii

LIST OF ABBREVIATIONS xviii

ACKNOWLEDGEMENTS xix

1. INTRODUCTION 1

1.1. *Rhodobacter capsulatus* 1

1.1.1. *R. capsulatus* taxonomy and characteristics 1

1.1.2. *R. capsulatus* genomic characteristics 1

1.2. Bacterial motility 2

1.2.1. Adaptive responses 2

1.2.2. Distribution, regulation, and types of bacterial motility 2

1.3. Bacterial flagellum-mediated motility 4

1.3.1. Flagellum structure and function 4

1.3.2. Aqueous substrate flagellar swimming 6

1.3.3. Solid substrate flagellar swarming 6

1.4. Bacterial pilus-mediated motility 7

1.4.1. Pilus structure and function 7

1.4.2. Solid substrate pilus twitching 10

1.5. Bacterial gliding motility 11
1.5.1. Gliding mechanisms and function 11
1.5.2. Cytoskeletal rearrangement in gliding 11
1.5.3. Extrusion in gliding 13
1.5.4. Focal adhesion in solid substrate gliding 14
1.6. Bacterial sliding motility 15
1.7. Bacterial taxis 16
1.7.1. Light-responsive motility 16
1.7.2. Energy taxis 17
1.7.3. Phototaxis 19
1.7.4. Tactic responses 21
1.8. Research approach to study solid substrate motility in *R. capsulatus* 22
2. MATERIALS AND METHODS 24
2.1. Bacterial strains, plasmids, growth conditions, and enumeration of cells 24
2.2. Bacterial motility assays 33
2.2.1. Design of chambers used for motility assays 35
2.2.2. Treatment of polystyrene plates used for motility assays 37
2.3. ^{32}P-orthophosphate cell labelling 37
2.4. Phase contrast negative stain capsule microscopy 38
2.5. Phase contrast and Nomarski microscopy 38

2.6. Cy3 fluorescence microscopy 39
2.7. Transmission electron microscopy 39
2.8. SDS-polyacrylamide gel electrophoresis (SDS-PAGE) 40
2.9. Cell surface protein enrichment 40
2.10. Protein sequencing 41
2.11. DNA manipulations 41
2.12. Alignments and database homology searches 41
2.13. Construction of mutants 42
2.14. Creation and screening of Tn5 library for flagellum-independent motility deficient mutants 46
2.15. Whole cell absorption spectrum 46
2.16. RNA isolation and microarray analysis 47
2.17. Statistical analysis of cell movement 47
3. RESULTS 49
3.1. Solid substrate motility 49
3.1.1. Solid substrate motility in interfaces generated on plastic or glass substrates 49
3.1.2. Modification of plastic substrates for variation of the interstice 50
3.1.3. Investigation of solidification agents used to generate a glass-substrate taxis interstice 51
3.1.4. Medium volume effects on taxis in a glass-agar interstice 53
3.1.5. Study of oxygen requirements for taxis in a glass-agar interstice 55
3.1.6. Occurrence of solid substrate motility in several *R. capsulatus* strains 57

3.2. Investigation of directional solid substrate motility 58

3.2.1. Directed taxis of cells in the glass-agar interstice 60

3.2.2. Glass substrate effects on directional motility in the interstitial interface 62

3.2.3. Dipole magnetism effects on directional motility 62

3.2.4. Temperature effects on directional motility 64

3.2.5. Effect of incident light during inoculation on directional motility 65

3.2.6. Effect of incident light during incubation on directional motility 66

3.2.7. Use of square plates to reduce the variability in motility toward incident light 70

3.3. Flagellum-mediated and flagellum-independent motility 72

3.3.1. Multiple motility phenotypes in the glass-agar interstice 72

3.3.2. Disruption of the gene encoding the flagellar structural subunit flagellin 73

3.3.3. Electron microscopy of *R. capsulatus* cells 76

3.3.4. Cell motility in the glass-agar interstice 77

3.3.5. Light microscopy visualization of cell movements in the glass-agar interstice 78

3.4. Pilus-mediated motility 80

3.4.1. Electron microscopy of pilus-like structures on cells 80

3.4.2. Peptide sequence analysis of extracellular proteins 80

3.4.3. Bioinformatics analyses of putative pilus biogenesis clusters and predicted gene homologues 83

3.4.4. Mutagenesis of a predicted pilus secretin 88

3.4.5. Mutagenesis of a predicted pilus assembly ATPase 89

3.4.6. Mutagenesis of a predicted pilus prepilin peptidase 91

3.5. Experiments related to the possibility of gliding-mediated motility 93

3.5.1. Fluorescence labelling of extracellular amine groups 97

3.5.2. Cell capsule effects on solid substrate motility 98

3.5.3. The role of a putative glycoprotein in solid substrate motility 101

3.5.4. Transposon mutagenesis to search for components of the solid substrate motility mechanism 105

3.6. Coordinated directional motility 105

3.6.1. Coordinated long-range solid substrate motility 105

3.6.2. Long-range solid substrate social motility 106

3.6.3. Evaluation of the role of the photosynthetic apparatus and pigments on motility 109

3.6.4. Evaluation of the effects of a photoactive yellow protein gene knockout on motility 112

3.6.5. Comparison of absorption profiles and potential photoresponsive movement 114

3.6.6. Evaluation of possible quorum sensing-mediated processes on motility 117

3.6.7. Evaluation of possible effects of RpoN on motility 118

3.6.8. Evaluation of possible SenC effects on motility 121

3.6.9. Evaluation of possible RegA effects on motility 123

3.6.10. Summary of angular directional motility assessments 124

4. DISCUSSION 127

4.1. Cell movements of *R. capsulatus* 127

4.1.1. Substrate-dependent effects on *R. capsulatus* solid substrate movement 128

4.1.1.1. Impaired motility of R. capsulatus on polystyrene 128

4.1.1.2. Changes in *R. capsulatus* motility in response to medium solidifying agent and concentration 129

4.1.1.3. Effect of medium moisture on *R. capsulatus* motility 131

4.1.2. Motility patterns in the plate-medium interstice 131

4.1.3. Directed *versus* stochastic motility in the plate-medium interstice 133

4.1.4. Possible chemotaxis in the plate-medium interstice 134

4.2. Light-induced cell movements in *R. capsulatus* 136

4.2.1. Action spectrum of *R. capsulatus* solid substrate, photoresponsive movement 138

4.2.2. Mutations affecting the direction of *R. capsulatus* solid substrate movement 139

4.3. Flagellum-dependent and flagellum-independent cell movements in *R. capsulatus* 142

4.3.1. Flagellum-dependent contributions to *R. capsulatus* solid substrate movement 143

4.3.1.1. Changes in flagellum-dependent movement contributions of *R. capsulatus* mutants 144

4.3.2. Flagellum-independent contributions to *R. capsulatus* solid substrate movement 147

4.3.2.1. Changes in flagellum-independent contributions to *R. capsulatus* movement 149

4.3.2.2. Investigation of twitching contributions to *R. capsulatus* solid substrate movement 149

4.3.2.3. Investigation of gliding contributions to *R. capsulatus* solid substrate movement 150

4.4. Concluding remarks 151

REFERENCES 154

APPENDIX A 191

APPENDIX B 233

APPENDIX C 236

C.1. Photoresponsive motility using optical filters to generate light of defined wavelength ranges 236

C.2. Photoresponsive motility induction using light-emitting diodes (LEDs) to generate light of specific wavelength ranges 239

LIST OF TABLES

Table 1-1: Types of bacterial motility.....3

Table 2-1: Bacterial strains.....25

Table 2-2: Plasmids. 30

Table 2-3: Primers for PCR amplification of *R. capsulatus* DNA.....43

Table 3-1: Average motility values of samples incubated anaerobically in the dark in the interstice of an agar medium.....57

Table 3-2: Magnetic field strengths on *R. capsulatus* cells inoculated into the glass-agar interstice. 63

Table 3-3: Average motility values of samples incubated in the interstice of an agar medium near magnetic fields.....64

Table 3-4: Annotation of the *R. capsulatus* flagellin gene product amino acid sequence. 74

Table 3-5: Alignment comparison of the *R. capsulatus* putative pilus anchor protein to TadG-domain proteins.....83

Table 3-6: Annotation of the *R. capsulatus* putative pilus gene cluster product amino acid sequences...84

Table 3-7: Average cell movement distances and directions in stab-plate tests of putative *R. capsulatus* pilus mutants. 93

Table 3-8: Alignment analysis search for putative gliding motility homologues in *R. capsulatus*.....94

Table 3-9: Putative polysaccharide synthesis/export gene cluster in *R. capsulatus*. 102

Table 3-10: Average motility values of wild type strain B10 and *flaA* mutant bKSDF time-course test samples incubated in the glass-agar interstice with halogen white light.....109

Table 3-11: Alignment comparison of the *R. capsulatus rpoN* gene product to similar proteins. 119

Table 3-12: Statistical evaluation of the distribution of *R. capsulatus* motility in stab-plates illuminated with halogen white light. 126

Table A-1: Average motility values of samples incubated in the glass-medium interstice of medium solidification agent titrations. 192

Table A-2: Average motility values of samples incubated in the glass-medium interstice of agar medium volume titrations. 193

Table A-3: Average evaporation values of agar medium volume titration samples. 193

Table A-4: Average motility values of samples incubated in the glass-agar interstice with various incubation temperatures. 194

Table A-5: *R. capsulatus* proteins identified by peptide sequencing of cell surface protein-enrichment resolved by SDS-PAGE 195

Table A-6: Average motility values of wild type strain B10 samples incubated in the glass-agar interstice with filtered directional incident light. 199

Table A-7: Average motility values of *flaA* mutant strain bKSDF samples incubated in the glass-agar interstice with defined emission LED directional incident light. 200

Table A-8: Average motility values of *flaA* mutant strain bKSDF and *flaA/pyp* mutant strain bKSDFpyp samples incubated in the glass-agar interstice with defined emission LED directional incident light. 202

Table A-9: *R. capsulatus* transcripts upregulated >2 fold identified by transcriptome comparison of solid substrate medium-harvested cell total RNA to early stationary phase aqueous medium-harvested cell total RNA. 204

LIST OF FIGURES

Figure 1-1: Representation of a typical bacterial flagellum 5

Figure 1-2: Representation of a typical motility pilus 9

Figure 1-3: Representation of a bacterial cytoskeletal rearrangement mechanism 12

Figure 1-4: Representation of a bacterial extrusion mechanism 13

Figure 1-5: Representation of a bacterial focal adhesion mechanism 15

Figure 1-6: Representation of a bacterial energy taxis pathway 18

Figure 2-1: Orientation of reference points used for incubation chamber control tests of stab-plate motility assays 34

Figure 2-2: Incubation chambers used for illumination of stab-plate motility assays 36

Figure 3-1: *R. capsulatus* motility on agar surfaces of polystyrene and borosilicate Petri plates in the air-agar or plate-agar interface 49

Figure 3-2: *R. capsulatus* motility in the interstice of polystyrene Petri plates etched with sodium hydroxide or abraded with sandpaper 50

Figure 3-3: *R. capsulatus* motility when inoculated into various medium solidifiers of different concentrations 52

Figure 3-4: *R. capsulatus* motility when inoculated into various agar medium volumes 54

Figure 3-5: *R. capsulatus* motility when inoculated into various agar medium volumes compared to relative moisture lost to evaporation 55

Figure 3-6: *R. capsulatus* motility in the glass-agar interstice of borosilicate Petri plates under anerobic or aerobic incubation conditions 56

Figure 3-7: *R. capsulatus* motility of environmental isolates, wild type, and laboratory wild type strains in the glass-agar interstice of borosilicate Petri plates 58

Figure 3-8: Representation of the measurement system used to determine the angular direction of motility in agar plates incoulated with *R. capsulatus* cells into the glass-agar interstice of borosilicate Petri plates 59

Figure 3-9: Agar-stab assays of *R. capsulatus* cells inoculated into the glass-agar interstice of borosilicate Petri plates exhibiting random, and directed motility 60

Figure 3-10: Graphical representation of the measured angular direction of motility in the glass-agar interstice of borosilicate Petri plates incubated in the dark 61

Figure 3-11: Influence of the glass plate on directed cell motility in agar-stab assays of *R. capsulatus* cells inoculated into the glass-agar interstice of borosilicate Petri plates 62

Figure 3-12: Influence of dipole magnetic fields on directed motility in agar-stab assays of *R. capsulatus* cells inoculated into the glass-agar interstice of borosilicate Petri plates 63

Figure 3-13: Influence of incident light during inoculation on directed cell motility in agar-stab assays of *R. capsulatus* cells inoculated into the glass-agar interstice of borosilicate Petri plates.....66

Figure 3-14: Influence of incident light during incubation on directed cell motility in agar-stab assays of *R. capsulatus* cells inoculated into the interstice of circular Petri plates.....67

Figure 3-15: Graphical representation of the measured angular direction of *R. capsulatus* wild type strain B10 motility in the glass-agar interstice of borosilicate Petri plates incubated with illumination.....68

Figure 3-16: Graphical representation of the measured angular direction of *R. capsulatus* wild type and mutant strain motility in the glass-agar interstice of borosilicate Petri plates incubated with illumination.....70

Figure 3-17: Directed motility of cells toward incident light during incubation in agar-stab assays of *R. capsulatus* cells inoculated into the interstice of square Petri plates.....71

Figure 3-18: Graphical representation of the measured angular direction of motility in the glass-agar interstice of square Petri plates incubated with illumination 72
Figure 3-19: Multiple motility phenotypes observed in agar-stab assays of *R. capsulatus* wild type strain B10 cells inoculated into the glass-agar interstice of borosilicate Petri plates 73
Figure 3-20: *R. capsulatus* flagellum-encoding genomic locus mutagenesis 75
Figure 3-21: Soft agar tubes and agar-stab assays of *R. capsulatus* FlaA-dependent motility through soft agar and in the glass-agar interstice of borosilicate Petri plates 76
Figure 3-22: Transmission electron micrograph negative stain of *R. capsulatus* flagellar filaments in wild type and flagellar mutant strains 77
Figure 3-23: Agar-stab assay of viable and non-viable ^{32}P-orthophosphate-labelled *R. capsulatus* cells in the glass-agar interstice of borosilicate Petri plates 78
Figure 3-24: Nomarski and phase contrast microscopy of *R. capsulatus* cell movements in the glass-agar interface of borosilicate Petri plates 79
Figure 3-25: Transmission electron micrograph negative stain of *R. capsulatus* pilus-like cell surface appendages 80
Figure 3-26: SDS-PAGE resolution of *R. capsulatus* cell surface protein enrichments and corresponding bands excised for peptide sequencing 82
Figure 3-27: Predicted *R. capsulatus* pilus-encoding genomic loci 84
Figure 3-28: Soft agar tubes and agar-stab assays of *R. capsulatus* CpaC-dependent motility in the glass-agar interstice of borosilicate Petri plates 89
Figure 3-29: Soft agar tubes and agar-stab assays of *R. capsulatus* CpaF-dependent motility in the glass-agar interstice of borosilicate Petri plates 90
Figure 3-30: Soft agar tubes and agar-stab assays of *R. capsulatus* CpaA-dependent motility in the glass-agar interstice of borosilicate Petri plates 92

Figure 3-31: Fluorescence microscopy of dye-labelled *R. capsulatus* cells and free amine-containing extracellular material.....98
Figure 3-32: Phase contrast bacterial capsule negative strain microscopy of *R. capsulatus*.....99
Figure 3-33: Soft agar tubes and agar-stab assays of *R. capsulatu*s capsule-dependent motility in the glass-agar interstice of borosilicate Petri plates.....100
Figure 3-34: *R. capsulatus* predicted *hcpA*-encoding genomic locus.....101
Figure 3-35: Soft agar tubes and agar-stab assays of *R. capsulatus* HcpA-dependent motility in the glass-agar interstice of borosilicate Petri plates.....104
Figure 3-36: Agar-stab assay ^{32}P-orthophosphate evidence of coordinated *R. capsulatus* motility in the glass-agar interface of borosilicate Petri plates 106
Figure 3-37: Agar-stab assay time-course of *R. capsulatus* wild type strain B10 motility in the glass-agar interface of borosilicate Petri plates 107
Figure 3-38: Agar-stab assay time-course of *R. capsulatus flaA* mutant strain bKSDF motility in the glass-agar interface of borosilicate Petri plates 108
Figure 3-39: Soft agar tubes and agar-stab assays of *R. capsulatus* PuhA-dependent and BchA/CrtB-dependent motility in the glass-agar interstice of borosilicate Petri plates 111
Figure 3-40: Soft agar tubes and agar-stab assays of *R. capsulatus* PYP-dependent motility in the glass-agar interstice of borosilicate Petri plates.....113
Figure 3-41: Graphical representation of the measured angular direction of PYP-dependent motility in the glass-agar interstice of Petri plates incubated in the LED chamber with LED light illumination.....114
Figure 3-42: Graphical representation of action spectra data overlaid with absorbtion spectra from *R. capsulatus* whole cells.....116

Figure 3-43: Soft agar tubes and agar-stab assays of *R. capsulatus* GtaI-dependent motility in the glass-agar interstice of borosilicate Petri plates.....118
Figure 3-44: Soft agar tubes and agar-stab assays of *R. capsulatus* RpoN-dependent motility in the glass-agar interstice of borosilicate Petri plates.....120
Figure 3-45: Soft agar tubes and agar-stab assays of *R. capsulatus* SenC-dependent motility in the glass-agar interstice of borosilicate Petri plates.....122
Figure 3-46: Soft agar tubes and agar-stab assays of *R. capsulatus* RegA-dependent motility in the glass-agar interstice of borosilicate Petri plates.....124
Figure 4-1: Chemical structures of Gelrite and agarose 130
Figure B-1: Graphical representation of the measured angular direction of motility in the glass-agar interstice of Petri plates with *bchA*/*crtB* mutant cells incubated in the aquarium chamber with white light 233
Figure B-2: Graphical representation of the measured angular direction of motility in the glass-agar interstice of Petri plates with *flaA*/*gtaI* mutant cells incubated in the aquarium chamber with white light 234
Figure B-3: Graphical representation of the measured angular direction of motility in the glass-agar interstice of Petri plates with *senC* mutant cells incubated in the aquarium chamber with white light 234
Figure B-4: Graphical representation of the measured angular direction of motility in the glass-agar interstice of Petri plates with *regA* mutant cells incubated in the aquarium chamber with white light 235
Figure B-5: Graphical representation of the measured angular direction of motility in the glass-agar interstice of Petri plates incubated in the LED chamber with white LED light 235

Figure C-1: Graphical representation of the measured angular direction of motility in the glass-agar interstice of Petri plates incubated in the filter chamber with filtered light illumination.....237
Figure C-2: Graphical representation of the measured angular direction of motility in the glass-agar interstice of Petri plates incubated in the filter chamber with white light illumination 238
Figure C-3: Spectral region of the visible wavelength action spectrum tested with LED lamps.....239
Figure C-4: Graphical representation of the measured angular direction of motility in the glass-agar interstice of Petri plates incubated in the LED chamber with LED light illumination 241

LIST OF ABBREVIATIONS

BChl:	Bacteriochlorophyll	ORF:	Open reading frame
BPhe:	Bacteriopheophytin	PE:	Phosphatidylethanolamine
Crt:	Carotenoid	PYP:	Photoactive yellow protein
DIC:	Differential interference contrast	P_Z:	Wilcoxon probability
EM:	Electron microscopy	RC:	Reaction center
ETC:	Electron transport chain	RFP:	Red fluorescent protein
IM:	Inner membrane	SP:	Signal peptide
IMF:	Ion motive force	Tad:	Tight adherence
IR:	Infra red	TEM:	Transmission electron microscopy
IQR:	Interquartile range	T4P:	Type IV pilus
Flp:	Fimbrial low-molecular weight protein	T4aP:	Type IV a pilus
LH1:	Light harvesting 1	T4bP:	Type IV b pilus
LH2:	Light harvesting 2	TIRF:	Total internal reflection fluorescence
MCP:	Methyl-accepting chemotaxis protein	TPR:	Tetratricopeptide repeat
MS-MS:	Tandem mass spectroscopy	UV:	Ultraviolet
T:	Tesla	Q_1:	First quartile
OM:	Outer membrane	Q_3:	Third quartile

ACKNOWLEDGEMENTS

I have received support from many people while I have completed my thesis. I thank all individuals that have assisted and encouraged me during the period of time that I worked on my doctoral thesis.

I am grateful to my supervisor, Tom Beatty, for allowing me the opportunity to work and learn in his lab group. His insight, enthusiasm, and experience have been an invaluable asset over the years.

I also appreciate the helpful comments, advice, and critical analysis of my thesis provided by the members of my advisory committee, Lindsay Eltis, Bill Mohn, and George Spiegelman.

1. INTRODUCTION

1.1. *Rhodobacter capsulatus*

1.1.1. *R. capsulatus* taxonomy and characteristics

R. capsulatus is a member of the Rhodobacterales order in the alpha class within the proteobacterial phylum of the eubacteria (Imhoff, 2006). Cultures consist of single cells or chains, as nearly spherical cells or distinct rods, cell size ranging from 1 to 6 μm long and 0.5 to 1 μm wide (Van Niel, 1944), cells produce a capsule, and the organism can be found throughout freshwater and soil environments (Overmann et al., 1991). *R. capsulatus* is a facultatively phototrophic purple non-sulfur bacterium that exemplifies the biological properties of the *Rhodobacter* genus (Weaver et al., 1975). Under anaerobic conditions, such organisms are capable of anoxygenic photosynthesis, using light for generating a proton gradient without the generation of oxygen (Blankenship, 2002). Some non-sulfur bacterial species can use hydrogen sulfide at low concentrations as the electron donor for chemotrophic ATP synthesis, however high H_2S concentrations are toxic (Hansen and van Gemerden, 1972).

Pigmentation is induced under low oxygen tension (Ma et al., 1993), and ranges from bright red under semi-aerobic to yellow-brown in anaerobic conditions (Van Niel, 1944). *R. capsulatus* is metabolically versatile, capable of nitrogen fixation and growth on a range of carbon sources (Weaver et al., 1975), making it a useful model organism for the study of nitrogen fixation, photosynthetic and respiratory electron transfer, carbon fixation, and other areas of research.

1.1.2. *R. capsulatus* genomic characteristics

The genome of *R. capsulatus* strain SB1003 (Yen and Marrs, 1976), derived from strain B10 (Marrs, 1974), contains 3.9 mega base pairs (Mbp), consisting of a 3.74 Mbp chromosome and a plasmid of 133 kb. The sequence, essentially completed in 2007 but not assembled and well-annotated until

2010, encodes a predicted 3740 genes: 3587 chromosomal and 153 plasmid genes. The availability of the genome sequence and the amenability of *R. capsulatus* to genetic and biochemical manipulation greatly facilitate the characterization of its physiology.

1.2. Bacterial motility

1.2.1. Adaptive responses

Environmental conditions influence the physiological and biochemical state of organisms. Cells may respond differently to environmental factors such as nutrients, temperature, and light (Parkinson, 1993). Adaptive responses allow organisms to tailor their biochemistry and physiology to shifts in the state of their immediate surroundings. Temporal or spatial sensory perception can assess the state of immediate surroundings, and induce an adaptive response to maintain conditions ideal for growth and proliferation (Alexandre et al., 2004). Bacterial cells are small enough such that the surface area of cells is considered insufficient to effectively perceive spatial stimuli, because of the short length across the cell and the rapid rate of diffusion (Armitage, 1992). Thus bacterial cells were thought to be limited to temporal sensory regulation mechanisms for adaptive responses (Macnab and Koshland, 1972), although recent research indicates this may not be true (Thar and Kuhl, 2003). Adaptive bacterial responses induced by temporal sensory perception modulate the state of the cell by various methods, involving transcriptional, translational, and post-translational regulation (Wadhams and Armitage, 2004), and physiological modulations such as changes in cell structure, cell morphology (Shi and Xia, 2003), and motility (Manson, 1992).

1.2.2. Distribution, regulation, and types of bacterial motility

Bacterial motility plays a large role in many biological phenomena, such as commensal relationships, virulence, DNA uptake, biofilms and community structure (Rudel et al., 1995b; Moens and Vanderleyden, 1996; Wood et al., 2006). Adaptive motility may be thought of as consisting of four

stages: 1) sensory integration; 2) signal transduction; 3) modulation of propulsion; and 4) adaptation of the system. Microorganisms have developed several methods of regulating the coordination of these stages, including transcriptional regulation, translational regulation, post-translational processing, and allosteric modification (Macnab, 1992; Aldridge and Hughes, 2002; Tamayo et al., 2007). Bacterial motility is regulated in a temporal manner by the allosteric modification of the sensory integration and signal transduction components of the pathway, enabling cells to detect and respond to fluctuations in stimuli against a range of background conditions, by comparing current conditions with those recently encountered. These signals are then transduced to the propulsion component and cells are translocated by an energy-dependent process that can be mediated by several different mechanisms. I will briefly review the motility mechanisms of flagellar rotation, pilus retraction, cytoskeletal rearrangement, exopolysaccharide extrusion, focal adhesion, and sliding (Harshey, 2003). Several types of motility, mechanisms, and movement speeds are summarized in Table 1-1.

Table 1-1: Types of bacterial motility.

Type of motility	Mechanism	Medium	Speed
swimming	flagellum rotation	aqueous	~30 – 150 μm/sec
swarming	flagellum rotation	semi-solid, solid	~0.05 – 40 μm/sec
twitching	pilus retraction	semi-solid, solid	~0.01 – 0.3 μm/sec
gliding	changes in envelope structure	aqueous	~5 – 25 μm/sec
	changes in envelope structure	semi-solid, solid	~0.07 – 0.25 μm/sec
	cytoskeletal rearrangement	semi-solid, solid	~1 – 4 μm/sec
	extrusion/secretion	semi-solid, solid	~0.02 – 0.1 μm/sec
	focal adhesion	semi-solid, solid	~0.02 – 10 μm/sec
sliding	secretion	semi-solid, solid	~0.02 – 6 μm/sec

Data taken from: (Magariyama et al., 1995); (Ren et al., 2002); (McCarter, 2010); (Harshey, 2003); (Fall et al., 2006)

1.3. Bacterial flagellum-mediated motility

1.3.1. Flagellum structure and function

Flagellar motility has been found in many Gram-positive and Gram-negative genera (Houwink and van Iterson, 1950), and despite some differences in flagella between microbial species there are several conserved core flagellar genes (Macnab, 1992). In general, flagellum biogenesis and function requires ~50 genes encoding cytoplasmic, periplasmic, and extracellular components that create a propeller-like force to drive cell motility (Macnab, 2003). Flagella are driven by a membrane-bound motor complex coupled to an ion motive force (IMF) to power the rotation of a helical flagellar filament (Berg and Anderson, 1973; Atsumi et al., 1992). A chemiosmotic sodium ion or proton gradient across the cell membrane is channelled through pores coupled to stator complexes associated with the flagellum motor. As shown in Figure 1-1, a rod assembly runs through multimeric protein rings, which act as bearings, in the cell wall and membrane(s). The rod is fixed to an extracellular hook structure, generating an axis around which rotation occurs. The hook is fixed to a flagellar filament, composed of repeating flagellin monomers, that translates the rotation into propulsion (Berg, 2003).

The production of the bacterial flagellum is regulated by transcriptional, translational, and post-translational mechanisms (Aldridge and Hughes, 2002; Llewellyn et al., 2005) resulting in a progressive assembly pattern (Macnab, 2003; Minamino and Namba, 2004). This progressive assembly can be used to classify flagellar genes into three transcriptional classes (I, II, and III) based on the promoter sequence involved in gene expression (Chilcott and Hughes, 2000), or four assembly classes (I, II, III, and IV) based on assembly checkpoints (Jenal, 2000). The bacterial flagellin (encoded by *flaA*) is a class III transcript, and a class IV assembly component. Flagellin is produced after the transport, motor, membrane-spanning rotor complex, and extracellular coupling structures of the flagellum are assembled (Anderson and Newton, 1997). Flagellin subunits are secreted through the 200 to 250 Å diameter central channel

(Craig et al., 2004) of the structure, and added to the flagellum distal end (Suzuki et al., 1978).

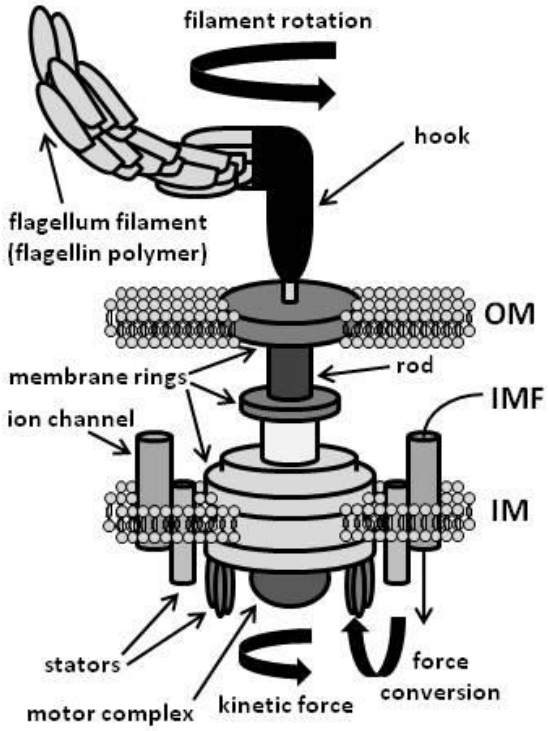

Figure 1-1: Representation of a typical Gram-negative bacterial flagellum. The rotational force from an inner membrane motor complex, generated by an ion motive force (IMF), is translated by a rotor assembly to an extracellular semi-helical filament to generate propulsion. OM, outer membrane; IM, inner membrane. Cell wall not shown.

Flagellum rotation is controlled by a multimeric protein switching complex that functions in conjunction with sensory pathways to regulate the rate and direction of rotation (Macnab and Aizawa, 1984). Flagellar movements consist of periods of smooth counter-clockwise rotations punctuated by short cessations, or clockwise reversals, of flagellar rotation. These modulations of flagellar rotation allow Brownian movements or induce cell tumbles that reorient the cell randomly (Macnab and Aizawa, 1984). Flagellar biogenesis and function may be regulated in response to the local conditions of the cellular environment, and some species possess more than one type of flagellum that may be expressed differentially in response to environmental conditions (Macnab and Koshland, 1972; Atsumi et al., 1992).

1.3.2. Aqueous substrate flagellar swimming

Aqueous flagellar swimming may be driven by a single flagellum, as in *Rhodobacter sphaeroides* (Armitage et al., 1999), or a bundle of flagella as in *Salmonella typhimurium* (Flores et al., 2005). Cells swim through aqueous media in a series of curved lines punctuated by periods of reorientation. Homogeneous environments induce random patterns of swimming in which short periods of smooth swimming are punctuated by short changes in direction (Porter et al., 2008). In the presence of stimuli that induce directed taxis, the sensory apparatus and signal transduction system respond to temporal changes over the time in which a cell moves several lengths (Macnab and Koshland, 1972). Random swimming patterns become biased in heterogeneous environments, because smooth runs of swimming are prolonged as cells move away from repellents, or toward attractants (Porter et al., 2008).

Cessation of rotation of a single flagellum induces a relaxation of the helical structure to a short wavelength, high amplitude coil (Armitage, 1992); the slow rotation of the cell as the flagellum conformation returns to a smooth swimming state, as well as Brownian movement, causes the cell to reorient the direction of taxis. Multiple flagella may be driven together into a bundle by counter-clockwise rotations that propel cells forward, in which case periodic reversals of rotation (to clockwise) dissociate this bundle, and induce the cell to reorient the direction of taxis (Armitage, 1992). The bundle is then reconstituted as flagella revert to counter-clockwise rotations and drive the smooth swimming state. In both cases Brownian motion and cell tumbling result in a reorientation of cells before smooth swimming is resumed.

1.3.3. Solid substrate flagellar swarming

Solid substrate flagellar motility can be driven by a polar flagellar bundle as in *Pseudomonas aeruginosa* (Kohler et al., 2000), lateral flagella punctuated across the surface of the cell as in *Vibrio parahaemolyticus* (Jaques and McCarter, 2006), or periplasmic sheathed flagella called axial filaments in

the spirochaete *Leptospira interrogans* (Bromley and Charon, 1979). A variety of factors such as growth medium viscosity, cell contact, the rate of flagellar rotation, cell density, or nutrients such as amino acids act as stimuli to induce the differentiation of cells from a vegetative to a swarming state, as described below. Hyper-flagellation is the most prominent feature of the swarming state, allowing swarming or crawling across substrates (Fraser and Hughes, 1999). Swarming cells aggregate into masses that undergo movements along the long axis of cells in coordinated rafts. Alignments of cells along their long axis and close cell to cell contact often occur during swarming migration (Darnton et al., 2010). Swarming cells may secrete compounds such as exopolysaccharides and other exopolmers to facilitate swarming motility (Neu, 1996). These secreted compounds may reduce the surface tension of the growth medium, increase the surface fluidity on the substrate over which the cells are moving, or encapsulate the rafts to keep cells together and tightly organized (Caiazza et al., 2005). Flagellar rotations are thought to be coordinated by extracellular signals, cell-cell contact, and signal transduction pathways within the cell. These signals are transduced to the motility apparatus by two-component regulatory systems, cytosolic regulators, and the chemotactic pathway (Fraser and Hughes, 1999). Flagellar movements function in the same manner as for aqueous swimming: counter-clockwise rotations propel cells forward, whereas the frequency of cessations and clockwise rotations are responsible for reorientations.

1.4. Bacterial pilus-mediated motility

1.4.1. Pilus structure and function

Pilus-driven motility has been observed in the Gram-positive bacterium *Clostridium perfringens*, and well-studied in the Gram-negative *Neisseria*, *Pseudomonas*, and *Myxococcus* genera (Wall and Kaiser, 1999; Varga et al., 2006). Bacterial pili are involved in a multitude of cellular functions such as DNA uptake, biofilm formation, virulence, cell-cell adhesion, phage infection, and pilus-dependent motility (McBride, 2001). Pilus-mediated motility has been characterized predominantly in bacteria that

assemble a Type IV pilus (T4P) (Mattick, 2002), and has been observed to function both independently of, or in conjunction with, flagellum-based motility (O'Toole and Kolter, 1998). T4P biogenesis and function are mediated by conserved genes (Strom and Lory, 1993) that encode cytoplasmic, periplasmic, and extracellular components secreted via a *sec*-dependent pathway (Bose et al., 2002) . Accessory components such as peptidases (Wolfgang et al., 2000) localize at the internal side of the cell membrane, whereas the ATPase motors and other membrane-associated components are translocated across the cell membrane by the *sec* secretion pathway (Bose et al., 2002).

T4P are composed of repeating pilin subunits, translated as pre-pilin proteins with a short N-terminal signal peptide (SP) that is involved in the localization of the pilin protein in the inner membrane (Strom and Lory, 1987). The SP sequence of T4P prepilins, the class III SP, is distinct from most signal peptides (class I SP and class II SP) in exported proteins (Michaelis and Beckwith, 1982) because the signal cleavage site precedes the hydrophobic residue stretch (Johnson et al., 1986; Nunn and Lory, 1991; Paetzel et al., 2002; Szabó et al., 2007). An inner membrane-associated endopeptidase (Wolfgang et al., 2000), or prepilin peptidase recognizes the N-terminal region of up to eight positively charged amino acids, followed by a stretch of 6 to 15 uncharged hydrophobic residues. After cleavage at a specific site within the SP (Michaelis and Beckwith, 1982), the pilin protein is polymerized at the cell membrane by a secretion ATPase. Pilus secretion requires the hydrolysis of ATP for the extension of the pilus (Chiang et al., 2008; Proft and Baker, 2009), as a 50 to 80 Å diameter (Craig et al., 2004) helical filament through a secretin portal in the cell wall (and outer membrane in Gram-negative bacteria). The secretin protein assembles in the outer membrane with the aid of an associated pilotin protein (Nudleman et al., 2006), to form a multimeric complex of 12 to 14 subunits (Collins et al., 2001) that extends into the periplasmic space and interacts with the peptidoglycan matrix to form a plugged barrel (Chami et al., 2005). The cavity of the secretin pore is approximately 55 Å in diameter (Bitter et al., 1998), and contains a gated channel (Wolfgang et al., 2000) through which the pilus is extruded. The

pilus culminates in a globular head structure generated by two C-terminal cysteine residues in what is termed the D-region of the pilin protein. These residues are buried along the length of the pilus and exposed only at the distal tip of the filament (Craig et al., 2004).

The pilus is retracted by a membrane-bound ATPase that lacks a structurally conserved N-terminal sequence of 160 to 175 amino acid residue domain present in secretion ATPases (Jakovljevic et al., 2008). These ATPases are members of the AAA+ family (Chiang et al., 2005), and depolymerize pilin subunits from the cell-proximal end of the pilus (LeBrasseur, 2002). This depolymerisation is responsible for generating the force that draws cells across the translocation surface in twitching motility (Jakovljevic et al., 2008) (Figure 1-2).

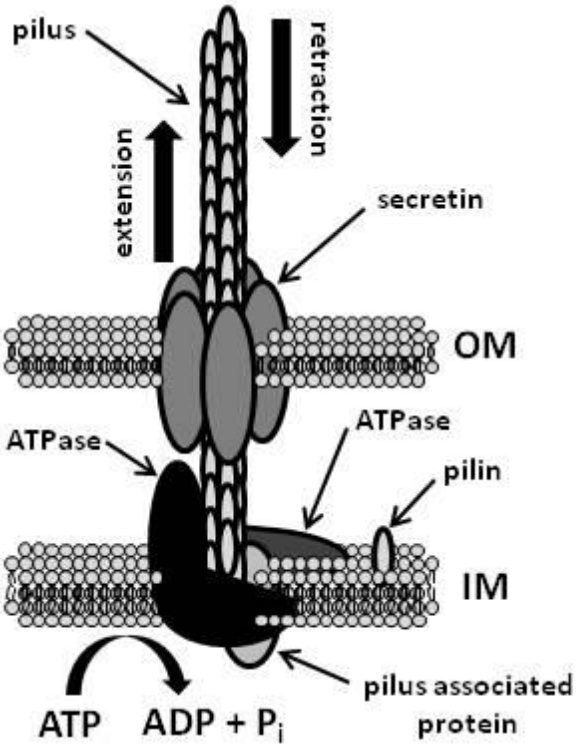

Figure 1-2: Representation of a typical motility pilus. The polymerization and depolymerisation of an extracellular filament of pilin proteins at an inner membrane motor complex mediated through a secretin complex to generate propulsion. OM, outer membrane; IM, inner membrane. Cell wall not shown.

1.4.2. Solid substrate pilus twitching

Twitching motility over solid substrates is driven by bundles of pili displayed at the poles of cells (Craig et al., 2004). Factors such as cell contact, substrate adherence, and nutrient availability have been shown to induce pilus biogenesis; however the role of these factors in T4P synthesis and function are not clearly understood. Twitching motility is a social form of bacterial motility, in which cells cluster together and align into ordered rafts to translocate as a cell mass with coordinated extensions and retractions of pili from the cell poles (Henrichsen, 1972; Burrows, 2005). Twitching motility is manifested as relatively slow, intermittent movements or smooth linear cell translocations, dependent on the organism and the conditions of the substrate (Semmler et al., 1999). Pilus extensions and retractions are achieved by the polymerization and depolymerization of long, thin polar filaments. Conserved structural and functional core components mediate the assembly and disassembly of the pilus, in conjunction with accessory components that may vary from organism to organism (Alm and Mattick, 1997). Two types of T4P have been characterized at the time of this thesis, classified on the basis of signal peptide and mature sequence lengths of the pilin: (a) the T4a pilus with separate ATPase motors for extension and retraction of the pilus filament (Whitchurch et al., 1991; Turner et al., 1993; Whitchurch and Mattick, 1994; Jakovljevic et al., 2008); and (b) the T4b pilus that appears to lack multiple ATPase motors (Craig et al., 2004; Craig and Li, 2008) and the ability to retract (with the exception of enteropathogenic *E. coli*). The T4aP mediates motility (Chiang et al., 2008), whereas the T4bP is capable of pilus extension but has yet to be proven capable of driving cell movements.

The pilus is extruded through a secretin complex and, upon extension an adhesin displayed on the end of the pilus adheres to the taxis substrate (Rudel et al., 1995a). An ATP-dependent depolymerisation motor retracts the pilus, thereby drawing the cell toward the anchored distal tip of the appendage, generating forward taxis (Merz et al., 2000). Cells move forward by coordinated extension and retraction of pili from the leading edge poles of the taxis raft, whereas reversals are achieved by

pilus activity at the lagging poles of cells in the raft (Sun et al., 2000). Because individual pili on the same cell seem to extend and retract independently (Mattick, 2002), it is unclear whether all cells in the raft contribute to pilus driven movement or if some cells are carried along by elasticotaxis (Stanier, 1942). Disassociation of the ordered cell raft, followed by realignment of cells along the long axis of a dissociated cell, might account for a method of directional reorientation.

1.5. Bacterial gliding motility

1.5.1. Gliding mechanisms and function

Gliding motility has been identified in several diverse bacterial phyla, in both aqueous media and on solid substrates. Gliding is a mode of flagellum/pilus-independent motility that may be driven by chemiosmotic gradients (sodium-ion or proton) across the cell membrane (Pate and Chang, 1979; Agarwal et al., 1997), however ATP hydrolysis may also be involved (McBride, 2001). Gliding motility mechanisms are characterized by smooth movements of cells in a linear manner, although these movements may occur consist of continuous translocations or sporadic advancements (Youderian, 1998). While still largely a mystery, gliding motility appears to be achieved by three separate mechanisms including rearrangements of cell shape, secretion of cell material, or localized adhesions of the cell to the substrate (Burchard, 1981; McBride, 2001). In some cases it appears that a combination of these mechanisms contributes to gliding motility, in which a motor complex pushes against helical cytoskeletal elements and extrudes material across adhesins (Harshey, 2003). The three mechanisms are described in more detail below.

1.5.2. Cytoskeletal rearrangement in gliding

Cytoskeletal and cell surface rearrangements have been implicated in the gliding motility of *Spiroplasma* (Wolgemuth et al., 2006) and *Synechococcus* (Ehlers et al., 1996). Gliding motility is thought to be achieved by conformational changes in cytoskeletal filaments (Shaevitz et al., 2005), or by

the activity of large proteins found on the cell surface that affect the cell structure (Samuel et al., 2001). Changes in the helical shape of the cell (Shaevitz et al., 2005), or rotation of surface components about a point (Samuel et al., 2001), are postulated to induce kinks or travelling waves in the surface of the cell that propagate motility (Ehlers et al., 1996) (Figure 1-3).

The outer membrane oscillin fibrils of *Oscillatoria* cyanobacteria were proposed to direct thrust during gliding motility. Oscillin contains Ca^{2+}-binding motifs (Brahamsha, 1999) similar to the S-layer SwmA protein that was postulated to translate longitudinal waves along the cell body of *Synechococcus* (Ehlers et al., 1996). Localized surface rearrangements were postulated to occur in *M. xanthus* cells observed to flex along the cell body, and may be associated with gliding motility (Spormann and Kaiser, 1995; Spormann and Kaiser, 1999). When combined with extrusion or focal adhesion models, these postulated travelling waves might also contribute to a gliding motility mechanism on solid substrates.

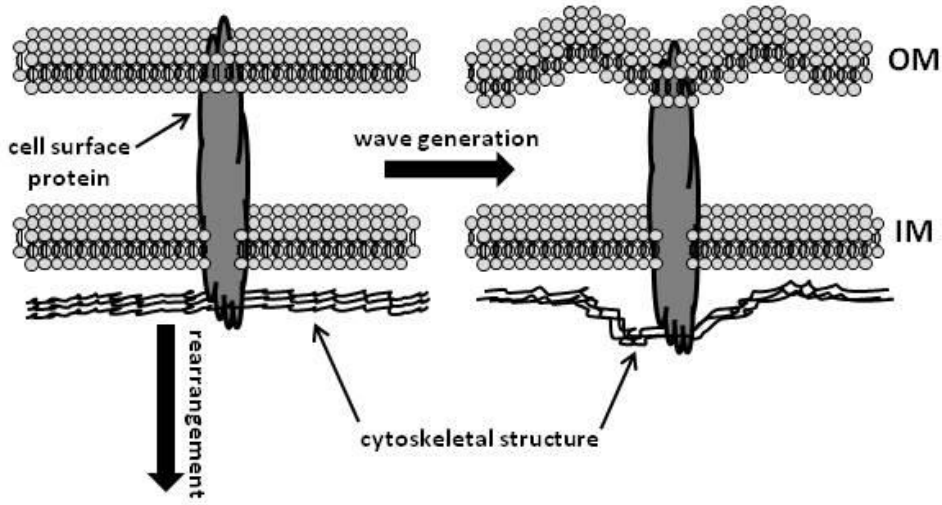

Figure 1-3: Representation of a Gram-negative bacterial cytoskeletal rearrangement mechanism. The transfer of energy to a localized point on the extracellular surface creates standing waves that generate propulsion. OM, outer membrane; IM, inner membrane. Cell wall not shown.

1.5.3. Extrusion in gliding

Extrusion-dependent gliding motility has been proposed to mediate solid substrate movement by slime secretion (Hoiczyk and Baumeister, 1998; Hoiczyk, 2000; Yu and Kaiser, 2007). Observations of slime trails left behind *M. xanthus* (Yu and Kaiser, 2007) cells translocating across solid substrates indicate that the secretion of polysaccharide facilitates gliding movements (Wolgemuth et al., 2002) (Figure 1-4).

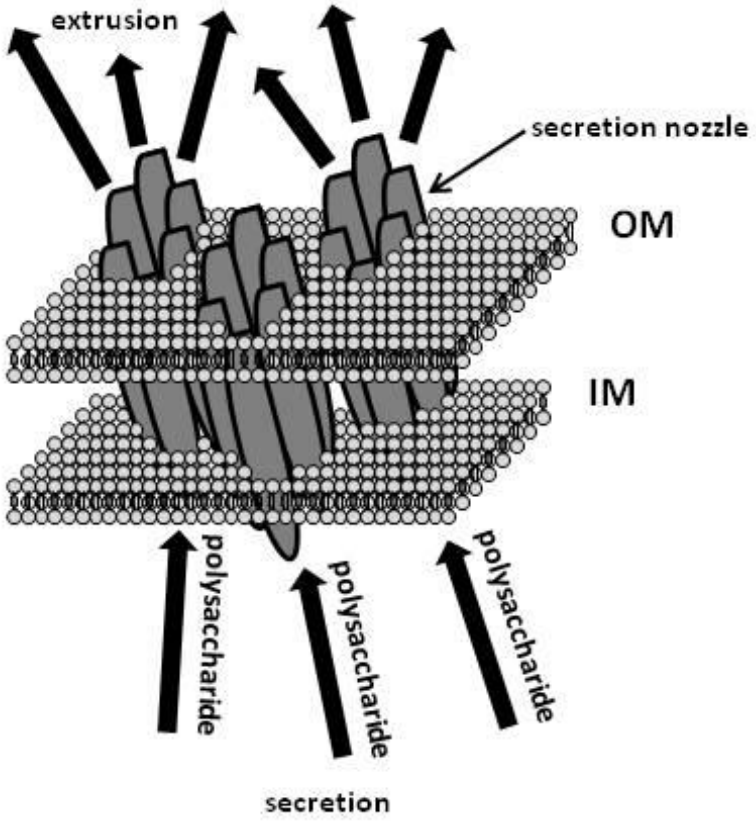

Figure 1-4: Representation of a Gram-negative bacterial extrusion mechanism: The transport and hydration of semi-hydrated polysaccharides through the nozzle as hydrated extracellular polysaccharides generates propulsion. OM, outer membrane; IM, inner membrane. Cell wall not shown.

Proteins involved in the biosynthesis (Yu and Kaiser, 2007) and transport (White and Hartzell, 2000; Youderian et al., 2003) of polysaccharides, and several proteins involved in the transport of molecules across the outer membrane have been implicated in some bacterial species. The directional

secretion of polysaccharides across a cell girdle, or from the poles, is thought to propel cells across the substrate (Hoiczyk and Baumeister, 1998; Hoiczyk, 2000). The secretion of polysaccharides may provide a surfactant, to reduce surface tension and friction in translocation across a substrate (Dworkin et al., 1983). Additionally, the extrusion and hydration of semi-hydrated polysaccharides within the nozzle may propel the cell across the substrate (Wolgemuth et al., 2002).

1.5.4. Focal adhesion in solid substrate gliding

Focal adhesion has been proposed as a mechanism of solid substrate motility in *Flavobacterium* (Braun et al., 2005), *Myxococcus* (Mignot et al., 2007), and *Mycoplasma* (Miyata, 2008). *Flavobacterium* and *Myxococcus* focal adhesions form along the entire cell body (Sliusarenko et al., 2007; Nelson et al., 2008), whereas *Mycoplasma* focal adhesions occur at only in the head-like structure at the leading cell pole (Miyata and Uenoyama, 2002). These adhesion mechanisms differ (Jarrell and McBride, 2008), but the underlying principle of translocation appears to be the same. It is thought that a point on the surface of the cell adheres to the substrate, while the cell mass is translocated with respect to this fixed point (Mignot et al., 2007). Focal adhesion studies of *Flavobacterium johnsoniae* and *Mycoplasma pneumoniae* identified short filaments distributed over the entire surface of the outer membrane believed to adhere to the substrate (Liu et al., 2007). Other localized surface proteins were also proposed to act as cell surface adhesins that anchor the outer membrane to the substrate (Hasselbring and Krause, 2007b), while cytoplasmic and transmembrane components transduce a signal to periplasmic proteins that induce a movement of the cell relative to the point of adhesion (Nelson et al., 2008) (Figure 1-5).

Alternatively, some motile bacteria lacking a cell wall (*i.e. Mycoplasma* species) develop a polarity in the shape and structure of the cell (Krause and Balish, 2001; Balish and Krause, 2006), an asymmetry where the leading edge of cells is narrowed and elongated. Gliding motility appears to be

facilitated by focal adhesions at the leading edge of the cell utilizing large molecular weight surface proteins as adhesins (Adan-Kubo et al., 2006). These focal adhesions are thought to be connected to the cytoskeletal elements of the cell, and so taxis is achieved by either rearrangements of the cytoskeletal proteins (Henderson and Jensen, 2006), or coupling of conformational changes in adhesins to the cytoskeleton (Hasselbring and Krause, 2007a). Focal adhesions are then released as the leading edge of the cell passes the adhesion point.

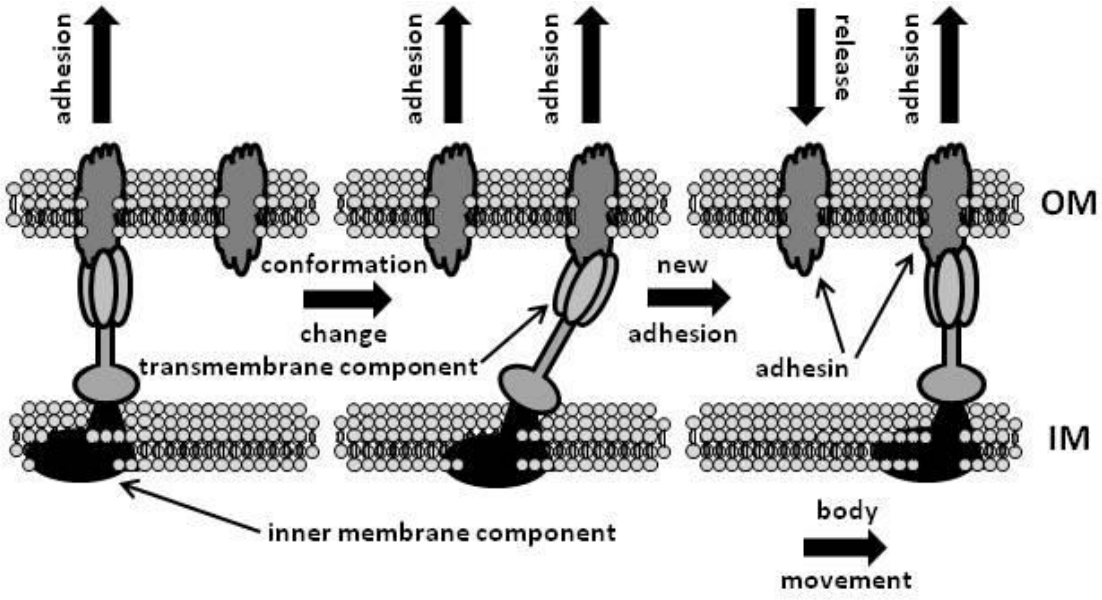

Figure 1-5: Representation of a Gram-negative bacterial focal adhesion mechanism. A conformational change in a linker assembly is driven by an inner membrane motor complex. The focal adhesion of an extracellular structure translates this conformational change to motility. OM, outer membrane; IM, inner membrane. Cell wall not shown.

1.6. Bacterial sliding motility

Sliding motility occurs on solid substrates in the absence of flagella and pili found in many bacterial species (Henrichsen, 1972). Surfactants are required for sliding movements across moist surfaces (Harshey, 2003). Lipopolysaccharides, glycopeptidolipids, and other surface-active compounds act as surfactants that reduce the surface tension on a substrate (Martinez et al., 1999). The

serrawettin lipopeptide is required for the sliding motility of *Serratia liquefaciens* (Lindum et al., 1998). Sliding motility is a passive mechanism of movement driven by the expansive force of cell proliferation on a reduced surface tension. Division in the central mass of a group of cells exerts pressure on the surrounding cells. This pressure is translated as force by cell-cell contact to the edge of the cell mass. The edge of the cell mass is moved when the force of the cell mass exceeds the adhesion between cells and the substrate, which is reduced by surfactants secreted by the cells. As a result the peripheral mass of sliding cells moves outward in a passive manner.

1.7. Bacterial taxis

Bacterial movement can be random or directed, and taxis is a property that confers directionality and adaptation to motility. Cells move in response to different stimuli (Hazelbauer et al., 1993), including: chemotaxis (Adler, 1966; Bibikov et al., 1997; Rebbapragada et al., 1997), movement in response to chemical gradients; galvanotaxis (Adler and Shi, 1988; Shi et al., 1996), movement in response to an electrical current; hydrotaxis (Pringault and Garcia-Pichel, 2004), movement in response to moisture; magnetotaxis (Blakemore, 1975), movement in response to a magnetic field; rheotaxis (Rosengarten et al., 1988), movement in response to fluid flow; thermotaxis, movement in response to temperature gradients (Gluch et al., 1995; Nara et al., 1996); and phototaxis (Ragatz et al., 1994; Gest, 1995), movement in response to light.

1.7.1. Light-responsive motility

Regardless of the mode of motility employed by bacterial cells, adaptive motility responses require sensory mechanisms to detect stimuli, which must be transduced to the motility apparatus and used to induce directed migration (Nultsch and Hader, 1988). Signal reception and transduction are critical components of any adaptive response regardless of the stimulus perceived and response induced. Light is pervasive on the Earth's surface and can act as a stimulus to induce adaptive responses

(Hader, 1987). Incident light has been shown to affect bacterial gene expression and/or cellular behaviour. Light-induced taxis responses have been reported in bacteria since scientists first began to study microbes (Engelmann, 1883; Gest, 1995), and may be subdivided into two classes based on whether the incident light is perceived in an energetically dependent or independent manner.

1.7.2. Energy taxis

The term energy taxis refers to a mechanism by which organisms modify tactic behaviour in response to the energetic state of the cell (Schweinitzer and Josenhans, 2010). The stimulus for induction of taxis originates within a central energetic regulator of the cell, the electron transport chain (ETC) (Alexandre et al., 2004). The generation of energy is a primary concern for cells, and bacteria must rapidly adapt to shifts resulting from changes in local conditions. The flow of electron transport in the bacterial membrane is the origin of the signal for this adaptive response (Alexandre, 2008), and may reflect the presence of a gradient of nutrients, cofactors, electron donors and acceptors, or light in the localized environment (Figure 1-6).

Energy taxis has been observed in many species. Examples include metabolism-dependent chemotaxis (Jeziore-Sassoon et al., 1998; Alexandre, 2008), *E. coli* aerotaxis (Bibikov et al., 1997), and scotophobic (*Schreckbewegung*) light intensity-dependent swimming in a variety of photosynthetic bacteria (including *R. capsulatus*) (Gest, 1995). Energy taxis may be initiated by the detection of chemical gradients by methyl-accepting MCPs that span the cytoplasmic membrane (Gestwicki and Kiessling, 2002), or by the transport and metabolism of chemoattractants (Jeziore-Sassoon et al., 1998).

The cytoplasmic chemoreceptor TplD of *Helicobacter pylori* was proposed to detect perturbations in the redox state of the electron transport chain. Decreases in intracellular energy levels resulting from exposure to electron transport inhibitors disrupted chemotactic motility, whereas artificial electron donors that restore the flow of electrons through the ETC restored concentration-

dependent chemotaxis (Alexandre, 2008). The availability of chemoattractants or their metabolic intermediates, as electron donors, cofactors and electron acceptors, bias *H. pylori* motility by energy taxis (Alexandre et al., 2004; Alexandre, 2008).

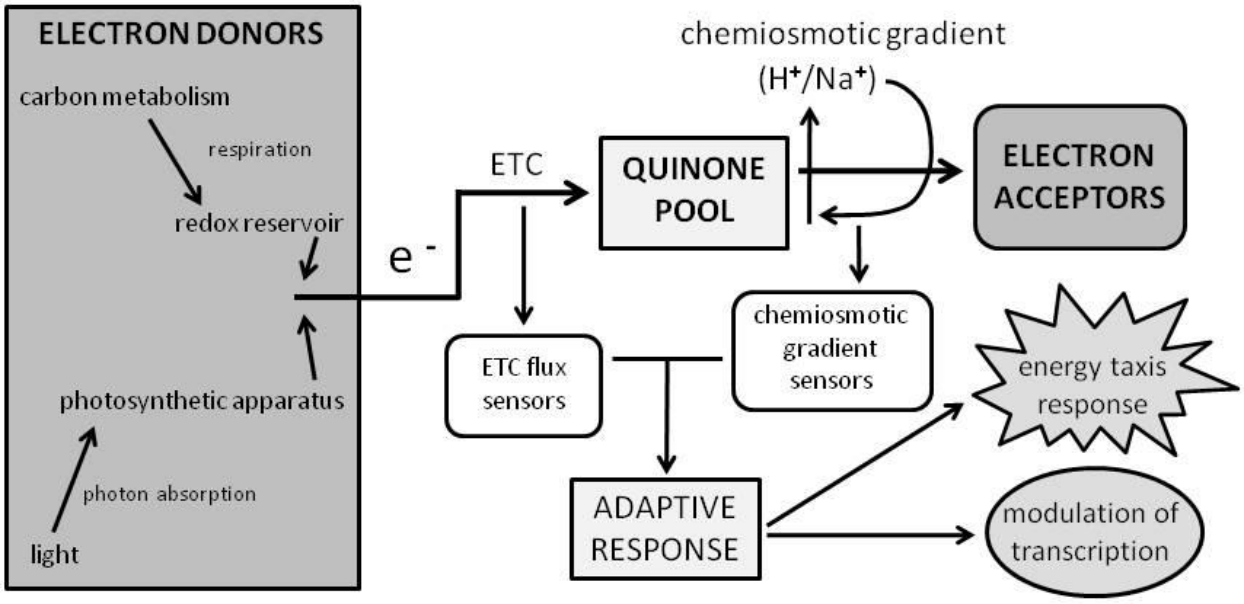

Figure 1-6: Representation of bacterial energy taxis pathway. Signals from energy-dependent stimuli are transduced through the energetic potential of the ETC to cytoplasmic effectors that modulate motility. Figure adapted from Taylor *et al.*, 1999.

In *E. coli*, aerotaxis dependent on the cytoplasmic membrane-anchored MCP-like Aer protein regulates swimming toward optimal oxygen concentrations (Armitage and Schmitt, 1997). The Aer protein is coupled to the redox state of the ETC via a N-terminal, non-covalently bound FAD cofactor (Schweinitzer et al., 2008). Thus donors and acceptors of the electron transport chain modulate the direction of motility to ensure a maximal electron transport rate (Armitage and Schmitt, 1997).

The scotophobic (fear of darkness) response causes motile phototrophic cells to change direction after a transition from a region of high to low illumination. As cells pass across a light/dark boundary, a decrease in the redox state of the ETC induces a tumble that reorients the direction of flagellar swimming. These dark-induced tumbles cause cells to accumulate in the zone of illumination

(Gest, 1995). The photosynthetic apparatus, which is integrated into the ETC, perceives the stimulus, and the taxis response is mediated by the flow of electrons through the ETC (Armitage and Schmitt, 1997). The scotophobic response is different from genuine phototaxis (described below) because it is dependent on energy production.

1.7.3. Phototaxis

Phototaxis is a process in which organisms use light as a stimulus to induce directed cell motility (Armitage, 1997). Phototaxis may cause the movement of cells in response to incident light, and is dependent on the quality (wavelength) of light. Phototactic signal reception may occur independently of the flow of electrons through the ETC (Giovannoni et al., 1987), and allows organisms to move to optimal positions within their growth environment with respect to the direction, wavelength, and intensity of incident light (Gest, 1995). A negative phototaxis response, as observed in *E. coli* (Yang et al., 1995), could serve to move cells away from unfavourable illumination, such as UV light that might induce superoxide radicals and DNA damage (Krinsky and Deneke, 1982). Conversely, positive phototactic migration, as reported in *Synechococcus* and *Rhodospirillum centenum* (Ragatz et al., 1994; Yoshihara and Ikeuchi, 2004), might be employed to locate cells at favourable positions within biofilms and other stratified environments, where conditions are improved for photosynthesis or other light-dependent biological processes (Nultsch and Hader, 1988).

A phototactic response will typically have an action spectrum, with differing responses to different wavelengths of light. An action spectrum may provide insight into the photoreception molecule(s) used by cells. The phototactic responses of the α-proteobacterium *R. centenum* (Ragatz et al., 1995), the unicellular cyanobacterium *Synechocystis* sp. PCC 6803 (Yoshihara and Ikeuchi, 2004), and the archaeon *Halobacterium salinarium* (Krah et al., 1994) have been defined by their activation spectra.

R. centenum cells move away from light in the visible spectrum (~400 to 800 nm), but toward infrared light (Ragatz et al., 1994). Positive phototaxis toward 800 to 875 nm light corresponds to the absorption profile of reaction center (RC) and light-harvesting (LH) photosynthetic complex-coupled bacteriochlorophyll (BChl). The negative phototaxis was found to be triggered by the blue/green/orange region of the spectrum, corresponding to the BChl absorption at 590 nm, and 475 to 550 nm absorption profiles of carotenoid pigments. Although the photosynthetic RC initiates this response, it differs from scotophobic movement because the light wavelength instead of intensity determines the direction of movement, generating a multiple wavelength action spectrum (Ragatz et al., 1995). It was found that a gene called *ptr*, which encodes a chemotaxis receptor-like protein homologue, is needed for both positive and negative phototaxis (Jiang and Bauer, 2001).

Synechocystis cells move toward yellow/red light and away from UV light. Positive movements toward 560 to 720 nm light are offset by negative phototaxis from 360 nm light (Choi et al., 1999). Studies indicate that several photoreceptors are active in *Synechocystis* cells, because negative responses were also observed with both 470 nm blue and 600 to 700 nm red light. Furthermore, absorption of 435 nm blue light overrides positive phototaxis in the 560 to 720 nm light range (Yoshihara and Ikeuchi, 2004). It appears that the *Synechocystis* phototaxis response has photoreceptors that elicit a positive or negative response based on the illumination conditions.

H. salinarium phototaxis has a simple action spectrum that includes a positive green/orange (~590 nm) light response and a negative blue/green (~480 nm) light response (Mironova et al., 2005). This is because the photoreceptors are two rhodopsin molecules, sensory rhodopsin I (SRI) and phoborhodopsin (SRII). Positive phototaxis is mediated by SRI absorption of 587 nm light (Imamoto et al., 1991), whereas negative phototaxis is due to the activation of SRII by 480 nm light (Dai et al., 2010)

Several classes of energy-independent photoreceptors have been identified, such as rhodopsins, cryptochromes, BLUF-domain proteins, LOV-domain proteins, and bacteriophytochromes (van der Horst and Hellingwerf, 2004). These molecules are capable of light-induced isomerizations (Hoff et al., 1994) that, when coupled to a biochemical reaction and signal pathway, are capable of transducing the light stimulus independently of the electron transport chain (Gordeliy et al., 2002).

1.7.4. Tactic responses

Motility is a physiological characteristic observed in a broad range of bacteria, and both Gram-positive and Gram-negative species have evolved several mechanisms of movement (Henrichsen et al., 1972; Williams and Schwarzhoff, 1978; Burchard, 1981; Henrichsen, 1983), which allow the directed translocation of bacterial cells in response to fluctuations in environmental states. Bacterial adaptive responses are induced not only by transient fluctuations in environmental conditions (Boyd and Simon, 1982), but they are also able to respond to long-lived environmental stimuli (Goy et al., 1977). Methylation modulates receptor sensitivity to allow the adjustment of sustained tactic responses from temporal sensory mechanisms during prolonged exposure to long-lived environmental stimuli, such as temperature, viscosity or high solute concentrations (Block et al., 1982; Hauri and Ross, 1995).

The methyl-accepting chemotaxis proteins (MCPs) that function as *Escherichia coli* chemotaxis receptors are allosterically modified to modulate receptor sensitivity (Clausznitzer et al., 2010). MCPs form mixed trimeric complexes of receptor homodimers (Studdert and Parkinson, 2004) that bind extracellular molecules and transduce a signal across a transmembrane segment to an autophosphorylating cytoplasmic domain (Boyd and Simon, 1982). This cytoplasmic domain is constitutively methylated by CheR (Springer and Koshland, 1977). Autophosphorylation induces a signal cascade that is transduced to the motility apparatus, but also results in the demethylation of the MCP by the phosphorylated CheB protein (Yonekawa et al., 1983), generating a feedback loop that regulates

the degree of MCP sensitivity. This feedback loop is further amplified by functional interactions between receptor clusters that modify the sensitivity of nearby MCPs (Li and Hazelbauer, 2005). Methylated MCPs have a higher affinity for the substrate than unmethylated receptors (Spiro et al., 1997), and so the feedback loop provides a temporal "memory" that can compare current conditions with those recently encountered. This "memory" modulation provides adaptation to prolonged stimuli by changing the substrate sensitivity of receptors.

The number of chemoreceptors encoded in a genome seems to reflect the niche of the organism; organisms in confined environments with stable environmental conditions have fewer chemoreceptors, whereas those isolated from aquatic and soil environments, subject to environmental fluctuations, typically have a large number of chemoreceptors (Alexandre et al., 2004). Various environmental conditions induce motility (Armitage, 1992), and many bacterial species are equipped with alternative mechanisms of motility for different environmental conditions (Kohler et al., 2000).

1.8. Research approach to study solid substrate motility in *R. capsulatus*

In the γ-proteobacteria and δ-proteobacteria, flagellum-independent bacterial motility has been observed in aqueous cultures (Brahamsha, 1999) and on solid substrates (Henrichsen, 1972), and mechanisms have been defined (Henrichsen, 1972; Spormann, 1999; Harshey, 2003; Yu and Kaiser, 2007). Flagellum-independent motility has not been characterized in the α-proteobacteria, although several potential homologues with weak similarity (% identity ranged from 7 to 46%) of genes identified to be involved in flagellum-independent motility of other bacteria (Table 3-6 and Table 3-8) were found in the genome sequence of *R. capsulatus*. This led me to hypothesize that perhaps *R. capsulatus* was capable of a similar mechanism of motility.

The overall objective of my research was to investigate flagellum-independent motility in *R. capsulatus*. I also investigated whether there is a light-responsive taxis feature of flagellum-

independent motility on solid substrates. I elucidated the contributions of flagellum-dependent and flagellum-independent mechanisms to motility (Shelswell et al., 2005), and cell movement toward illumination (Chapter **3.3**). I also investigated a possible role of pilus homologues (Chapter **3.4**), and gliding motility (Chapter **3.5**) in this taxis. In addition to mechanisms propelling cell motility, I examined the role of incident light on the initiation of this adaptive response (Chapter **3.6**). The results are discussed in terms of factors influencing the distance and frequency of movement, light-dependent directed motility, and the mechanism driving cell movement.

2. MATERIALS AND METHODS

2.1. Bacterial strains, plasmids, growth conditions, and enumeration of cells

The *E. coli* strains used (Table 2-1) were DH5α (Gibco-BRL, CA, USA), DH10B (Gibco-BRL, CA, USA), JM109[λ-pir] (Penfold and Pemberton, 1992) and the *dam*$^-$ mutant RB404 (Brent and Ptashne, 1980). Strains S17-1 (Simon et al., 1983), S17-1[λ-pir] (Herrero et al., 1990), HB101 (pRK2013) (Boyer and Roulland-Dussoix, 1969), and Tec5 (Taylor et al., 1983) were used to conjugate plasmids into *R. capsulatus*. *E. coli* strains were grown at 37 °C in LB medium (Sambrook et al., 1989) supplemented with the appropriate antibiotics at the following concentrations: ampicillin, 100 μg/mL; gentamicin sulphate, 10 μg/mL; kanamycin sulphate, 50 μg/mL; spectinomycin-2HCL, 25 μg/mL; tetracycline-HCL, 10 μg/mL.

The *R. capsulatus* strains are described in Table 2-1. Strains B10 (Marrs, 1974) and SB1003 (Solioz and Marrs, 1977) were used as the parental strains for mutant construction, and strain B10 was used as the source of DNA for genetic manipulations. DNA sequence information was obtained from the B10 derived rifampicin-resistant strain SB1003. The culture media were centered around a defined minimal medium (RCV) that contains malate as the carbon source and ammonium as the nitrogen source (Beatty and Gest, 1981), and a complex medium (YPS) containing yeast extract and peptone (Wall et al., 1975). *R. capsulatus* strains were grown at 30 °C; aerobically using RCV medium, anaerobically in the dark using a 50:50 YPS:RCV medium supplemented with 20 mM fructose and 30 mM dimethyl sulfoxide (DMSO), or photosynthetically using YPS medium. Media were supplemented with the appropriate antibiotics at the following concentrations: gentamicin sulphate, 1 μg/mL; kanamycin sulphate, 10 μg/mL; spectinomycin-2HCL, 10 μg/mL; tetracycline-HCL, 1 μg/mL.

The *R. centenum* strains used are described in Table 2-1. Strains 51521 (Favinger et al., 1989) and M3-8 (C. E. Bauer, personal communication) were used as Western blot controls for flagellar

expression. *R. centenum* strains were grown at 37 °C aerobically in CENS medium (Ragatz et al., 1995), supplemented when appropriate with spectinomycin-2HCl, at 50 μg/mL.

The *R. sphaeroides* strain 2.4.1 (Van Niel, 1944) was used as a western blot control for flagellar expression, and grown at 30 °C aerobically in RCV medium.

Culture turbidity was monitored by measuring light scattering with a Klett-Summerson photometer (filter #66; red). One hundred Klett units are equivalent to approximately 3 x 10^8 cells per mL. Plasmids are described in Table 2-2.

Table 2-1: Bacterial strains.

Strain	Relevant properties	Reference or source
E. coli		
DH10B	*F-mcrA* Δ *(mrr-hsdRMS-mcrB)*, *endA*1, *recA*1, Δ(*ara*, *leu*)7697, *araD*139, *galU*, *galK*, *nupG*, *rspL*, *ϕ*80d*lacZ*ΔM15 used for plasmid subcloning	(Lorow and Jessee, 1990)
DH5α	*F-, endA*1, *hsdR*17 (r_K^-, m_K^+), *supE*44, *thi*-1, *λ*-, *recA*1, *gyrA*96, *relA*1, *ϕ*80d*lacZ*ΔM15 used for plasmid subcloning	(Hanahan, 1985) (Hanahan, 1986)
HB101	*supE*44, *hsdS*20(r_B^-, m_B^-), *recA*13, *ara*-14, *proA*2, *lacY*1, *galK*2, *rpsL*20, *xyl*-5, *mtl*-1, *leuB*6, *thi*-1 used as mobilization strain with pRK2013 mobilization plasmid for conjugation to *R. capsulatus*	(Boyer and Roulland-Dussoix, 1969)
JM109[λ-pir]	*recA*1, *endA*1, *gyrA*96, *thi*, *hsdR*17, *supE*44, *relA*1, Δ(*lac-proAB*), [F', *traD*36, *proAB*$^+$, *lacI*^{q}, *lacZ*ΔM15], λ-pir used for suicide plasmid subcloning	(Penfold and Pemberton, 1992)

Strain	Relevant properties	Reference or source
E. coli		
RB404	*dam*-3, *dcm*-6, *metBI*, *galK*2, *galT*22, *his*-4, *thi-i*, *tonA*31, *tsx*-78, *mtl-l*, *supE*44	(Brent and Ptashne, 1980)
	used to obtain unmethylated plasmid DNA	
S17-1	Tp^r, Sm^r, *recA*, *thi, pro*, hsdR (r_K^-, m_K^+), *RP4-2-Tc::Mu-Km::Tn7*	(Simon et al., 1983)
	used for Tn5 transposon plasmid conjugation to *R. capsulatus*	
S17-1[λ-pir]	Tp^r, Sm^r, *recA*, *thi, pro*, hsdR (r_K^-, m_K^+), *RP4-2-Tc::Mu-Km::Tn7*, λ-pir	(Herrero et al., 1990)
	used for suicide plasmid conjugation to *R. capsulatus*	
Tec5	C600 (pDPT51) mobilization plasmid	(Taylor et al., 1983)
	used for recombination-based conjugation to *R. capsulatus*	
R. capsulatus		
37b4	environmental isolate no cell capsule	(Biebl and Drews, 1969; Weckesser et al., 1972; Trieschmann et al., 1996)
B6	environmental isolate from St. Louis pond sample	(Marrs, 1974)
	no GTA production	
B10	wild type	(Marrs, 1974)
	environmental isolate from St. Louis pond sample	
BCKF	*ctrA*::KIXX	(Lang and Beatty, 2002)
	no GTA production, reduced flagellar transcription, derived from B10	

Strain	Relevant properties	Reference or source
R. capsulatus		
bKSDF	Δ*flaA* no flagellum, derived from B10	this thesis
bKSDFcpaA	Δ*flaA*, *cpaA*::KIXX no flagellum, no pilus prepilin peptidase, derived from KSDF	this thesis
bKSDFcpaC	Δ*flaA*, *cpaC*::KIXX no flagellum, no pilus secretin, derived from KSDF	this thesis
bKSDFcpaF	Δ*flaA*, *cpaF*::KIXX no flagellum, no pilus ATPase, derived from KSDF	this thesis
bKSDFgtaI	Δ*gtaI*, Δ*flaA* no C16-HSL synthesis, no quorum sensing, derived from BLKI	this thesis
bKSDFhcpA	Δ*flaA*, *hcpA*::KIXX, no *hcpA*-encoded glycoprotein, derived from bKSDF	this thesis
bKSDFpyp	Δ*flaA*, Δ*pyp*::KIXX, no *pyp*-encoded PYP, derived from bKSDF	this thesis
bKSDFrpoN	Δ*flaA, rpoN*::KIXX no nitrogen fixation, no flagellum, derived from bKSDF	this thesis
BLKI	Δ*gtaI* no C16 acyl-HSL synthesis, no quorum sensing, derived from B10	M. Leung Ph.D. thesis (Schaefer et al., 2002)

Strain	Relevant properties	Reference or source
R. capsulatus		
BY1653	*bchA165, crtB4,* Rif ^{r}	(Marrs, 1981)
	P670 accumulated, no carotenoids, no photosynthesis, pale colour, derived from Y165 mutant of SB1003	(Yen and Marrs, 1976)
DE442	*crtD*, unknown mutations	(Yen et al., 1979; Gari et al., 1992)
	GTA overproducer, accumulates neurosporene carotenoid, green colour	
DW5	*puhA*	(Wong et al., 1996)
	no LH1, no LH2, no RC, no photosynthesis, derived from SB1003	
KSDF37b4	Δ*flaA*	this thesis
	no cell capsule, no flagellum, derived from 37b4	
LJ1	*rpoN*::KIXX	(Wall et al., 1984)
	no nitrogen fixation, derived from B10	(Kranz and Haselkorn, 1985)
LS01	*senC*::KIXX	(Swem et al., 2005)
	reduced cytochrome c activity, derived from SB1003	
REG1	*regA*::KIXX	(Sganga and Bauer, 1992)
	reduced anaerobic photosynthetic expression, derived from SB1003	
SB1003	Rif ^{r}	(Solioz and Marrs, 1977)
	laboratory wild type, derived from B10 via B100	
sbKSDF	Δ*flaA*	this thesis
	no flagellum, derived from SB1003	

Strain	Relevant properties	Reference or source
R. capsulatus		
sbKSDFby	*bchA165, crtB4, flaA*, Rif ^{r}	this thesis
	P670 accumulated, no carotenoids, no photosynthesis, pale colour, no flagellum, derived from BY1653	
sbKSDFdw5	*puhA*, *flaA*	this thesis
	no LH1, no LH2, no RC, no photosynthesis, no flagellum, derived from DW5	
sbKSDFregA	*regA*::KIXX, ∆*flaA*	this thesis
	reduced anaerobic photosynthetic expression, no flagellum, derived from REG1	
sbKSDFsenC	*senC*::KIXX, ∆*flaA*	this thesis
	reduced cytochrome c activity, no flagellum, derived from LS01	
SP36	environmental isolate from Bloomington, IN settling pond	(Weaver et al., 1975)
	no GTA production, no GTA uptake	
Y262	unknown mutations	(Yen et al., 1979)
	GTA overproducer	
YW1	environmental isolate from Yellowwood State Forest, IN	(Weaver et al., 1975)
	no GTA production, no GTA uptake	
YW2	environmental isolate from Yellowwood State Forest, IN	(Weaver et al., 1975)
	no GTA production	

Strain	Relevant properties	Reference or source
R. centenum		
51521	wild type	(Favinger et al., 1989)
M3-8	*fliE*, Sp^r	C. E. Bauer, unpublished
	lateral hook mutant, derived from 51521	
R. sphaeroides		
2.4.1	wild type	(Van Niel, 1944)

Table 2-2: Plasmids.

Plasmid	Relevant properties	Reference
pCR2.1 -TOPO	subcloning vector	Invitrogen
	pUC origin, f1 origin, LacZα blue/white screening, Amp^r, Km^r	
pDPT51	recombination/conjugation vector	(Warren et al., 1979; Meyer and Shapiro, 1980; Taylor et al., 1983)
	broad-host-range IncP-1 plasmid R751/ ColE1 RSF2011 fusion, ColE1 *mobC* mobilization region, Amp^r	
pKS050	pUC19:: KJS10-KJS11	this thesis
	markerless Δ*cpaF* ORF RCC00505 construct, *lacZ*, Amp^r	
pKS053	pUC19::KJS01	this thesis
	flaA ORF RCC03525, *lacZ*, Amp^r	
pKS055	pUC19::KJS09[KIXX]	this thesis
	KIXX disrupted *cpaF* ORF RCC00505, *lacZ*, Amp^r, Km^r	

Plasmid	Relevant properties	Reference
pKS056	pUC19::KJS09	this thesis
	cpaF ORF RCC00505, *lacZ*, Amp^r	
pKS057	pUC19:KJS01[KIXX]	this thesis
	KIXX disrupted *flaA* ORF RCC03525, *lacZ*, Amp^r, Km^r	
pKS064	pUC19::KJS15	this thesis
	cpaC ORF RCC00502, *lacZ*, Amp^r	
pKS065	pUC19::KJS15[KIXX]	this thesis
	KIXX disrupted *cpaC* ORF RCC00502, *lacZ*, Amp^r, Km^r	
pKS067	pUC19::KJS02-KJS03	this thesis
	markerless Δ*pyp* ORF RCC01066 construct, *lacZ*, Amp^r	
pKS068	pUC19::KJS02-KJS03[KIXX]	this thesis
	KIXX disrupted *pyp* ORF RCC01066, *lacZ*, Amp^r, Km^r	
pKS071	pCR2.1TOPO::KJS10	this thesis
	upstream *cpaF* ORF RCC00505 region, *lacZ*, Amp^r, Km^r	
pKS072	pUC19::KJS03	this thesis
	upstream *pyp* ORF RCC01066 region, *lacZ*, Amp^r	
pKS073	pUC19::KJS02	this thesis
	downstream *pyp* ORF RCC01066 region, *lacZ*, Amp^r	
pKS074	pUC19::KJS05	this thesis
	upstream *flaA* ORF RCC03525 region, *lacZ*, Amp^r	

Plasmid	Relevant properties	Reference
pKS075	pUC19::KJS06	this thesis
	downstream *flaA* ORF RCC03525 region, *lacZ*, Amp^r	
pKS080	pUC19::KJS11	this thesis
	downstream *cpaF* ORF RCC00505 region, *lacZ*, Amp^r	
pKS087	pUC19::KJS05-KJS06	this thesis
	markerless Δ*flaA* ORF RCC03525 construct, *lacZ*, Amp^r	
pKS089	pZJD29A::KJS12	this thesis
	markerless suicide vector Δ*flaA* ORF RCC03525 construct, *lacZ*, Gm^r	
pKS091	pUC19:: KJS10-KJS11[KIXX]	this thesis
	KIXX disrupted Δ*cpaF* ORF RCC00505 construct, *lacZ*, Amp^r, Km^r	
pKS094	pZJD29A::KJS23	this thesis
	markerless suicide vector Δ*pyp* ORF RCC01066 construct, *lacZ*, Gm^r	
pKS100	pUC19::KJS24	this thesis
	cpaA ORF RCC00510, *lacZ*, Amp^r	
pKS101	pUC19::KJS24[KIXX]	this thesis
	KIXX disrupted *cpaA* ORF RCC00510, *lacZ*, Amp^r, Km^r	
pKS108	pUC19::KJS32	this thesis
	hcpA ORF RCC00178, *lacZ*, Amp^r	
pKS109	pUC19::KJS32[KIXX]	this thesis
	KIXX disrupted *hcpA* ORF RCC00178, *lacZ*, Amp^r, Km^r	

Plasmid	Relevant properties	Reference
pRK2013	mobilization vector broad-host-range IncP-1 plasmid RK2 derivative, ColE1 origin, Km^r	(Figurski and Helinski, 1979)
pSUP2021	Tn5 transposon donor suicide vector ColEl origin, P-type mobilization region, Tn5, Amp^r, Cm^r, Tc^r	(Simon et al., 1983)
pUC4-KIXX	source of KIXX cartridge pBR322 origin, Amp^r, Km^r	(Barany, 1985)
pUC19	subcloning vector pMB1 origin, LacZα blue/white screening, Amp^r	(Yanisch-Perron et al., 1985)
pZJD29A	suicide vector R6K origin, RP4 mobilization region, LacZα blue/white screening, *puc* promoter driving *sacB* expression, Gm^r	J. Jiang and C. E. Bauer (unpublished plasmid construction)

Amp^r, Cm^r, Gm^r, Km^r, and Sp^r signify resistance to ampicillin, chloramphenicol, gentamicin, kanamycin, and spectinomycin, respectively.

2.2. Bacterial motility assays

Flagellum-dependent motility was assayed by stab inoculation of 8 mL YPS soft agar (0.4% w/v) in 13 x 125 mm test tubes. Cells from an exponential phase aerobic culture were collected by centrifugation at 10410 X g for 1 minute at room temperature. Supernatants were removed by aspiration and the resulting cell pellets were sampled using an inoculation needle, and the agar tube was stabbed and incubated under photosynthetic conditions at 30 °C for 72 hours, unless otherwise stated (Lang and Beatty, 2002). For photosynthetic growth, cultures were illuminated from one side by halogen lamps (Capsylite, Sylvania) at an intensity of ~190 $\mu E \cdot m^{-2} \cdot s^{-1}$.

Unless otherwise stated, flagellum-independent motility was assayed by stab inoculation of 20 mL YPS agar (1.5% w/v) in a Petri plate. Other media were not investigated because the focus of this thesis was on the surface properties of the movement substrate, mechanism of motility, and dynamics of the pattern of cell movement. Cells from an exponential phase aerobic culture were collected by centrifugation and the resulting cell pellets were sampled using a sterile square toothpick, to inoculate the plate-agar interstice and incubated under aerobic conditions at 30 °C for 48 hours, unless otherwise stated (Shelswell et al., 2005). Because pigmented cells were often visible in the plate-medium interstice after inoculation, the toothpick stab must introduce at least 10^6 cells to the interstice (see section **3.6.2**). Control samples in a separate chamber were arranged in the same orientation as experimental samples (Figure 2-1) and incubated under aerobic conditions at 30 °C for 48 hours in the absence of the experimental magnetic, temperature, or light stimuli, unless otherwise stated.

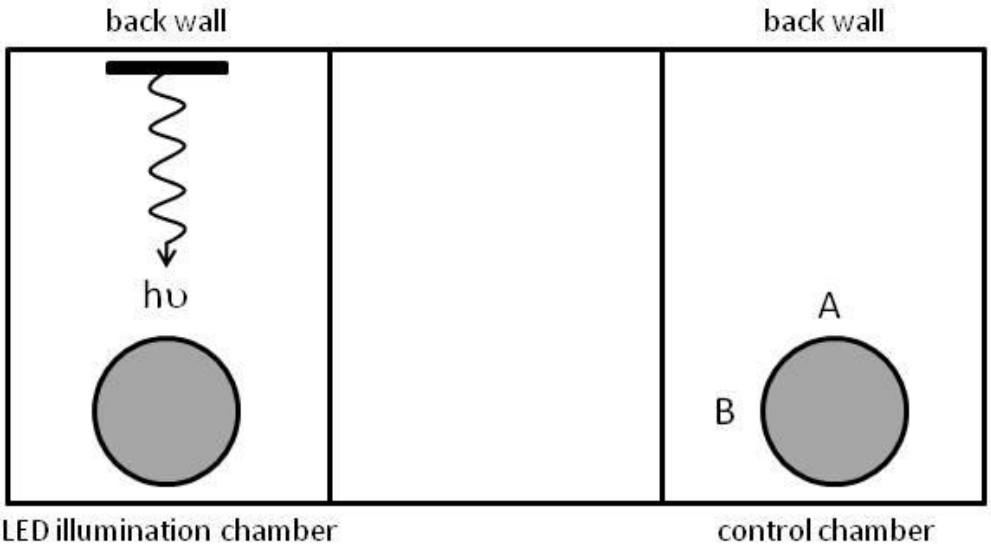

Figure 2-1: Orientation of the 0° reference points marked on plates, relative to the back wall of the chamber, used for control tests. The "A" orientation reference mark was used for plate reuse, magnet, aquarium chamber, and LED chamber controls. The "B" orientation reference mark was used for temperature gradient and filter chamber controls. A top down view is presented, and the gray circles indicate a stack of plates.

2.2.1. Design of chambers used for motility assays

The “aquarium” chamber consisted of a glass aquarium immersed in temperature-controlled ~32 °C water within a second aquarium. The inner aquarium was masked on 3 sides with black felt, leaving an unmasked side facing a bank of halogen lamps (see above) 14 cm away from plates. Two stacks of 8 plates were illuminated in an experiment. The “LED” control chamber (see below) was used for controls without illumination (Figure 2-2a,b).

The “LED” chamber consisted of two chambers on a level shelf enclosed in cardboard and tinfoil to exclude light, in an air temperature-controlled ~30 °C incubator room. The control chamber was located 60 cm to the right of the LED chamber, with the power source for the lamps placed in the middle. Plates in the control chamber were further enclosed in a stainless steel canister, and the entire assembly was draped in black felt. The LED samples were illuminated by an array of bulbs located opposite the access point at the front of the chamber 14 cm away from plates. The dark control reference point was also similarly positioned opposite the access point at the front of the chamber. A stack of 12 plates were illuminated in an experiment in the LED chamber, whereas a stack of 6 to 12 plates were used in an experiment in the dark control chamber (Figure 2-2c,d).

The “filter” chamber consisted of a tinfoil-enclosed cardboard chamber with an illumination port on one side, on a level shelf in an air temperature-controlled ~30 °C incubator room. The three interior sides of the chamber surrounding the plates were covered in black felt, and the edges of the chamber were lined with black felt. A single lamp was used to illuminate samples 60 cm away from plates to reduce heat. Filters were fixed in the port to control the wavelengths of light illuminating samples. A stack of 12 plates were illuminated in an experiment, and controls without illumination were incubated in the “LED” control chamber on a shelf directly below the experimental samples. The

orientation of the reference point of control samples was the same as the direction of the light source for the filter chamber (Figure 2-2e,f).

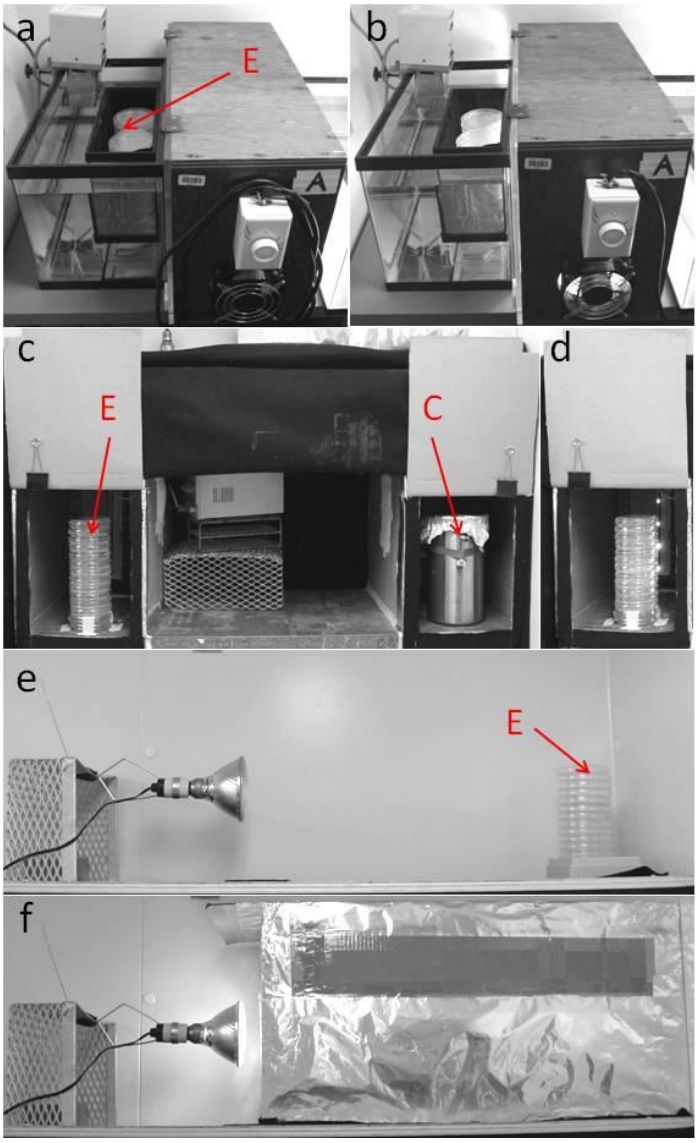

Figure 2-2: Incubation chambers used for illumination of stab-plate photoresponsive motility assays. (a) aquarium chamber; (b) aquarium chamber with illumination; (c) LED chamber, with shielded access doors open, compare with Figure 2-1; (d) LED chamber with illumination, with shielded access door open; (e) filter chamber; (f) filter chamber with illumination and shield. "E" designates experimental illumination chamber, "C" designates control dark chamber. The LED control chamber was also used for dark controls of aquarium chamber and filter chamber tests.

2.2.2. Treatment of polystyrene plates used for motility assays

Sodium hydroxide-etched plastic Petri plates were obtained by addition of 5 mL of 1 M NaOH and incubation for 10 minutes at room temperature, rinsed with 10 mL of dH_2O, incubated three times for 10 minutes with 10 mL of dH_2O at room temperature, and sterilized by 254 nm UV irradiation for 90 seconds (GS Gene Linker [BIORAD Laboratories, Richmond, CA, USA]). Sandpaper-abraded Petri plates were randomly scraped with P600C grit sandpaper (Task, Delta, BC, Canada) for 3 minutes, rinsed with 10 mL of dH_2O, incubated three times for 10 minutes with 10 mL of dH_2O at room temperature, and sterilized by UV irradiation as described above. Plates were washed with dH_2O at room temperature on a rocking platform tilting at a rate of 8 cycles per minute. UV-sterilization was verified by testing one plate from each batch with YPS agar medium.

2.3. ^{32}P-orthophosphate cell labelling

Radioactive labelling of cells was achieved by incubating cells with ^{32}P-orthophosphate (Amersham/GE Healthcare, NJ, USA). A starter culture of *R. capsulatus* cells was aerobically cultured in YPS medium (in darkness) to 200 Klett units and used to inoculate a photosynthetic YPS culture grown anaerobically to 300 Klett units. A 1 mL aliquot of photosynthetic culture was then transferred to 30 mL of 1% w/v MOPS-buffered YPS medium containing 2.5 mCi of ^{32}P-orthophosphate and incubated overnight photosynthetically. The ^{32}P-orthophosphate-labelled culture was separated into two 15 mL volumes to create viable and non-viable samples. The viable culture sample was diluted with 7 mL of sterile dH_2O while 7 mL of 37% formaldehyde was added to the non-viable fraction to create a 12% formaldehyde solution, and samples were incubated on ice for 1.5 hours. Cells were collected by centrifugation at 7740 X g for 10 minutes at 4 °C and washed with 1 mL of YPS medium four times, to remove unincorporated ^{32}P-orthophosphate. Viable and non-viable cells were then inoculated into the glass-agar interstice of borosilicate Petri plates as described above (see section **2.2**), and incubated under aerobic illuminated conditions for 48 hours.

2.4. Phase contrast negative stain capsule microscopy

Aerobic cultures were grown in RCV medium to an optical density of 250 Klett Units. A 10 μl drop of culture mixed with a 10 μl drop of negative stain solution (10% Nigrosin, 0.5% formalin) was spread over a slide, and dried at room temperature for 5 minutes. Slides were then flooded with Crystal violet stain (2.5% crystal violet, 25% EtOH, 10% ammonium oxalate), incubated at room temperature for 1 minute, thoroughly rinsed with dH_20 and dried at room temperature for 5 minutes. Capsule stain microscopy samples were visualized by phase contrast microscopy as described below.

2.5. Phase contrast and Nomarski microscopy

Agar plates were stab-inoculated with *R. capsulatus* wild type strain B10 and *flaA* mutant strain bKSDF cells taken from aqueous cultures grown aerobically for 48 hours at 30 °C. Cells were inoculated into the glass-agar interstice of glass bottom polystyrene Petri plates (Electron Microscopy Sciences, Hatfield, PA, USA), and incubated at 30 °C with directional illumination. Samples were examined after incubation times of 30 minutes, 4 hours, and 24 hours. Microscopy samples were examined under oil immersion with either phase contrast or differential interference contrast/Nomarski interference contrast (DIC/NIC) microscopes. Phase contrast samples were examined using a Zeiss Axioskop 50 microscope (100 X magnification) at room temperature. Images were recorded over a period of 240 minutes using a Sony ASC-S75 Cybershot camera to yield high resolution JPEG images. DIC/NIC samples were examined using a Zeiss 510 Meta scan head mounted on an Axiovert 200M inverted microscope (100 X magnification) at room temperature. Images were recorded over a period of 180 minutes using a Zeiss AxioCam HRm CCD camera controlled by Zeiss LSM Software. Images were edited and converted to JPEG images and AVI movies using Axio Vision LE version 4.5 (Carl Zeiss Canada Ltd., ON, CND).

2.6. Cy3 fluorescence microscopy

Microscope slides and coverslips were incubated in 10 mL of 95% ethanol for 20 minutes to remove residual oils from the manufacturing process, rinsed with 10 mL of dH_2O, incubated three times for 10 minutes with 10 mL of dH_2O at room temperature, air dried, and sterilized by 254 nm UV irradiation for 90 seconds. Microscope slide incubations were performed at room temperature on a rocking platform tilting at a rate of 8 cycles per minute. *R. capsulatus* cells were harvested from early stationary phase aerobic aqueous culture by centrifugation, as for agar-stab experiments, and washed three times in 1 mL labelling buffer (50 mM KH_2PO_4, pH 8.0, 5 mM $MgCl_2$, 25 mM EDTA). Washed cells were resuspended in 0.5 mL labelling buffer supplemented with 11 mL of Cy3 dye (GE Healthcare, NJ, USA) dissolved in DMSO (0.09 mg/mL), and incubated for 1 hour at room temperature in the dark. Cy3-stained cells were collected by centrifugation, washed three times in 1 mL labelling buffer, and resuspended in 0.5 mL of RCV medium. A 1-μL droplet of labelled *R. capsulatus* wild type strain B10 and *flaA* mutant strain bKSDF cells was spotted on a microscope slide, and a coverslip was placed over the droplet. Fluorescence samples were examined through a fluorescein FITC-filter set using a Leica DMI 600B inverted microscope (60 X magnification) at room temperature. Images were recorded over a period of 30 minutes using a Qimaging Retiga 200R fast 1394 time-lapse video recorder. Images were edited using Openlab version 4.0.2.

2.7. Transmission electron microscopy

Suspension culture cells were collected by centrifugation and agar stab-plate interstitial culture cells were collected by scraping cells from motility plates. Cells were gently resuspended in 1 mL YPS medium and 10 μL were spotted on a 300 mesh 0.4% formvar-coated copper grid for 10 minutes at room temperature. Adhered samples were washed with a 50 μL drop of distilled dH_2O and blotted dry with hardened # 50 Whatman paper. The wash was repeated 3 times, samples were air dried for 2 minutes at room temperature, and stained with 10 μL 2% uranyl acetate for 1 minute at room

temperature. Excess stain was removed by washing disks with four subsequent 50 μL drops of distilled dH_2O each of which was blotted with hardened # 50 Whatman paper, and samples were then air dried for 2 minutes at room temperature.

2.8. SDS-polyacrylamide gel electrophoresis (SDS-PAGE)

Laemmli buffer (Laemmli, 1970) electrophoresis was used to separate proteins on 10% resolving gels with 5% stacking gels (acrylamide/bisacrylamide 29:1). Protein samples were boiled in SDS-PAGE loading buffer (50 mM pH 6.8 Tris-Cl, 2% SDS, 10% glycerol, 0.1% bromophenol blue, 1% β-mercaptoethanol) for 5 minutes before loading the gel. Gels were run in the Mini-PROTEAN II (BIORAD Laboratories, CA, USA) apparatus at 30 V through the stacking gel and at 100 V through the resolving gel.

2.9. Cell surface protein enrichment

Samples for cell surface protein enrichments were isolated from the interstice of the agar medium in borosilicate glass Petri plates. Proteins were separated from the surface of cells by mechanical shearing or heat-shock shedding. For mechanical shearing 100 μL of cells scraped from the interstice were suspended in 100 μL of PBS and vigorously vortexed in an Eppendorf tube for 15 minutes at room temperature. Cells and large debris were removed by centrifugation and the supernatant was concentrated by two methods: (i) concentration ~5-fold with an Amicon 10-kDa molecular weight cut-off filter (Millipore, Billerica, MA, USA); (ii) precipitation with 20% trichloroacetic acid (TCA) for 1 hour at 0 °C, followed by centrifugation at 16000 X g for 45 minutes at 4 °C, suspension of pellet in 10 mL acetone chilled on ice for 20 minutes, and centrifugation again to yield a protein pellet.

For heat-shock shedding of protein, cells were suspended in 500 μL of PBS and incubated for 20 minutes at 65 °C. Cells and cell debris were removed by centrifugation and supernatants were incubated for 24 hours at 4 °C to increase flocculation of proteins. Aggregates of protein were pelleted

by centrifugation at 57000 X g for 20 minutes at 4 °C. All concentrated samples were stored in 10 mM Tris-HCl (pH 8.0) at -20 °C.

2.10. Protein sequencing

Proteins were separated by SDS-PAGE and stained with Coomassie Brilliant Blue as previously described (see **2.8** above). Plates, spacers, combs, gel assembly apparatus, SDS-PAGE reservoir, staining trays, and razor blades were washed in Liquinox detergent (Alconox, White Plains, NY, USA) diluted to a 1% solution according to the manufacturer's specifications, rinsed with 10 mL of dH_2O five times, rinsed with 5 mL 95% ethanol twice, and air dried at room temperature in an attempt to remove any contaminants from previous use. Air-dried equipment was further washed in 10 mL methanol three times followed by three rinses with 10 mL distilled dH_2O to reduce keratin contamination. Protein bands were excised as gel fragments for peptide sequence identification. Peptide sequences were determined by tandem mass spectrometry performed by the UBC MSL/LMB Proteomics Core Facility.

2.11. DNA manipulations

Standard methods for DNA isolation, purification, restriction enzyme digestion, ligation, and other modification techniques were used (Sambrook et al., 1989). DNA sequencing was performed by the UBC NAPS facility using the BigDye v3.1 Terminator (Applied Biosystems, Foster City, CA, USA) system on the PRISM 377 automated capillary sequencer (Applied Biosystems, Foster City, CA, USA) apparatus. Sequencing was done using vector-based M13 primers (Table 2-3) (Messing, 1983).

2.12. Alignments and database homology searches

Database searches were performed against the *R. capsulatus* genome sequence (http://www.ncbi.nlm.nih.gov/sites/entrez?Db=genome&Cmd=Search&Term=txid272942[orgn]) of ORFs using the BLASTp program (Altschul et al., 1997). Local alignments were done using full length sequences. The resulting BLASTp sequence alignments were used to identify putative protein domains.

Alignment of full length sequences was done using ClustalW (Thompson et al., 1994) to evaluate functions and determine % of amino acid sequence identities. Pairwise alignments were performed using the EMBOSS ClustalW global alignment program using the Blosum62 matrix, a gap opening penalty of 10, and a gap extension penalty of 0.5 for % identities.

2.13. Construction of mutants

Gene disruptions were made by interposon mutagenesis using the *neo* gene on a *Sma I* fragment (KIXX cartridge) from the plasmid pUC4-KIXX (Barany, 1985). The KIXX cartridge was ligated into the cloned gene deletion constructs to be disrupted, and these pUC19 plasmid-borne disruptions were recombined *in vivo* with pDPT51 (Taylor et al., 1983). Mobilization of plasmids containing a ColEI origin of replication from *E. coli* into the *R. capsulatus* GTA overproducer strain Y262 or DE442 (Yen et al., 1979) was done by conjugation from *E. coli* mobilization strain Tec5 (Taylor et al., 1983). The mutations were then integrated into the *R. capsulatus* chromosome by GTA transduction as previously described (Solioz et al., 1975; Yen et al., 1979). Markerless gene disruptions were made by cloning the deletion construct from pUC19 into the *λpir*-dependent suicide plasmid pZJD29A. Plasmid pZJD29A derivatives were mobilized by conjugation from the IncP mobilizing *E. coli* strain S17-1[*λpir*] to recipient *R. capsulatus* strains, and chromosomal integration was determined by Gm^r. Allele replacement was identified by sucrose counter selection and change in fragment size after PCR amplification of the disrupted gene. Primers used for sequencing or PCR amplification of genomic DNA for plasmid-based cloning (see Table 2-2) are listed in Table 2-3.

Table 2-3: Primers for PCR amplification of *R. capsulatus* DNA.

Primers	Relevant properties	Oligonucleotide sequence
KJS01F	ORF RCC03525 (*flaA*) forward primer	5'- GCC AAA GAC GAA GGA CCT G -3'
KJS01R	ORF RCC03525 (*flaA*) reverse primer	5'- AAT ACC TTC CAG TGG CGA GA -3'
KJS02F	ΔORF RCC01066 (*pyp*) downstream forward primer	5'- GGG GTA CCT GCA GGG TCG GTT CGA C -3'
KJS02R	ΔORF RCC01066 (*pyp*) downstream reverse primer	5'- GCT CTA GAT CGT GAA GCG GGC CTG AG -3'
KJS03F	ΔORF RCC01066 (*pyp*) upstream forward primer	5'- GCT CTA GAC GTC CCG AAC GGA ATG ATT TC -3'
KJS03R	ΔORF RCC01066 (*pyp*) upstream reverse primer	5'- GCC GAA GCT TCG GAG CTG CGA CAC -3'
KJS05F	ΔORF RCC03525 (*flaA*) upstream forward primer	5'- CGA GAT CTG GTC CGA GAG AG -3'
KJS05R	ΔORF RCC03525 (*flaA*) upstream reverse primer	5'- GTG TTG ATG GTC GAC ATG TCA -3'
KJS06F	ΔORF RCC03525 (*flaA*) downstream forward primer	5'- CGA TCC TGT CGA CCT TCA AGT -3'
KJS06R	ΔORF RCC03525 (*flaA*) downstream reverse primer	5'- ACG ATC GCA TGC CAG ATC CT -3'
KJS09F	ORF RCC00505 (*cpaF*) forward primer	5'- CGA TTT CGT GCC CTA TCC GCT -3'
KJS09R	ORF RCC00505 (*cpaF*) reverse primer	5'- ATG ATG CCG AAT TCG GTG CCC -3'
KJS10F	ΔORF RCC00505 (*cpaF*) upstream forward primer	5'- CTC CCG GGA CGT CTC GAA TTT C -3'
KJS10R	ΔORF RCC00505 (*cpaF*) upstream reverse primer	5'- TAA CCC GGG AAC ATG ACG GTC TCC GGG C -3'
KJS11F	ΔORF RCC00505 (*cpaF*) downstream forward primer	5'- GAC CCG GGT CAG GCC TGA CGG AGA GCC AA -3'
KJS11R	ΔORF RCC00505 (*cpaF*) downstream reverse primer	5'- CCG GCA TTG TAG AAC AGC ACG -3'
KJS12F	ΔORF RCC03525 (*flaA*) suicide plasmid forward primer	5'- TGT AAA ACG ACG GCC AGT GAA TTC -3'
KJS12R	ΔORF RCC03525 (*flaA*) suicide plasmid reverse primer	5'- CCA AGC TTG AGC TCC AGA TCC TC -3'
KJS15F	ORF RCC00502 (*cpaC*) forward primer	5'- CGA CAG ATC CCG GGG TAG CAG C -3'

Primers	Relevant properties	Oligonucleotide sequence
KJS15R	ORF RCC00502 (*cpaC*) reverse primer	5'- GCG CAT GCC CGG GCC CCC AAG -3'
KJS23F	∆ORF RCC01066 (*pyp*) suicide plasmid forward primer	5'- GCG GAA GAG CTC CCA ATA CGC -3'
KJS23R	∆ORF RCC01066 (*pyp*) suicide plasmid reverse primer	5'- GTG AAT TCG AGC TCG GTA CCT G -3'
KJS24F	ORF RCC00510 (*hcpA*) forward primer	5'- GAC GCA CGA GCT CTT TGA GCG C -3'
KJS24R	ORF RCC00510 (*hcpA*) reverse primer	5'- GCG GCA AGC TTT CCG GGC TG -3'
KJS32F	ORF RCC00178 (*hcpA*) forward primer	5'- GGA CAG GAA TTC GTT GCG CTG -3'
KJS32R	ORF RCC00178 (*hcpA*) reverse primer	5'- GTC GCA AGC TTT GCC CTC AG -3'
-21m13	m13 sequencing primer forward primer	5'- CGC CAG GGT TTT CCC AGT CAC GAC -3'
m13R	m13 sequencing primer reverse primer	5'- AGC GGA TAA CAA TTT CAC ACA GG -3'

Strain bKSDF was constructed from strain B10 by replacing the *flaA* gene with a markerless deletion construct. The genomic sequences directly upstream and downstream of the *flaA* ORF, including the start and stop codons, were amplified by PCR and ligated together to generate the pKS089 suicide plasmid, an in-frame 394 amino acid deletion of ORF RCC03525, resulting in a 6 amino acid ORF construct recombined into the B10 genome.

Strain sbKSDF was constructed from strain SB1003, strain KSDF37b4 was constructed from strain 37b4, strain sbKSDFdw5 was constructed from strain DW5, strain sbKSDFby was constructed from strain BY1653, strain bKSDFgtaI was constructed from strain BLKI, strain sbKSDFsenC was constructed from strain LS01, and strain sbKSDFregA was constructed from strain REG1, all as described above for bKSDF.

Strain bKSDFcpaC was constructed from strain bKSDF by replacing the *cpaC* gene with a KIXX-disrupted version. The ORF RCC00502 *cpaC* coding region from nucleotides 730 to 733 (inclusive) was

duplicated by Klenow enzyme fill-in of *Sty I*-digested plasmid pKS064, and the KIXX cartridge was inserted into this site to generate pKS065.

Strain bKSDFcpaF was constructed from strain bKSDF by replacing the *cpaF* gene with a KIXX-disrupted version. The genomic sequences directly upstream and downstream of the *cpaF* ORF, including the start and stop codons, were amplified by PCR and ligated together to generate pKS050, an in-frame 480 amino acid deletion of ORF RCC00505. The KIXX cartridge was inserted into a unique *Sma I* site of the resulting 7 amino acid ORF to generate pKS091.

Strain bKSDFcpaA was constructed from strain bKSDF by replacing the *cpaA* gene with a KIXX-disrupted version. The *cpaA* coding region was amplified by PCR and cloned to create plasmid pKS100. The KIXX cartridge was inserted into the unique *Stu I* site of ORF RCC00510 to generate pKS101.

Strain bKSDFhcpA was constructed from strain bKSDF by replacing the *hcpA* gene with a KIXX-disrupted version. The ORF RCC00178 *hcpA* coding region from nucleotides 79 to 1384 (inclusive) was deleted by *Nru I* digestion and the KIXX cartridge inserted to generate plasmid pKS109.

Strain bKSDFpyp was constructed from strain bKSDF by replacing the *pyp* gene with a KIXX-disrupted version. The genomic sequences directly upstream and downstream of the *pyp* ORF, including the start and stop codons, were amplified by PCR and ligated together to generate pKS067, a frameshift deletion of ORF RCC01066. The KIXX cartridge was inserted into a unique Klenow-filled *Xba I* site of the resulting 13 amino acid ORF to generate pKS068.

Strain bKSDFrpoN was constructed from strain bKSDF by replacing the *rpoN* gene with a deleted, KIXX-disrupted version (Wall et al., 1984). The *rpoN::KIXX* lesion was transduced to the bKSDF genome using GTA particles harvested from the *rpoN* mutant strain LJ1.

2.14. Creation and screening of Tn5 library for flagellum-independent motility deficient mutants

A transposon Tn5 mutant library was constructed from the *flaA* mutant *R. capsulatus* strain bKSDF by use of the IncP mobilizing *E. coli* strain S17-1 carrying the plasmid pSUP2021 (Simon et al., 1983). This was achieved by biparental mating between bKSDF and S17-1(pSUP2021) with a subsequent selection for kanamycin resistant *R. capsulatus* conjugants on RCV agar. The ColE1 origin of replication of plasmid pSUP2021 carrying Tn5 cannot replicate in *R. capsulatus*, so any resulting kanamycin-resistant conjugant bKSDF cells should have contained the Tn5 transposon inserted at some locus in the genome. The conjugant colonies were screened for solid substrate motility in the interstice of YPS agar (1.5% w/v) medium circular plates. Kanamycin-resistant members of the transposition library were stab inoculated into the glass-agar interstice of borosilicate glass Petri plates at a density of 40 bKSDF::Tn5 strains per plate, and incubated for 48 hours at 30 °C with directional illumination. Strains that were capable of movement in the interstice were discarded whereas strains with inhibited motility were retained. These bKSDF::Tn5 strains that did not exhibit cell movement from the point of stab-inoculation were harvested from the surface colony growth at the air-agar interface and rescreened for motility.

2.15. Whole cell absorption spectrum

The whole cell spectrum was measured from *R. capsulatus* strain SB1003 cells cultured in RCV medium (Beatty and Gest, 1981). Approximately 15 mL of culture grown photosynthetically at 32 °C to 400 Klett units was centrifuged (see above) and the resulting cell pellet was resuspended in 1 mL 10 mM Tris-HCl (pH 8.0) and sonicated to lyse cells. The cell debris was removed by centrifugation (see above) and the supernatant (membranes and cytoplasmic fractions together) was retained for the absorption spectrum, measured at a 1:10 dilution.

2.16. RNA isolation and microarray analysis

R. capsulatus cells were inoculated into the glass-agar interstice of agar medium in borosilicate Petri plates and incubated for 24 hours at 30 °C with directional illumination (white light from an incandescent lamp, ~190 $\mu E/m^2/s$). Cells were harvested from the interstice at the leading edge of cell movement and RNA was extracted using the RNeasy Kit (Qiagen Inc., Mississauga, ON, Canada) in accordance with the manufacturer's protocol. Whole-genome expression 100-3660 arrays were constructed by Affymetrix Inc. (Santa Clara, CA, USA) through a custom design by Dr. A. S. Lang generated using a preliminary version of the complete *R. capsulatus* genome sequence. These custom arrays contain oligonucleotide probes for 3635 open reading frames (ORFs) and 1452 intergenic regions greater than 90 bp, with 11 probe pairs representing each ORF. RNA sample processing was performed at the Michael Smith Genome Sciences Centre (Vancouver, BC, Canada). Synthesis of cDNA, probe labelling, and hybridization was performed as described for prokaryotic samples in the Affymetrix expression Analysis Technical Manual.

Data from cells harvested from the glass-agar interstice were compared to data from early stationary phase aqueous culture samples (generously provided by R. Mercer and A. S. Lang). Using GeneSpring version GX (Agilent Technologies, Santa Clara, CA, USA), the signal intensities from scanned arrays were normalized to the 50^{th} percentile per chip such that the median normalized signal intensity equalled 1, and the differential expression threshold limit was set to 2-fold signal intensity for gene lists generated from solid substrate culture samples relative to aqueous culture samples.

2.17. Statistical analysis of cell movement

The average and standard deviation of the distance and the direction (relative to an arbitrary reference mark or experimental stimulus) of movement travelled by cells were calculated to assess the effects of experimental factors on motility. Standard deviation values were presented in parentheses

following average values. Experimental replicates were required to determine the overall distance and direction travelled by cells inoculated into the plate-agar interstice. Experimental sample and control sets were compared to determine whether differences in the average distance or direction of motility were significant. Control sets consisted of parental strains incubated under the same conditions or samples incubated in the absence of the experimental stimulus.

Data were analyzed with SOCR Analysis program suite (Che et al., 2009). The parametric unequal variance Student's t (P_T) test (Student, 1908), which assumes normally distributed data, was unsuitable for the comparison of directional motility because the distribution of the data from experiments did not conform to a normal Gaussian curve. Therefore, the non-parametric two-independent sample Wilcoxon (P_Z) test, which does not assume normally distributed data (Stephens, 2004), was used. The Wilcoxon test assigns a rank to each data point and compares the ranked sum of the distributions, whereas the Student's t-test compares the shape of the distributions. A Wilcoxon ranked sum test was used to analyze distance-travelled data, whereas a Wilcoxon ranked sign test was used to analyze direction of movement data. Mutations may have resulted in increased or decreased motility responses, so a two-tailed analysis model was applied to data based on the assumption that one data set parameter was not greater or lesser than the other data set parameter. P_Z values were determined for the 0.95 confidence interval to represent differences between samples that were not the result of random chance. P_Z values of ≥ 0.05 were considered to represent no statistically significant difference in the distance or direction of motility. P_Z values of <0.05 were considered to represent statistically significant differences in the distance or direction of motility, and are noted with an asterisk. Statistical evaluations are summarized in section **3.6.10**.

3. RESULTS

3.1. Solid substrate motility

Solid substrate motility was evaluated using a stab-plate technique shown to be effective with *M. xanthus* and *P. aeruginosa* (Rashid and Kornberg, 2000; Murray and Kazmierczak, 2008). The dimensions of the gap between the Petri plate base and the agar were unknown, and free-swimming flagellar motility may have occurred in this interstice. However, I suggest that the motility observed in this interstice is not free-swimming motility between the two solid substrates, but rather a mixture of flagellar swarming and flagellum-independent movement components. These components appeared to depend on the nature of both the "upper" and "lower" solid substrate surface in the interstice where motility was detected, as described below.

3.1.1. Solid substrate motility in interfaces generated on plastic or glass substrates

R. capsulatus wild type strain B10 motility was assayed on the surface of the air-agar and in the interstice of plate-agar interfaces, using plastic and glass Petri plates. Solid substrate cell taxis was not observed on the air-agar interface using either polystyrene plastic or borosilicate glass plates. Cells inoculated to the air-agar surface interface grew as a localized cell mass at the point of inoculation (Figure 3-1a,b) and rarely exhibited movement across the surface (data not shown).

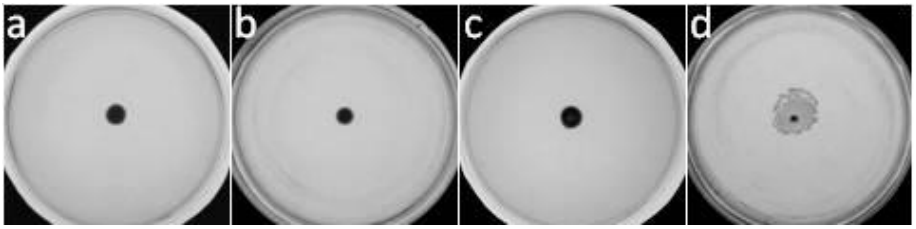

Figure 3-1: Representative agar plates inoculated with wild type strain B10, and incubated in the dark: (a) air-agar surface inoculation in a polystyrene plate; (b) air-agar surface inoculation in a borosilicate plate; (c) plastic-agar interstitial inoculation in a polystyrene plate; (d) glass-agar interstitial inoculation in a borosilicate plate.

Cells inoculated into the polystyrene plastic-agar interstice grew as a localized cell mass at the point of inoculation, whereas cells inoculated into the borosilicate glass-agar interstice exhibited movement from the point of inoculation (Figure 3-1c,d). These results indicated that differences in the physical or chemical properties between plastic and glass resulted in different degrees of motility in the plate-agar interstice.

3.1.2. Modification of plastic substrates for variation of the interstice

In attempts to determine whether a physical difference between the plastic and glass Petri plates affected cell motility, the surface of plastic plates was modified by etching with 2 M NaOH (Kahn, 1984), or abrasion with sandpaper (see section **2.2**). The rationale was that the glass plates had been used, washed, and re-used many times, perhaps resulting in abrasion of the glass surface. The plastic plates, however, were new.

Solid substrate cell taxis was not observed in either the plastic-agar interstice of NaOH-etched or sandpaper-abraded polystyrene plastic plates. Cells inoculated into the interstice grew as a distinct localized cell mass at the point of inoculation (Figure 3-2a,b).

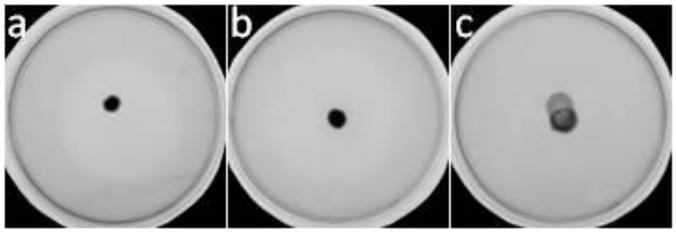

Figure 3-2: Representative agar medium inoculated with wild type strain B10, and incubated in the dark: (a) etched polystyrene surface; (b) abraded polystyrene surface; (c) borosilicate insert on the native polystyrene surface.

Insertion of a borosilicate glass microscope slide at the bottom of polystyrene plastic plates generated a glass-agar interstice in which solid substrate cell taxis was observed, as cells exhibited movement from the point of inoculation and cell growth (Figure 3-2c). Cell movement was not affected in etched or abraded borosilicate plates (data not shown). I concluded that the reason cells did not

move in the plastic-agar interstice was an inherent chemical or physical difference between polystyrene plastic and borosilicate glass that was not mimicked by etching or abrasion. These properties of the plate materials may have influenced cell movement directly by affecting the interstice, or the medium surface.

3.1.3. Investigation of solidification agents used to generate a glass-substrate taxis interstice

In previous work, agar concentrations of 0.5 to 0.8% supported swarming (with some species able to swarm on concentrations of up to 1 or 2%), whereas twitching motility occurred on concentrations up to around 1.5%. Concentrations for gliding motility ranged from 1 to 2%, and 0.3 to 0.7% concentrations supported sliding motility (Harshey, 2003). Several solidification agents were used to vary the composition of the solid medium poured into glass plates. I found that, in general, *R. capsulatus s*olid substrate movement was affected by the type and concentration of the medium solidifier.

Agar, agarose, and Gelrite were used to solidify media, and motility responses were tested. Cells inoculated into the glass-agar interstice of 1.5% (w/v) agar-solidified media moved away from the point of inoculation. Cells inoculated into the glass-agar interstice of agarose-solidified (0.25 to 1.5% w/v) media moved, but the average distance travelled was less in 0.25% agarose than on higher concentrations. Cells inoculated into the glass-agar interstice of Gelrite-solidified (0.25 to 1.5% w/v) media also moved, but the average distance travelled was greater in 0.25% Gelrite than on higher concentrations (Figure 3-3, **APPENDIX A** Table A-1).

Motility on the surface of the air-medium interface was observed on 11% of 1.25 and 1.5% agarose-solidified media, and 4% of 1.25 and 1.5% (w/v) Gelrite-solidified media. Samples exhibiting cell growth at a distance $\leq$4 mm from the site of inoculation were not considered to have moved.

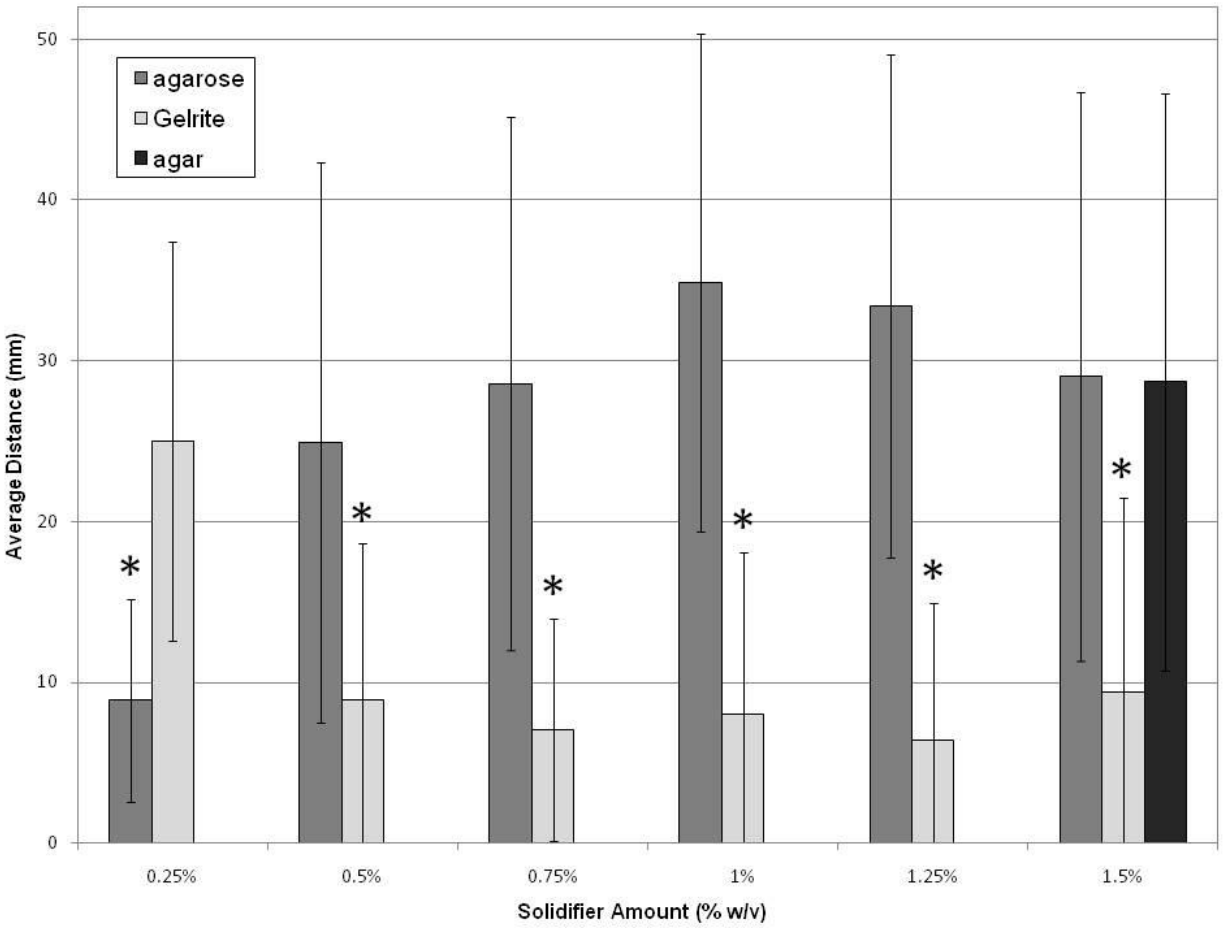

Figure 3-3: Average distance travelled by wild type strain B10 cells inoculated into medium solidifier agent titration plates, and incubated anaerobically with halogen white light. (grey) agarose-solidified medium; (light grey) Gelrite-solidified medium; (dark grey) agar-solidified medium. Error bars represent 1 standard deviation. The P_Z value is the probability that a difference from the 1.5% agar value is due to random chance – hence a P_Z value < 0.05 means that the difference is statistically significant. Asterisks indicate cases where $P_Z < 0.05$.

Using the method described in section **2.17**, the distribution of the distance travelled by cells was compared to 1.5% agar samples. The occurrence of movement >4 mm from the site of inoculation was used to determine the frequency of movement. The average distance of cell movement was reduced in 0.25% agarose-solidified and 0.5 to 1.5% Gelrite-solidified samples when compared to 1.5% agar medium plates. The average distance and frequency of cell movements was comparable to 1.5% agar in 0.5 to 1.5% agarose-solidified and 0.25% Gelrite-solidified samples, and the average distance

travelled by motile cells was longest in 1.0% agarose-solidified medium. The frequency of movement was also reduced in 0.25% agarose and 0.5 to 1.5% Gelrite-solidified samples (see **APPENDIX A** Table A-1). These results indicated that the type and amount of solidification agent employed in the taxis substrate had an influence on the occurrence and distance of solid substrate interstitial motility. Because there were differences in the motility depending on the type and concentration of the solid medium used, it appeared the medium directly interacted with cells, and that *R. capsulatus* cells moved on the lower surface of the solid medium.

3.1.4. Medium volume effects on taxis in a glass-agar interstice

The effect of moisture evaporation through the overlaying medium was examined by testing various medium volumes. The rationale was that greater volumes (thicker plates) would result in smaller fractions of total moisture loss, and hence increased hydration as time passed for the cells in the glass-agar interstice. Cells were inoculated into the interstice of borosilicate Petri plates containing 5, 10, 15, 20, or 25 mL of YPS medium solidified with 1.5% (w/v) agar. Cells moved from the point of inoculation in all 5 medium volumes, however, the frequency and average distance travelled varied with respect to the amount of medium (Figure 3-4, **APPENDIX A** Table A-2).

The large standard deviations indicated that the distribution of data was non-parametric. Using the method described in section **2.17**, the distribution of the distances travelled by cells was compared to 20 mL agar samples. There was not a clear trend in the average distance of cell movement as a function of medium volume. The average distance travelled by cells in 15 mL medium volumes was significantly reduced relative to the 20 mL volumes, according to the statistical method used. However, in the absence of a clear trend, it appeared that the volume of agar may not have been the only factor that affected the distance travelled by cells.

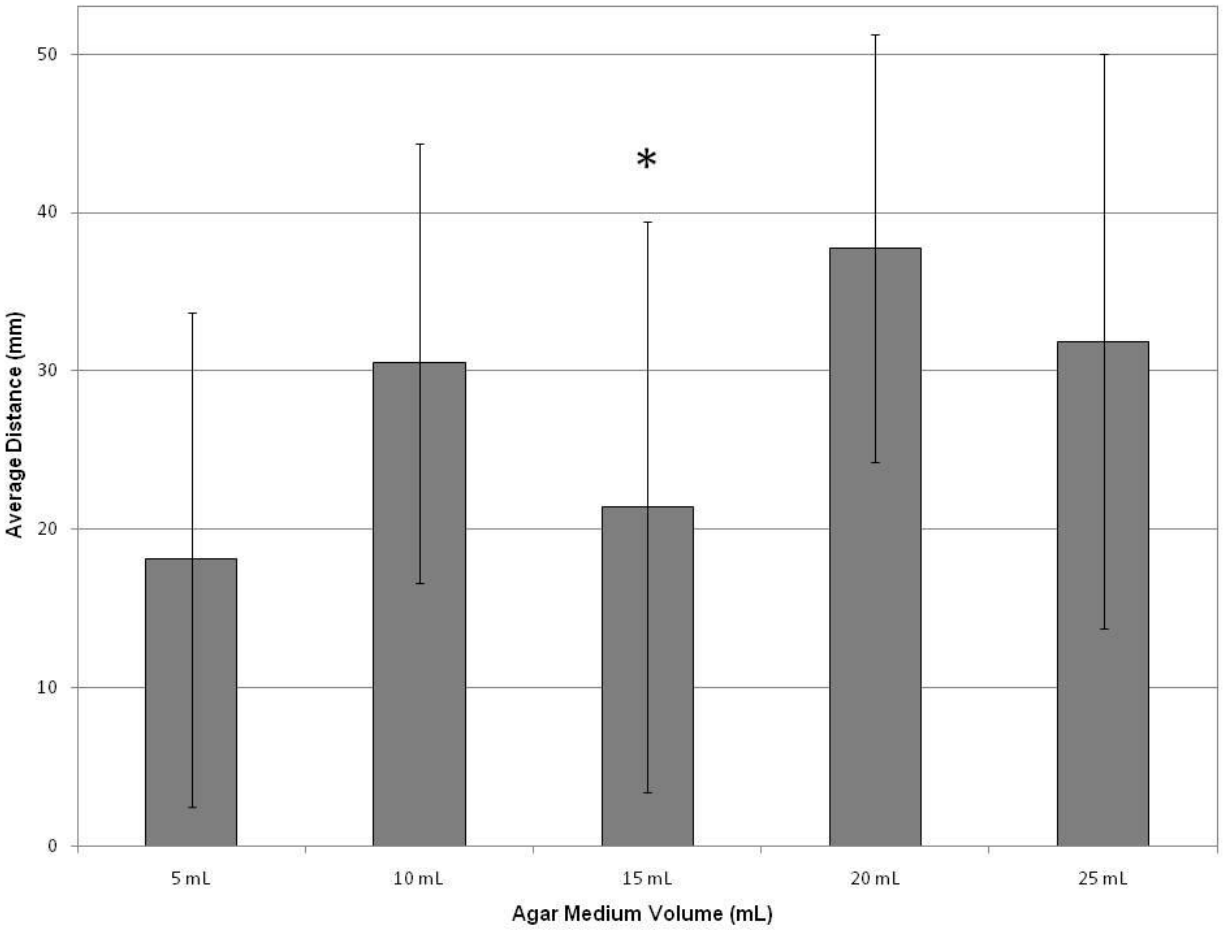

Figure 3-4: Average distance travelled by wild type strain B10 cells inoculated into agar medium volume titration plates, and incubated in the dark. Error bars represent 1 standard deviation. The P_Z value is the probability that a difference from the 20 mL agar value is due to random chance – hence a P_Z value < 0.05 means that the difference is statistically significant. The asterisk indicates where P_Z < 0.05.

The weight of plates after medium solidification was compared to the weight after incubation at 30 °C for 16 hours in the dark (Figure 3-5; **APPENDIX A**, Table A-3). The average moisture lost to evaporation was similar for all 5 stab-plate volumes, as expected, ranging from 0.42 to 0.45 g ($\pm$0.7 to $\pm$0.12 g, n = 10). The amount of moisture lost relative to the initial medium weight differed, and generated a decreasing trend with increasing volume. When plots of "relative" moisture loss and average movement distance were compared (Figure 3-4), the statistically significant difference of the 15 mL volume found in Figure 3-4 did not appear to be due to moisture loss. In summary, it appeared that

the volume of medium had an effect on the distance of cell movements, but it could not be linked to moisture loss.

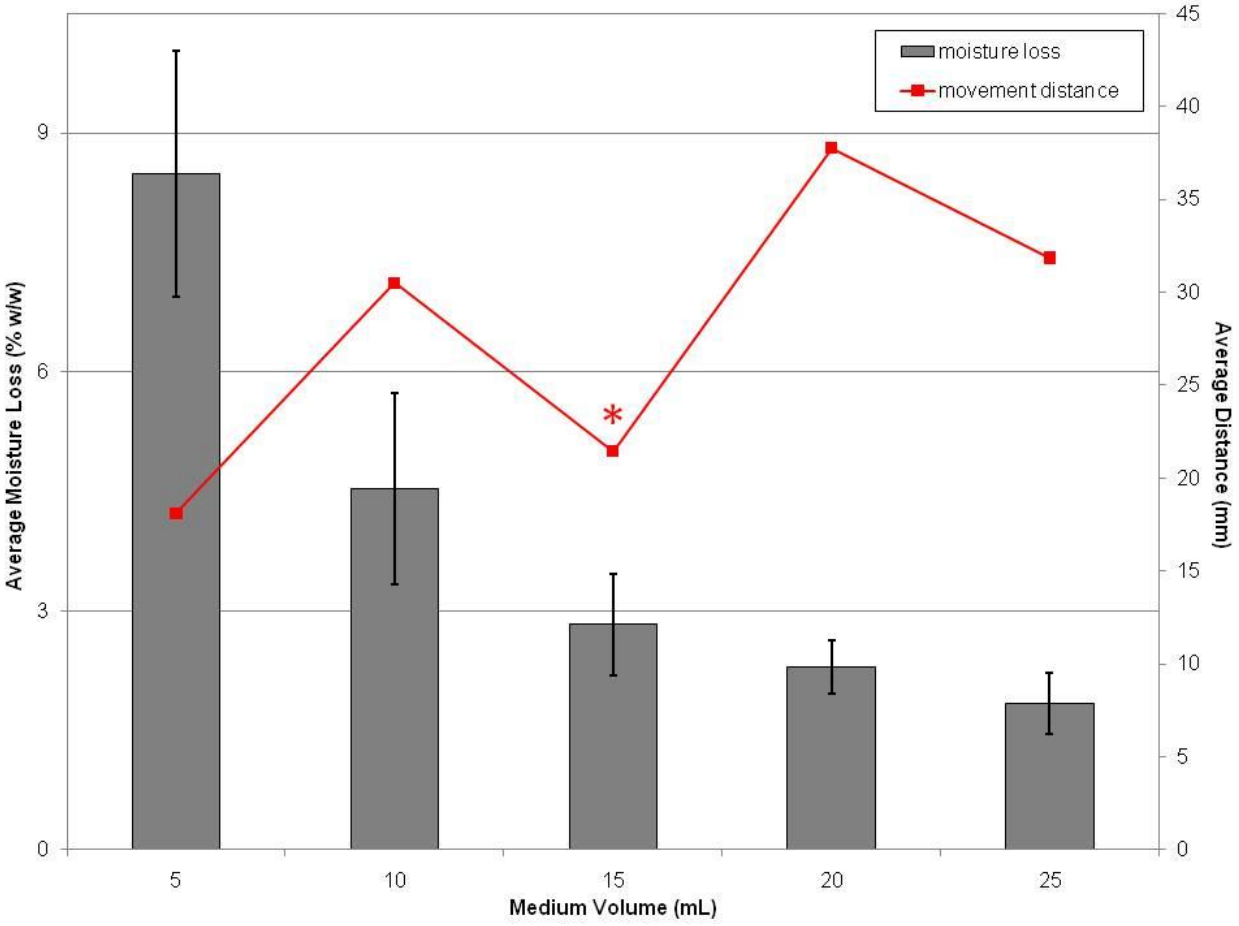

Figure 3-5: Average distance travelled compared to relative moisture lost to evaporation. Wild type strain B10 cells inoculated into agar medium volume titration plates, and incubated in the dark. The P_Z value is the probability that a difference from the 20 mL agar value is due to random chance – hence a P_Z value < 0.05 means that the difference is statistically significant. The asterisk indicates where P_Z < 0.05.

3.1.5. Study of oxygen requirements for taxis in a glass-agar interstice

The role of oxygen on the occurrence of solid substrate cell taxis was investigated by comparison of aerobic and anaerobic incubation conditions, using a modified YPS:RCV medium supplemented with fructose and DMSO to allow for anaerobic respiration in the absence of light (Saeki

and Kumagai, 1998). The CtrA response regulator of *R. capsulatus* was shown to modulate the transcription of motility genes (Lang and Beatty, 2002), and so the movement of the *ctrA*-deficient strain BCKF was also tested. Wild type B10 and *ctrA* mutant BCKF strains were incubated both aerobically and anaerobically in the dark, and cells moved away from the point of inoculation under both conditions (Figure 3-6).

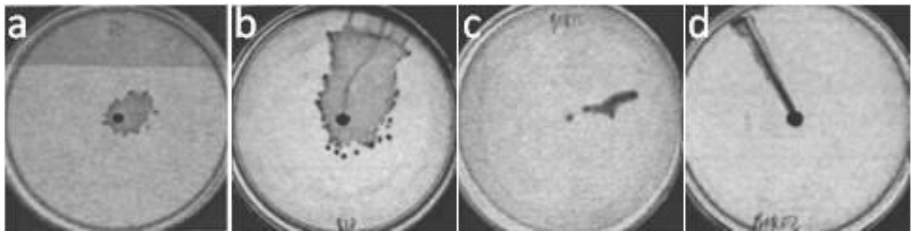

Figure 3-6: Representative fructose/DMSO-supplemented 50:50 YPS:RCV agar medium inoculated with *R. capsulatus* cells, and incubated in the dark: (a) anaerobic conditions, wild type strain B10; (b) aerobic conditions, wild type strain B10; (c) anaerobic conditions, *ctrA* mutant strain BCKF; (d) aerobic conditions, *ctrA* mutant strain BCKF.

Using the method described in section **2.17**, the distribution of the distance travelled by aerobically and anaerobically incubated cells was compared (Table 3-1). Oxygen was not required for the solid substrate taxis of *R. capsulatus*, but these results indicated that the absence of oxygen resulted in significantly reduced cell movement distances, perhaps because fructose oxidation under anaerobic dark conditions generates approximately 4-fold less ATP (Madigan et al., 1980; Grammel et al., 2003; Herrmann et al., 2008). Movement under anaerobic conditions was reduced both away from the site of inoculation (distance) and outward from the path of movement (width).

Table 3-1: Average motility values of samples incubated anaerobically in the dark in the interstice of an agar medium.

Strain	Strain name	Oxygen	Average motility distance [(a)] (mm)	Average motility width [(b)] (mm)	P_z	# Samples
wild type	B10	aerobic	40 (14)	24 (9)		17
		anaerobic	12 (15)	12 (2)	0.000021 [(c)] *	28
					0.00004 [(d)] *	
ctrA	BCKF	aerobic	37 (17)			17
		anaerobic	12 (13)		0.000072 [(c)] *	27

(a) Taxis distance as measured from the point of inoculation to farthest point of visible cell growth, with standard deviation in parentheses.

(b) Taxis distance as measured outward from the middle across the broadest point of visible cell growth, with standard deviation in parentheses.

(c) Two-tailed two-independent sample Wilcoxon rank sum test of significant difference compared to aerobic control sample distances. For a >0.95 probability that the movement was different from aerobic controls, $P_z < 0.05$. Asterisks indicate cases where $P_z < 0.05$.

(d) Two-tailed two-independent sample Wilcoxon rank sum test of significant difference compared to aerobic control sample widths. For a >0.95 probability that the movement was different from aerobic controls, $P_z < 0.05$. Asterisks indicate cases where $P_z < 0.05$.

3.1.6. Occurrence of solid substrate motility in several *R. capsulatus* strains

The possibility of widespread occurrence of this solid substrate motility was tested in different strains. The environmental isolate strains B6 (Marrs, 1974), SP36, YW1, and YW2 (Weaver et al., 1975) were compared to the wild type environmental isolate strain B10, and its rifampicin-resistant derivative SB1003. Solid substrate cell taxis was observed in all five of the environmental isolate strains as well as SB1003 (Figure 3-7). These results indicated that solid substrate motility is a conserved characteristic in *R. capsulatus*.

Using the method described in section **2.17**, the distribution of the distance travelled by strains B6, SP36, YW1, YW2, and SB1003 was compared to strain B10. No difference was observed in the

distance travelled by cells, although the number of samples was too small for a rigorous statistical evaluation (data not shown).

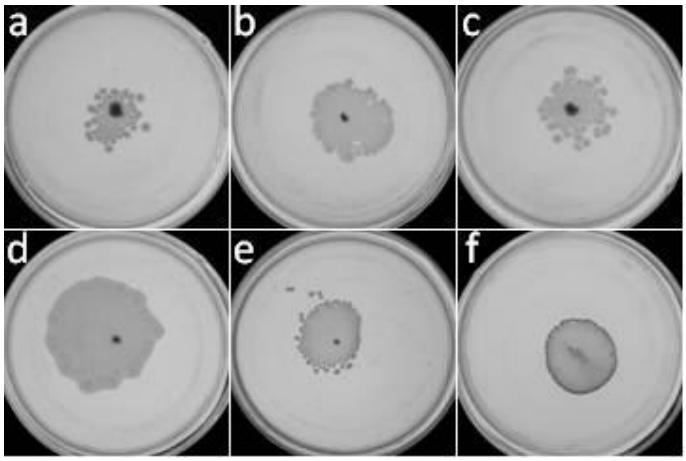

Figure 3-7: Representative agar plates inoculated with *R. capsulatus* strains, and incubated in the dark: (a) B6; (b) SP36; (c) YW1; (d) YW2; (e) B10; (f) SB1003.

3.2. Investigation of directional solid substrate motility

Subsequent experiments on the direction of motility were analyzed using a 2-D geometrical evaluation, to measure the direction of cell movement. The direction of cell movement corresponded to the farthest point of visible cell growth from the point of stab inoculation. Directional motility was measured as an angular value between the direction of cell taxis and a fixed reference point at the edge of the plate. For samples incubated in the absence of a known stimulus, this fixed reference point corresponded to the back wall of the room when facing the incubation shelf, or the position of the magnetism/heat/illumination source for samples incubated with the corresponding stimulus (Figure 3-8). Statistical evaluations are summarized in section **3.6.10**.

The reference point on the Petri plate corresponding to the direction of a specific point in the incubator (to correspond with LED-illuminated plate orientations; see section **C.2**), or the position closest to the source of magnetism, heat, or illumination was designated as the 0° reference point. Samples were assessed such that movement within the hemisphere of the 0° reference point

constituted movement toward the stimulus, while those samples moving within the 180° hemisphere constituted movement away from the stimulus (Figure 3-8). Samples incubated in the dark were assessed using the same model, with the 0° reference point positioned similarly to when a stimulus was present. The 0° reference point is positioned at the top of plates presented in figures throughout this thesis. The radius of cell growth at the air-medium interface varied from approximately 1 to 4 mm, so samples moving less than 4 mm from the point of stab inoculation were considered to not move.

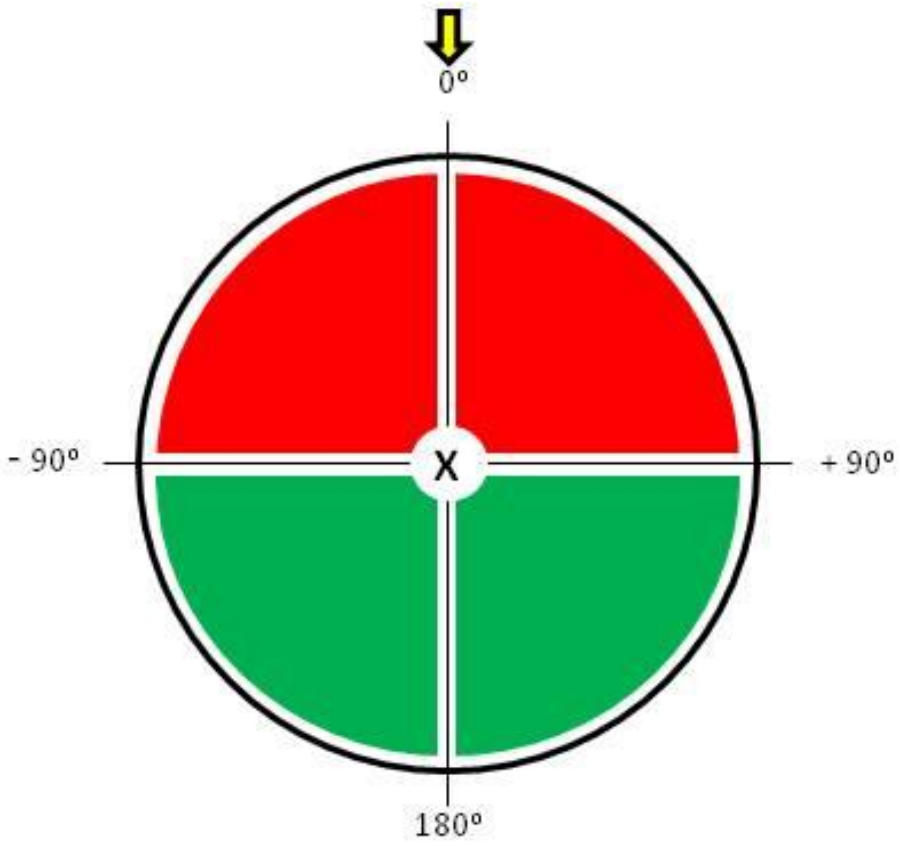

Figure 3-8: Representation of the system used to determine the angular direction of motility in agar plates with *R. capsulatus* strains inoculated into the glass-agar interstitial region of borosilicate Petri plates: (X) point of stab inoculation; (yellow arrow) direction of stimulus; (red) movement of cells scored toward stimulus; (green) movement of cells scored away from stimulus.

3.2.1. Directed taxis of cells in the glass-agar interstice

In a subset of experiments *R. capsulatus* cells moved in an obviously directed manner. The difference between movement and "obvious directed" movement is shown in Figure 3-9. The appearance of plates inoculated with the wild type strain B10 showing the absence of obvious directed movement is shown in Figure 3-9a,b, while prominent directional movement of B10 is shown in Figure 3-9c,d.

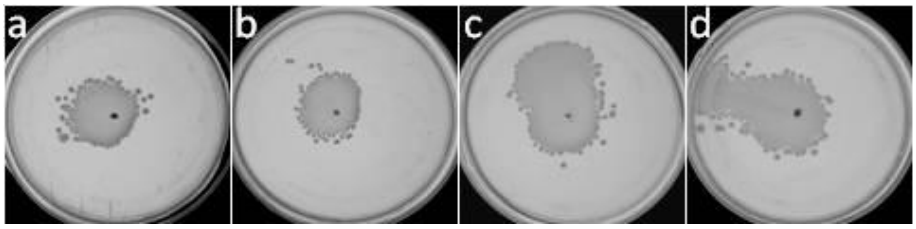

Figure 3-9: Representative agar plates inoculated with wild type strain B10, and incubated in the dark: (a) -102° movement (b) 17° movement; (c) prominent directed -16° movement; (d) prominent directed -73° movement.

A graphical representation of the angular direction of cell movement in plates incubated in the dark indicated that cells were predisposed to move in certain directions. The direction of cell motility appeared to be biased toward the 0° to $\pm$ 90° hemisphere (based on the arbitrary designation of zero in Figure 3-8), but using the calculation of the interquartile range (IQR), the data did not appear to present a normal distribution. The IQR, which consists of the central half of the data between the first and third quartiles, is a measure of the spread of a distribution (Kleinbaum, 1998). The movement of 206 (50%) samples was between -52° and 87°, while 253 (62%) samples travelled within -90° to 90° (Figure 3-10). The IQR can be used to identify outliers, data that fall outside the observed trend in the distribution of the data. Outliers can be an outside or a detached value and are $\geq$3 standard deviations from the mean, (Kleinbaum, 1998). An outside value is greater than $\pm$1.5xIQR (with a probability of 0.05), while a detached value is greater than $\pm$3xIQR (with a probability of 0.005). None of the data appeared to be

outliers, and although the majority of samples moved within one hemisphere, this apparent bias may have been due to chance.

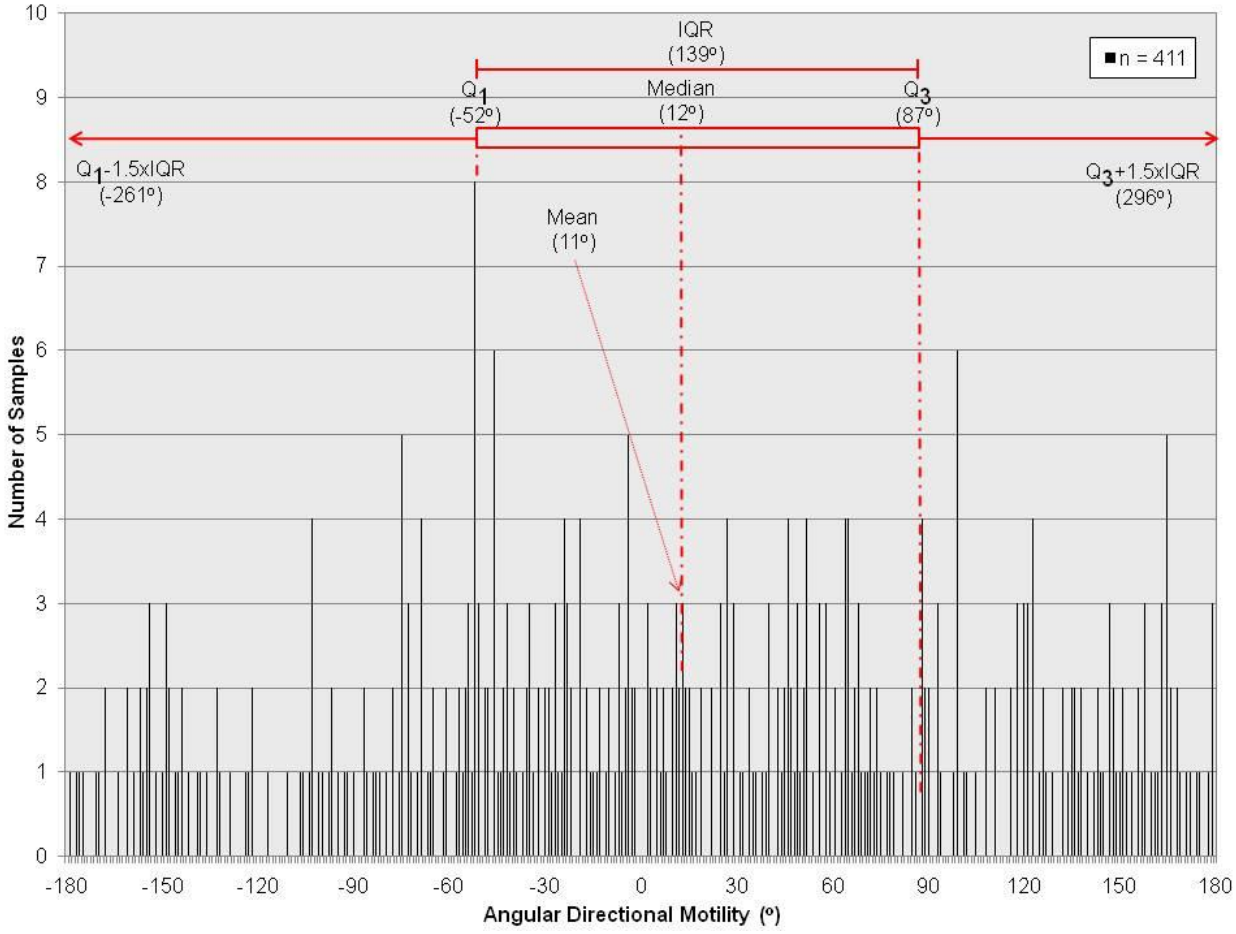

Figure 3-10: Graphical representation of the measured angular direction of motility of wild type strain B10 inoculated into the glass-agar interface of borosilicate Petri plates, and incubated in the dark with no known stimulus. The 0° angle corresponds to a particular direction in the incubator. Q_1, first quartile; Q_3, third quartile; IQR, interquartile range; n, total number of samples.

The possibility that environmental stimuli influenced the directional taxis of cells in the glass-agar interstice of plates was addressed in experiments described in following sections, using strains that lacked the flagellum in some experiments. Two types of mutations were used to create strains that lacked the flagellum: a knockout of the *ctrA* gene, which is needed for flagellar gene transcription (Lang

and Beatty, 2002; Mercer et al., 2010); or a knockout of the *flaA* gene, which encodes the flagellum protein flagellin (Shelswell et al., 2005).

3.2.2. Glass substrate effects on directional motility in the interstitial interface

The *ctrA* mutant strain BCKF was used to test for the influence of the plate surface of the interstice on the direction of cell motility. This was assessed by reusing a set of borosilicate plates. The orientation of cell movement was recorded on the base of plates, the Petri plates were washed, randomly reoriented, reused, and the subsequent direction of cell movement recorded. Of 106 samples, 85 subsequently exhibited directed motility. In these experiments, the subsequent direction of movement was considered to be the same as the previous direction if the motility was within the same quadrant (±22.5°). Of the 85 samples, 21 moved within 22.5° of the direction of taxis observed in the initial experiment, and so 75% of motility did not correspond with the previous direction (Figure 3-11). These data indicated that the direction of solid substrate motility was not a result of irregularities in the glass interface of the glass-agar interstice. The influence of other environmental conditions was investigated in an attempt to elucidate stimuli that induced directed motility (see below).

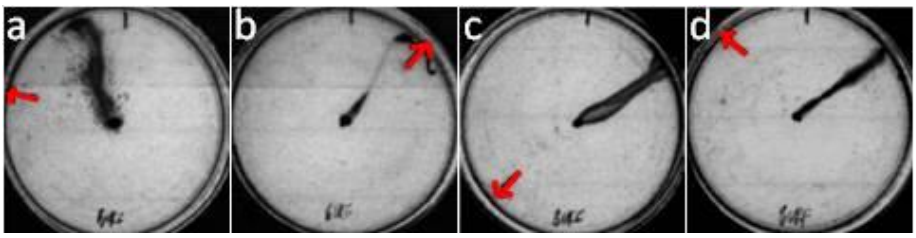

Figure 3-11: Representative agar plates inoculated with *ctrA* mutant strain BCKF, and incubated with incident halogen white light from the top of the image: (a-d) directional variability of motility with illumination; red arrows indicate the direction of motility observed in previous experiments.

3.2.3. Dipole magnetism effects on directional motility

Some bacteria exhibit directed motility in response to a magnetic field (Matsunaga, 1991), so the influence of a dipole magnetic field on the direction of cell taxis was investigated by fixing Teflon-

encased magnetic stir-bars to the edge of experimental plates at a 0° reference point. Magnets (length = 37 mm, radius = 5 mm) were arranged in tangential and radial orientations and fixed to the plate with laboratory tape during incubation (Figure 3-12). The magnetic field strength (Table 3-2) was measured in Tesla (T) units (measured with the assistance of Dr. J. Nakane) using a FW Bell 9200 Gaussmeter with a HAB92-2502 probe (Toronto Surplus & Scientific Inc., Richmond Hill, ON).

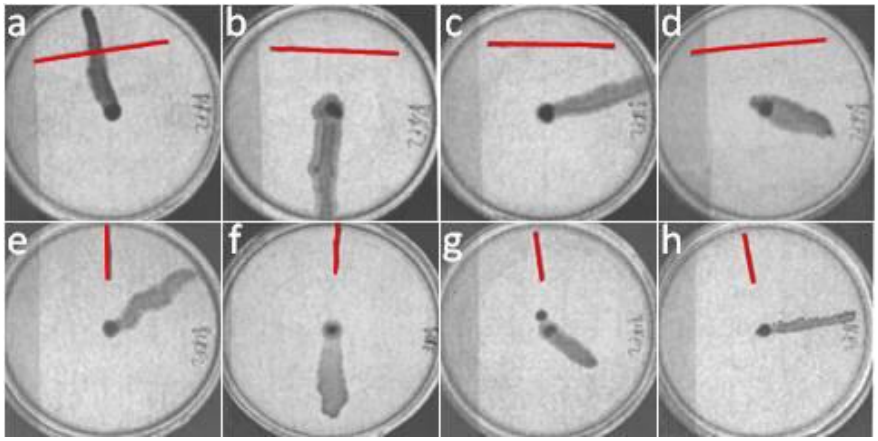

Figure 3-12: Representative agar plates inoculated with *ctrA* mutant strain BCKF, and incubated in the dark near a dipole magnet: (a-d) directional variability of motility with tangentially oriented magnetism; (e-h) directional variability of motility with radially oriented magnetism; red lines indicate the orientation of the magnet.

Table 3-2: Magnetic field strengths on *R. capsulatus* cells inoculated into the glass-agar interstice.

Magnet orientation	Distance from point of inoculation (mm)[(a)]	Magnetic field (mT)[(b)]
tangential	27 (1.7)	12.7 (3.5)
radial	21 (1.3)	29.5 (9.9)

(a) Closest vector distance from point of stab inoculation to magnet, with standard deviation in parentheses.

(b) For tangential orientation the field was determined at the magnet girdle; for radial orientation the field was determined at the magnet pole. Standard deviations are in parentheses.

Using the method described in section **2.17**, the distribution of the direction of movement of the samples incubated with magnetism was compared to samples without magnetism. Statistical analysis showed no difference in the distribution of angular direction in the presence of tangentially or radially

arranged magnetism compared to controls without magnetism (Table 3-3). These results indicated that the direction of solid substrate cell movements was not influenced by the presence or orientation of a dipole magnetic field or that the field generated by the magnets was not sufficient to influence directional cell movements.

Table 3-3: Average motility values of samples incubated in the interstice of an agar medium near magnetic fields.

Magnetism orientation	Average motility distance [(b)] (mm)	Average angular motility direction [(c)] (°)	P_Z [(d)]	# Samples
tangential	28 (17)	6 (143)	0.62	28
control (tangential)[(a)]	27 (19)	-28 (124)		25
radial	20 (15)	-20 (117)	0.42	29
control (radial) [(a)]	18 (15)	42 (135)		25

(a) Controls for each type of orientation lacked a magnet.

(b) Taxis distance as measured from the point of inoculation to farthest point of visible cell growth, with standard deviation in parentheses.

(c) Taxis direction from the point of inoculation to the farthest point of visible cell growth relative to an arbitrary 0° point, with standard deviation in parentheses.

(d) Two-tailed two-independent sample Wilcoxon rank sum test of significant difference compared to control samples without magnets. For a >0.95 probability that the movement was different from controls, $P_Z < 0.05$.

3.2.4. Temperature effects on directional motility

Since illumination of plates from one direction using halogen lamps (see section **3.2.6**) could create a temperature gradient, along with potential liquid convective movements, the influence of temperature on motility was assessed by observing the effects of a directed heat source on the orientation of wild type cell movements. Plates were shielded from light by black felt and incubated near a heat source that created a temperature gradient decreasing from 45 °C to 30 °C (the temperature

of the incubator) such that side of the plate nearest the heat source was 32, 34, 36, or 40 °C (as measured with a thermometer).

Using the method described in section **2.17**, the distribution of the direction of movement of the samples incubated relative to the temperature gradient was compared to samples at 30 °C with no gradient. Cells incubated along the temperature gradient at 32, 34, 36, and 40 °C exhibited movement from the point of inoculation, but Wilcoxon statistical analysis of the direction did not show any significant differences in the distribution of angular direction when compared to 30 °C controls (see **APPENDIX A**, Table A-4). These results indicated that *R. capsulatus* cells did not respond to a temperature stimulus along a gradient from 30 to 40 °C. However, the number of samples was too small to provide a rigorous statistical analysis of directed movement.

3.2.5. Effect of incident light during inoculation on directional motility

The influence of directional incident light during stab inoculation on the direction of *flaA* mutant strain bKSDF (see section **3.3.2**) cell movement was investigated by noting a reference point (0°) on plates during inoculation. These reference points were arranged in the same position for stab inoculation, which lasted for approximately 5 minutes. The plates were incubated aerobically in the dark, and the direction of cell movement was determined as described in Figure 3-8.

Representative plates are shown in Figure 3-13, and analysis revealed that cells travelled at an average angle of -35° $\pm$89° (n = 16). The range of direction for movement was from -178 to 133°. These results indicated that the direction of cell migration in the glass-agar interstice of borosilicate Petri

plates under aerobic dark conditions was not influenced by light perceived during inoculation.

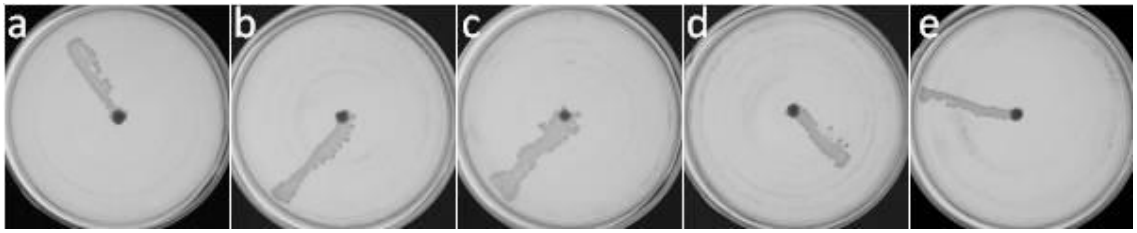

Figure 3-13: Representative agar plates inoculated with *flaA* mutant strain bKSDF, and incubated in the dark to show the variability in directional motility relative to the orientation during inoculation. Plates are displayed in the same position as used for inoculation.

3.2.6. Effect of incident light during incubation on directional motility

The influence of directional incident light during incubation on the direction of cell movement was investigated by noting the direction relative to the orientation of plates during incubation, with respect to the location of the incident light. The direction of incident light was observed to influence the orientation of directed cell motility. Wild type strain B10 cells showed a bias towards the light, which was similar for tungsten filament, halogen and LED white light sources (Figure 3-14a,b,c). The variability in the direction of motility is shown in Figure 3-14d,e,f, using halogen white light in these examples.

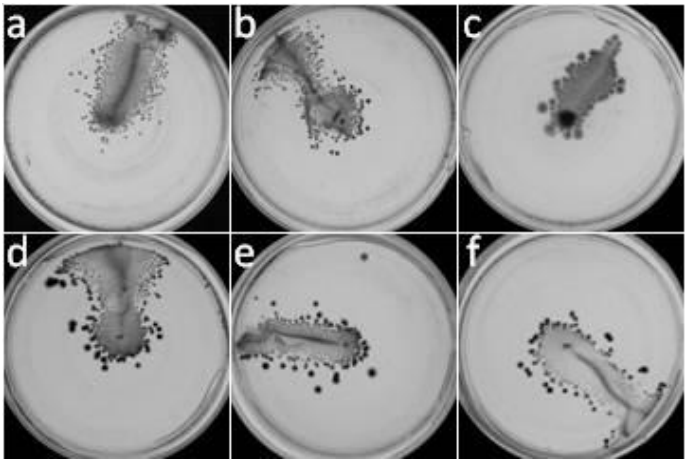

Figure 3-14: Representative agar plates inoculated with wild type strain B10, and incubated with incident white light from the top of the image: (a) tungsten filament lamp illumination; (b) halogen lamp illumination; (c) LED lamp illumination; (d-f) directional variability of motility with halogen illumination.

The degree of variability was recorded for white light-illuminated tests using wild type strain B10 inoculated into 20 mL, 1.5% agar medium plates. Cells moved in 271 of 328 experiments (83%), and travelled an average distance of 35 $\pm$14 mm from the point of inoculation. Cells travelled in a range of directions. The average angle from the direction of the light was -1 $\pm$73°, and cells appeared to move toward the light. The distribution of the direction of movement for tests is presented in Figure 3-15, where the height of the bars indicates the number of times that cells travelled in a specific angular direction.

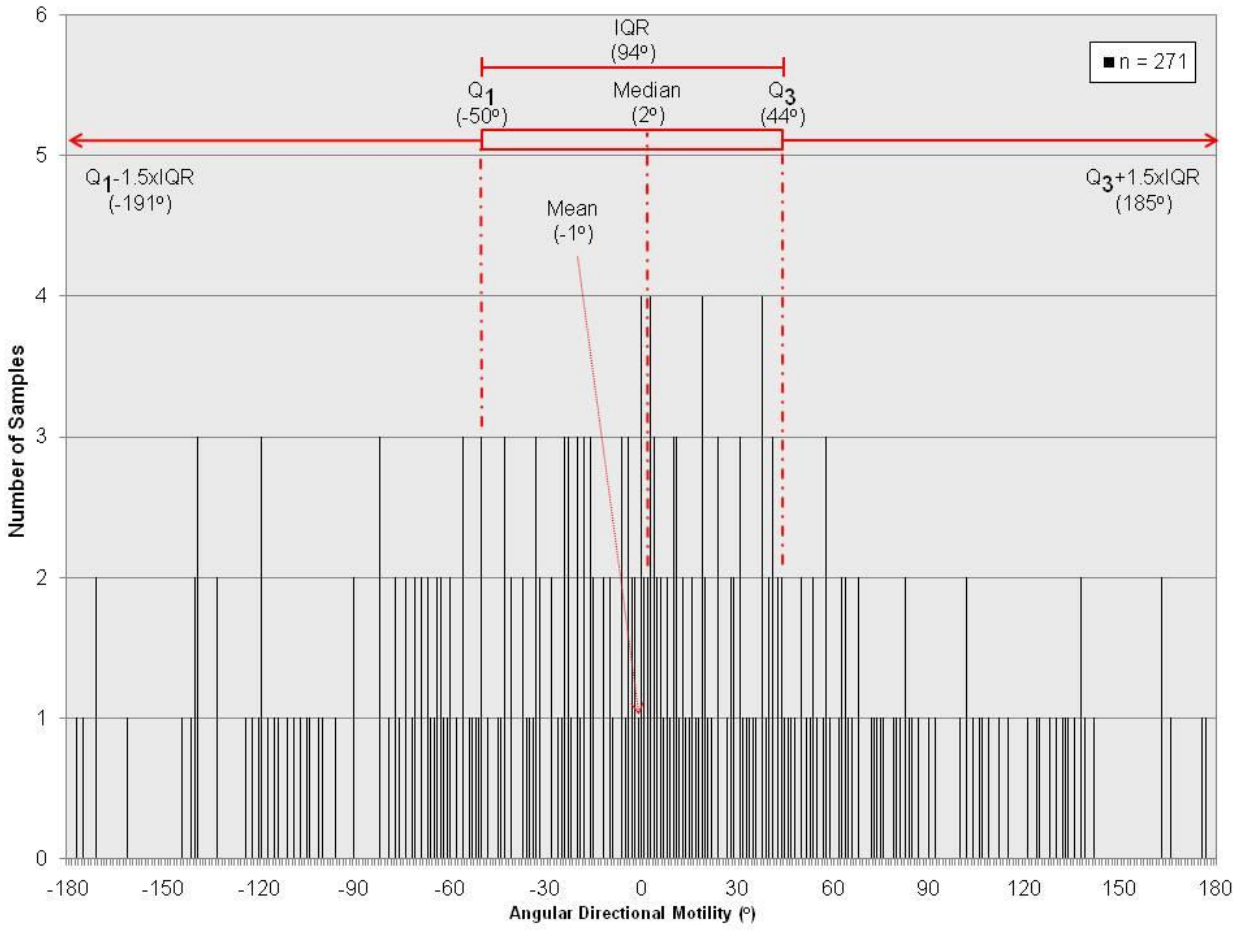

Figure 3-15: Graphical representation of the measured angular direction of motility from agar plates with wild type strain B10 inoculated into the glass-agar interstitial region of circular borosilicate Petri plates, and incubated with incident white light. 0° indicates movement directly toward the light source, and ± 180° indicates movement directly away from the light. Q_1, first quartile; Q_3, third quartile; IQR, interquartile range; n, total number of samples.

The data did not follow a normal distribution, but the direction of cell motility appeared to be biased between -90° and 90°. It was found that 135 (50%) of the motile samples travelled between -50° and 44°. Furthermore, 209 (77%) samples travelled within 90° of the light, considered to be toward the light source (Figure 3-15). These results indicated that cell movement was predisposed toward the direction of illumination during incubation.

The large variability in the data (Figure 3-15) presented uncertainty in whether the observations really reflected a phototactic response. The sample size was increased by including all 1.5% w/v agar-solidified medium stab-plate experiments incubated aerobically with white light illumination in the glass-agar interstice of plates. By including all strains (B10, SB1003, bKSDF, sbKSDF, BCKF, bKSDFcpaC, bKSDFcpaF, bKSDFcpaA, 37b4, KSDF37b4, bKSDFhcpA, DW5, sbKSDFdw5, BY1653, sbKSDFby, BLKI, bKSDFgtaI, LS01, sbKSDFsenC, REG1, and sbKSDFregA; see Table 2-1) the sample size was increased from 236 to 1836 (Figure 3-16).

The statistical distribution of directional motility did not change significantly with increased sample numbers (Figure 3-16), and yielded similar mean, median, and IQR values as in Figure 3-15. Of the 1836 tests, 1326 (72%) of the cell movements were within the -90° to 90° hemisphere. These results indicated that the distribution pattern of directional cell movement under white light-illumination in plates was not random, although greatly variable. It was thought that cells moved toward the light, but the optical properties of the circular plates were at least partly responsible for the variability in the direction of white light-illuminated cell movement.

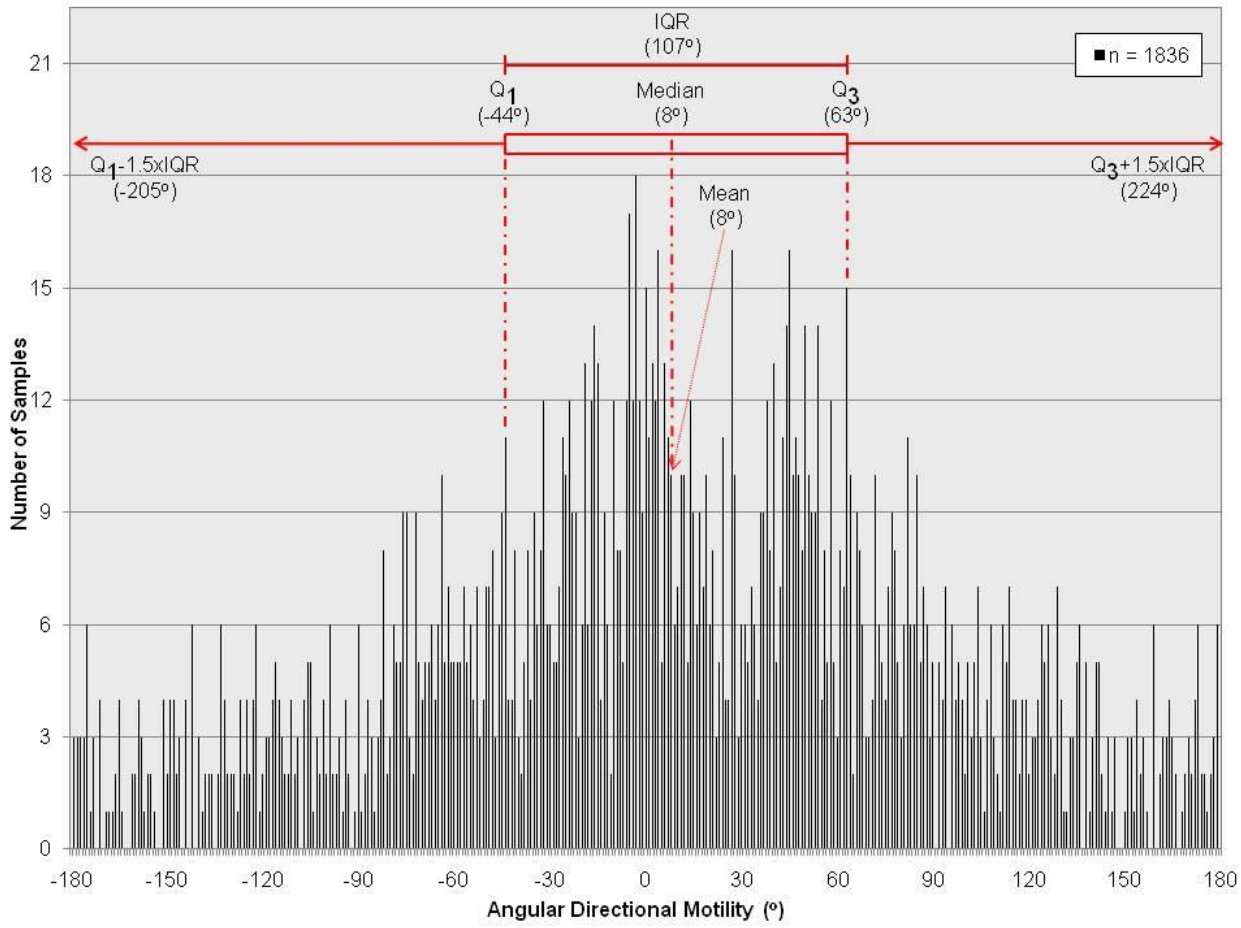

Figure 3-16: Graphical representation of the measured angular direction of motility from agar plates inoculated with *R. capsulatus* cells incubated with halogen lamp white light. 0° indicates movement directly toward the light source, and ± 180° indicates movement directly away from the light. Q_1, first quartile; Q_3, third quartile; IQR, interquartile range; n, total number of samples.

3.2.7. Use of square plates to reduce the variability in motility toward incident light

It seemed likely that the optical properties of circular glass plates influenced the direction of cell motility relative to the light source. Therefore cell movement was assayed using square, polystyrene plastic Petri plates (Figure 3-17). To create the glass-agar interstice needed for motility, a borosilicate glass slide was inserted after the addition of agar, which then solidified around it at the base of the plate. The borosilicate slides were rectangular, and placed with one edge directly against the plate wall incubated closest to the light source. Results indicated that the orientation and position of the slides

did not influence the direction of cell movement (data not shown), however motility did not progress past the edges of the slides across the polystyrene-agar interstice.

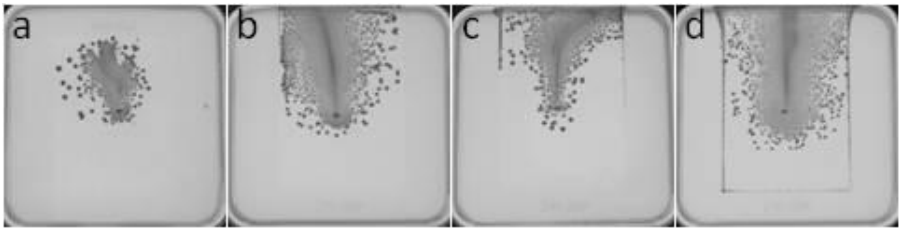

Figure 3-17: Representative agar plates with wild type strain B10 inoculated into the glass-agar interstitial region of polystyrene Petri plates with a borosilicate glass insert, and incubated with incident halogen white light from the top of the image: (a-d) reproducible taxis toward incident broad spectrum light.

Cell motility was observed in 166 of 197 samples (83%) in square plates illuminated with halogen white light. Of these 166 motile samples, the directional movement of 84 (50%) tests was between -16° and 20° (Figure 3-18). 153 (94%) samples moved within 90° of the direction of incident light, while 125 (77%) moved within 45° of the incident light. Therefore, less directional variability was observed than when using circular plates (Figure 3-17a,b,c,d), consistent with the idea that the circular plates caused changes in the direction of light sensed by cells.

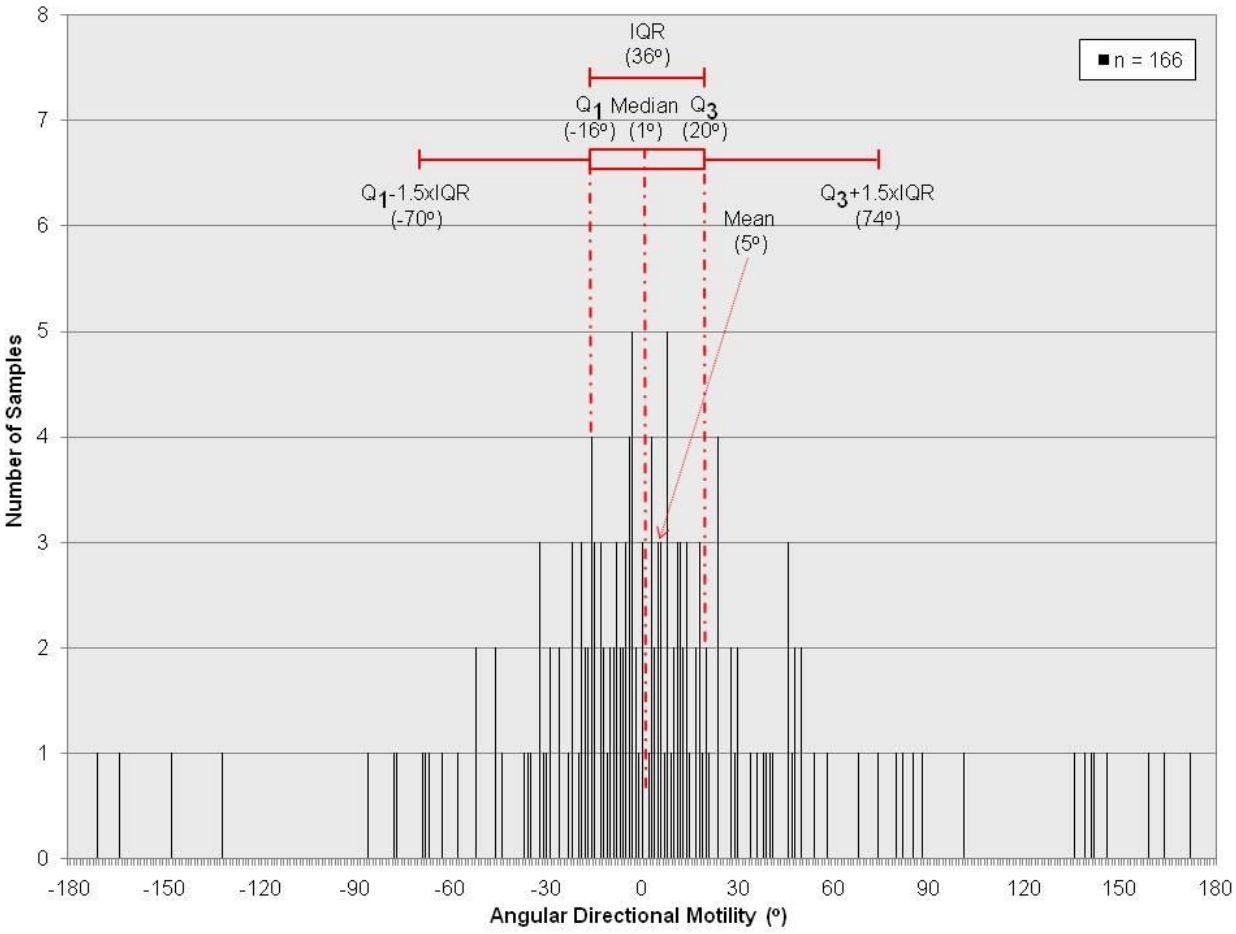

Figure 3-18: Graphical representation of the measured angular direction of motility from agar plates with *R. capsulatus* cells inoculated into the glass-agar interstice of square polystyrene Petri plates with a borosilicate insert, and incubated with incident white light. 0° indicates movement directly toward the light source, and ± 180° indicates movement directly away from the light. Q_1, first quartile; Q_3, third quartile; IQR, interquartile range; n, total number of samples.

3.3. Flagellum-mediated and flagellum-independent motility

3.3.1. Multiple motility phenotypes in the glass-agar interstice

R. capsulatus wild type strain B10 cells inoculated into the glass-agar interstice of borosilicate Petri plates that were incubated in darkness exhibited somewhat concentric, random taxis patterns from the point of inoculation (Figure 3-19a). However, skewed patterns of movement were sometimes observed, producing a heavy line of cell density within the general area of cell proliferation (Figure

3-19b). This heavy line of growth was more obvious in plates incubated under illumination (Figure 3-19c).

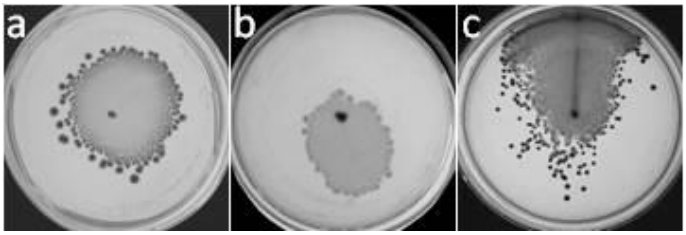

Figure 3-19: Representative agar plates inoculated with wild type strain B10, and incubated for 48 hrs: (a) random diffusive taxis in the absence of illumination; (b) diffusive 164° taxis in the absence of illumination; (c) directed and diffusive 4° taxis under directional incident halogen white light from the top of the image.

This dense line within a broad zone of cells moving away from the point of stab inoculation indicated that at least two modes of motility were occurring in the glass-agar interstice of borosilicate glass Petri plates. This phenomenon was also observed in square plates (Figure 3-17). Furthermore, in many experiments cells moved away from the mass of motile cells, sometimes a great distance, before stopping to give rise to a colony. This behaviour was more prominent in flagellated strains than in strains lacking the flagellum (compare Figure 3-13 and Figure 3-14). The contributions of flagellar and flagellum-independent processes are described in following sections.

3.3.2. Disruption of the gene encoding the flagellar structural subunit flagellin

The role of the bacterial flagellum in solid substrate motility was analyzed by mutagenesis of the gene *flaA,* encoded by RCC03525, predicted to encode the structural subunit of the flagellar filament. The *R. capsulatus* RCC03525, which contained an amino-terminal flagellin-N superfamily domain (PFAM 00669) (DeRosier, 1995), was compared to the polar and sub-polar flagellin protein sequences from *R. sphaeroides* and the four flagellin subunits of the *Sinorhizobium meliloti* flagellar bundle (Shah et al., 2000; Sourjik et al., 2000; del Campo et al., 2007) (Table 3-4).

Table 3-4: Annotation of the *R. capsulatus* flagellin gene product amino acid sequence.

Gene	Gene product	Length (aa)	Characterized homologue[(a)]	Identity (%)	E value[(b)]
flaA	flagellin	398	FlaA, *Rhodobacter sphaeroides* (YP_001033838)	37	$9e^{-36}$
			FliC, *Rhodobacter sphaeroides* (YP_353145)	24	$5e^{-11}$
			FlaD, *Sinorhizobium meliloti* (NP_384777)	34	$4e^{-43}$
			FlaB, *Sinorhizobium meliloti* (AAB81423)	34	$5e^{-24}$
			FlaA, *Sinorhizobium meliloti* (AAB81420)	33	$6e^{-25}$
			FlaC, *Sinorhizobium meliloti* (AAB81421)	32	$2e^{-25}$

(a) Gene product name, species (NCBI accession number).

(b) Top E-value scores from local pairwise protein alignment BLASTp.

The protein encoded by RCC03525 was the reciprocal best hit of FlaA and FlaD in *R. sphaeroides* and *S. meliloti*, respectively (Table 3-4). The RCC03525 *flaA* was disrupted by creating a translationally in-frame deletion in the wild type strain B10, and the rifampicin-resistant strain SB1003 (a derivative of B10) (Figure 3-20), to create the mutant strains bKSDF and sbKSDF, respectively (Table 2-1).

Soft agar (0.4% w/v) stab tubes were used to evaluate flagellar swimming outward from the column of stab inoculation through the medium. The direction of illumination was perpendicular to the long axis of the test tube. Stab tubes rotated freely during incubation, so no specific side of the tube corresponded to the direction of the light. Stab-plates were also used to evaluate movement. Stab plates were fixed so that a specific side of the plate corresponded to the direction of the light.

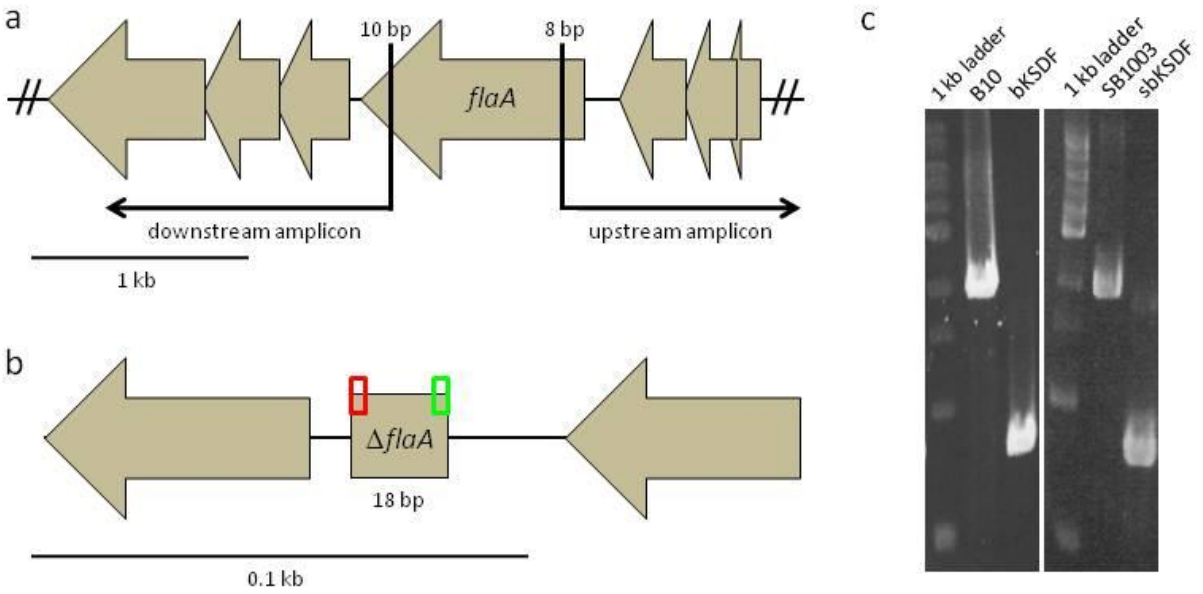

Figure 3-20: The *R. capsulatus* flagellin-encoding *flaA* gene RCC03525 mutagenesis: (a) flagellar locus containing the flagellin-encoding *flaA* gene RCC03525, and showing the positions in the coding sequence of mutagenic primers used for PCR; (b) result of PCR-based mutagenesis scheme to create an in-frame deletion of *flaA*, with the start codon represented by a green box and the stop codon represented by a red box; (c) genomic screening of *flaA* deletion mutagenesis, showing decreased size of *flaA* locus.

Strains bKSDF and sbKSDF were impaired in movement outward from the inoculation stab in soft agar, consistent with the need for flagellum-dependent swimming motility to move through agar (Figure 3-21a,b,e,f). However, flagellum-deficient bKSDF and sbKSDF mutants still exhibited motility and moved away from the point of inoculation in the glass-agar interstice. This flagellum-independent taxis lacked the diffusive appearance of the wild type strains (Figure 3-21c,g), but retained directed linear motility (Figure 3-21d,h).

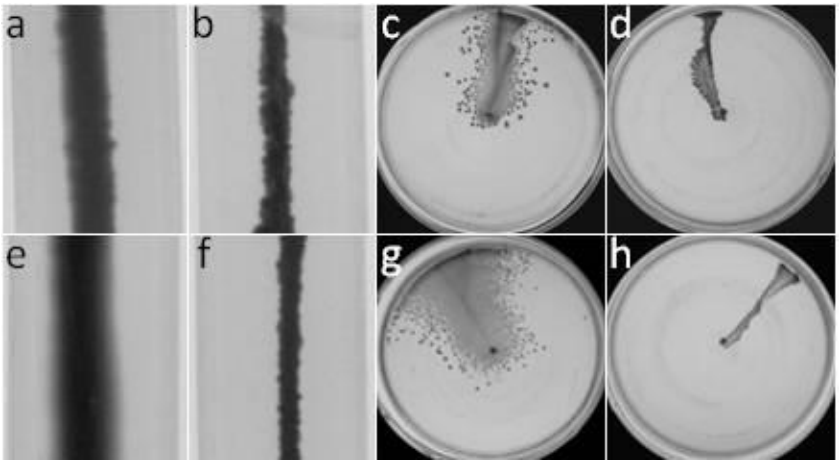

Figure 3-21: Representative differential motility phenotypes of wild type and *flaA* mutant strains incubated with halogen white light. Tubes were illuminated with incident light from the side, whereas stab-plate illumination was from the top of the image: (a) wild type strain B10 soft agar stab; (b) *flaA* mutant strain bKSDF soft agar stab; (c) wild type strain B10 stab-plate; (d) *flaA* mutant strain bKSDF stab-plate; (e) wild type strain SB1003 soft agar stab; (f) *flaA* mutant strain sbKSDF soft agar stab; (g) wild type strain SB1003 stab-plate; (f) *flaA* mutant strain sbKSDF stab-plate.

3.3.3. Electron microscopy of *R. capsulatus* cells

Support for the presence of flagellar filaments was obtained from strain B10 cells grown in aqueous culture (data not shown), and in the glass-agar interstice of borosilicate glass Petri plates (Figure 3-22a). Flagellar filaments were not observed on BCKF (*ctrA*$^-$) or bKSDF (*flaA*$^-$) mutant cells from aqueous culture (data not shown) or from the interstitial region of plates (Figure 3-22b,c).

Sequence comparison of the ~40 kDa strain SB1003 flagellin protein with the ~50 kDa sub-polar Fla1 (FliC) and ~28 kDa polar Fla2 (FlaA) proteins of the closely related *R. sphaeroides* (Table 3-4) indicated that *R. capsulatus* flagellin is likely a polar FlaA homologue (del Campo et al., 2007). The *R. capsulatus* flagellin shared 45 and 55% sequence identity with the amino and carboxy terminal domains (covering 68% of the protein sequence) of Fla2, but only 23% sequence identity with that of Fla1. While it was not possible to clearly identify the attachment site of the flagellum, the number of flagellar

filaments observed in micrographs (data not shown) suggested that *R. capsulatus* produced a single, polar flagellum that was absent in strains BCKF and KSDF.

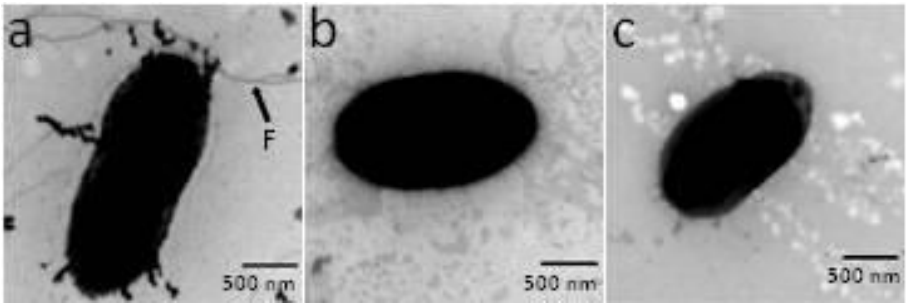

Figure 3-22: Electron micrograph negative stain of *R. capsulatus* cells from agar plates inoculated at the glass-agar interstitial region of borosilicate Petri plates: (a) wild type strain B10; (b) *ctrA* mutant strain BCKF; (c) *flaA* mutant strain bKSDF. 'F' indicates flagellar filament.

3.3.4. Cell motility in the glass-agar interstice

Tracking of radioactively labelled cells was used to determine whether the light-responsive cell motility was a passive phenomenon or an active, adaptive response. *R. capsulatus ctrA* mutant strain BCKF was used instead of wild type strain B10 to reduce signal dispersal in the broad diffusive pattern of movement. BCKF cells were labelled with ^{32}P-orthophosphate, and half the culture was killed by treatment with formaldehyde prior to stab inoculation. Photographs and radiographs of plates were taken after inoculation and incubation, to compare cell growth and movement to radioactive signal dispersal (Figure 3-23).

Labelled mutant *ctrA* strain BCKF cells treated with sterile water moved in the glass-agar interstice, whereas no movement of radioactivity was observed in plates inoculated with formaldehyde-killed cells. The radioactivity was dispersed over the zone of taxis and growth of the water-treated cells (Figure 3-23a,b), whereas the radioactivity from formaldehyde-killed cells remained localized at the point of inoculation (Figure 3-23c,d). This comparison of formaldehyde-killed and viable ^{32}P-labelled

cells indicated that dead cells did not move, and therefore movement appeared to be a biological response driven by a motility mechanism.

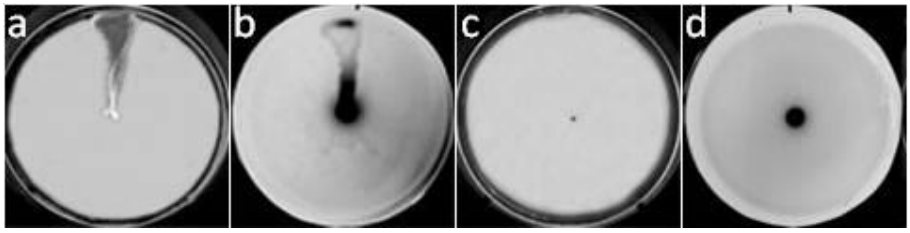

Figure 3-23: Representative agar plates inoculated with ^{32}P-orthophosphate-labelled *ctrA* mutant strain BCKF cells inoculated into the glass-agar interface of borosilicate Petri plates, and incubated at 30 °C aerobically for 48 hrs with incident light from the top of the image: (a) photograph of viable cells; (b) radiograph of viable cells; (c) photograph of non-viable cells; (d) radiograph of non-viable cells.

3.3.5. Light microscopy visualization of cell movements in the glass-agar interstice

As another method of tracking cell movement, light microscopy was used after stabbing cells into the glass-agar interstice of plates. The plates were observed using 100 X magnification, focusing on the edge of confluent cell growth, to yield time-lapse videos and images. Movement of cells at the edges of the confluent growth was recorded both in wild type strain B10 and flagellum-deficient strain bKSDF. Within uncolonized pockets in the main mass of cell growth, wild type strain B10 cells were observed to exhibit continuous rapid randomized motions (Video 1). No rapid random movements were observed by B10 cells at the periphery of the cell mass (Video 2). Flagellum-deficient strain bKSDF cells were not observed to exhibit rapid random movements within uncolonized pockets or at the cell mass periphery.

Both wild type strain B10 and *flaA* mutant strain bKSDF cells moved with intermittent, discontinuous patterns at the periphery of the cell mass at an approximate rate of 1.1 to 1.6 μm/sec (Videos 3,4,5). Cells occasionally underwent lateral or rotational movements when located within approximately one cell length of another cell, resulting in cell-cell contact in a longitudinally oriented configuration initiated by what appeared to be a pole-mediated interaction (Figure 3-24a-d).

Cell movements were also observed independent of the proximity of other cells, over a distance of several cell lengths (Figure 3-24e-j). Because cells did not move continuously, this intermittent movement which occurred at an approximate rate of at least 0.14 μm/sec did not reflect the maximal rate of movement. Cell movements occasionally underwent reversals in the direction of motility along the long axis of the cells. These observations showed that individual cells in the glass-agar interstice were capable of long-distance movement, even in the bKSDF strain that lacked the flagellum.

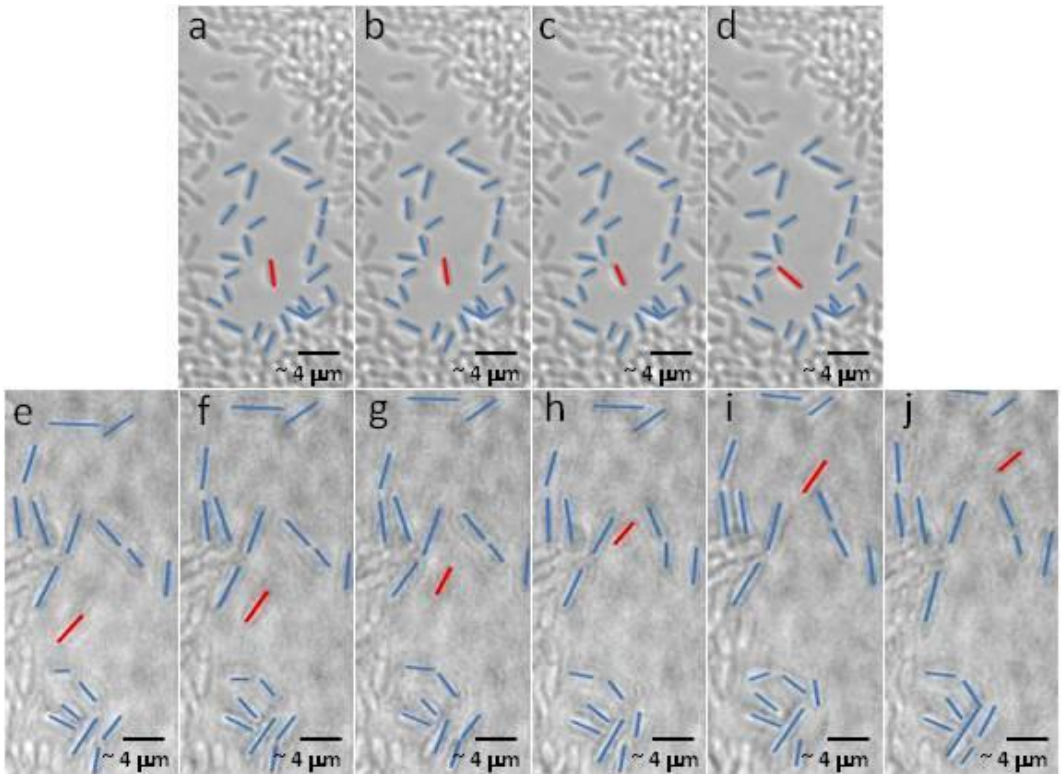

Figure 3-24: Oil Immersion microscopy of *flaA* mutant strain bKSDF cells at the glass-agar interface of polystyrene Petri plates with a borosilicate coverslip base replacing the plastic: (a-d) short range lateral cell movements, phase contrast images captured as described in section 2.5; (e-j) long range longitudinal cell movements, DIC/NIC images captured as described in section 2.5. Red designates motile cell of interest, blue designates surrounding stationary cells. Surrounding cells were not necessarily immobile. An image was captured each 0.25 seconds for lateral movement panel and each 20 seconds for the longitudinal movement panel.

3.4. Pilus-mediated motility

3.4.1. Electron microscopy of pilus-like structures on cells

The presence of surface appendages in *R. capsulatus* was examined by transmission electron microscopy (TEM). Negative staining of cells showed non-flagellar appendages (based on filament structure, diameter, and length) that appeared to originate from foci at the poles of cells (Figure 3-25)

These appendages formed structures ranging from what appeared to be individual 7 nm (70 Å) wide filaments, to bundles with diameters of approximately 60 nm (600 Å), and resembled pili (Craig et al., 2004). The flagellum and pilus-like filaments were observed on wild type strain B10 cells from aqueous culture (data not shown), and the glass-agar interstice of borosilicate Petri plates (Figure 3-25a). Only pilus-like filaments were observed on *flaA* $^{-}$ mutant strain bKSDF cells from aqueous culture (data not shown) or the glass-agar interstice of borosilicate Petri plates (Figure 3-25b).

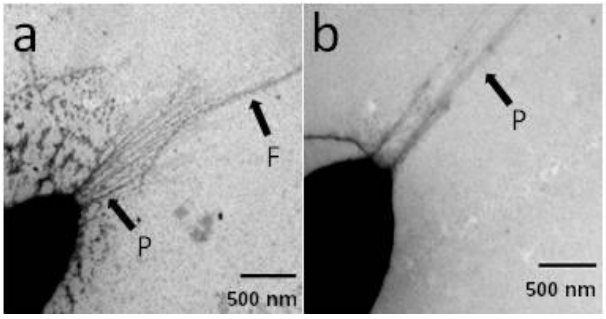

Figure 3-25: Electron micrograph negative stain of *R. capsulatus* strain cells isolated from the glass-agar interface of Petri plates: (a) wild type B10 strain exhibiting splayed appendages; (b) *flaA* mutant bKSDF strain exhibiting bundled appendages. 'F' indicates flagellar filament, 'P' indicates pilus-like appendage.

3.4.2. Peptide sequence analysis of extracellular proteins

The sequences of surface-expressed proteins were investigated by tandem mass spectroscopy (MS-MS) in hopes of identifying peptides from a pilus or some other motility structure. Samples of *flaA* mutant strain bKSDF were treated in two ways: 1) by heat shock to release cellular appendages

(Karkhanis, 1983); and 2) vortex agitation to mechanically shear cellular appendages (Dodd and Eisenstein, 1982; Salit et al., 1983). These methods were further processed by two methods: A) precipitation of liquid culture supernatant (with trichloroacetic acid); B) concentration of liquid sample by molecular cut-off filter (10-kDa). Proteins resolved by SDS-PAGE yielded approximately 40 bands in total from the 3 treatments. The T4P consists of repeating pilin monomers polymerized into a thin ~6 nm diameter filament of up to several μm in length (Craig et al., 2004). Pili occasionally do not fully dissociate in SDS-PAGE systems, forming ladder-like banding patterns (Ho et al., 1990). Ladder-like banding patterns were observed when *R. capsulatus* proteins were separated by SDS-PAGE (Figure 3-26). From Method 1A band #6 was chosen for sequencing because it was part of a ladder-like pattern. Bands #15 and #19 from Method 2B were selected for sequencing because they were the smallest and largest clearly resolved bands, respectively. From Method 2A Band #29 was chosen as a control sample, because it appeared to consist of a clearly resolved single band with minimal degradation that should have yielded successful peptide sequencing and protein identification. Polar pilin proteins range from 5 kDa to 20 kDa (Burrows, 2008) so the unresolved smear #33 from Method 2A was chosen because it was a complex low molecular weight band that might contain pili or degradation products from pili and other cell surface proteins (Figure 3-26).

After MS-MS, a total of 1074 peptide sequences were identified. Of these, 84 peptides were mapped to ORFs in the *R. capsulatus* genome sequence (see **APPENDIX A**, Table A-5). Unmapped peptides may have been components of the complex medium (yeast extract, peptone) used to culture cells. Of the 84 *R. capsulatus* peptides, only one mapped to a gene encoding a putative homologue of a bacterial pilus component. This single peptide provided 3% coverage of the predicted amino acid sequence of RCC0356 (annotated as a conserved hypothetical protein), which was predicted to contain a putative N-terminal fimbrial low molecular weight protein (Flp) pilus TadG protein domain (COG4961)

(de Bentzmann et al., 2006) (Table 3-5). Because of the presence of a putative TadG domain, this protein encoded by RCC0356 might have been a component of a T4P.

Bands # 6 and #15 were the porin encoded by RCC00259 while bands # 19 and # 29 were unassigned peptides. All other peptides were identified in band # 33. This approach was not pursued further because of the large number (~61%) of peptide assignments to cytoplasmic proteins, which indicated that these samples were not highly enriched for surface-expressed proteins (see **APPENDIX A**, Table A-5). This may have been the result of cell lysis during culture growth and/or vortex agitation.

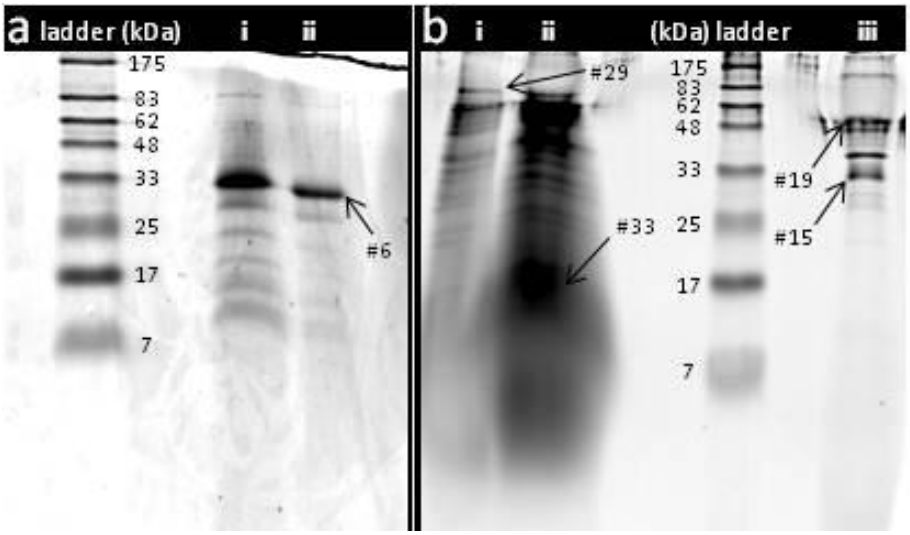

Figure 3-26: Cell surface proteins from *flaA* mutant strain bKSDF cells isolated in the interstitial interface of agar medium on borosilicate Petri plates resolved by SDS-PAGE and visualized with Coomassie staining: (a) heat shock release treated samples; (b) vortex agitation release treated samples; (a-i) 30 μL heat shock precipitate; (a-ii) 5 μL heat shock precipitate; (b-i) 5 μL TCA precipitated supernatant; (b-ii) 30 μL TCA precipitated supernatant; (b-iii) 10 kDa molecular weight cut-off filtered TCA precipitated supernatant.

Table 3-5: Alignment comparison of the *R. capsulatus* putative pilus anchor protein to TadG-domain proteins.

Gene	Gene product	Length (aa)	TadG-domain homologue	Identity (%)	E value [(c)]
RCC0356	putative pilus anchor	628	TadG, *Fulvimarina pelagi* (ZP_01438428) [(a)]	21	$5e^{-18}$
			TadG, *A. actinomycetemcomitans* (AAP43994) [(b)]	15	$2e^{-10}$

(a) Hypothetical protein annotated by bioinformatic domain conservation (gene product name, species, and NCBI accession number).

(b) Gene product name, species (NCBI accession number).

(c) Top E-value scores from local pairwise protein alignment BLASTp.

3.4.3. Bioinformatics analyses of putative pilus biogenesis clusters and predicted gene homologues

The region of the *R. capsulatus* chromosome from base pair 533727 to 544504 is predicted to encode 12 proteins (ORF RCC00499 through ORF RCC00510, transcribed in the same orientation) (Figure 3-27). BLASTp analyses and global alignment comparisons to the corresponding type IV pili (T4P) proteins of *Actinobacillus actinomycetemcomitans*, *C. crescentus*, and *P. aeruginosa* indicated that ORF RCC00499 through RCC00510 may encode homologues of proteins involved in the biogenesis and function of bacterial pili (Bernard et al., 2009). The predicted proteins from *R. capsulatus* to known T4P proteins had low % identity alignments, so protein domains identified in the putative *R. capsulatus* proteins were also considered. The local alignment scores (E values) of the predicted protein sequences to the top protein domains were also provided (Table 3-6).

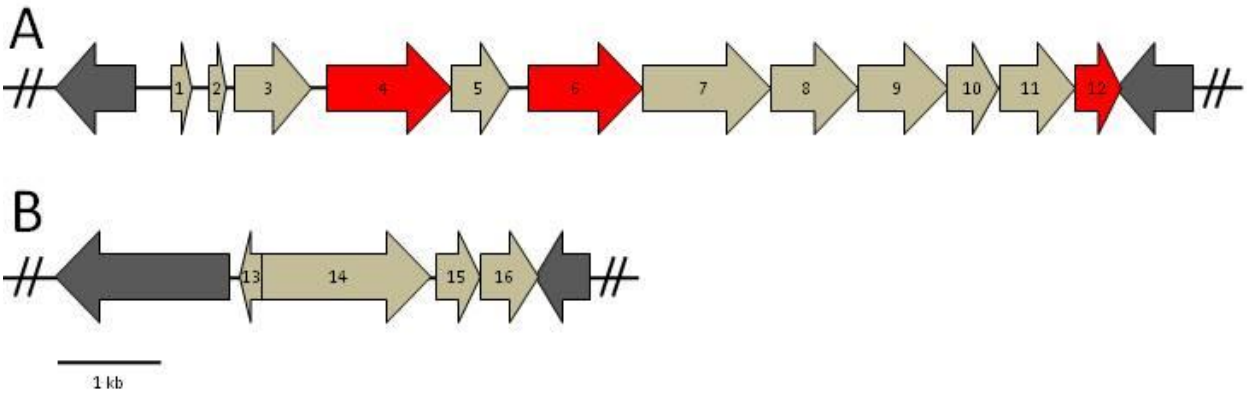

Figure 3-27: Genomic loci encoding putative Flp/Tad pilus genes in *R. capsulatus* discovered by peptide sequencing and BLAST alignment with characterized Flp/Tad secretins and assembly ATPases. (A) primary putative pilus locus: (1) RCC00499 *flp1* pilin; (2) RCC00500 *flp2* pilin; (3) RCC00501 *cpaB* outer membrane assembly protein; (4) RCC00502 *cpaC* secretin; (5) RCC00503 OmpA-family protein; (6) RCC00504 *cpaE* localization ATPase; (7) RCC00505 *cpaF* assembly ATPase; (8) RCC00506 *tadB* inner membrane assembly protein; (9) RCC00507 *tadC* inner membrane assembly protein; (10) RCC00508 TPR-domain assembly protein; (11) RCC00509 TPR-domain assembly protein; (12) RCC00510 *cpaA* prepilin peptidase. (B) secondary putative pilus locus: (13) protein of unknown function; (14) RCC03056 *tadG* pilus anchor; (15) RCC03057 *tadE* pseudopilin; (16) RCC03058 protein of unknown function. Genes that were knocked out are highlighted in red, genes flanking the pilus clusters are highlighted in dark grey.

Table 3-6: Annotation of the *R. capsulatus* putative pilus gene cluster product amino acid sequences.

Gene	Gene product	Length (aa)	Domain or characterized homologue [(a)]	Identity (%)	E value[(b)]
RCC00498	lytic transglycosylase	291	Lytic Transglycosylase Goose Egg-White Lysozyme domain (cl00222)		$6.7e^{-24}$
RCC00499	hypothetical protein	64			
RCC00500	hypothetical protein	55			
RCC00501	assembly component	289	CpaB domain (COG3745)		$5.5e^{-22}$
			CpaB, *C. crescentus* (AAF40191)	26	
RCC00502	secretion portal	469	CpaC secretin domain (COG4964)		$8.0e^{-88}$
			RcpA, *P. aeruginosa* (AAG07692)[(c)]	32	
			CpaC, *C. crescentus* (NP_421739)	31	
			RcpA, *A. actinomycetemcomitans* (AAP43985)	27	
			PilQ, *P. aeruginosa* (AAP22531)	16	
			OmpA, *E. coli* (ABJ00366)	6	

Gene	Gene product	Length (aa)	Domain or characterized homologue [a]	Identity (%)	E value[b]
RCC00503	outer membrane protein	216	OmpA_C-like domain (cd07185)		$1.9e^{-21}$
RCC00504	localization / assembly component	421	CpaE ATPase domain (COG4963)		$3.4e^{-26}$
			CpaE, *C. crescentus* (AAF40194)	20	
RCC00505	assembly ATPase	486	CpaF ATPase domain (COG4962)		$7.8e^{-108}$
			CpaF/TadA, *C. crescentus* (AAF40195)	46	
			TadA, *A. actinomycetemcomitans* (AAP43988)	40	
			TadA, *P. aeruginosa* (NP_252992)[c]	38	
			PilT, *P. aeruginosa* (NP_249086)	19	
			PilB, *P. aeruginosa* (NP_253216)	18	
			PilU, *P. aeruginosa* (AAA25965)	17	
RCC00506	inner membrane assembly component	322	TadB domain (COG4965)		$4.8e^{-67}$
			TadB, *C. crescentus* (AAF40196)	26	
RCC00507	inner membrane assembly component	337	TadC domain (COG2064)		$4.4e^{-20}$
			TadC, *P. aeruginosa* (AAG07688)[c]	24	
RCC00508	TPR protein	187	Tetratricopeptide repeat domain (cd00189)		$3.3e^{-8}$
			TadD, *P. aeruginosa* (NP_252989) [c]	20	
RCC00509	TPR protein	286	Tetratricopeptide repeat domain (cd00189)		$9.7e^{-3}$
			TadD, *C. crescentus* (NP_421732)	22	
RCC00510	peptidase	167	A24 peptidase domain (PF01478)		$9.3e^{-7}$
			CpaA, *C. crescentus* (AAF40190)	27	
			FppA, *P. aeruginosa* (AAG07683)[c]	23	
			TadV, *A. actinomycetemcomitans* (ABG45872)	21	
			PilD, *P. aeruginosa* (AAG07916)	15	
			LepA, *E. coli* (YP_001731497)	5	
RCC00511	erythritol kinase	286	Erythritol kinase domain (PRK14608)		$8.8e^{-65}$
RCC03055	DNA primase	654	DNA primase domain (PRK05667)		$5.5e^{-158}$
			DnaG, E. Coli (AAA24600)	30	
	Hypothetical protein	61			

Gene	Gene product	Length (aa)	Domain or characterized homologue [(a)]	Identity (%)	E value[(b)]
RCC03056	anchor protein	628	TadG domain (COG4961)		$8.5e^{-3}$
			TadG, *A. actinomycetemcomitans* (AAP43994)	15	
RCC03057	pseudopilin	152	TadE, *C. crescentus* (YP_002518419)	19	
RCC03058	hypothetical protein	210			
RCC03059	transcriptional regulator	195	AcrR transcriptional regulator domain (COG1309)		$1.2e^{-4}$
			TetR_N family domain (Pfam00440)		$4.3e^{-4}$

(a) Characterized protein domain (domain name, domain number) or homologue of experimentally verified function (gene product name, species, NCBI accession number). Cluster I and cluster II are separated by a dashed line.

(b) Top E-value scores from local pairwise protein domain alignment BLASTp.

(c) Hypothetical protein characterized by sequence similarity and domain conservation.

In ascending order of gene annotation number, the sequence predictions were: RCC00499, hypothetical protein; RCC00500, hypothetical protein; RCC00501, *cpaB* outer membrane assembly factor; RCC00502, *cpaC* secretin portal protein (Skerker and Shapiro, 2000); RCC00503, OmpA-domain outer membrane protein; RCC00504, FrtZ/MinD-like pilus localization/assembly component; RCC00505, *cpaF* pilus assembly ATPase; RCC00506, *tadB* pilus inner membrane assembly component; RCC00507, *tadC* pilus inner membrane assembly component; RCC00508 and RCC00509, tetratricopeptide repeat assembly proteins; and RCC00510, a putative aspartyl-peptidase domain *cpaA* prepilin peptidase (Skerker and Shapiro, 2000). The locus was flanked on one side by ORF RCC00498 that was predicted to encode a lytic transglycosylase, perhaps performing cell wall rearrangements required for pilus extrusion (Koraimann, 2003). The other flanking sequence, ORF RCC00511, was predicted to encode an erythritol kinase required for isoprenoid biosynthesis. The *R. capsulatus* amino acid sequences were the reciprocal best hits to the highest % identity alignment protein sequences from the other organisms (Table 3-6), unless otherwise stated.

The first ORF in the Flp pilus clusters of *A. actinomycetemcomitans* (Inoue et al., 1998), *C. crescentus* (Skerker and Shapiro, 2000), and *P. aeruginosa* (de Bentzmann et al., 2006) are pilin genes. However, the T4bP pilin sequences from these organisms did not share significant similarity with proteins of *R. capsulatus*, and there are no *pilA* pilin homologues in *R. capsulatus*. Furthermore, BLASTp alignments with the NCBI non-redundant protein database using the first two *R. capsulatus* protein sequences (RCC00499 and RCC00500) in the putative pilus cluster returned only conserved hypothetical proteins. Although T4aP and T4bP proteins share little sequence similarity in the C-terminal region, both have N-terminal class III signal peptides (SP), of which the T4bP class is longer (Craig et al., 2003). Analysis of the *R. capsulatus* genome for genes encoding the T4P SPs (generously done by Dr. M. Pohlschröder) identified 5 ORFs encoding putative class III SPs (Michaelis and Beckwith, 1982). Two of these ORFs were the first two genes in the putative Flp pilus cluster. Thus it was thought that RCC00499 and RCC00500 possibly encoded pilins.

The OmpA-domain protein (RCC00503) may have a role in mediating pilus/secretin interactions with the peptidoglycan cell wall (Wang, 2002), and the FrtZ/MinD-like ATPase protein may localize the pilus apparatus to the cell poles (Mignot et al., 2005). The predicted inner membrane TadB and TadC proteins may drive pilin monomers into the growing pilus structure (Craig et al., 2006; Tomich et al., 2007). The tetratricopeptide repeat domain proteins (TPR) had no discernable similarity to known Flp/Tad pilus components, and were not the reciprocal hits to TadD proteins from *P. aeruginosa* or *C. crescentus*. However, TPR domains are often found in proteins that assist in the assembly of protein complexes (D'Andrea and Regan, 2003). Perhaps proteins encoded by RCC00508 and RCC00509 mediate pilus complex assembly by ensuring components are within close proximity to one another. The protein encoded by RCC00510 was also not the reciprocal hits to prepilin peptidase amino acid sequences from the organisms listed in Table 3-6, although the predicted peptidase domain and genomic location indicated it might encode a prepilin peptidase.

A separate putative pilus-related locus (Figure 3-27B) was discovered in chromosomal base pair 3248082 to 3251201 (predicted to encode 2 pilus-related proteins). In ascending order of gene annotation number, the ORFs were predicted (by BLAST analysis) to encode: RCC03056, *tadG* Flp pilus anchor protein; RCC03057, *tadE* pilus initiation pseudopilin (Durand et al., 2005; Tomich et al., 2006); and RCC03058, protein of unknown function. However, RCC03056 and RCC03057 were not the reciprocal best hits of the T4P amino acid sequences listed in Table 3-6, and might not have encoded components of a pilus. This locus was flanked on one side by ORF RCC03055, predicted to encode a DNA primase for RNA synthesis; and on the other side by ORF RCC03059, predicted to encode a TetR family transcriptional regulator.

This information was used to design knockouts of putative homologues predicted to encode conserved components of the pilus structure and function, to investigate whether these genes were involved in mediating movements in the glass-agar interstice.

3.4.4. Mutagenesis of a predicted pilus secretin

One of the genes (RCC00502) in the Flp/Tad clusters was annotated as an outer membrane secretion protein. T4P secretins form a gated, hexameric homomultimer portal complex that allows the extrusion of the assembled pilus through the peptidoglycan wall and outer membrane (Bayan et al., 2006). T4P secretins differ significantly in structure and size when compared to classical outer membrane proteins with higher β-strand membrane-spanning structure (Chami et al., 2005; Bayan et al., 2006). Therefore, alignments were compared between the putative protein encoded by the gene RCC00502 (Figure 3-27) and: the T4aP PilQ and T4bP RcpA secretins of *P. aeruginosa* strain PA01 (Martin et al., 1993; de Bentzmann et al., 2006); the T4bP CpaC secretin of *C. crescentus* strain CB15 (Skerker and Shapiro, 2000); the T4bP RcpA secretin of *A. actinomycetemcomitans* (Haase et al., 1999); and the classical OmpA protein of *E. coli* strain DH10B (Wang, 2002). As summarized in Table 3-6, the highest-

scoring alignments (31-32 % identity) occurred with the RcpA sequences, whereas the OmpA alignment was confined to a small conserved domain. Thus RCC00502 was predicted to encode an orthologue of the T4P secretin protein CpaC (Viollier et al., 2002), which is thought to be responsible for extrusion of a fimbrial low-molecular weight protein (Flp)/tight adherence (Tad) T4b pilus, based on this sequence analysis and the genomic context (see section **3.4.3**) of RCC00502. The potential role of this putative outer membrane pilus secretin protein in solid substrate motility was investigated, by creating a strain deficient in the gene for this protein.

RCC00502 was disrupted by inserting an antibiotic resistance marker using the flagellin-deficient strain bKSDF as a background, to create the strain bKSDFcpaC (Table 2-1). Strain bKSDFcpaC was impaired in movement outward from the inoculation stab in soft agar (Figure 3-28c), which confirmed a lack of flagellar motility due to the *flaA* deletion. The bKSDFcpaC mutant moved away from the point of inoculation in the interstice of plates, and therefore retained flagellum-independent motility (Figure 3-28e).

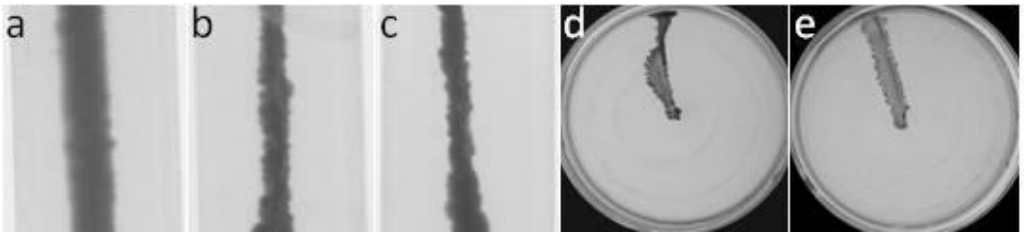

Figure 3-28: Representative soft agar tubes or agar plates inoculated with *R. capsulatus* cells incubated with halogen white light. Tubes were illuminated with incident light from the side, whereas stab-plate illumination was from the top of the image: (a) wild type strain B10 soft agar stab; (b) *flaA* mutant strain bKSDF soft agar stab; (c) *flaA/cpaC* mutant strain bKSDFcpaC soft agar stab; (d) *flaA* mutant strain bKSDF stab-plate; (e) *flaA/cpaC* mutant strain bKSDFcpaC stab-plate.

3.4.5. Mutagenesis of a predicted pilus assembly ATPase

Another gene (RCC00505) in the putative Flp/Tad clusters (Figure 3-27) was annotated as a secretory protein kinase. The putative protein has a Walker-type ATP binding site containing a Walker A

triphosphate binding motif and a Walker B Mg^{+2} coordination motif (Minamino et al., 2006), as well as hexameric interface sites characteristic of AAA+ ATPases associated with cellular activities (Kaiser, 2000). The RCC00505 sequence was compared by BLASTp and complete sequence alignments to T4P ATPases: the CpaF/TadA protein of *C. crescentus* strain CB15 (Viollier and Shapiro, 2003; Entcheva-Dimitrov and Spormann, 2004); the PilB, PilT, PilU, and TadA proteins of *P. aeruginosa* strain PA01 (Chiang et al., 2005; de Bentzmann et al., 2006); and the TadA protein of *A. actinomycetemcomitans* (Bhattacharjee et al., 2001). As summarized in Table 3-6, the highest-scoring alignments (40-46% identity) occurred with TadA sequences. Thus RCC00505 was predicted to encode an orthologue of the T4P ATPase motor protein CpaF (Tomich et al., 2007) , which is thought to be responsible for the assembly of a Flp/Tad T4b pilus (Mattick, 2002; Jakovljevic et al., 2008), and which is consistent with the genomic context (see section **3.4.3**) of RCC00505. The potential role of this putative pilus ATPase protein in solid substrate motility was investigated by creating a strain deficient in the gene for this protein.

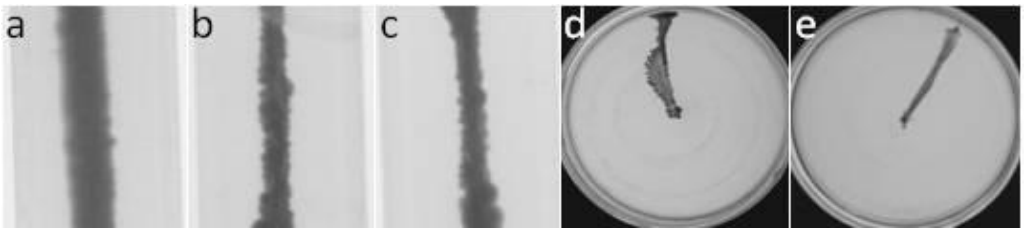

Figure 3-29: Representative soft agar tubes or agar plates inoculated with *R. capsulatus* cells incubated with halogen white light. Tubes were illuminated with incident light from the side, whereas stab-plate illumination was from the top of the image: (a) wild type strain B10 soft agar stab; (b) *flaA* mutant strain bKSDF soft agar stab; (c) *flaA/cpaF* mutant strain bKSDFcpaF soft agar stab; (d) *flaA* mutant strain bKSDF stab-plate; (e) *flaA/cpaF* mutant strain bKSDFcpaF stab-plate.

RCC00505 was disrupted by a combination of a deletion and insertion of an antibiotic resistance marker, using the flagellin-deficient strain bKSDF as a background, to create the strain bKSDFcpaF (Table 2-1). Strain bKSDFcpaF was impaired in movement outward from the inoculation stab in soft agar

(Figure 3-29c), which confirmed a lack of flagellar motility due to the *flaA* deletion. The bKSDFcpaF mutant moved away from the point of inoculation in the interstice of plates, toward white light, and therefore retained flagellum-independent motility (Figure 3-29e).

3.4.6. Mutagenesis of a predicted pilus prepilin peptidase

A third gene (RCC00510) in the putative Flp/Tad clusters (Figure 3-27) was annotated as a hypothetical membrane spanning protein. The putative protein was predicted to contain an aspartic-type A24SA peptidase family domain, and so alignments were performed with the T4bP CpaA signal peptidase of *C. crescentus* (Skerker and Shapiro, 2000), the *P. aeruginosa* T4aP PilD and T4bP FppA signal peptidases (Nunn and Lory, 1991; de Bentzmann et al., 2006); the *A. actinomycetemcomitans* T4bP TadV peptidase protein (Tomich et al., 2006), and the LepB Type I signal peptidase of *E. coli* (Wolfe et al., 1983). All these sequences appeared to be widely divergent and the best alignment (27% identity) occurred against the T4bP class III peptidase CpaA of *C. crescentus* (Table 3-6). Given the genomic context (see section **3.4.3**) and sequence alignments, RCC00510 may encode an orthologue of a Flp/Tad T4bP class III prepilin signal peptide (SP) endopeptidase CpaA. Prepilin peptidases process the immature prepilin to the mature pilin protein by cleaving a short N-terminal fragment of the peptide (Dev and Ray, 1990). Removal of the SP generates the mature pilin protein that is polymerized into the pilus (Strom and Lory, 1992). The potential role of this putative *R. capsulatus* peptidase protein in solid substrate motility was investigated by creating a strain deficient in the gene for this protein.

RCC00510 was disrupted by inserting an antibiotic resistance marker using the flagellin-deficient strain bKSDF as a background, to create the strain bKSDFcpaA (Table 2-1). Strain bKSDFcpaA was impaired in movement outward from the inoculation stab in soft agar (Figure 3-30c), which confirmed a lack of flagellar motility due to the *flaA* deletion. The bKSDFcpaA mutant moved away from the point of

inoculation in the interstice of plates, toward white light, and therefore retained flagellum-independent motility (Figure 3-30e).

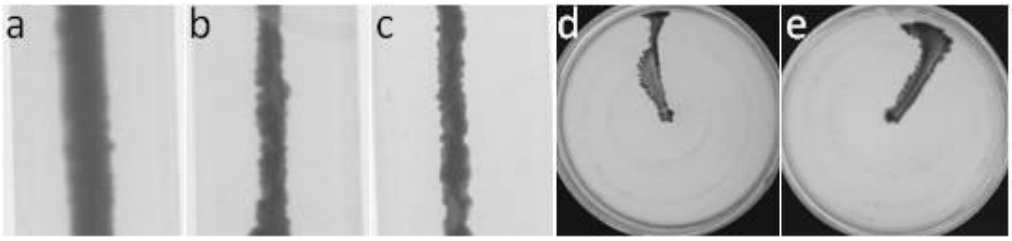

Figure 3-30: Representative soft agar tubes or agar plates inoculated with *R. capsulatus* cells incubated with halogen white light. Tubes were illuminated with incident light from the side, whereas stab-plate illumination was from the top of the image: (a) wild type strain B10 soft agar stab; (b) *flaA* mutant strain bKSDF soft agar stab; (c) *flaA/cpaA* mutant strain bKSDFcpaA soft agar stab; (d) *flaA* mutant strain bKSDF stab-plate; (e) *flaA/cpaA* mutant strain bKSDFcpaA stab-plate.

Using the method described in section **2.17**, the distribution of the direction of movement in bKSDFcpaC, bKSDFcpaF, and bKSDFcpaA mutants in illuminated stab-plates was compared to the parental *flaA* mutant strain bKSDF (Table 3-7). Statistical analysis showed an insignificant difference in the distribution of angular direction of bKSDFcpaC and bKSDFcpaA, when compared to bKSDF controls. The distribution of angular direction of bKSDFcpaF showed less deviation than bKSDF controls (Table 3-7). These results indicated that these putative pilus proteins were not required for photoresponsive solid substrate motility.

Table 3-7: Average cell movement distances and directions in stab-plate tests of putative *R. capsulatus* pilus mutants.

Strain	Strain name	Average distance travelled [(a)] (mm)	Average angular motility direction [(b)] (°)	P_Z [(c)]	# Samples
flaA	bKSDF	33 (16)	6 (76)		273
flaA/*cpaC*	bKSDFcpaC	30 (20)	-18 (97)	0.11	41
flaA/*cpaF*	bKSDFcpaF	42 (10)	-15 (42)	0.031 *	26
flaA/*cpaA*	bKSDFcpaA	40 (14)	-10 (69)	0.54	28

(a) Taxis distance as measured from the point of inoculation to farthest point of visible cell growth, with standard deviation in parentheses.

(b) Taxis direction from the point of inoculation to the farthest point of visible cell growth, with standard deviation in parentheses. 0° indicates movement directly toward the light source, and ± 180° indicates movement directly away from the light.

(c) Two-tailed two-independent sample Wilcoxon rank sum test of significant difference compared to wild type bKSDF samples. For a >0.95 probability that the movement was different from controls, $P_Z < 0.05$. The asterisk indicates where $P_Z < 0.05$.

3.5. Experiments related to the possibility of gliding-mediated motility

Bacterial flagellum contributions (see section **3.3**) and genes encoding proteins predicted to be required for pilus biogenesis and function (see section **3.4**) were demonstrated to be unnecessary for cell movements in the glass-agar interstice of borosilicate Petri plates. Therefore, the role of gliding-mediated mechanism contributions to solid substrate cell movements was considered.

Known gliding motility proteins identified in *M. xanthus* (Youderian et al., 2003; Yang et al., 2004), *F. Johnsoniae* (Braun et al., 2005; Nelson et al., 2007; Nelson et al., 2008; Sato et al., 2010; Rhodes et al., 2011), *Synechococcus* (McCarren, 2005), and *M. mobile* (Adan-Kubo et al., 2006; Nonaka et al., 2010), as well as bacterial cytoskeletal elements (Shih and Rothfield, 2006), were compared to the *R. capsulatus* proteome in an attempt to identify potential gliding motility genes (Table 3-8). Sequence

identity was low for most protein alignments, ranging from 1 to 39%, and only 8 of the 59 query sequences were reciprocal best hits. Based on reciprocal best hit sequence conservation, the only likely candidate for mutagenesis was the *ctpA* gene encoded by RCC00075. It was plausible that a gliding motility mechanism might interact with the *R. capsulatus* cytoskeleton, so the presence of bacterial cytoskeletal element proteins were also considered (Table 3-8).

Table 3-8: Alignment analysis search for putative gliding motility homologues in *R. capsulatus*.

Gene	Gene product	Length (aa)	Domain or characterized homologue [(a)]	Identity (%)	E value [(b)]
tolQ	biopolymer transport protein	234	AglR, *M. xanthus* (AAO22892)	10	$3e^{-10}$
RCC00757	alpha/beta fold family hydrolase	246	AglS, *M. xanthus* (YP_634977)	16	$8e^{-1}$
RCC02069	TPR repeat domain-containing protein	617	AglT, *M. xanthus* (AAO66317)	16 *	$3e^{-5}$
trpB	tryptophan synthase, beta chain	402	AglU, *M. xanthus* (AAO22920)	11	$7e^{-1}$
exbD	biopolymer transport protein	168	AglV, *M. xanthus* (AAO22857)	39	$6e^{-23}$
tolB	translocation protein	437	AglW, *M. xanthus* (AAO22855)	30	$3e^{-44}$
tolQ	biopolymer transport protein	234	AglX, *M. xanthus* (AAO22858)	28	$3e^{-24}$
RCC00167	cell wall glycosyl transferase	2043	AglZ, *M. xanthus* (AAR39422)	13	$2e^{-17}$
amiC	N-acetylmuramoyl-L-alanine amidase	405	AgmA, *M. xanthus* (AAO66323)	18	$1e^{-19}$
rhlE	ATP-dependent RNA helicase	448	AgmB, *M. xanthus* (AAO66303)	9	1.2
RCC03330	glutamyl-tRNA(Gln) amidotransferase, subunit A	438	AgmC, *M. xanthus* (AAO22852)	6	$3e^{-1}$
trpS	tryptophanyl-tRNA synthetase	350	AgmD, *M. xanthus* (AAO22871)	37	$7e^{-52}$
parA	chromosome-partitioning protein	273	AgmE, *M. xanthus* (AAO22874)	27	$2e^{-32}$
rluD	ribosomal large subunit pseudouridine synthase	347	AgmF, *M. xanthus* (AAO22876)	36	$1e^{-48}$

Gene	Gene product	Length (aa)	Domain or characterized homologue [(a)]	Identity (%)	E value [(b)]
pldB	lysophospholipase L2	312	AgmG, *M. xanthus* (AAO22879)	4	$2e^{-1}$
pldB	lysophospholipase L2	312	AgmH, *M. xanthus* (AAO22882)	21 *	$2e^{-4}$
cobs	cobaltochelatase subunit	324	AgmI, *M. xanthus* (AAO22887)	5	$4e^{-1}$
dacC1	D-alanyl-D-alanine carboxypeptidase	538	AgmJ, *M. xanthus* (AAO22906)	10	2.5
RCC00512	TPR repeat domain-containing protein	572	AgmK, *M. xanthus* (AAO22907)	7	$8e^{-2}$
leuB	3-isopropylmalate dehydrogenase	369	AgmL, *M. xanthus* (AAO66296)	24	$3e^{-15}$
hom	homoserine dehydrogenase	432	AgmM, *M. xanthus* (AAO66299)	14	$8e^{-1}$
mutM	formamidopyrimidine-DNA glycosylase	281	AgmN, *M. xanthus* (AAO66306)	18	$5e^{-1}$
RCC01921	hypothetical protein	286	AgmO, *M. xanthus* (AAO66309)	12	1.4
tetA	tetracycline resistance protein	404	AgmP, *M. xanthus* (AAO66313)	31 *	$3e^{-24}$
RCC00158	M10 family peptidase	586	AgmQ, *M. xanthus* (AAO66326)	7 *	$8e^{-8}$
RCC02662	class II aldolase	677	AgmR, *M. xanthus* (AAO66301)	9	$1e^{-1}$
paaF	enoyl-CoA hydratase	258	AgmS, *M. xanthus* (AAO66327)	31	$6e^{-20}$
RCC01681	aminodeoxychorismate lyase family protein	390	AgmT, *M. xanthus* (AAO66328)	18 *	$6e^{-11}$
RCC01813	AMP-dependent synthetase/ligase	512	AgmU, *M. xanthus* (AAO66314)	8	2.4
RCC00697	hypothetical protein	186	AgmV, *M. xanthus* (AAO66319)	5	3.8
ctpA	C-terminal processing peptidase	454	AgmW, *M. xanthus* (AAO22866)	39 *	$1e^{-85}$
RCC03169	zinc finger domain-containing protein	433	AgmX, *M. xanthus* (AAO22908)	21	$8e^{-4}$
dctB	C4-dicarboxylate transport sensor protein	599	AgmZ, *M. xanthus* (AAO66297)	7	$1e^{-1}$
RCC02545	sensor histidine kinase/response regulator receiver protein	877	CglB, *M. xanthus* (AAB86642)	9	$3e^{-1}$
RCC02025	polyols ABC transporter, ATP-binding protein	332	MglA, *M. xanthus* (AAA25389)	15	$4e^{-1}$

Gene	Gene product	Length (aa)	Domain or characterized homologue [a]	Identity (%)	E value [b]
lnt	apolipoprotein N-acyltransferase	511	MglB, *M. xanthus* (AAA25388)	4	$8e^{-2}$
RCC00012	ABC transporter ATP-binding protein	305	GldA, *F. johnsoniae* (AAC19751)	28	$2e^{-40}$
glpK2	glycerol kinase	490	GldB, *F. johnsoniae* (AAD42888) GldD, *F. johnsoniae* (AAG00560)	8	$9e^{-2}$
RCC01863	hypothetical protein	449	GldE, *F. johnsoniae* (AAG00559)	27	$3e^{-48}$
RCC00619	ABC transporter permease	372	GldF, *F. johnsoniae* (AAK63181)	13	$3e^{-2}$
RCC00597	hypothetical protein	699	GldG, *F. johnsoniae* (AAK63182)	9	$4e^{-1}$
sufS1	cysteine desulfurase	406	GldH, *F. johnsoniae* (AAM92019)	7	$5e^{-1}$
lypB	lipoyltransferase	220	GldI, *F. johnsoniae* (AAM92025)	4	6.5
gap3	glyceraldehyde-3-phosphate dehydrogenase	333	GldJ, *F. johnsoniae* (AAM92031)	5	$9e^{-2}$
RCC00632	hypothetical protein	543	GldK, *F. johnsoniae* (AAW78679)	12	$6e^{-3}$
RCC00812	hypothetical protein	367	GldL, *F. johnsoniae* (AAW78680)	13	$1e^{-1}$
gph2	phosphoglycolate phosphatase	224	GldM, *F. johnsoniae* (AAW78681)	11	1.3
RCC02788	hypothetical protein	1037	GldN, *F. johnsoniae* (AAW78682)	4	$3e^{-1}$
ugpA	sn-glycerol-3-phosphate transport system permease protein	314	PorT, *F. johnsoniae* (ABQ04498)	12	1.4
fliF	flagellar M-ring protein	566	SprA, *F. johnsoniae* (AAW49009)	5	$3e^{-2}$
mreC	rod shape-determining protein	299	SprB, *F. johnsoniae* (ABL60886)	1	1.5
paaK	phenylacetate-CoA ligase	406	SprC, *F. johnsoniae* (ABL60884)	15	$3e^{-1}$
tkt2	transkelotase	672	SprD, *F. johnsoniae* (ABL60885)	10	$3e^{-1}$
RCC01362	hemolysin-type calcium-binding repeat protein	607	SwmA, *Synechococcus* (AAQ13434)	24	$5e-^{13}$
RCC01900	hemolysin-type calcium-binding repeat protein	2065	SwmB, *Synechococcus* (NP_ 897046)	5	$3e^{-4}$
RCC01756	2-isopropylmalate synthase/homocitrate synthase	540	Gli349, *M. mobile* (BAC23068)	3	4.5

Gene	Gene product	Length (aa)	Domain or characterized homologue [(a)]	Identity (%)	E value [(b)]
rnpA	ribonuclease P	162	Gli521, *M. mobile* (BAC23069)	1 *	6.6
RCC01231	ubiquinone biosynthesis hydroxylase	404	P1, *M. pneumoniae* (CAB37298)	8 *	$6e^{-1}$
mreB	rod shape-determining protein	409	MreB, *M. xanthus* (YP_ 634906)	47 *	$2e^{-105}$
			MreB, *P. aeruginosa* (AAG07869)	49 *	$5e^{-108}$
ftsZ	cell division protein	575	FtsZ, *M. xanthus* (YP_ 633736)	31 *	$8e^{-70}$
			FtsZ, *P. aeruginosa* (AAA95993)	33 *	$5e^{-71}$
mipZ	chromosome partitioning protein	269	MinD, *P. aeruginosa* (AAG06632)	20	$4e^{-5}$

(a) Homologue of experimentally verified function (gene product name, species, NCBI accession number). Gliding motility genes and bacterial cytoskeletal element genes are separated by a dashed line. Asterisks indicated cases where the proteins were reciprocal best hits.

(b) Top E-value scores from local pairwise protein alignment BLASTp.

3.5.1. Fluorescence labelling of extracellular amine groups

The possible role of secreted material in the solid substrate taxis of *R. capsulatus* was examined using fluorescence microscopy. Cells from stab-plate assay cultures were stained with the amino-specific dye Cy3, and placed as a suspension on a microscope slide under a coverslip. The Cy3 NHS-ester dye binds any available free amine group, such as on DNA bases, proteins, lipids, or sugars (Mujumdar et al., 1993).

A broad comet-like trail of Cy3-labelled material was observed behind three cells in a field of approximately 300 when visualized at 60 X magnification. One of these cells is presented in Figure 3-31a. This phenomenon was not found in a replicate experiment. The staining resembled that of polysaccharides secreted by *M. xanthus* cells during movement on a glass substrate (Wolgemuth et al., 2002). This suggested a Cy3-stained substance was excreted by *R. capsulatus* cells. This extrusion may have mediated solid substrate movement.

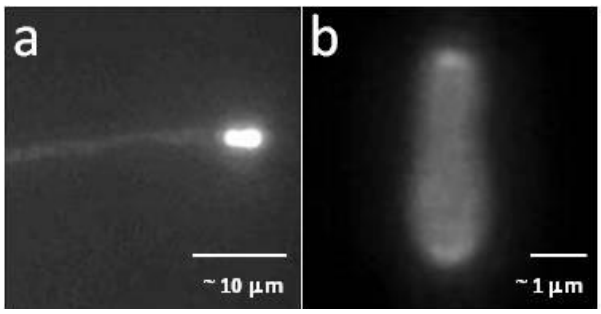

Figure 3-31: Possible free-amine containing material deposited during motility, as visualized by oil immersion microscopy: (a) fluorescence microscopy of Cy3 dye stained *flaA* mutant strain bKSDF; (b) fluorescence microscopy of Cy3 dye stained signal localization at cell poles of *flaA* mutant strain bKSDF.

Closer examination of cells indicated that the Cy3 signal was highest at the cell poles (Figure 3-31b), which indicated that *R. capsulatus* cells may have spatially distributed NHS-ester-reactive substrates in the cell. The concentrated signal at the poles may have been due to an increased accessibility of the dye to this region of the cell, although the concentrated Cy3-binding at cell poles may also have indicated that *R. capsulatus* cells are capable of a polar protein organization, possibly similar to the polar slime secretion mechanism proposed for *M. xanthus* movement (Yu and Kaiser, 2007).

3.5.2. Cell capsule effects on solid substrate motility

The bacterial cell capsules vary between species, and have been classified as a rigid, flexible, integral, or peripheral component. Rigid capsules exclude particles, flexible capsules do not exclude particles; integral capsules are intimately associated with the cell surface, and peripheral capsules may be shed into the surroundings (Costerton et al., 1981). *R. capsulatus* produces a thick polysaccharide envelope consisting of both a thick rigid integral capsule and an irregular peripheral capsule (Flammann et al., 1984).

I observed that centrifugation of aqueous culture B10-derived exponential phase cells yielded a dense pellet, whereas early stationary culture cells yielded a biphasic pellet: a compact phase below a loose one. Cell pellets from the natural isolate strain 37b4 (Biebl and Drews, 1969) consisted of only a

compact phase regardless of growth phase (data not shown). Strain 37b4 is considered to embody the characteristic features of wild type *R. capsulatus* strains, except that it is unencapsulated (Omar et al., 1983b; Brautigam et al., 1988) (Figure 3-32). The forgoing observations and information indicated that the peripheral capsule (and possibly also the integral capsule) of strain B10 and derivatives may be secreted during stationary phase. Contributions from the cell capsule to the solid substrate cell taxis were investigated using the natural isolate strain 37b4, which lacks a capsule, in comparison to capsule-replete strains.

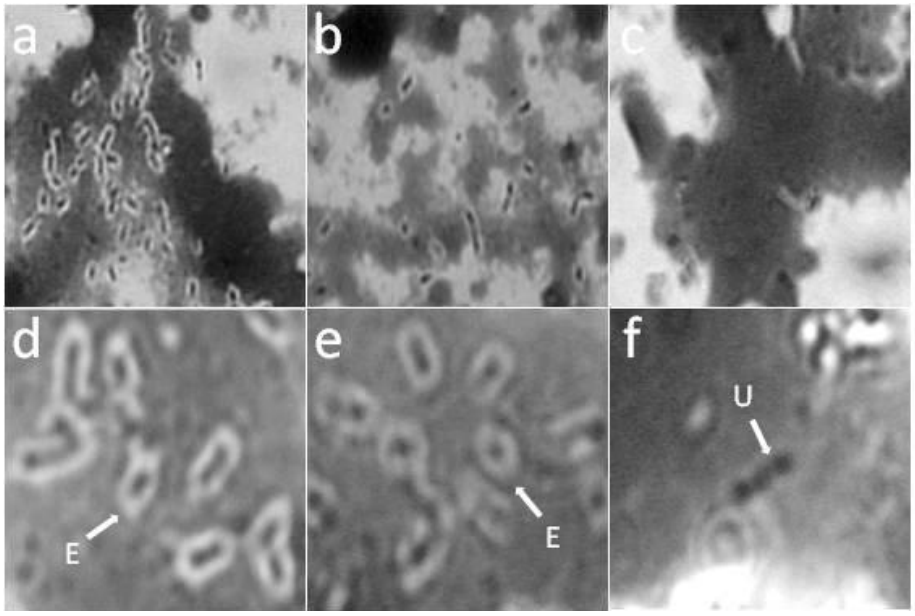

Figure 3-32: Bacterial capsule negative strain micrograph of *R. capsulatus* cells inoculated into aqueous cultures and incubated at 30 °C aerobically for 48 hrs in the dark: (a,d) wild type strain B10; (b,e) *flaA* mutant strain bKSDF cells; (c,f) natural isolate strain 37b4 cells. (a-c) 40 X magnification; (d-f) 100 X magnification. "E" indicates encapsulated cell, "U" indicates unencapsulated cell.

The motility of capsule-deficient strain 37b4 cells was mainly limited to the column of stab inoculation in soft agar stabs (Figure 3-33c); however 37b4 cells appeared to exhibit flagellar movement at small diffusive nodes along the stab column, possibly due to irregularities in the composition of the agar (Figure 3-33c inset). When the 37b4-derived *flaA* mutant strain KSDF37b4 was inoculated into soft

agar tubes, cell movement was limited to the column of stab inoculation and nodes along the stab column appeared less diffuse (Figure 3-33d), resembling the phenotype exhibited by the *flaA* mutant strain bKSDF (Figure 3-33b).

When inoculated into the interstice of plates, 37b4 cells moved away from the point of stab inoculation in a broad, diffusive manner similar to that of wild type strain B10, and therefore retained flagellum-dependent motility (Figure 3-33e,g). The capsule-deficient *flaA* mutant strain KSDF37b4 cells also moved away from the point of stab inoculation, but did so in the dense linear pattern characteristic of *flaA* mutant strain bKSDF, and therefore retained flagellum-independent motility (Figure 3-33f,h).

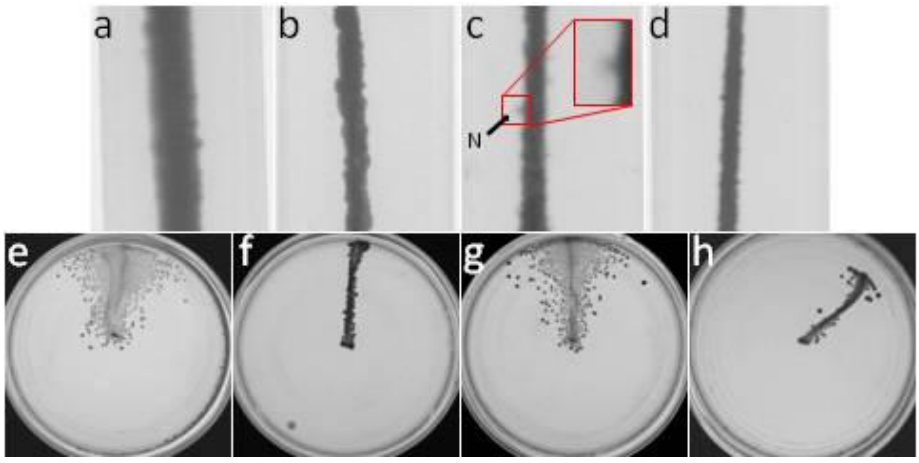

Figure 3-33: Representative soft agar tubes or agar plates inoculated with *R. capsulatus* cells incubated with halogen white light. Tubes were illuminated with incident light from the side, whereas stab-plate illumination was from the top of the image: (a) wild type strain B10 soft agar stab; (b) *flaA* mutant strain bKSDF soft agar stab; (c) capsule mutant strain 37b4 soft agar stab; (d) capsule-deficient *flaA* mutant strain KSDF37b4 soft agar stab; (e) wild type strain B10 stab-plate; (f) *flaA* mutant strain KSDF stab-plate; (g) capsule mutant strain 37b4 stab-plate; (h) capsule-deficient *flaA* mutant strain KSDF37b4 stab-plate. 'N' indicates node of flagellar swimming through soft agar.

Using the method described in section **2.17**, the distribution of the direction of movement of the capsule mutants in illuminated stab-plates was compared to that of the wild type strain. Statistical analysis showed a significant difference in the distribution of angular direction when compared to wild

type controls (P_Z = 0.015). Although my results indicated that the capsule was not required for solid substrate motility, it was unclear whether it was involved in photoresponsive movement Also, the data indicated that the capsule was required for maximal flagellum-dependent swimming through soft agar.

3.5.3. The role of a putative glycoprotein in solid substrate motility

The gene RCC00178 was annotated as an iron-regulated cell surface protein, and is located in a region of the genome annotated as containing genes required for the cell capsule, including synthesis of the sugar rhamnose and capsule export (Figure 3-34 and Table 3-9). Rhamnose is known to be a component of the *R. capsulatus* capsule (Omar et al., 1983a). RCC00178 had a low sequence identity with the closest characterized protein, CsxB (Braun et al., 1999), so protein domains identified in the putative *R. capsulatus* proteins were also considered. The local alignment scores (E values) of the predicted protein sequences to the top protein domains were also provided (Table 3-9).

The genes surrounding, but transcribed separately from RCC00178 are shown to illustrate that this is a region of the chromosome associated with capsule biosynthesis.

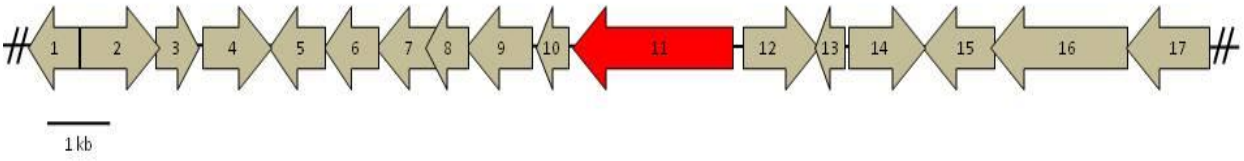

Figure 3-34: Genomic context of the putative cell surface hemolysin-type Ca^{+2} binding domain protein encoded by ORF RCC00178, identified by MS-MS peptide sequencing: (1) *kpsM* capsule export inner membrane permease; (2) *kpsE* capsule export inner membrane protein; (3) *kpsT* capsule export inner membrane ATP-binding subunit; (4) RCC00171 protein of unknown function; (5) glycosyltransferase protein; (6) *rmlA* glucose-1-phosphate thymidylytransferase; (7) *rmlD* dTDP-4-dehydrorhamnose reductase; (8) RCC00175 protein of unknown function; (9) *rmlB* dTDP-D-glucose 4,6-dehydratase; (10) *rmlC* dTDP-4-dehydrorhamnose epimerase; (11) RCC00178 hemolysin-type Ca^{+2} binding domain protein; (12) *ilvA* threonine deaminase; (13) RCC00180 hypothetical protein; (14) RCC00181 response regulator; (15) *hlyD* hemolysin transport protein; (16) RCC00183 ATP-binding efflux permease protein; (17) RCC00184 outer membrane efflux protein. Mutagenized ORF RCC00178 gene highlighted in red.

The protein encoded by RCC00178 was not the reciprocal best hit to the amino acid sequence from the hypothetical *C. rectus* CsxB. While CsxB was the best hit in the *C. rectus* genome queried with RCC00178, three other hemolysin-type calcium-binding repeat family proteins in the *R. capsulatus* genome returned higher alignment scores to the *C. rectus* CsxB than RCC00178. Thus I was unable to determine a function for the RCC00178 protein. This RCC00178 gene was chosen for mutagenesis in part because two peptides (providing ~2.3% coverage) from the protein it encoded were possibly on the cell surface, as indicated by peptide mass analysis (see section **3.4.2** and **APPENDIX A**, Table A-5). Also, BLASTp comparison of the *R. capsulatus* proteome with the sequence of the *Synechococcus* SwmA protein identified several proteins, including RCC00178, which shared sequence similarity with the hemolysin-type Ca^{+2} binding domains of SwmA. SwmA is required for *Synechococcus* flagellum-independent swimming (McCarren and Brahamsha, 2009), and so the potential role of this predicted outer membrane surface-associated protein in solid substrate motility was investigated, by creating a strain deficient in RCC00178.

Table 3-9: Putative polysaccharide synthesis/export gene cluster in *R. capsulatus*.

Gene	Gene product	Length (aa)	Domain or characterized homologue [(a)]	Identity (%)	E value [(b)]
kpsM	capsule export inner membrane permease	267	ABC-type polysaccharide export permease domain (COG1682)		$3.8e^{-17}$
			KpsM, *A. hydrophila* (AAM22565)	23	
kpsE	capsule export inner membrane protein	409	capsule exopolysaccharide export domain (COG3524)		$2.2e^{-49}$
			KpsE, *E. coli* (ABC88655)	24	
kpsT	capsule export inner membrane ATP-binding subunit	227	ABC KpsT Wzt transport subfamily domain (cd03220)		$3.8e^{-63}$
			KpsT, *E. coli* (ABC88663)	43	
			CtrD, *N. meningitides* (AAA25453)	43	
RCC00171	hypothetical protein	371	DUF2793 domain (Pfam10983)		$1.7e^{-27}$
wbbT	glycosyltransferase	306	GT2-like glycosylase domain (cd04196)		$5e^{-54}$
			WbbT, *Y. enterocolitica* (CAA79348)	34	
			RfbG, *P. fluorescens* (ABC71789)	27	

Gene	Gene product	Length (aa)	Domain or characterized homologue [(a)]	Identity (%)	E value[(b)]
rmlA	glucose-1-phosphate thymidylytransferase	291	G1P TT short form domain (cd02538)		$1.6e^{-110}$
			RmlA, *E. coli* (ACA24816)	61	
rmlD	dTDP-4-dehydrorhamnose reductase	361	L-rhamnose substrate binding domain (Pfam04321)		$1.5e^{-71}$
			dTDP-4-dehyrorhamnose reductase domain (COG1091)		$5.8e^{-58}$
			RmlD, *S. elodea* (AAP57701)	38	
RCC00175	hypothetical protein	225			
rmlB	dTDP-D-glucose 4,6-dehydratase	353	dTDP-D-glucose 4,6-dehyratase domain (COG1088)		$6.6e^{-151}$
			RmlB, *E. coli* (ABG81797)	61	
rmlC	dTDP-4-dehydrorhamnose epimerase	187	dTDP-4-dehyrorhamnose epimerase domain (Pfam00908)		$2.4e^{-73}$
			RmlC, *G. stearothermophilus* (AAQ23680)	55	
RCC00178	hypothetical protein	879	peptidase M10 serralysin C-terminal domain (Pfam08548)		$1.2e^{-4}$
			CsxB, *C. rectus* (AAD02003)	16	
ilvA	threonine deaminase	415	threonine dehydratase domain (COG1171)		$1.6e^{-92}$
			IlvA, *B. subtilis* (P37946)	45	
RCC00180	hypothetical protein	109	Hpt domain (Pfam01627)		$2.5e^{-3}$
RCC00181	response regulator	409	signal receiver domain (cd00156)		$5.6e^{-25}$
hlyD	Type I secretion membrane fusion protein	390	HlyD Type I secretion membrane fusion protein domain (TIGR01843)		$4e^{-67}$
RCC00183	ABC efflux ATP-binding permease	750	ABC-type bacteriocin exporter domain (COG2274)		$1.6e^{-118}$
RCC00184	outer membrane efflux protein	446	outer membrane efflux protein domain (Pfam02321)		$3.8e^{-4}$
			HrdC, *Chromohalobacter sp*. 160 (BAD35012)	21	

(a) Characterized protein domain (domain name, domain number) or homologue of experimentally verified function (gene product name, species, accession number).

(b) Top E-value scores from local pairwise protein domain alignment BLASTp.

RCC00178 (tentatively designated *hcpA* for hemolysin-type Ca^{+2} binding protein) was disrupted by insertion of an antibiotic resistance marker using the flagellin-deficient strain bKSDF as the background, to create the strain bKSDFhcpA (Table 2-1). Strain bKSDFhcpA was impaired in movement outward from the inoculation stab in soft agar (Figure 3-35c), which confirmed a lack of flagellar motility due to the *flaA* deletion. The bKSDFhcpA mutants moved away from the point of inoculation in the interstice of plates, and therefore retained flagellum-independent motility (Figure 3-35d).

Using the method described in section **2.17**, the distribution of the direction of movement of the *hcpA* mutants in illuminated stab-plates was compared to that of the wild type strain. Statistical analysis showed a significant difference in the distribution of angular direction when compared to wild type controls, although bKSDFhcpA cells moved toward the light in a less dispersive pattern than wild type controls ($P_Z = 0.028$). These results indicated that RCC00178 was not required for solid substrate motility, but perhaps the protein encoded by RCC00178 changed the photoresponse such that motility was less dispersed.

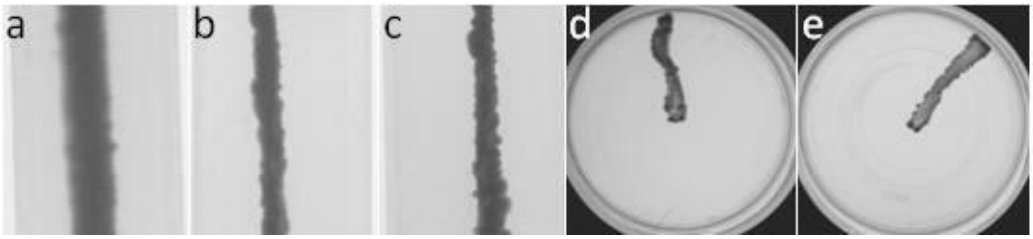

Figure 3-35: Representative soft agar tubes or agar plates inoculated with *R. capsulatus* cells incubated with halogen white light. Tubes were illuminated with incident light from the side, whereas stab-plate illumination was from the top of the image: (a) wild type strain B10 soft agar stab; (b) *flaA* mutant strain bKSDF soft agar stab; (c) *flaA/hcpA* mutant strain bKSDFhcpA soft agar stab; (d) *flaA* mutant strain bKSDF stab-plate; (e) *flaA/hcpA* mutant strain bKSDFhcpA stab-plate.

3.5.4. Transposon mutagenesis to search for components of the solid substrate motility mechanism

A transposon (Tn5) mutagenesis library was constructed in an attempt to identify genes required for flagellum-independent solid substrate taxis. A transposon library of 1503 isolates was generated and assayed for loss of flagellum-independent motility. The library was not assayed for random insertion and may have contained siblings. The stab-plate assay was not a high-throughput platform, as only a single strain was screened in each Petri plate, so the technique was modified to include 40 stabs per plate to generate a high-throughput system. Tn5 mutants judged to not move were assayed again whereas motile strains were discarded. After more than 38 stab-plate iterations needed to test and re-test all library samples, this screen failed to identify mutants that were deficient in solid substrate motility. It was possible that a larger insertion library was needed, made with a transposon with a higher frequency of transposition (Larsen et al., 2002).

3.6. Coordinated directional motility

3.6.1. Coordinated long-range solid substrate motility

R. capsulatus cell distribution in the plate-medium interstice was examined after movement away from the point of stab inoculation occurred, using ^{32}P radiography (Figure 3-36). Exposure profiles that corresponded to radioactive signal varied along what was thought to be the movement path in the interstitial region (Figure 3-36b), and arranged in what may have been a coordinated pattern. The signal intensity from cells labelled with ^{32}P -orthophosphate was divided into three groups, based on the intensity in the region of movement and growth. Cells at the leading edge of the taxis zone (Figure 3-36e) had a strong signal compared to cells located closer to the point of inoculation (Figure 3-36c,d). The cells between the edge of the plate and the point of inoculation appeared to contain less ^{32}P, which was attributed to dilution of the ^{32}P signal following cell divisions. These results were interpreted to

mean that the cells at the edge of the plate (Figure 3-36e) rapidly translocated from the point of inoculation to the plate perimeter in a coordinated manner, which resulted in a strong ^{32}P signal.

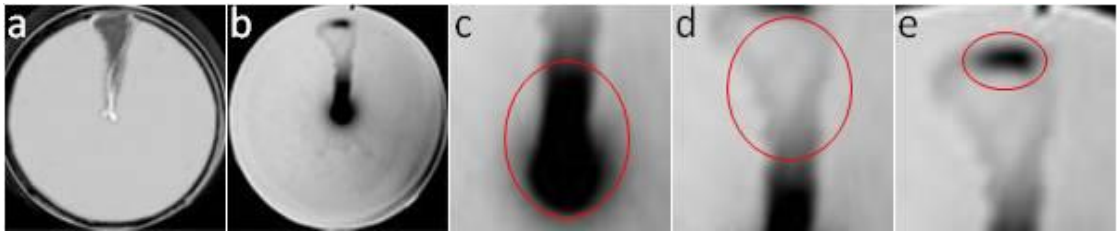

Figure 3-36: Cells were labelled with ^{32}P-orthophosphate, and agar plates were inoculated with *ctrA* mutant strain BCKF, and incubated with incident light from the top of the image: (a) photograph of macroscopic cell proliferation; (b) autoradiogram showing ^{32}P signal profile; (c) high signal intensity near the point of inoculation; (d) low signal intensity along taxis path; (e) high signal intensity at leading edge of taxis. Regions of interest are indicated with red circles.

3.6.2. Long-range solid substrate social motility

A time-course approach was used to further investigate cell group motility, because the ^{32}P labelling experiment did not provide information regarding what occurred between stab inoculation and the macroscopic growth observed by eye at the end of the experiment (~48 hours after stabbing the plates).

A series of observations of cell density and location over time indicated that some stab-inoculated cells rapidly move from the point of inoculation (Figure 3-37 and Figure 3-38). An isolated cluster of wild type strain B10 cells was observed at the edge of the circular plate incubated under incident light after 16 hours (Figure 3-37h). In a similar experiment on the flagellum-deficient (*flaA*$^-$) strain bKSDF, a cluster of cells was visible after only 12 hours (Figure 3-38g).

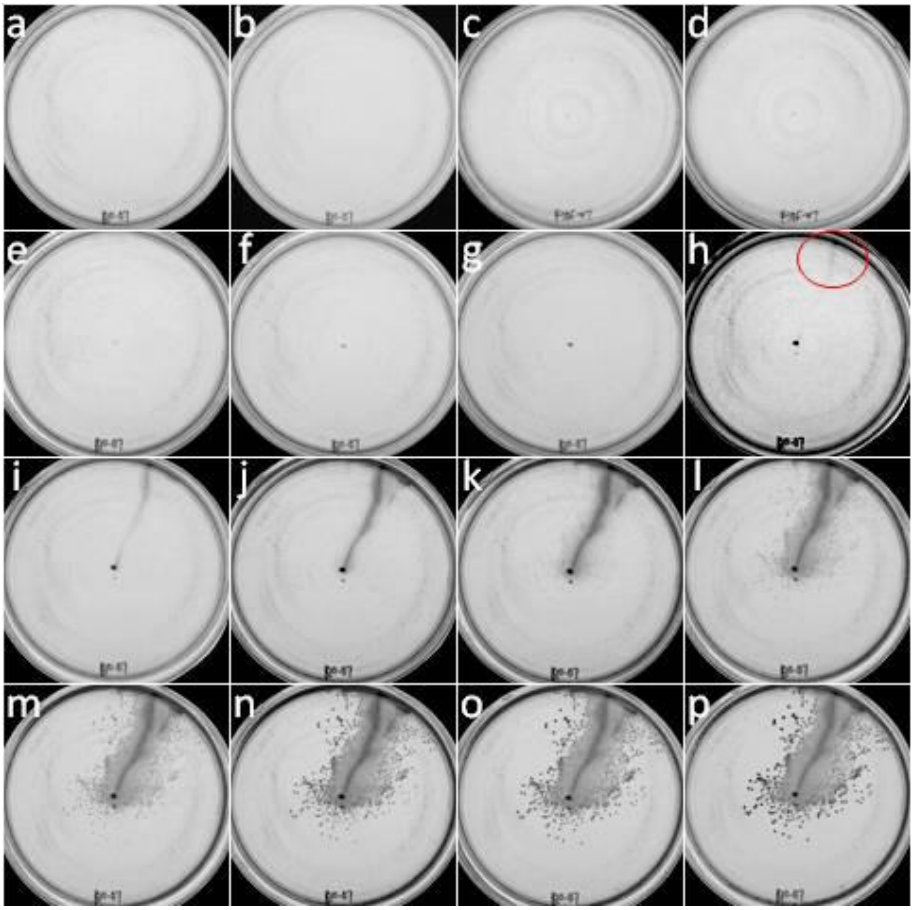

Figure 3-37: Representative agar plates inoculated with wild type strain B10, and incubated with incident halogen white light from the top of the image: (a) 0 hrs; (b) 0.5 hrs; (c) 1 hr; (d) 2 hrs; (e) 4 hrs; (f) 8 hrs; (g) 12 hrs; (h) 16 hrs; (i) 20 hrs; (j) 24 hrs; (k) 28 hrs; (l) 32 hrs; (m) 36 hrs; (n) 40 hrs; (o) 44 hrs; (p) 48 hrs. The macroscopically visible first appearance of a satellite cluster is indicated with a red circle.

These groups of cells at the plate edge appeared to be "satellite clusters" because they were not connected to the site of inoculation by any visible cell growth. A single visible pin-point colony contains approximately 10^6 cells. If *R. capsulatus* cells doubled every 2.5 hours, approximately 45 hours (18 generations) would be required for a single cell to form the visible satellite clusters. Therefore, these satellite clusters appeared to have been formed by a group of cells at the site of inoculation that moved as an aggregated mass.

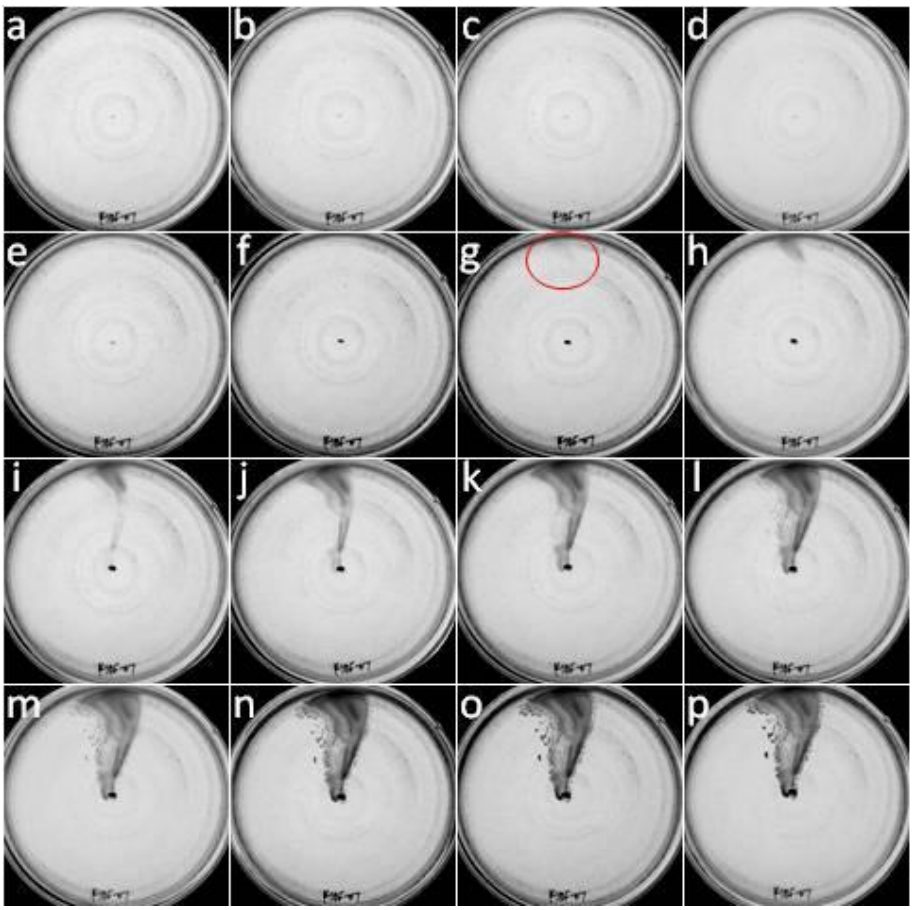

Figure 3-38: Representative agar plates inoculated with *flaA* mutant strain bKSDF, and incubated with incident halogen white light from the top of the image: (a) 0 hrs; (b) 0.5 hrs; (c) 1 hr; (d) 2 hrs; (e) 4 hrs; (f) 8 hrs; (g) 12 hrs; (h) 16 hrs; (i) 20 hrs; (j) 24 hrs; (k) 28 hrs; (l) 32 hrs; (m) 36 hrs; (n) 40 hrs; (o) 44 hrs; (p) 48 hrs. The macroscopically visible first appearance of a satellite cluster is indicated with a red circle.

With both strains, these clusters of cells were connected to the point of stab inoculation by subsequent growth of intervening cells. These intervening cells either moved more slowly, started to move at a later time, were populated by reversal in the movement of cells that had moved closer to the edge of the plate, or stopped sooner. Furthermore, the diffusive flagellum-dependent taxis away from the path of dense linear motility appeared to occur after the flagellum-independent cell movement. However, flagellum-dependent and -independent movement may have occurred at the same time, although flagellar dispersal may have resulted in a low cell density not visible macroscopically until much later.

Using the method described in section **2.17**, the distribution of the direction of movement of the bKSDF mutants in illuminated stab-plates was compared to that of the wild type strain. Statistical analysis showed no significant difference in the distribution of angular direction when compared to wild type controls (Table 3-10). Long-range cell movement was observed regardless of the flagellum, and some cells moved rapidly in a flagellum-independent manner at a rate of > 1.04 μm/sec, toward white light.

Table 3-10: Average motility values of wild type strain B10 and *flaA* mutant bKSDF time-course test samples incubated in the glass-agar interstice with halogen white light.

Strain	Strain name	Average motility distance [(a)] (mm)	Average angular motility direction [(b)] (°)	P_Z [(c)]	# Samples
wild type	B10	45 (1)	-4 (39)		8
flaA	bKSDF	43 (6)	2 (29)	0.83	8

(a) Taxis distance as measured from the point of inoculation to farthest point of visible cell growth, with standard deviation in parentheses.

(b) Taxis direction from the point of inoculation to the farthest point of visible cell growth, with standard deviation in parentheses. 0° indicates movement directly toward the light source, and ± 180° indicates movement directly away from the light.

(c) Two-tailed two-independent sample Wilcoxon rank sum test of significant difference compared to wild type B10 illuminated samples. For a >0.95 probability that the movement was different from controls, $P_Z < 0.05$.

3.6.3. Evaluation of the role of the photosynthetic apparatus and pigments on motility

A possible role of the photosynthetic apparatus and pigments in coordinating light-responsive adaptive motility was first investigated using the photosynthetic reaction center (RC) mutant strain DW5 (Wong et al., 1996), and subsequently using the photosynthetic pigment mutant strain BY1653 (lacks BChl and carotenoid) (Marrs, 1981). Neither of these strains grows anaerobically under photosynthetic conditions.

The RC mutant strain DW5 (*puhA*$^-$) and was capable of weak flagellar motility through soft agar in the aerobic zone of the tube, while movement was reduced in the anaerobic region of the tube. The *puhA*/*flaA* double mutant strain sbKSDFdw5 movement was impaired in movement outward from the stab, which confirmed a lack of flagellar motility due to the *flaA* deletion. The growths of both strains were reduced in the anaerobic region of the tube (Figure 3-39e,f). The *puhA* mutant strain DW5 was capable of directed movement away from the point of stab inoculation in plates in a manner characteristic of flagellum-dependent diffusive motility (Figure 3-39g), and the *puhA*/*flaA* double mutant strain sbKSDFdw5 was capable of directed motility in a flagellum-independent manner (Figure 3-39h).

Soft agar stab analysis of the BChl/carotenoid pigment-deficient strain BY1653 (*bchA*$^-$/*crtB*$^-$), and the *bchA*/*crtB*/*flaA* triple mutant strain sbKSDFby, indicated that growth was limited to the upper aerobic zone of the stab tube. The pigment-deficient strain BY1653 was capable of weak flagellar movement outward from the top of the stab (Figure 3-39i), and movement of the triple mutant strain sbKSDFby outward from the stab was impaired, which confirmed a lack of flagellar motility due to the *flaA* deletion (Figure 3-39j). Strain BY1653 moved in a diffuse directed flagellar manner in stab-plate assays (Figure 3-39k), however, strain sbKSDFby exhibited what appeared to be diffuse directed taxis in the absence of the flagellum (Figure 3-39l). When inoculated into the glass-agar interstice, sbKSDFby cells lacked the dense linear motility pattern characteristic of flagellum-deficient strain sbKSDF motility (Figure 3-39d). Instead sbKSDFby cells created a diffuse pattern of growth unlike either SB1003 or sbKSDF cells (compare Figure 3-39k and Figure 3-39l).

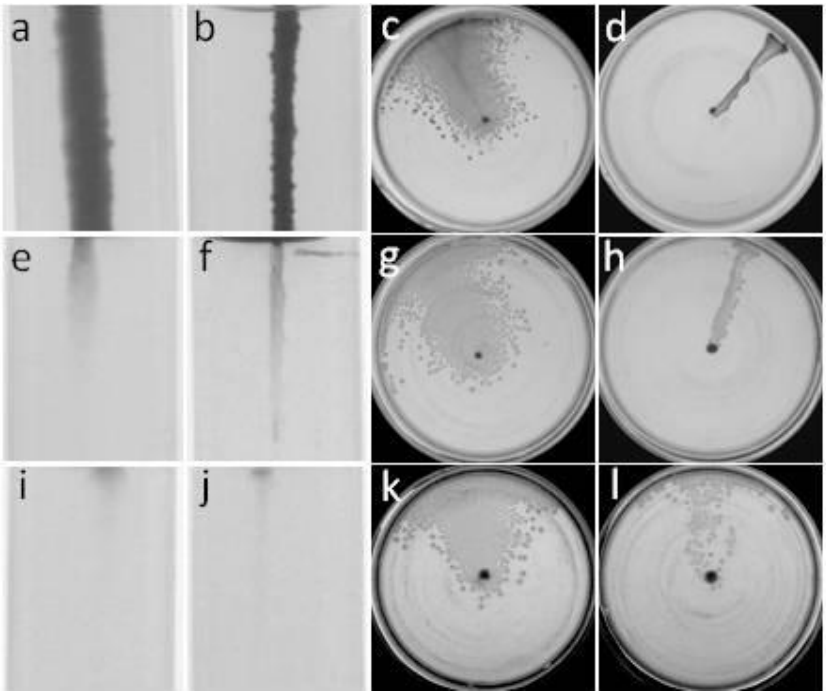

Figure 3-39: Representative soft agar tubes or agar plates inoculated with *R. capsulatus* cells incubated with halogen white light. Tubes were illuminated with incident light from the side, whereas stab-plate illumination was from the top of the image: (a) strain SB1003 soft agar stab; (b) *flaA* mutant strain sbKSDF soft agar stab; (c) strain SB1003 stab-plate; (d) *flaA* mutant strain sbKSDF stab-plate; (e) *puhA* mutant strain DW5 soft agar stab; (f) *flaA/puhA* mutant strain sbKSDFdw5 soft agar stab; (g) *puhA* mutant strain DW5 stab-plate; (h) *flaA/puhA* mutant strain sbKSDFdw5 stab-plate; (i) *bchA/crtB* mutant strain BY1653 soft agar stab; (j) *flaA/bchA/crtB* mutant strain sbKSDFby soft agar stab; (k) *bchA/crtB* mutant strain BY1653 stab-plate; (l) *flaA/bchA/crtB* mutant strain sbKSDFby stab-plate.

Using the method described in section **2.17**, the distribution of the direction of movement of the *puhA* and *bchA*/*crtB* mutants in illuminated stab-plates was compared to that of the wild type strain. Statistical analysis of *puhA* mutant direction showed no significant difference in the distribution of angular direction when compared to wild type controls ($P_Z = 0.56$). Therefore, a functional RC did not appear to be needed for directed motility.

However, statistical analysis of *bchA*/*crtB* mutant direction showed a significant difference in the distribution of angular direction when compared to wild type controls ($P_Z = 0.00075$). Therefore the photosynthetic pigments and/or precursors appeared to have been needed for photoresponsive

movement to white light in the glass-agar interstice of plates. The BChl and/or carotenoid pigments, but not a functional RC, were required for dense, linear flagellum-independent cell movement (compare Figure 3-39h and Figure 3-39l).

3.6.4. Evaluation of the effects of a photoactive yellow protein gene knockout on motility

The photoactive yellow protein (PYP) is a classified as a xanthopsin, based on the coumarate chromophore of the protein (Rajagopal and Moffat, 2003; van der Horst and Hellingwerf, 2004). The *R. capsulatus* PYP, encoded by RCC01066, is a small, water-soluble protein with a PAS signalling domain (Pellequer et al., 1998) and a *p*-hydroxycinnamic acid chromophore. The *R. capsulatus* PYP absorbs 435 and 375 nm light, resulting in *trans-cis* conformational changes to the chromophore (Hoff et al., 1994; Kyndt et al., 2004). It seemed possible that the *R. capsulatus* PYP was involved in the activation of solid substrate motility in response to blue light, so the potential role of this PYP in solid substrate motility was investigated, by creating a strain deficient in the gene for this protein.

RCC01066 was disrupted by insertion of an antibiotic resistance marker using the flagellin-deficient strain bKSDF as a background, to create the strain bKSDFpyp (Table 2-1). Strain bKSDFpyp was impaired in movement outward from the inoculation stab in soft agar, which confirmed a lack of flagellar motility due to the *flaA* deletion (Figure 3-40c). The bKSDFpyp mutant moved away from the point of inoculation in the interstice of plates, and therefore retained flagellum-independent motility (Figure 3-40d,e).

Strain bKSDFpyp was tested for PYP-dependent photoresponsive movement under white, 435, and 375 nm illumination, because these wavelengths were shown to cause conformational changes in the PYP protein (Kyndt et al., 2004). The average direction of taxis, standard deviations, and P_Z values of LED-illuminated sample sets were determined, and plotted in Figure 3-41.

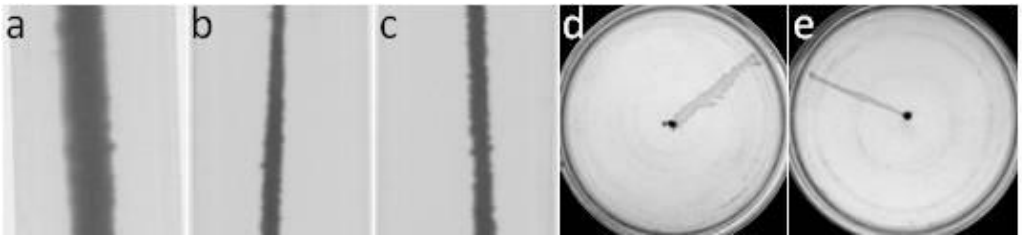

Figure 3-40: Representative soft agar tubes or agar plates inoculated with *R. capsulatus* cells incubated with halogen white light. Tubes were illuminated with incident light from the side, whereas stab-plate illumination was from the top of the image: (a) wild type strain B10 soft agar stab; (b) *flaA* mutant strain bKSDF soft agar stab; (c) *flaA/pyp* mutant strain bKSDFpyp soft agar stab; (d) *flaA* mutant strain bKSDF stab-plate; (e) *flaA/pyp* mutant strain bKSDFpyp stab-plate.

Using the method described in section **2.17**, the distribution of the direction of movement of the *flaA*/*pyp* mutant in stab-plates was compared to the parental bKSDF (*flaA*$^-$) strain in illuminated and dark experiments (see **APPENDIX A**, Table A-8). Statistical analysis showed no significant difference in the distribution of angular direction of bKSDFpyp cells when compared to bKSDF controls. These results indicated that the *pyp* encoded by RCC01066 was not required for photoresponsive, directional solid substrate motility toward white, 435 or 375 nm light.

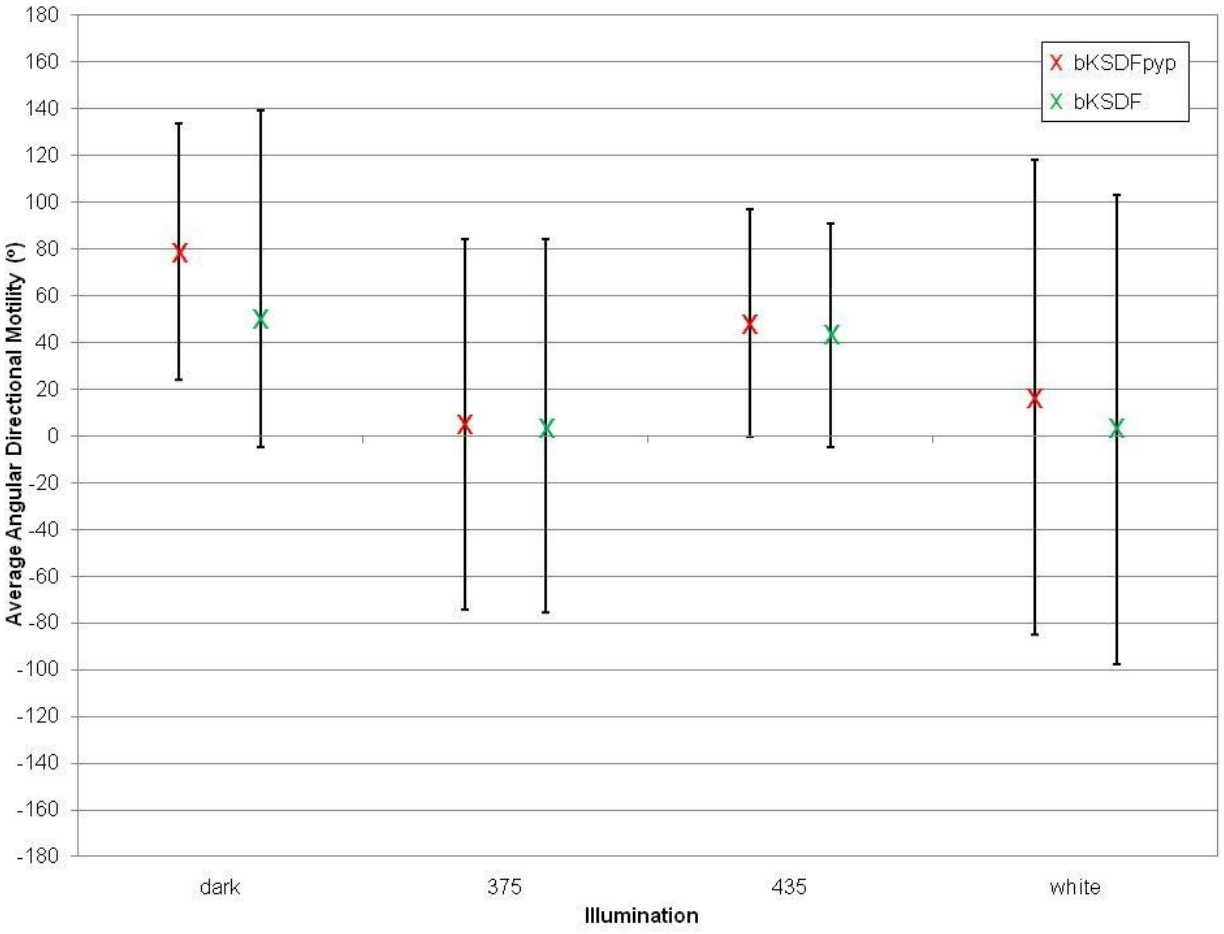

Figure 3-41: Graphical representation of the average angular direction of *R. capsulatus* motility in agar plates incubated in the LED chamber with illumination. The vertical axis gives the angle of movement, and the presence/absence of light, and wavelengths, are given on the horizontal axis. 0° indicates movement directly toward the light source, and ± 180° indicates movement directly away from the light. The average direction of movement is denoted with an "X" . Error bars represent 1 standard deviation. The P_z value is the probability that a difference from the control value is due to random chance – hence a P_z value < 0.05 means that the difference is statistically significant. In these experiments, none of the bKSDFpyp data yielded cases where P_z < 0.05 compared to bKSDF controls incubated with the same illumination.

3.6.5. Comparison of absorption profiles and potential photoresponsive movement

R. capsulatus cells moved toward white light, but how the illumination was perceived was unclear. It was hoped that an action spectrum might indicate which regions of the white light spectrum induced motility, and the potential photoreceptors responsible for movement. However, the lack of a

statistically significant difference between the distribution of directional movement of white light illuminated and dark controls made the interpretation of the data extremely difficult. For this reason, the action spectrum data is presented in **APPENDIX C**, without extensive interpretation of the data.

The direction of movement for illuminated samples was compared with the absorption spectrum from a whole cell crude lysate from an *R. capsulatus* strain SB1003 culture (Figure 3-42). The angular direction represented the average direction of movement under each wavelength region measured. As in other experiments, 0° represents directly toward the lamp, and 180° represents directly away from the lamp (see Fig 3-8).

Several absorption peaks corresponded to the regions of wavelengths tested in the action spectrum (**APPENDIX C**), and could speculatively be associated with known photoreceptive molecules. The >900 nm photoresponse may have been perceived by the BChl of the LH1 complex, although the absorption peak shoulder barely overlapped this wavelength range. The 750 nm wavelength coincided with the absorption peak of BPhe. The 700 nm wavelength did not coincide with any membrane fraction peaks, although some unknown cytoplasmic protein(s) appeared to absorb in this region.

The 572 nm wavelength coincided with an absorption peak from BChl, while the 490, 470, and 450 nm wavelengths corresponded to a peak for carotenoid compounds. The 425 nm wavelength overlapped with the shoulders of the carotenoids, BChl, and PYP peaks, as well as some unknown cytoplasmic protein(s). The 395, 385, and 375 nm wavelengths coincided with both a BChl, PYP, and unknown cytoplasmic protein(s) absorption peak (Jones, 2009). However, it is possible that photoreceptors involved in movement toward white light were not present in sufficient amounts to generate visible peaks in the spectra.

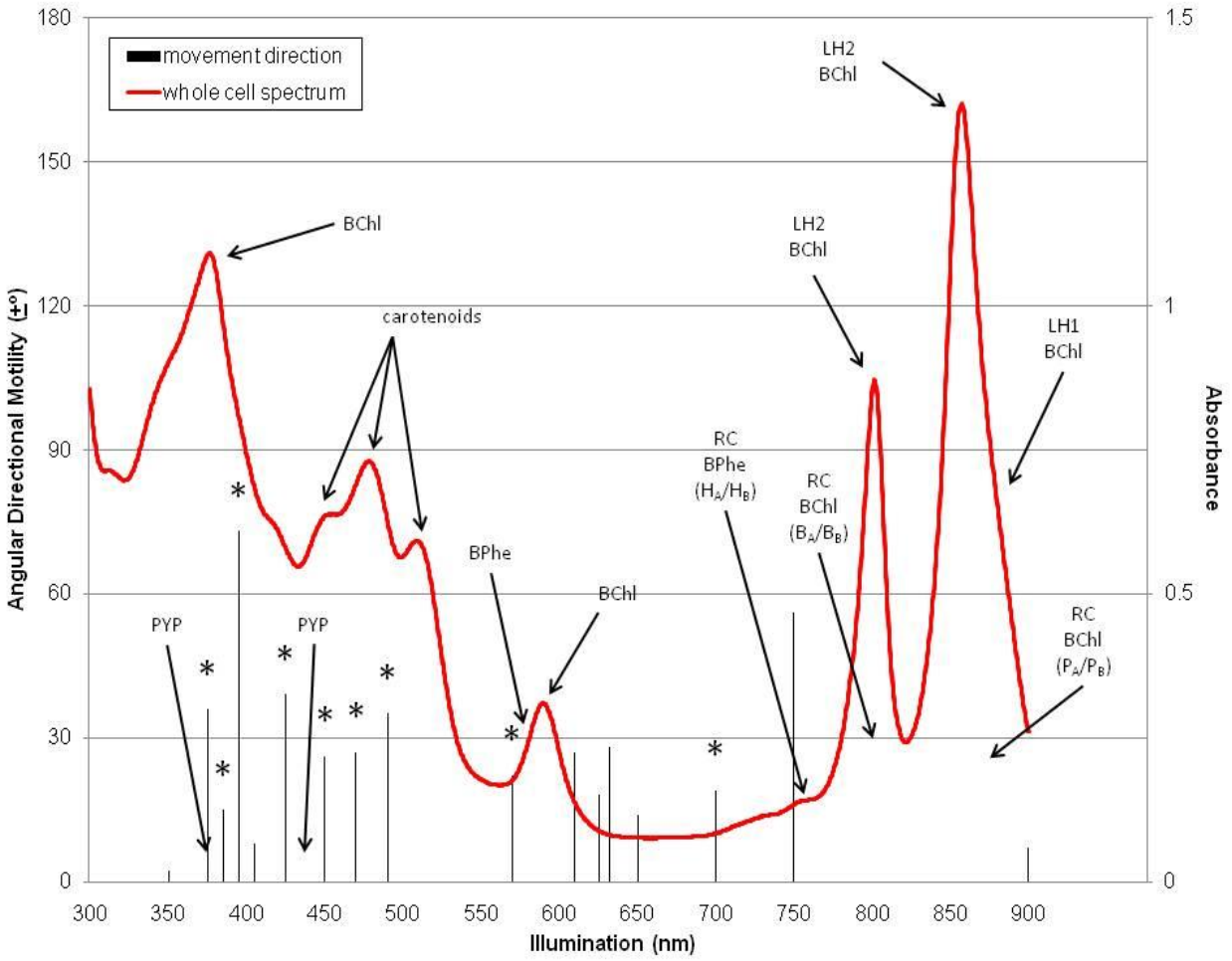

Figure 3-42: Action spectra data overlaid with absorption spectra. The height of the black bars represents the absolute average direction of motility of cells illuminated with that wavelength. The vertical axes give the angle of movement and the absorbance units, and wavelengths are given on the horizontal axis. The red line is the absorption spectrum from *R. capsulatus* whole cell lysate supernatant. The absorption peaks of known photoreceptive molecules are designated with arrows on the membrane fraction spectrum. The RC absorption profile is masked by the LH absorption profiles. The PYP absorption profiles are masked by the pigment profiles. The P pigments are the special pair BChl dimer, whereas the H and B forms are monomeric pigments. The A subscript refers to RC L subunit-bound pigments, while the B subscript refers to RC M subunit-bound pigments. The P_Z value is the probability that a difference from the white light control is due to random chance – hence a P_Z value < 0.05 means that the difference is statistically significant. Asterisks indicate cases where $P_Z < 0.05$ compared to white light tests.

3.6.6. Evaluation of possible quorum sensing-mediated processes on motility

R. capsulatus was shown to use a 16C acyl-homoserine lactone (HSL) quorum sensing system to induce gene transfer (Schaefer et al., 2002). I found that cells moved rapidly as a group (a local area of high density) away from the point of stab-inoculation (see section **3.6.2**), and so it was considered that quorum sensing may be needed for coordinated cell movement. If quorum sensing were required for group movement, the macroscopic pattern of flagellum-independent movement should not resemble the dense linear pattern of *flaA* mutant strain bKSDF cells. Instead, the cell movement pattern might be expected to result in a dispersed manner if the organization of motility were dependent on the 16C acyl-HSL signal. The potential role of quorum sensing in solid substrate motility was investigated in strains deficient in the HSL synthase protein GtaI, encoded by the gene RCC00329.

Cells of the *gtaI*$^-$ strain BLKI (Table 2-1) stabbed into tubes of soft agar moved outward from the inoculation stab, but to a lesser extent than was observed in the wild type strain B10 (Figure 3-43a,c). The flagellum-dependent movement of BLKI cells in the interstice was less diffuse than that of the wild type strain B10 (Figure 3-43e,g). Strain bKSDFgtaI (*flaA*$^-$/*gtaI*$^-$) was impaired in movement outward from the inoculation stab in soft agar (Figure 3-43d), which confirmed a lack of flagellar motility due to the *flaA* deletion. The bKSDFgtaI mutant moved away from the point of inoculation in the interstice of plates, and therefore retained flagellum-independent motility (Figure 3-43h).

Using the method described in section **2.17**, the distribution of the direction of movement of the *gtaI* mutants in illuminated stab-plates was compared to that of the wild type strain. Statistical analysis showed a significant difference in the distribution of angular direction when compared to the wild type strain illuminated controls ($P_Z = 0.00000014$). These results indicated that *gtaI* was required for photoresponsive solid substrate motility. Furthermore, these results indicated that the 16C acyl-HSL synthesized by GtaI for quorum sensing was not required for production of the flagellum. However, GtaI

may have been required for maximal flagellar activity, because flagellum-dependent motility in the *gtaI* mutant strain BLKI was decreased (compare Figure 3-43a to Figure 3-43c, and Figure 3-43e to Figure 3-43g).

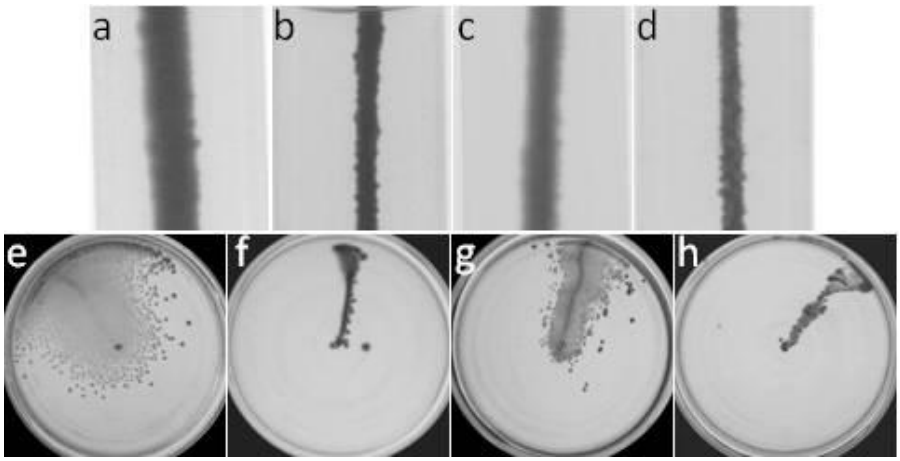

Figure 3-43: Representative soft agar tubes or agar plates inoculated with *R. capsulatus* cells incubated with halogen white light. Tubes were illuminated with incident light from the side, whereas stab-plate illumination was from the top of the image: (a) wild type strain B10 soft agar stab; (b) *flaA* mutant strain bKSDF soft agar stab; (c) *gtaI* mutant strain BLKI soft agar stab; (d) *flaA/gtaI* mutant strain bKSDFgtaI soft agar stab; (e) wild type strain B10 stab-plate; (f) *flaA* mutant strain bKSDF stab-plate; (g) *gtaI* mutant strain BLKI stab-plate; (h) *flaA/gtaI* mutant strain bKSDFgtaI stab-plate.

3.6.7. Evaluation of possible effects of RpoN on motility

R. capsulatus contains a single σ^{54} RNA polymerase transcription factor (Cannon et al., 1996). This alternative sigma factor (encoded by gene RCC00568) is a homologue of RpoN proteins that have been shown to modulate the expression of motility genes in several well-characterized bacteria such as *P. aeruginosa* (Ishimoto and Lory, 1989), *Synechocystis* (Bhaya et al., 1999), *H. pylori* (Fujinaga et al., 2001), and *V. fischeri* (Wolfe et al., 2004). The RpoN of *R. capsulatus* shows up to 50% amino acid sequence identity with RpoN proteins known to regulate the transcription of motility genes (Totten et al., 1990; Anderson et al., 1995; Martin et al., 2006) (Table 3-11). Based on this, RpoN was predicted to be involved in the regulation of the expression of *R. capsulatus* motility genes. However, the promoter

recognition activity of the *R. capsulatus* RpoN was found to differ from previously characterized RpoN proteins and the *R. capsulatus* RpoN protein lacks an acidic amino acid residue region associated with melting promoter DNA (Cannon et al., 1996). Thus the *R. capsulatus* RpoN protein may constitute a subclass of σ^{54} RNA polymerase transcription factors (Cannon et al., 1996), and this difference may be reflected in the activity of the RpoN on the expression of motility genes in *R.* capsulatus. The *R. sphaeroides* RpoN protein was the highest-scoring BLAST alignment in the NCBI database to the *R. capsulatus* RpoN sequence. Furthermore, the *R. capsulatus* protein encoded by RCC00568 was the reciprocal best hit of RpoN in each of *R. sphaeroides*, *C. crescentus*, and *P. aeruginosa* (Table 3-11).

Table 3-11: Alignment comparison of the *R. capsulatus rpoN* gene product to similar proteins.

Gene	Gene product	Length (aa)	Characterized homologue [(a)]	Identity (%)
rpoN	RNA polymerase σ^{54}	428	RpoN, *R. sphaeroides* (YP_353600)	50
			RpoN2, *R. sphaeroides* (YP_353144)	41
			RpoN3, *R. sphaeroides* (AAA26134)	39
			RpoN4, *R. sphaeroides* (YP_352929)	36
			RpoN, *C. crescentus* (CAA48553)	30
			RpoN, *P. aeruginosa* (AAA19793)	29

(a) Gene product name, species (NCBI accession number).

Using the *Pseudomonas putida* RpoN-binding consensus sequence TGGYAYNNNNNTTGC (where Y = C or T and N = A or C or G or T) with an unconserved 5 nucleotide spacer (N) between the two DNA/protein contact sequences (Kohler et al., 1994), three potential binding sites were found within the *R. capsulatus* genomic regions encoding the flagellar genes, and three potential binding sites were found within the putative pilus-encoding genomic locus. A perfect consensus sequence match upstream of RCC03526 (upstream of *flaA*), a sequence with a 7 nucleotide spacer upstream of the gene encoding the *flbT* ORF RCC03523, and a sequence with a 9 nucleotide spacer upstream of the gene encoding the *fliE* ORF RCC03518 were identified. A modified **C**GGY**T**YNNNNNTTGC consensus sequence match upstream of the gene encoding *flp1* ORF RCC00499, another modified **C**GG**CCG**NNNNNTTGC consensus sequence

match upstream of the gene encoding *flp2* ORF RCC00500, and a 7 nucleotide spacer modified **C**GGY**TG**NNNNTTGC consensus sequence match upstream of the gene encoding *cpaC* ORF RCC00502 were also identified. However, only the sequences identified upstream of *flp2* and *cpaC* overlapped with predicted promoter sites suitably located upstream of the predicted ORFs.

The role of RpoN in motility was investigated, using a derivative of the strain B10 that was deficient in the alternative RNA polymerase sigma cofactor gene RCC00568 for this protein (Wall et al., 1984). RpoN-deficient strain LJ1 cells stabbed into tubes of soft agar moved from the column of stab inoculation, similar to wild type strain B10 cells (Figure 3-44a,c). In contrast, growth of the *flaA*/*rpoN* double mutant strain bKSDFrpoN was limited to the column of stab inoculation, like the *flaA* mutant strain bKSDF cells, and therefore lacked flagellar motility (Figure 3-44b,d). When cells were inoculated into the interstice of plates, RpoN-deficient LJ1 cells moved similarly to wild type B10 cells (Figure 3-44e,g), and FlaA/RpoN-deficient strain bKSDFrpoN movements resembled the motility of *flaA* mutant strain bKSDF (Figure 3-44f,h).

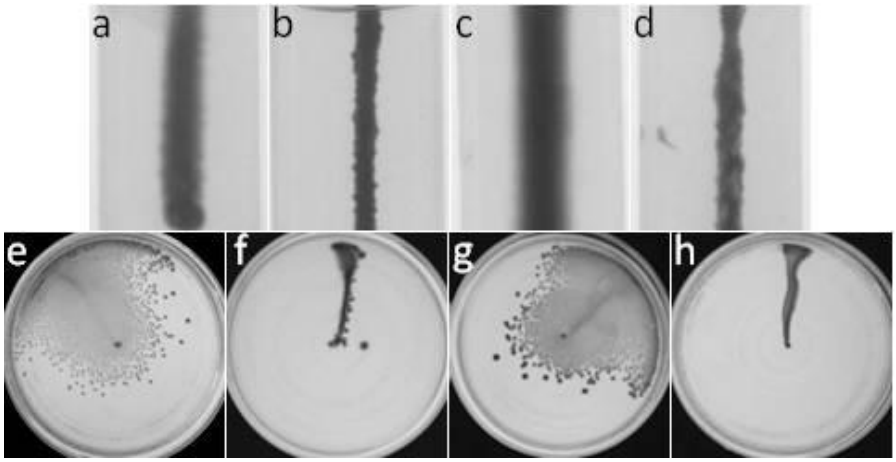

Figure 3-44: Representative soft agar tubes or agar plates inoculated with *R. capsulatus* cells incubated with halogen white light. Tubes were illuminated with incident light from the side, whereas stab-plate illumination was from the top of the image: (a) wild type strain B10 soft agar stab; (b) *flaA* mutant strain bKSDF soft agar stab; (c) *rpoN* mutant strain LJ1 soft agar stab; (d) f*laA/rpoN* mutant strain bKSDFrpoN soft agar stab; (e) wild type strain B10 stab-plate; (f) f*laA* mutant strain bKSDF stab-plate; (g) *rpoN* mutant strain LJ1 stab-plate; (h) f*laA/rpoN* mutant strain bKSDFrpoN stab-plate.

Using the method described in section **2.17**, the distribution of the direction of movement of the *rpoN* mutants in illuminated stab-plates was compared to that of the wild type strain. Statistical analysis showed an insignificant difference in the distribution of angular direction when compared to the wild type strain illuminated controls ($P_Z = 0.9$). These results indicated that *rpoN* was not required for photoresponsive solid substrate motility. These data also indicated that the RpoN σ^{54} protein was not required for production of a functional GTA transduction particle, as the *rpoN* lesion was GTA-transduced from strain LS01 to bKSDF to create bKSDFrpoN.

3.6.8. Evaluation of possible SenC effects on motility

The *R. capsulatus* SenC protein (encoded by gene RCC00044) is predicted to be a 23.2 kDa polypeptide with a conserved copper/iron binding domain, and an amino-terminal membrane-spanning motif thought to be associated with the inner membrane. SenC may indirectly regulate photosynthetic gene expression and cellular respiration (Buggy and Bauer, 1995), through the assembly of the cbb_3-type cytochrome *c* oxidase complex (Schulze and Rodel, 1989; Swem et al., 2005).

A transcriptome (microarray) comparison of strain bKSDF (*flaA*$^-$) cells from glass-agar interstice cultures to cells from aqueous cultures, done in collaboration with Dr. A. L. Lang, indicated that transcription of *senC* was increased 2.45 fold in the glass-agar interstice (**APPENDIX A**, Table A-9). Therefore the SenC protein was tested for a possible involvement in the regulation of solid substrate motility, using the SB1003-derived *senC* mutant strain LS01 (Swem et al., 2005).

LS01 cells inoculated into soft agar tubes moved away from the column of stab inoculation, similar to the parental strain SB1003 (Figure 3-45a,c), but LS01 growth and flagellar movement were much reduced in the aerobic upper region of the stab. Strain sbKSDFsenC was impaired in movement outward from the inoculation stab in soft agar (Figure 3-45d), which confirmed a lack of flagellar motility

due to the *flaA* deletion. In the stab-plate motility assay, LS01 cells moved away from the point of stab inoculation like the parental strain SB1003 (Figure 3-45e,g). The sbKSDFsenC mutant moved away from the point of inoculation in the interstice of plates, and therefore retained flagellum-independent motility (Figure 3-45h).

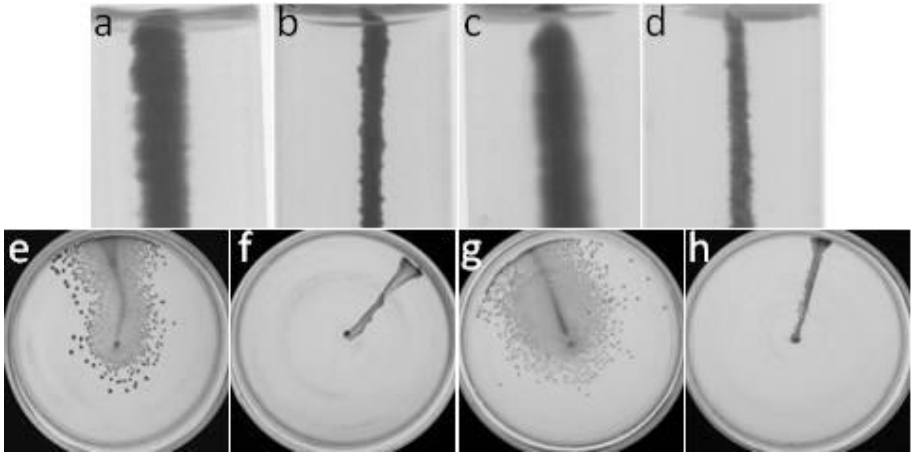

Figure 3-45: Representative soft agar tubes or agar plates inoculated with *R. capsulatus* cells incubated with halogen white light. Tubes were illuminated with incident light from the side, whereas stab-plate illumination was from the top of the image: (a) strain SB1003 soft agar stab; (b) *flaA* mutant strain sbKSDF soft agar stab; (c) *senC* mutant strain LS01 soft agar stab; (d) *flaA*/*senC* mutant strain sbKSDFsenC soft agar stab; (e) strain SB1003 stab-plate; (f) *flaA* mutant strain sbKSDF stab-plate; (g) *senC* mutant strain LS01 stab-plate; (h) *flaA*/*senC* mutant strain sbKSDFsenC stab-plate.

Using the method described in section **2.17**, the distribution of the direction of movement of the *senC* mutant in illuminated stab-plates was compared to that of the wild type strain. Statistical analysis showed a significant difference in the distribution of angular direction when compared to the wild type strain illuminated controls ($P_Z = 0.00012$). Although *senC* was not required for solid substrate motility, it appeared that SenC was involved in photoresponsive movement. Also, because of the decrease in flagellum-dependent motility at the top of the soft agar stabbed with the *senC* mutant strain LS01 (Figure 3-45c), SenC may have been required for maximal aerobic flagellar motility.

3.6.9. Evaluation of possible RegA effects on motility

The *R. capsulatus* RegA (encoded by gene RCC00045) is a DNA-binding protein (Du et al., 1998; Vignais et al., 2005) that acts as a global response regulator (Elsen et al., 2004). Some of the processes regulated by RegA include: the aerobic synthesis of heme and cytochromes (Swem and Bauer, 2002; Smart et al., 2004); the light-dependent (Sganga and Bauer, 1992) transcription of core photosynthesis genes (Mosley et al., 1994); and the anaerobic transcription of photosynthetic pigments (Willett et al., 2007).

A transcriptome (microarray) comparison of strain bKSDF (*flaA*$^-$) cells from solid substrate interstice cultures to cells from aqueous cultures, done in collaboration with Dr. A. L. Lang, indicated that *regA* transcription was increased 2.85 fold in the glass-agar interstice (**APPENDIX A**, Table A-9). Therefore, the activity of the RegA protein on coordinated cell motility was tested, using the SB1003-derived *regA* mutant strain REG1 (Sganga and Bauer, 1992).

REG1 cells inoculated into soft agar tubes moved away from the column of stab inoculation in the upper aerobic zone of the column. REG1 cells moved less than the parental strain SB1003, and motility of REG1 cells in the lower, anaerobic zone appeared to be limited to the column of stab inoculation (Figure 3-46a,c). Strain sbKSDFregA was impaired in movement outward from the inoculation stab in soft agar (Figure 3-46d), which confirmed a lack of flagellar motility due to the *flaA* deletion. In the stab-plate motility assay, REG1 cells moved away from the point of stab inoculation like the parental strain SB1003 (Figure 3-46e,g). The sbKSDFregA mutant moved away from the point of inoculation in the interstice of plates, and therefore retained flagellum-independent motility (Figure 3-46h).

Using the method described in section **2.17**, the distribution of the direction of movement of the *regA* mutant in illuminated stab-plates was compared to that of the wild type strain. Statistical analysis

showed a significant difference in the distribution of angular direction when compared to the wild type strain illuminated controls (P_Z = 0.0082). Although the results indicated that *regA* was not required for solid substrate motility, it appeared that RegA was involved in determining the direction of photoresponsive movement. Also, RegA may have been required for anaerobic flagellar motility, because of the decrease in flagellum-dependent motility at the bottom of the soft agar stabbed with the *regA* mutant strain REG1 (Figure 3-46c).

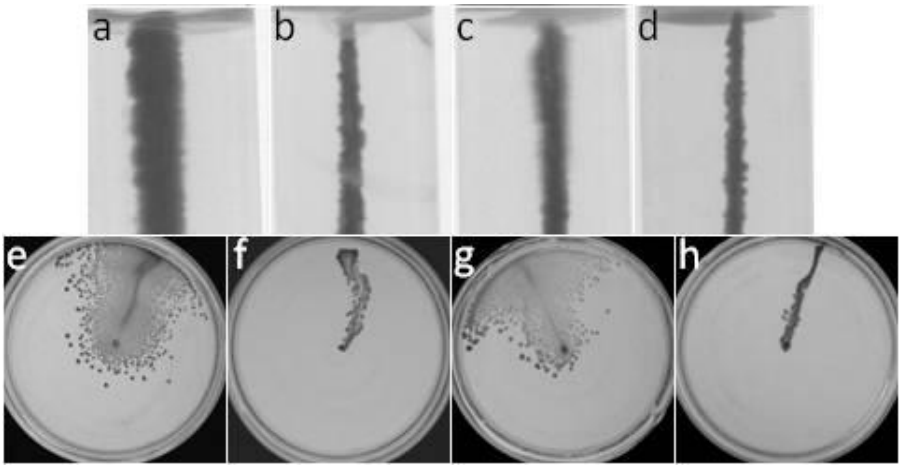

Figure 3-46: Representative soft agar tubes or agar plates inoculated with *R. capsulatus* cells incubated with halogen white light. Tubes were illuminated with incident light from the side, whereas stab-plate illumination was from the top of the image: (a) strain SB1003 soft agar stab; (b) *flaA* mutant strain sbKSDF soft agar stab; (c) *regA* mutant strain REG1 soft agar stab; (d) *flaA/regA* mutant strain sbKSDFregA soft agar stab; (e) strain SB1003 stab-plate; (f) *flaA* mutant strain sbKSDF stab-plate; (g) *regA* mutant strain REG1 stab-plate; (h) *flaA/regA* mutant strain sbKSDFregA stab-plate.

3.6.10. Summary of angular directional motility assessments

I would expect that the movement in mutant cells would be greatly reduced relative to the wild type strain if the mutation(s) in question contributed to a structure needed for motility. The average distances travelled by cells are summarized in Table 3-12, but the flagellum-independent, solid substrate movement of cells did not appear to be affected in any of the mutant strains I tested. However, some genes were implicated in the effectiveness of flagellar motility.

Some mutations, however, did appear to affect the direction of cell movement. The direction of *R. capsulatus* cells moving in the plate-medium interstice of stab-plates appeared to respond to environmental stimuli (Figure 3-9). One stimulus affecting the direction of cell movement appeared to be white light, which seemed to be a prominent cue that overrode other signals (Figure 3-18). How white light was prioritized as a primary taxis cue is unknown, but perhaps involved some signal integration mechanism like in chemotaxis (Khan et al., 1995). Wild type *R. capsulatus* cells moved toward white light, in a coordinated group (Figure 3-38). The directional motility of mutants illuminated with white light was compared to that of wild type strain cells because mutations affecting photoresponsive motility were expected to cause changes in the response to white light illumination. The average angles of motility and P_Z values for the distributions of angular direction in response to white light illumination are summarized in Table 3-12. Data were pooled to increase the statistical reliability if no statistically significant difference in the distribution of directional movement was observed between a mutant and the parental strain.

The contributions of cellular components to motility summarized in Table 3-12 were considered in the following text of the Discussion (section **4**). The potential effects of mutations on the function of the flagellum, and the role of mutated components as signalling components in a directional movement response were considered with regards to the movement and taxis of characterized bacterial systems in other bacterial species.

Table 3-12: Statistical evaluation of the distribution of *R. capsulatus* motility in stab-plates illuminated with halogen white light.

Strain	Strain name	Average motility distance (mm)	Average angular motility direction (°)	P_Z [(a)]	# Samples
wild type	B10	29 (17)	0 (73)		355
wild type [(b)]	B10	29 (21)	-2 (90)	0.42	293
bchA$^-$/*crtB*$^-$	sbKSDFby and BY1653	39 (10)	-31 (74)	0.00075 *	72
capsule$^-$	37b4	41 (8)	25 (67)	0.015 *	47
cpaA$^-$	bKSDFcpaA	40 (14)	-10 (69)	0.081	28
cpaC$^-$	bKSDFcpaC	30 (20)	-18 (97)	0.24	41
cpaF$^-$	bKSDFcpaF	42 (10)	-15 (42)	0.064	36
ctrA$^-$	BCKF	20 (18)	5 (83)	0.5	125
flaA$^-$	bKSDF and sbKSDF	34 (16)	8 (75)	0.29	331
flaA$^-$/*pyp*$^-$	bKSDFpyp	28 (17)	17 (102)	0.39	30
gtaI$^-$	bKSDFgtaI	43 (7)	53 (57)	0.00000014*	31
hcpA$^-$	bKSDFhcpA	44 (3)	23 (54)	0.028 *	45
puhA$^-$	sbKSDFdw5 and DW5	41 (9)	8 (74)	0.56	61
regA$^-$	sbKSDFregA and REG1	41 (8)	22 (68)	0.0082*	60
rpoN$^-$	bKSDFrpoN and LJ1	34 (14)	-6 (85)	0.9	69
senC$^-$	sbKSDFsenC and LS01	38 (11)	34 (78)	0.00012 *	66

(a) Two-tailed two-independent sample Wilcoxon rank sum test of the angle of movement compared to wild type illuminated samples (standard deviation values presented in parentheses). For a >0.95 probability that the movement was different from the control, $P_Z < 0.05$. A P_Z value of ≥ 0.05 means no statistically confident determination regarding the distribution of movement direction could be made. Asterisks indicate cases where $P_Z < 0.05$.

(b) Incubated aerobically in the dark.

4. DISCUSSION

In this thesis, I investigated the occurrence, characteristics, and mechanism(s) of solid substrate motility in *R. capsulatus*. Solid substrate motility has become recognized in an increasing range of prokaryotic species (Harshey, 2003; Jarrell and McBride, 2008), and my results demonstrated that *R. capsulatus* is also capable of solid substrate motility. The occurrence of this motility in independently isolated *R. capsulatus* strains B6, B10, SP36, YW1, and YW2 (Table 2-1, Figure 3-7), indicated that it is a common trait in this species.

Solid substrate motility assays involve the introduction of cells to the assay surface and the measurement of cell movement. Cells on the assay surface may or may not be able to move. If cells do move, this movement can be either random or directed. Directed movement involves the reception of stimuli, integration of these signals, and cell orientation to generate a suitable movement direction. In probing the mechanism by which *R. capsulatus* cells achieve solid substrate taxis, I identified several fundamental characteristics of this motility. In probing the stimuli that influence the direction in which cell moved on a solid substrate, I found that *R. capsulatus* cells exhibited phototaxis toward white light.

4.1. Cell movements of *R. capsulatus*

Bacterial solid substrate motility can be assayed on the surface, or in the interstitial region of plates. The surface assay involves the introduction of cells onto the air-medium interface of the substrate, whereas stab-plate assay cells are introduced into the plate-medium interstice. In both cases, non-motile cells remain at the site of inoculation whereas motile cells can move away from the site of inoculation across the substrate. Twitching, gliding and sliding motility can be assayed either on the air-medium surface or in the interstitial region, whereas swarming motility is assayed on the air-medium surface (Burchard, 1970; Alm and Mattick, 1995; Martinez et al., 1999; Semmler et al., 1999). Swarming motility requires a film of fluid on the surface of the substrate (Fraser and Hughes, 1999). Because a fluid layer exists between the plate and the medium (Rashid and Kornberg, 2000), flagellar motility

contributions were expected to occur in the interstitial region. *R. capsulatus* cells moved both on the air-medium surface and in the plate-medium interstice, but movement in the interstitial region was observed much more frequently (approximately 10 and 85%, respectively). Perhaps conditions could have been optimized to yield a more robust surface assay, but I chose to focus on results from the stab-plate assay.

4.1.1. Substrate-dependent effects on *R. capsulatus* solid substrate movement

Bacterial motility on solid media is affected by the composition of the taxis surface (Henrichsen, 1975a; Harshey, 2003), but in my work it was unclear where in the plate-medium interstice cell movements occurred. *R. capsulatus* cells may have moved on the plate surface, medium surface, or within the interstitial fluid layer between these surfaces. The roles of these three phases were examined by testing the effects of the plate material, medium composition, and moisture content on movement.

4.1.1.1. Impaired motility of R. capsulatus on polystyrene

Numerous studies have reported bacterial taxis in the plate-agar interstitial region of plastic Petri plates (McMichael, 1992; Alm and Mattick, 1995; Semmler et al., 1999; Li et al., 2005; Han et al., 2008) and on glass surfaces (McBride, 2001). Polystyrene is a polymer of repeating aromatic styrene molecules organized in an ordered sheet made up of parallel strands with a hydrophobic surface (James and Castor, 2000; Stamm and Carlowitz, 2000). Borosilicate is an amorphous composition primarily composed of approximately: 81% silica (SiO_2) and 13% boron oxide (B_2O_3) with a polar surface (Varshneya, 1994; Vogel, 1994). *R. capsulatus* unexpectedly did not move in the plate-agar interstice of polystyrene plates, but cell movements occurred in borosilicate plates (Figure 3-1). *R. capsulatus* movement on polystyrene may have been impaired because of the presence or absence of adhesive forces between cells and the polystyrene surface. The movements of some gliding bacteria are limited

by adhesion on hydrophobic surfaces (Burchard et al., 1990). *R. capsulatus* cells may have been immobilized by hydrophobic interactions between the cell surface and the plastic, depending on the hydrophobicity of the cell surface (Gerson and Scheer, 1980; van Loosdrecht et al., 1987; van Loosdrecht et al., 1990). Alternatively, cell motility would be impaired if the movement mechanism required adhesion and cells were unable to adhere to the hydrophobic, ordered structure of the plate (Miyata et al., 2000; De La Fuente et al., 2007). While I did not directly test the adhesion between polystyrene and *R. capsulatus* cells, I suggest that *R. capsulatus* cell movement occurred on the surface of the growth medium, and that too much adhesion with the polystyrene surface inhibited this movement.

4.1.1.2. Changes in *R. capsulatus* motility in response to medium solidifying agent and concentration

The type and amount of solidification agent can affect the movement of cells across a medium surface. Individual *M. xanthus* gliding movements are negligible on 0.3% agar, but cells move readily on 1.5% agar (Shi and Zusman, 1993). Similarly, the average distance traveled by *R. capsulatus* in the plate-medium interstice was greatest with higher agarose concentrations, and shortest with 0.25% agarose (Figure 3-3). The increase in average distance traveled as the agarose concentration rose from 0.25% to 1% would seem to indicate that a certain amount of substrate rigidity was needed to facilitate cell movement. However, there appeared to be the opposite effect of Gelrite concentration on motility. The average distance traveled on Gelrite-solidified media was greatest with 0.25% and lesser with 0.5% and greater concentrations (Figure 3-3). Nevertheless, these data are consistent with the idea that *R. capsulatus* solid substrate motility occurs on the surface of the solid medium, as opposed to the surface of the plate.

Movement on both agarose and agar is not uncommon (Burchard, 1982; Shi and Zusman, 1993) but few bacterial motility studies have used Gelrite to solidify the medium. The leaf pathogen *Xylella fastidiosa* twitching motility occurs on 0.9% Gelrite-solidified medium (Hill and Purcell, 1995; Chen et al.,

2007) but *Cytophaga johnsonae* cells that can glide on 1.5% agar and 0.7% agarose do not move on 0.4% Gelrite (Wolkin and Pate, 1984).

Gelrite is a linear deacetylated gellan polysaccharide (Figure 4-1a) composed of a repeating tetrasaccharide polymer of rhamnose, glucose, and glucuronic acid (Kang et al., 1982; Colegrave, 1983; Shungu et al., 1983). Agarose and agar have as the primary component, a polysaccharide consisting of alternating anhydro-galactose and galactose disaccharides (Lahaye and Rochas, 1991). Agarose is the purified polysaccharide (Figure 4-1b) whereas agar contains approximately 30% agaropectin, a complex mixture of agarose polymers with sulphate-, methyl- and uronate-modified galactose side chains. The opposite effects of agarose and Gelrite concentrations on *R. capsulatus* motility indicated that the chemical composition of the solidifier polysaccharides had different effects on *R. capsulatus* motility, since movements were limited on Gelrite concentrations >0.5% but not higher agarose concentrations (Figure 3-3).

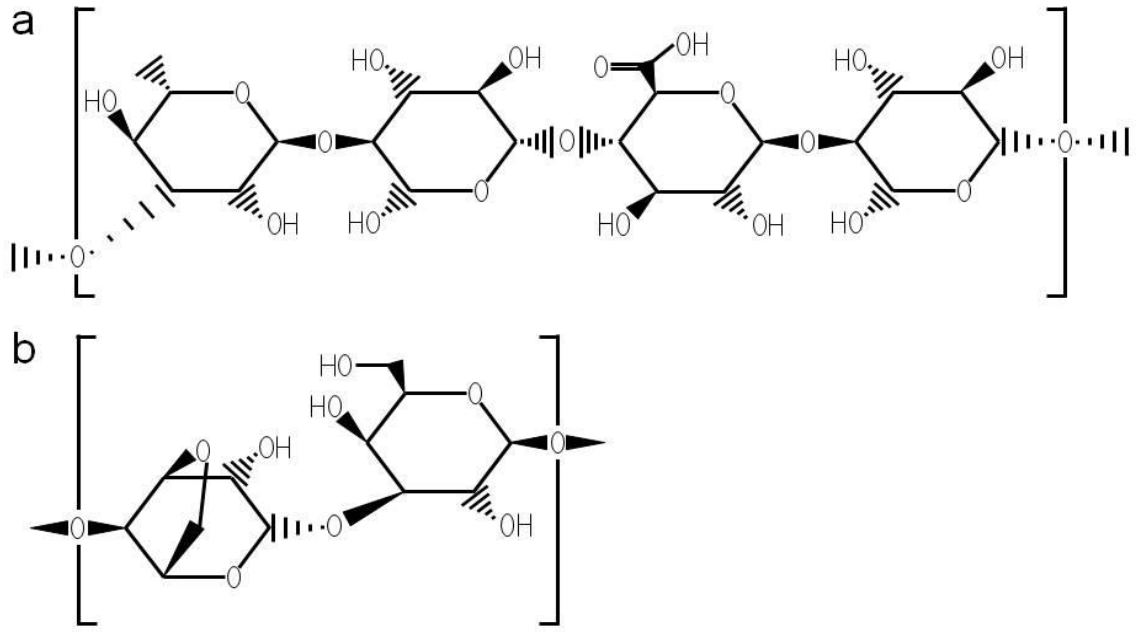

Figure 4-1: Chemical structures of solidification agents for bacterial growth medium. (a) the tetrasaccharide subunit of the Gelrite polymer; (b) the disaccharide subunit of the agarose polymer.

In summary, it appears that motility was affected by both the chemical composition of the medium solidifying agent, and the rigidity of the medium. These observations further indicated that motility in the plate-medium interstice occurred on the surface of the solidified medium. This is because if cells moved over the surface of the plates, or in the plate-medium interstice, the composition of the medium would not be thought to greatly affect movement.

4.1.1.3. Effect of medium moisture on *R. capsulatus* motility

The moisture content of the surface significantly effects solid substrate motility of prokaryotes (Henrichsen, 1975a; Berg, 2005). Swarming motility may be inhibited by too much or too little moisture (Alberti and Harshey, 1990; Harshey and Matsuyama, 1994; Ragatz et al., 1995). The fluid film associated with an interstitial region is beneficial to twitching motility (Henrichsen, 1972), and the hydration requirements of gliding motility can vary depending on the bacterial species (Harshey, 2003).

The moisture content of the solid substrate appeared to have affected the motility of *R. capsulatus*. Evaporation from 5 mL stab-plates reduced the moisture content by a greater percentage than evaporation from 20 mL plates, and the average distance and frequency of movements in 5 mL plates was less than in 20 mL plates (Figure 3-5, **APPENDIX A** Table A-2). Also, movement on the air-medium surface of plates occurred less frequently than in the plate-medium interstice. Therefore, I suggest that the reason why there was little movement at the air-medium surface may have been due to insufficient moisture.

4.1.2. Motility patterns in the plate-medium interstice

In the absence of a chemical gradient, bacterial twitching, gliding, or sliding motility on the air-medium or in the plate-medium interface typically occurs outward from the site of inoculation in a random manner (Rodriguez and Spormann, 1999; Rashid and Kornberg, 2000; Murray and Kazmierczak, 2008). When *R. capsulatus* cells were inoculated into the plate-medium interstice of stab-plates, cells

exhibited two motility patterns. One pattern appeared to be a broad, diffuse random movement, whereas another pattern resembled a dense, linear directed movement (Figure 3-19). Because of the published work on other species, a diffuse pattern characteristic of random movement was expected in the stab plate assay, and so the pattern interpreted as directed movement was unexpected. My comparisons of wild type and *flaA* mutant strains indicated that the flagellum was the major component driving the broad, diffuse type of motility, whereas a flagellum-independent mechanism drove the linear, directed movement (Figure 3-21).

Directed movement has previously been observed in solid substrate motility when cells perceive a suitable stimulus. Directed motility of cell groups was observed in *P. aeruginosa* and *M. xanthus* cells in a phosphatidylethanolamine (PE) gradient (Kearns and Shimkets, 1998; Kearns et al., 2001). These "social" cell masses moved in spearheads or rafts that spread out as large broad patterns up the PE gradient. *R. capsulatus* flagellum-independent movement generated a dense pattern with minimal spreading (Figure 3-21) that resembled a cell mass type of movement more similar to "adventurous" motility, which involves the movement of a single cell separately, than social motility.

While cells moving by adventurous motility often follow a non-linear path (Burchard, 1982; Wolgemuth et al., 2002), whereas *R. capsulatus* flagellum-independent movement was typically linear. *M. smegmatis* cells slide as a mass of cells at the front edge of an expanding colony that moves outward in a random pattern on agarose media. However, on 0.3% agar medium cells slide in linear masses (Martinez et al., 1999) that resemble the dense linear motility pattern of *R. capsulatus*. Along with the short period of time required to observe satellite colonies (see section **3.6.2**), this indicated that perhaps a group of *R. capsulatus* cell moved together in a directed manner, perhaps in response to some stimulus.

4.1.3. Directed *versus* stochastic motility in the plate-medium interstice

Motile cells on the surface or in the interstice of plates can exhibit either random or directed movement (Adler and Dahl, 1967). Any direction of movement is equally likely at all times for random motility, whereas directed movement, or taxis, has a bias in the direction of movement in response to a stimulus. For example, *E. coli* cells can travel up or down chemical gradients in the growth medium (Sourjik, 2004), whereas *M. magneticum* cells align their movement along magnetic fields in the environment (Philippe and Wu, 2010). *R. capsulatus* cells generated linear movement patterns in plates incubated in the dark, although the direction of movement was distributed over a broad range. All values fell within the outlier cut-off determined by the interquartile range (Figure 3-10). Outliers are data that do not follow the trend of the data and lie outside the normal distribution, being $\geq$3 standard deviations from the mean (Kleinbaum, 1998). In this statistical analysis, it was unclear whether this movement was due to a stochastic process or to a stimulus.

If the direction of *R. capsulatus* movement in plates incubated in the dark was not in response to a stimulus, perhaps the direction of movement was determined by a stochastic process (Hensel and Xiao, 2009) whereby motile cells do not reorient their direction of movement. Social solid substrate motility in *P. aeruginosa*, *M. xanthus*, and *R. centenum* involves the arrangement and coordination of groups of cells (Harshey, 1994; McBride, 2001). Cells in such a social mass undergo alignments along the long axis of the cells upon coming into contact with each other to organize into raft-like clusters (Semmler et al., 1999). Cells that join a social mass conform to the alignment of the raft, however it is unclear what factors would dictate the orientation of the first two cells coming together to form the initial nucleation stage of a social mass. It could be the adhesion of one cell to the substrate, an alignment partway between the original orientation of each cell, or a random Brownian motion that results in the orientation of the first cells. Perhaps the original alignment of *R. capsulatus* cells in a social mass was sufficient to predispose the direction of motility in the absence of a stimulus.

4.1.4. Possible chemotaxis in the plate-medium interstice

In the absence of an obvious stimulus, bacteria were expected to move outward from the site of inoculation as a circle (Berg, 1996), but flagellum-independent *R. capsulatus* movement was characterized by a dense, linear pattern. Either chemotaxis or energy taxis could have accounted for directed movement in response to stimuli in the plate-medium interstice. Chemotaxis involves the integration of multiple stimulus inputs to determine the direction of motility (Khan et al., 1995). *E. coli* chemotaxis MCP receptors detect one or several stimuli (Ames et al., 2002) and the input from simultaneous signals is integrated to determine, for example, whether an attractant or repellent will have a more profound effect (Adler and Tso, 1974). Energy taxis occurs in a similar manner. Movement to conditions favouring optimal metabolic activity is determined by the integration of multiple stimuli by membrane-associated or cytosolic receptors (Schweinitzer and Josenhans, 2010). Proteins with MCP signaling domains respond to cues that reflect the internal energetic conditions of the cell and transduce the energy taxis signal to the motility apparatus. These MCP proteins can be a single protein with a sensory and transduction domain, or can interact with a separate signal reception protein (Hendrixson et al., 2001; Greer-Phillips et al., 2003). In both chemotaxis and energy taxis, the stimulus strength, and the integration of multiple stimuli are the mediating factors for the direction of movement, and may have influenced *R. capsulatus* movement as discussed below.

Perhaps the direction of cell movement in the dark was a chemotactic response to multiple factors. A chemotactic integration of oxygen, carbon source, and nitrate/nitrite stimuli was proposed to drive swarming patterns in *Pseudomonas* strain KC cells (Emerson, 1999). However, as the *Pseudomonas* cells proliferated and depleted nutrients, they moved outward from the site of inoculation randomly (Emerson, 1999), whereas wild type *R. capsulatus* cells sometimes moved in a directed pattern (Figure 3-9). The directed movement was especially pronounced in strains lacking the flagellum (Figure 3-21). The *R. capsulatus* genome encodes 18 MCPs and a homologue of *nnrS*

(Haselkorn et al., 2001; Cabello et al., 2004). The NnrS protein of *R. sphaeroides* is required for chemotaxis toward nitrate (Bartnikas et al., 2002). Chemotaxis has not been demonstrated in *R. capsulatus*, but these MPCs and NnrS may potentially have directed motility as cells depleted the local concentration of nutrients. However, this directed *R. capsulatus* pattern did not seem to be consistent with a chemotaxis mechanism involving nutrient depletion, unless an aligned group of cells continued to move in the direction that was initially chosen randomly.

No known chemical gradients were established in the plate medium, but it is likely that the microenvironment around cells at the stab point quickly came to have reduced oxygen concentrations around respiring cells. Aerotaxis is a form of chemotaxis that responds to oxygen concentrations (Taylor et al., 1999). The membrane-anchored Aer protein of *E. coli* regulates swimming through the CheA-CheW chemotaxis signalling pathway. The oxygen-dependent modulation of flagellar rotation by Aer causes cells to move toward optimal oxygen concentrations (Armitage and Schmitt, 1997; Bibikov et al., 1997). Aerotaxis has not been demonstrated in *R. capsulatus*, but its RegA/RegB two-component system also acts as a global regulator similar to that of *R. sphaeroides* (Elsen et al., 2000; Swem et al., 2001). The RegB sensor-kinase has been shown to regulate aerotaxis in *R. sphaeroides*, apparently by sensing changes that originate in the aerobic respiratory chain (Romagnoli et al., 2002; Elsen et al., 2004). Different oxygen concentrations may have manifested as changes in the electron flow through the *R. capsulatus* ETC and in the proton gradient (Dang et al., 1986), which in turn may have been sensed by the RegB sensor-kinase that communicated with an aerotaxis system, as in the closely related *R. sphaeroides* (Romagnoli et al., 2002).

R. capsulatus also produces two aerobic repressor proteins, CrtJ and AerR, that regulate the expression of photosynthesis genes (Dong et al., 2002). It seems less likely that aerotaxis would have

been mediated through CrtJ or AerR, because these are transcription regulators and not known to modulate protein activity, as in the response of pilus and flagellar motility.

In summary, the initial movement of an aligned group of cells away from the mass at the site of inoculation, in response to depletion of oxygen, may have determined the direction of movement. Once cells began to move in a direction, they may have perceived entry into a zone of increased oxygen concentration, which may have resulted in continued movement in that direction. Thus, the random orientation of initial movement may have accounted for the broad distribution in the directional movement of *R. capsulatus* stab-plates incubated in the dark (Figure 3-10).

4.2. Light-induced cell movements in *R. capsulatus*

Because *R. capsulatus* flagellar swimming is photoresponsive, I thought that solid substrate motility may also respond to light. The rotation of the flagellum in swimming *R. capsulatus* cells is modulated by the intensity of light. Since the electrochemical proton gradient drives the flagellum rotation, decreases in the flow of electrons through the electron transfer chain (ETC) are thought to stop or slow flagellar rotation (Hellingwerf et al., 1998). Brownian motion alters the orientation of the cell such that when swimming resumes, the cell moves in a different direction. If the new direction of swimming does not result in a decrease in light intensity, there is less frequent pausing. The net result is that cells accumulate in zones of illumination, but this is not taxis toward light. Instead, it is a scotophobic (fear of darkness) behaviour that is an energetic response independent of the direction of the light (Drews, 2005).

The phototactic response in other species is determined by the integration of signal cascades from multiple wavelengths in accordance with the strength of the respective illumination stimuli (Armitage and Hellingwerf, 2003). *R. centenum* cells travel toward IR illumination, but in the presence of a sufficient intensity of visible wavelength illumination the IR spectrum stimulus is ignored and cells

travel away from the light (Ragatz et al., 1995). Similarly, the *H. salinarium* phototaxis signal for movement toward green/orange illumination is negated by sufficient blue/green light (Mironova et al., 2005). In my tests the illumination wavelengths and intensities were approximately constant, and so a phototactic movement should have had a consistent direction with a parametric distribution. When *R. capsulatus* circular stab-plates were illuminated with white light, the distribution of the directions of cell movement appeared less random than stab-plates incubated in the dark, with a bias toward the light (compare Figure 3-10 and Figure 3-15). The number of samples was increased by pooling all strains used in stab-plates and in the majority of tests cells travelled toward the light (Figure 3-16). However, movement in a significant portion of the illuminated stab-plates was in the hemisphere considered to be away from the light, and the data did not follow a parametric (normal) distribution.

The direction of movement in circular plates may have followed a parametric distribution, masked by the presence of random outlier data. The interquartile range (IQR) determined from the distribution of tests can be used to determine if data in the first and fourth quartiles are outliers (see section **3.2.1**). Outliers may be the result of random error, but they can also indicate the presence of unanticipated variables (Kleinbaum, 1998). The cut-off values for outlier data calculated by the IQR were beyond the maximal measured angle in both directions from the light source (Figure 3-16). Because no samples were outliers, directional cell movement of *R. capsulatus* in circular plates followed a non-parametric distribution.

It was thought that the curvature of, and irregularities in, the circular glass plates may have changed the perceived direction of the light source, Therefore, square polystyrene plates were used and found to yield a distribution of directional motility that was more tightly clustered than in circular plates (compare Figure 3-16 and Figure 3-18). In contrast to the circular plates, the data from the square plates yielded cut-off values for outliers that were within the hemisphere nearest the lamp ($\pm$90°). Cells reproducibly moved toward the white light in a parametric distribution, although a small outlier fraction

(6%) did not. Perhaps these outliers integrated multiple stimuli and responded in the direction of something other than light, or there still were optical effects, although to a lesser degree than in the circular plates. I believe there still was variability in the direction of light perceived by cells inoculated into square plates that were subsequently stacked and incubated in front of lamps.

If the illumination stimulus was not sufficient, another stimulus may have directed cell movement. Light is a primary source of energy for *R. capsulatus*, so if this organism were phototactic, light of specific (photosynthetic) wavelengths in sufficient quantities would be expected attract cells (Schweinitzer and Josenhans, 2010). It is worth considering the path of photons (or waves, because of the dual nature of light) from a lamp to the interior of a stabbed plate. Light leaves the lamp as a spray of photons that strike the surfaces of the plate at various angles (Weast and Astle, 1982). My experiments were done with stacks of plates, resulting in differences in the angle of incidence. As light waves move from air into glass they are refracted, or bent, depending on the angle of incidence, and again as they leave the glass. It is not clear what happens as light enters the agar medium, but it seems likely that there could be variable effects depending on the degree of homogeneity of the media. Light travelling through the agar may reflect from the top, the bottom or the sides of the plate. Finally, a certain amount of light may be diffracted (decomposed into constituent wavelengths due to differential refraction of wavelengths), and these wavelengths further refracted and reflected as they pass through the plate. Therefore, it is perhaps not surprising that it was so difficult to obtain reproducible data on phototaxis.

4.2.1. Action spectrum of *R. capsulatus* solid substrate, photoresponsive movement

The distribution of directional motility indicated that cells moved toward white light significantly more often than away from the light (Figure 3-18), but it did not indicate what wavelengths of light cell movement responded to. The induction and direction of taxis by specific wavelengths defines the action spectrum for photoresponsive movement (Harayama and Lino, 1976), and I tested the action

spectrum of *R. capsulatus* to determine which wavelengths affected cell movement, using circular plates.

Based on the average angular direction and distribution of directional movement, it could be argued that cells did not respond to 375, 385, 405, 470, 490, 525, 625, 632, 650, and 700 nm wavelengths (**APPENDIX C**, Figure C-1 and Figure C-4). Similarly, cells appeared to move toward 425, 450, 572, and 750 nm wavelengths. Furthermore, the >350, 610, and >900 nm illumination distribution was similar to white light controls, so perhaps cells moved toward these wavelengths. The distribution of motility to 395 nm illumination indicated cells may have moved away from this wavelength.

However, the lack of a random dark control that differed significantly from white light-illuminated tests, and the conflicting data from white light illumination in the aquarium/LED and filter chambers, rendered this action spectrum data suspect. Thus, a confident assessment of the effects of wavelengths tested could not be made for the action spectrum data available. In retrospect, because square plates appeared to give rise to fewer artefacts than circular plates (compare Figure 3-15 and Figure 3-18), it may have been better to use square plates for the action spectrum experiments (although this would not have compensated for the lack of a robust dark control).

4.2.2. Mutations affecting the direction of *R. capsulatus* solid substrate movement

The distribution of directional movements of mutants affected in photosynthetic pigments (BChl/Crt), HSL synthase production (GtaI), the membrane-associated SenC, and the response regulator RegA differed statistically from the wild type movements (Table 3-12), as discussed below. These experiments were plagued by variability, and it was sometimes difficult to see how graphical plots of the frequency of directional motility related to the statistical analysis.

Bacteriochlorophyll (BChl) and the carotenoid spheroidene are the part of the photosynthetic apparatus in *R. capsulatus* (Armstrong et al., 1990; Blankenship, 2002). Carotenoids protect the cell

from photo-oxidative damage and along with BChl are used to harvest light. The CrtB enzyme creates the first of a series of carotenoid intermediates early in the biosynthetic pathway. It converts geranylgeranyl diphosphate into phytoene. The *bchA* locus encodes chlorin reductase that converts chlorophyllide to 3-vinyl bacteriochlorophyllide *a*, which in four steps is converted to BChl (Willows and Kriegel, 2008). The direction of movement of the *bchA*/*crtB* mutant was broadly dispersed (see **APPENDIX B**, Figure B-1), which indicated that, in contrast to the wild type strain, this mutant was not biased to move toward white light. The BChl and carotenoid pigments may have been needed for directional cell movement toward white light by acting as photoreceptor molecules. The movement of the *puhA* mutant (lacking the photosynthetic RC) was not different than the wild type strain, and so it appeared that photoresponsive motility did not require a functional photosynthetic RC. If so, this would differ from the flagellum-driven *R. centenum* photoreception signal transduction model that is based on sensing of the photosynthesis-dependent redox state of the ETC by the chemotaxis-like Ptr protein (Jiang and Bauer, 2001). Alternatively, the BChl and carotenoid biosynthesis pathways may have affected motility independently of the photosynthetic apparatus. Perhaps the signal for photoresponsive movement was transduced directly from the LH1 and LH2 complexes, or from a biosynthetic intermediate. For example, protoporphyrin IX is a BChl/heme precursor in *R. capsulatus*, and the absorption of blue light by protoporphyrin IX affects the rotation of the flagellum in *E. coli* (Yang et al., 1995). By analogy it is possible that a BChl or carotenoid biosynthetic intermediate, as opposed to the end product, was a photoreceptor required for movement toward white light.

Modelling of *Synechocystis sp.* strain PCC6803 taxis indicated that cells had an excitation threshold. Excitation was a prerequisite for taxis and could be induced by other cells, or possibly by stimuli (Levy and Requeijo, 2008). The *R. capsulatus* 16C acyl-HSL synthesized by GtaI is a signal for quorum sensing (Schaefer et al., 2002), in a culture density-dependent mechanism for signalling between cells. The *gtaI* mutant moved as a coordinated mass, so a possible excitation phenomenon

was not inhibited by this mutation (Figure 3-43). However, in agreement with the statistical analysis (Table 3-12), a graphical representation indicated that the movement of the *gtaI* mutant was not biased toward white light (see **APPENDIX B**, Figure B-2). Without HSL production, there may have been a change in the expression of a gene that affected movement toward white light. Alternatively, perhaps the quorum sensing system was required to coordinate the orientation of a cell mass, to ensure the group moved in the direction of the white light source.

SenC, required for the assembly of the ccb_3-type cytochrome *c* oxidase, may have affected motility by altering the flow of electrons through the ETC, similar to photoresponsive movement in *R. sphaeroides* and *R. centenum* (Gauden and Armitage, 1995; Jiang et al., 1997; Romagnoli et al., 2002). However, the distribution of *senC* mutant directional motility was clustered around 34° relative to the orientation of the light source, and although there was great variability, most of the movement was in the hemisphere closest to the lamp (see Table 3-12, **APPENDIX B** Figure B-4). Perhaps a loss of SenC reduced electron flow by reducing amounts of the ccb_3-type cytochrome *c* oxidase, although the finding that the RC (*puhA*) mutant moved toward the light indicated that perturbation of electron flow did not have an effect on the direction of motility. The SenC protein itself may have transmitted a signal to the motility apparatus like the *R. centenum* Ptr protein (Jiang and Bauer, 2001), but despite the statistical significance of the data in Table 3-12, it was difficult to determine whether the *senC* mutant responded to white light.

While the statistical comparison of *regA* mutant movement to that of the wild type showed a significant difference (Table 3-12), the distribution of *regA* mutant directional movement appeared to be biased toward the light (see **APPENDIX B**, Figure B-4). Again, it is difficult to be unequivocal about whether the statistical analysis shows an absence of a response to illumination, or simply indicates a difference in the distribution of values compared to the wild type strain. If the *regA* mutant data represented random movement, the RegA protein could transduce a light stimulus upon

phosphorylation by RegB, a sensor kinase that senses the electron flow through the ETC (Masuda et al., 1999; Elsen et al., 2004). If RegA were required for movement toward white light, it would indicate that movement toward white light occurred in an energy taxis-dependent manner (Alexandre, 2010), because transcription of genes by RegA would have been modulated by RegB in response to the redox state of the ETC. However, as for the *senC* mutant, the finding that a *puhA* mutation did not affect the direction of motility (Table 14) indicated that a signal did not originate from electron flow through the ETC.

In summary, although the statistical analyses indicated some factors potentially involved in phototaxis, the experimental variability prevented a confident assignment. Perhaps the use of square plates would have helped in this series of experiments.

4.3. Flagellum-dependent and flagellum-independent cell movements in *R. capsulatus*

Two motility patterns were observed macroscopically in the plate-medium interstice, a broad diffusive pattern and a dense linear pattern (Figure 3-19). Prokaryotes move using a variety of structures, and some bacteria possess multiple mechanisms for movement under different conditions (Bardy et al., 2003). *R. centenum* switches from a polar flagellar swimming in aqueous environments to hyperflagellated swarming on solid substrates (McClain et al., 2002). *P. aeruginosa* can swim through aqueous conditions using a flagellum or move over solid substrates using swarming, twitching, or sliding mechanisms (Rashid and Kornberg, 2000; Murray and Kazmierczak, 2008). When *R. capsulatus* wild type cells in the plate-medium interstice were visualized by oil immersion microscopy, two types of motility were evident: 1) rapid random movement within uncolonized pockets; and 2) slow linear movements along the cell periphery and within cell masses (Video 1,3). As discussed below, my results showed that *R. capsulatus* was capable of at least two modes of motility: 1) a flagellum-dependent mechanism; and 2) a flagellum-independent mechanism.

In an attempt to identify a factor needed for solid substrate movement, several proteins and cell components were investigated for effects on motility, either by creating knockout mutations, or investigating previously isolated mutants. It was found that none of the following were required for motility in the glass-agar interstice of plates: the response regulator CtrA, a putative CpaC secretin, a putative CpaF ATPase, a putative CpaA peptidase, the cell capsule, a putative surface protein HcpA, the RC H subunit PuhA, the PYP protein, the HSL synthase GtaI, the sigma factor RpoN, the membrane-associated SenC, or the response regulator RegA.

4.3.1. Flagellum-dependent contributions to *R. capsulatus* solid substrate movement

The broad diffusive pattern of motility in stab-plates was driven by the *R. capsulatus* flagellum (Figure 3-21). In general, flagellar motility may move cells through a liquid medium, even if made viscous by low concentrations of solidifying agent, or on the surface of solidified media. Flagellum-driven movement on the surface of a solidified medium is called swarming motility. Hyperflagellation is typical of swarming motility (Fraser and Hughes, 1999), but wild type strain B10 cells from solid substrate culture did not appear hyperflagellated in EM images. However, hyperflagellation is not strictly required for swarming (McCarter, 2010), and so *R. capsulatus* cells may have swarmed in the absence of hyperflagellation. Whether flagellum-dependent movement in the plate-medium interstice was swarming was not addressed in these experiments, although the contributions of flagellar movement were assessed.

The flagellum-dependent movement in the plate-medium interface appeared to have occurred after the flagellum-independent movement. This is because in the time-course experiments the appearance of plates stabbed with wild type cells after ~16 to 20 hours resembled the appearance of later stages of plates stabbed with strains lacking the flagellum (compare Figure 3-37 and Figure 3-38).

The appearance of these plates indicated that flagellar contributions occurred after approximately 24 hours (Figure 3-37).

Different species of bacteria exhibit different trends in flagellar gene expression as cultures progress from the exponential through the stationary phase of growth. For example, *H. pylori* cells express two flagellin genes, *flaA* and *flab*, with transcription of *flaA* highest in late exponential phase, whereas *flab* transcription peaks in early to mid-exponential phase. Transcription of both genes is negligible in stationary phase (Niehus et al., 2002). *C. crescentus* flagellum genes are expressed at specific periods of the cell cycle (Wu and Newton, 1997), and flagellin transcription in *E. coli* is increased in mid- to late exponential growth phases (Sperandio et al., 2002). Similar to *E. coli*, *R. capsulatus* was found to induce the expression of flagellar genes as cultures progressed from exponential to stationary phase (Lang and Beatty, 2002). Perhaps flagellar gene expression during 16 to 20 hours after inoculation of stab-plates resembles the expression in liquid medium cultures in the early stationary phase. This would explain the induction of flagellar motility, as evidenced by the broadening of the line of growth, and the appearance of colonies, after 24 hours in wild type strain stab-plates.

Growth phase dependent flagellar transcription and a scotophobic response could also explain the pattern of flagellum-dependent motility in stab-plates illuminated with white light. The accumulation of cells (self-shading) may have contributed to changes in the transmission of light through the culture to individual cells. A decrease in light intensity may have induced flagellar tumble reorientations that resulted in movement away from the path of linear motility (Rushing et al., 2000), causing cells to travel outward as they moved toward the light source (Figure 3-19c).

4.3.1.1. Changes in flagellum-dependent movement contributions of *R. capsulatus* mutants

The flagellum-dependent movements of the rifampicin-resistant strain SB1003 appeared to be greater than wild type B10 (Figure 3-21). This was unexpected because strain SB1003 was derived from

strain B100, which is a phage-free derivative of B10 (Solioz and Marrs, 1977). The difference may have been due to the strength of flagellar propulsion. Because decreases in the proton motive force of *E. coli* and *Salmonella* reduce the rotational speed of the flagella (Minamino et al., 2003), I speculate that the SB1003 flagellum rotates at a faster rate than that of B10 cells due to a difference in the proton motive force. Regardless, some unknown mutation(s), changes associated with the loss of prophages, and/or properties of the rifampicin-resistant RNA polymerase β-subunit (O'Neill et al., 2000), increased the activity or effectiveness of the flagellum in strain SB1003.

Quorum sensing regulates the expression of bacterial flagellar genes, such as in *S. meliloti* and *H. pylori* (Rader et al., 2007; Hoang et al., 2008). The magnitude of *R. capsulatus* flagellum-dependent movement exhibited in the *gtaI* mutant BLKI appeared to be less than that of wild type B10. The GtaI protein synthesizes a 16C acyl-HSL that allosterically modifies the DNA-binding activity of the GtaR response regulator (Leung, 2010). Movement through soft agar indicated that BLKI cells produce a functional flagellum (Figure 3-43), so the difference may have due to been decreased flagellar propulsion controlled at the transcriptional level by GtaR.

The production of *S. meliloti* exopolysaccharide is also quorum sensing dependent (Hoang et al., 2008), and the absence of exopolysaccharide in the capsule-deficient *R. capsulatus* strain 37b4 reduced movement through soft agar (Figure 3-33). The loose material of the capsule may increase flagellar propulsion through soft agar by decreasing the friction and drag on cells. Perhaps the loss of quorum sensing in *R. capsulatus* also decreases capsule production, which resulted in an intermediate soft agar swimming phenotype.

The *puhA* mutant is not phototrophic, and thus cannot grow anaerobically unless supplemented with a suitable carbon source and terminal electron acceptor (Saeki and Kumagai, 1998). The growth profile of *puhA* mutant cells in soft agar tubes (Figure 3-39) provided a reference to evaluate O_2

diffusion into the unsupplemented soft agar. The *puhA* mutant growth in the upper region of the tube indicated that this region was aerobic, whereas the inhibition of growth in the lower region of the tube indicated this region was anaerobic. The middle region separated by the upper and lower phases appeared to be semi-aerobic, based on the limited growth of cells in this region. By comparison of flagellum-dependent movement to the *puhA* mutant in soft agar stab tubes, the *senC* and *regA* mutants appeared to be affected by the O_2 concentration gradient (see below).

Flagellar motility of the *senC* mutant was decreased in the upper aerobic region of soft agar stabs, while cells moved out through the agar in the lower semi-aerobic and anaerobic regions (Figure 3-45). The *R. capsulatus* SenC affects the redox state of the ETC, because SenC is needed for assembly of the ccb_3-type cytochrome *c* oxidase (Buggy and Bauer, 1995; Swem et al., 2005), which has a low affinity for oxygen and is produced under oxygen-saturating conditions (Swem and Bauer, 2002). Thus, a potential link between limited motility and SenC could be impairment of aerobic respiration by reducing the levels of ccb_3-type cytochrome *c* oxidase in the membrane. With impaired respiration in the aerobic zone of the soft agar stab, it is possible that the relatively high concentration of O_2 repressed photosynthesis (Ma et al., 1993), thus decreasing the proton gradient powering flagellar rotation.

In contrast, flagellar movement of the RegA mutant in soft agar was decreased throughout the stabs (Figure 3-46). The membrane-bound RegB sensor kinase senses the redox state of the ETC (Masuda et al., 1999; Elsen et al., 2004) by binding oxidized ubiquinone, which inhibits autophosphorylation. When the concentration of oxidized ubiquinone is low (*i.e.*, under anaerobic conditions), RegB autophosphorylates and transfers a phosphate to RegA (Swem et al., 2006). The *R. capsulatus* RegA is a global regulator of transcription (Elsen et al., 2004), including genes needed for anaerobic and aerobic respiration (Willett et al., 2007) and phosphorylated RegA represses the expression of photosynthesis genes under aerobic conditions (Sganga and Bauer, 1992). RegA may be

required for transcription of flagellar genes under anaerobic conditions, or perhaps RegA is linked to limited motility by impairment of anaerobic respiration. Phosphorylated RegA may be required for maximal transcription of flagellar genes under anaerobic conditions, or perhaps RegA is linked to motility by impairment of photosynthetic electron transfer, due to a decrease in the transcription of genes required for photosynthetic complex proteins and pigment biosynthesis (Willett et al., 2007). Decreased electron transfer would reduce the proton gradient powering flagellar rotation, reducing movement through the soft agar.

4.3.2. Flagellum-independent contributions to *R. capsulatus* solid substrate movement

The dense linear pattern of motility in *R. capsulatus* stab-plates was a flagellum-independent mechanism (Figure 3-21). Movement occurred in both the *flaA* mutant strain bKSDF that lacked the flagellar filament and the *ctrA* mutant strain BCKF that did not express flagellar genes (Lang and Beatty, 2002). The macroscopic appearance of flagellum-independent *R. capsulatus* movement resembled the directed movement of *Synechocystis sp.* strain PCC6803 and *R. centenum* (Ragatz et al., 1994; Burriesci and Bhaya, 2008).

Synechocystis individual cell motility was limited, but directed movement was enhanced by groups of cells moving together (Burriesci and Bhaya, 2008). Observations of *Synechocystis* twitching motility indicated that an "excitation" state was required for movement, and an excited cell could induce the excitation of other cells around it, forming a group of motile cells (Levy and Requeijo, 2008). The swarming phototaxis of *R. centenum* also occurred as a group of cells (Jiang et al., 1998).

As in *Synechocystis*, individual cell movements of *R. capsulatus* were punctuated by frequent stops, and stationary cells approached by motile cells occasionally became motile (Video 4). The linear macroscopic pattern of movement, the strong localized ^{32}P emission signal at the edge of plates stabbed with labelled cells (Figure 3-36), and the macroscopic appearance of satellite clusters within 12 hours of

inoculation (Figure 3-38), all indicated that long-range flagellum-independent *R. capsulatus* movement occurred as a coordinated group of cells.

The rate of flagellum-independent *R. capsulatus* cell movement determined by light microscopy was similar to that estimated in macroscopic examinations of time-course stab-plates. The flagellum-deficient *flaA* mutant strain bKSDF cells visualized in the plate-medium interstice by light microscopy exhibited only slow linear movements (Video 4,5). The rate of movement for these cells was determined to be ~1.1 to 1.6 μm/sec. Time-course results indicated that flagellum-independent movement in the plate-medium interface occurred before the flagellum-dependent movement, within 12 hours of inoculation (Figure 3-38). To have reached the plate edge from the site of inoculation within this time, the rate of cell movement had to be at least 1 μm/sec. Individual and social *M. xanthus* movement rates differed on 0.3 and 1.5% agar media (Shi and Zusman, 1993), so 1 μm/sec may not reflect the maximal rate of *R. capsulatus* flagellum-independent movement. The motility rate may differ with changes in medium composition.

My results indicated that the flagellum-independent microscopic linear movements observed in the plate-medium interstice led to the macroscopic movements in the time-course experiments. The rate of flagellum-independent movement indicated that motility may have been due to one of the gliding or sliding mechanisms listed in Table 1-1. A sliding mechanism seemed unlikely because sliding motility is a passive form of translocation (Matsuyama et al., 1995; Martinez et al., 1999). Sliding cells move outward in response to the increase in pressure of cell division within the cluster. This force translates in all directions, and would not be expected to generate directed movement. Thus the flagellum-independent movement observed in *R. capsulatus* may have been gliding motility.

4.3.2.1. Changes in flagellum-independent contributions to *R. capsulatus* movement

The flagellum-independent motility pattern of the *bchA*/*crtB*/*flaA* triple mutant was different from that of other *flaA* mutants in stab-plates. This was because the *bchA*/*crtB*/*flaA* mutant cells did not produce the dense, linear pattern characteristic of flagellum-independent movement (Figure 3-39). Statistical analysis of the distribution of directional movement of the triple mutant and wild type strains indicated that either BChl or carotenoid photoreception was also required for movement toward white light (Table 3-12). Perhaps coordinated cell movement required photoreception by BChl or carotenoids. It was suggested that the phototaxis of *Synechocystis* cells involved the transmission of an excited state from one cell to another. A sufficient mass of cells in this excitation state then moved as a group (Burriesci and Bhaya, 2008). If these pigments induce a light-dependent excited state, unpigmented cells would not reach an excitation state or transfer this state from cell to cell. Motile groups would not form and the dense linear pattern of movement would not be generated.

Alternatively, the pigments may have been used as a signalling component between cells in a motile mass. Carotenoids are cleaved to generate signalling molecules in animal cells (Giuliano et al., 2003), so perhaps spheroidene or a carotenoid precursor were a signalling molecule to organize cells into coordinated taxis masses. However, carotenoids are hydrophobic and found in the inner membrane of *R. capsulatus*, and so it seems unlikely that an uncleaved carotenoid would serve as an intercellular signalling molecule.

4.3.2.2. Investigation of twitching contributions to *R. capsulatus* solid substrate movement

R. capsulatus EMs showed polar, pilus-like appendages as splayed or bundled conformations (Figure 3-25), resembling other EMs of bacterial pili (Bakaletz et al., 2005; Li et al., 2005). No polar, pilus-like appendages were observed by fluorescence microscopy, but this may have been due to the limitations of the microscope(s) I used. The T4P and T4P-mediated twitching motility of *P. aeruginosa*

were visualized using a sophisticated total internal reflection fluorescence (TIRF) microscopy apparatus (Skerker and Berg, 2001). TIRF microscopy greatly reduces background fluorescence, so much higher sensitivity can be obtained than with conventional fluorescence microscopes (Axelrod, 1989). Perhaps a TIRF microscope would allow for the visualization of the pilus-like appendages seen in the *R. capsulatus* EMs (Figure 3-25).

Bacterial twitching motility is achieved by the extension, adhesion, and retraction of T4P in a range of bacteria, including *P. aeruginosa*, *M. xanthus*, and S*ynechocystis* (Henrichsen, 1975b; Mattick, 2002). A peptide from a protein predicted to be an Flp/Tad TadG pilus anchor was identified by MS-MS sequencing of *R. capsulatus* proteins (see **APPENDIX A**, Table A-5). This led to the bioinformatic identification of a putative T4bP gene cluster in the *R. capsulatus* genome (Figure 3-27), but *R. capsulatus* movement was not affected when several predicted homologues of genes required for the extension of a T4P in other bacteria (Craig and Li, 2008) were knocked out. Whether *R. capsulatus* cells make a pilus was not addressed by these experiments, but flagellum-independent motility (Table 3-7) was not mediated by proteins from the predicted pilus genes that were knocked out (Table 3-6). The rate measured for *R. capsulatus* movement was also greater than those of known twitching motility mechanisms (Table 1-1), which further indicated this was not twitching motility. This left a gliding mechanism as the likely candidate for flagellum-independent *R. capsulatus* movement.

4.3.2.3. Investigation of gliding contributions to *R. capsulatus* solid substrate movement

The rate of cell movement indicated that a gliding mechanism may drive the flagellum-independent motility of *R. capsulatus.* Gliding motility may have been achieved by a cytoskeletal rearrangement, extrusion, or adhesion mechanism, and movement rates vary from ~0.02 - 10 μm/sec (Table 1-1). The Cy3-labelled extracellular material observed in Figure 3-31 indicated that an extrusion gliding mechanism may be involved in *R. capsulatus* flagellum-independent motility. However, what this

free amine-containing material was, and where it originated from was unknown. In the absence of a clear candidate gene involved in gliding motility, it was hoped that a random mutagenesis approach would be fruitful using the Tn5 transposon (Matsunaga et al., 1992; Jacobs et al., 2003). The idea was to screen for the absence of flagellum-independent motility in stabbed plates, to identify a Tn5-tagged gene.

In theory, full genome saturation would require a mutant library consisting of approximately five times the number of genes in the genome (Jacobs et al., 2003; Pollock and Larkin, 2004; Salama et al., 2004). The *R. capsulatus* genome encoded a predicted 3685 genes, so approximately 18400 mutants were theoretically needed to have a 99% probability of hitting all genes. However, many gene mutations would be lethal, and so a smaller number should have sufficed. The bacterial flagellum requires more than 40 genes (Aizawa and Kubori, 1998; Macnab, 2003), T4P depend on approximately 30 to 40 gene products (Mattick, 2002; Salama et al., 2004), and *M. xanthus* gliding motility may involve around 70 genes (Hartzell and Youderian, 1995). Thus I reasoned that *R. capsulatus* flagellum-independent movement should require at least approximately 40 genes, and perhaps a library on the order of 1000 mutants would suffice. My library of 1503 mutants provided a theoretical ~8% coverage of the genome, but evidently was not large enough, because a mutant incapable of flagellum-independent motility was not obtained.

4.4. Concluding remarks

The results of this thesis focused on the finding of a previously unsuspected solid substrate taxis in *R. capsulatus*. I discovered several interesting aspects of this motility, although the mechanism responsible for flagellum-independent contributions was not determined. Several unanswered questions arose from the interpretation of my results, and suggest avenues for future research.

The action spectrum of photoresponsive motility provided preliminary data, and requires further investigation. My results indicated that a BChl-related and/or carotenoid-related molecule may act as a receptor for photoresponsive movement. Improvement of the reliability of the stab-plate assay could be achieved using a focused light source and square plates, and a greater number of replicates would be beneficial. To follow up on experiments on an improved wild type action spectrum, a variety of pigment biosynthesis and photosynthetic complex mutants exist (Yen and Marrs, 1976; Bollivar et al., 1994; Lilburn et al., 1995; Wong et al., 1996). These and similar mutants could be used in experiments to confirm whether the wild type action spectrum relates to a factor absent from one of these mutants.

The movement of the *R. capsulatus* cells forming satellite clusters in time-course experiments was intriguing. Whether cell groups arise from the association of cells dispersed around the site of inoculation could be addressed with further microscopy. It would also be interesting to determine if the method of coordinating this motile cell mass involves a diffusible signal, cell-cell contact, or possibly both. The dense linear movement pattern of flagellum-independent motility was disrupted in the flagellum/pigment mutant strain sbKSDFby, so a focus on how cells aggregate and coordinate group movement could begin with determining the exact role of BChl or carotenoids in coordinated movement.

The predicted pilus clusters identified by bioinformatics could be characterized more completely. My results indicated that at least some of these genes are not required for movement, but it would be interesting to determine whether *R. capsulatus* can produce a T4P. If the pilus-like appendages seen in *R. capsulatus* EMs were T4P encoded by these clusters, the *cpaC*, *cpaF*, and *cpaA* mutants should lack these structures. Mutagenesis of the predicted pilin genes would also be of interest. Complementation would be expected to rescue these phenotypes. Red fluorescent protein (RFP) fusion proteins (Campbell et al., 2002; Fradkov et al., 2002) of RCC00502 and RCC00505 could

determine the cellular localization of the proteins, and a purified His-tagged version of the protein (Terpe, 2003) encoded by RCC00505 could be evaluated for predicted ATP-hydrolysis *in vitro* (Koronakis et al., 1995; Chiang et al., 2008). If ORFs RCC00499 and RCC00500 are pilins, they could possibly be distinguished on the cell by epitope tagging (Li et al., 2002).

Determining the reason why *R. capsulatus* cells do not move in a polystyrene-agar interstice could also help in understanding the motility mechanism employed by cells. *P. aeruginosa* and *M. xanthus* cells can move on both plastic and glass substrates. Both flagellum-dependent and flagellum-independent movement was impeded in plastic plates. Perhaps the plate surface somehow affected the surface properties of the medium, altering the interaction between the substrate and the motility apparatus (Miyata et al., 2000; De La Fuente et al., 2007). Alternatively, the inability of *R. capsulatus* cells to move on a medium solidified in a polystyrene plate may be due to properties of the cell itself such as membrane hydrophobicity (Gerson and Scheer, 1980).

Finally, future approaches should focus on increasing the throughput of the mutant screen, so that a larger library may be screened effectively. The screening process was a problem because the frequency of movement in stab-plates was less than 100%, and many false-positives (clones that did not move) had to be retested. I believe a random, saturating mutagenesis approach would be the best way to identify genes required for this movement, perhaps using a high-frequency transposon, such as described by Larsen *et. al.* (2002).

In addition to the results described in my thesis, these experiments should help to characterize the basis of the conditions that induce flagellum-independent motility in *R. capsulatus*. These experiments may also clarify whether *R. capsulatus* solid substrate movement is driven by a gliding motility structure, or some uncharacterized mechanism.

REFERENCES

Adan-Kubo, J., Uenoyama, A., Arata, T., and Miyata, M. (2006) Morphology of isolated Gli349, a leg protein responsible for *Mycoplasma mobile* gliding via glass binding, revealed by rotary shadowing electron microscopy. *J Bacteriol* **188**: 2821-2828.

Adler, J. (1966) Chemotaxis in bacteria. *Science* **153**: 708-716.

Adler, J., and Dahl, M.M. (1967) A method for measuring the motility of bacteria and for comparing random and non-random motility. *J Gen Microbiol* **46**: 161-173.

Adler, J., and Tso, W.W. (1974) "Decision"-making in bacteria: chemotactic response of *Escherichia coli* to conflicting stimuli. *Science* **184**: 1292-1294.

Adler, J., and Shi, W. (1988) Galvanotaxis in bacteria. *Cold Spring Harb Symp Quant Biol* **53 Pt 1**: 23-25.

Agarwal, S., Hunnicutt, D.W., and McBride, M.J. (1997) Cloning and characterization of the *Flavobacterium johnsoniae* (*Cytophaga johnsonae*) gliding motility gene, *gldA*. *Proc Natl Acad Sci U S A* **94**: 12139-12144.

Aizawa, S.I., and Kubori, T. (1998) Bacterial flagellation and cell division. *Genes Cells* **3**: 625-634.

Alberti, L., and Harshey, R.M. (1990) Differentiation of *Serratia marcescens* 274 into swimmer and swarmer cells. *J Bacteriol* **172**: 4322-4328.

Aldridge, P., and Hughes, K.T. (2002) Regulation of flagelar assembly. *Curr Opin Microbiol* **5**: 160-165.

Alexandre, G. (2008) A sense of self-worth: energy taxis provides insight into how *Helicobacter pylori* navigates through its environment. *J Bacteriol* **190**: 3095-3097.

Alexandre, G. (2010) Coupling metabolism and chemotaxis-dependent behaviours by energy taxis receptors. *Microbiology* **156**: 2283-2293.

Alexandre, G., Greer-Phillips, S., and Zhulin, I.B. (2004) Ecological role of energy taxis in microorganisms. *FEMS Microbiol Rev* **28**: 113-126.

Alm, R.A., and Mattick, J.S. (1995) Identification of a gene, *pilV*, required for type 4 fimbrial biogenesis in *Pseudomonas aeruginosa*, whose product possesses a pre-pilin-like leader sequence. *Mol Microbiol* **16**: 485-496.

Alm, R.A., and Mattick, J.S. (1997) Genes involved in the biogenesis and function of type-4 fimbriae in *Pseudomonas aeruginosa*. *Gene* **192**: 89-98.

Altschul, S.F., Madden, T.L., Schaffer, A.A., Zhang, J., Zhang, Z., Miller, W., and Lipman, D.J. (1997) Gapped BLAST and PSI-BLAST: a new generation of protein database search programs. *Nucleic Acids Res* **25**: 3389-3402.

Ames, P., Studdert, C.A., Reiser, R.H., and Parkinson, J.S. (2002) Collaborative signaling by mixed chemoreceptor teams in *Escherichia coli*. *Proc Natl Acad Sci U S A* **99**: 7060-7065.

Anderson, D.K., and Newton, A. (1997) Posttranscriptional regulation of *Caulobacter* flagellin genes by a late flagellum assembly checkpoint. *J Bacteriol* **179**: 2281-2288.

Anderson, D.K., Ohta, N., Wu, J., and Newton, A. (1995) Regulation of the *Caulobacter crescentus rpoN* gene and function of the purified sigma 54 in flagellar gene transcription. *Mol Gen Genet* **246**: 697-706.

Armitage, J.P. (1992) Behavioral responses in bacteria. *Annu Rev Physiol* **54**: 683-714.

Armitage, J.P. (1997) Behavioural responses of bacteria to light and oxygen. *Arch Microbiol* **168**: 249-261.

Armitage, J.P., and Schmitt, R. (1997) Bacterial chemotaxis: *Rhodobacter sphaeroides* and *Sinorhizobium meliloti*--variations on a theme? *Microbiology* **143 (Pt 12)**: 3671-3682.

Armitage, J.P., and Hellingwerf, K.J. (2003) Light-induced behavioral responses ('phototaxis') in prokaryotes. *Photosynth Res* **76**: 145-155.

Armitage, J.P., Pitta, T.P., Vigeant, M.A., Packer, H.L., and Ford, R.M. (1999) Transformations in flagellar structure of *Rhodobacter sphaeroides* and possible relationship to changes in swimming speed. *J Bacteriol* **181**: 4825-4833.

Armstrong, G.A., Schmidt, A., Sandmann, G., and Hearst, J.E. (1990) Genetic and biochemical characterization of carotenoid biosynthesis mutants of *Rhodobacter capsulatus*. *J Biol Chem* **265**: 8329-8338.

Atsumi, T., McCarter, L., and Imae, Y. (1992) Polar and lateral flagellar motors of marine *Vibrio* are driven by different ion-motive forces. *Nature* **355**: 182-184.

Axelrod, D. (1989) Total internal reflection fluorescence microscopy. *Methods Cell Biol* **30**: 245-270.

Bakaletz, L.O., Baker, B.D., Jurcisek, J.A., Harrison, A., Novotny, L.A., Bookwalter, J.E. et al. (2005) Demonstration of Type IV pilus expression and a twitching phenotype by *Haemophilus influenzae*. *Infect Immun* **73**: 1635-1643.

Balish, M.F., and Krause, D.C. (2006) *Mycoplasmas*: a distinct cytoskeleton for wall-less bacteria. *J Mol Microbiol Biotechnol* **11**: 244-255.

Barany, F. (1985) Single-stranded hexameric linkers: a system for in-phase insertion mutagenesis and protein engineering. *Gene* **37**: 111-123.

Bardy, S.L., Ng, S.Y., and Jarrell, K.F. (2003) Prokaryotic motility structures. *Microbiology* **149**: 295-304.

Bartnikas, T.B., Wang, Y., Bobo, T., Veselov, A., Scholes, C.P., and Shapleigh, J.P. (2002) Characterization of a member of the NnrR regulon in *Rhodobacter sphaeroides* 2.4.3 encoding a haem-copper protein. *Microbiology* **148**: 825-833.

Bayan, N., Guilvout, I., and Pugsley, A.P. (2006) Secretins take shape. *Mol Microbiol* **69**: 1-4.

Beatty, J.T., and Gest, H. (1981) Generation of succinyl-coenzyme A in photosynthetic bacteria. *Arch Microbiol* **129**: 335-340.

Berg, H.C. (1996) Symmetries in bacterial motility. *Proc Natl Acad Sci U S A* **93**: 14225-14228.

Berg, H.C. (2003) The rotary motor of bacterial flagella. *Annu Rev Biochem* **72**: 19-54.

Berg, H.C. (2005) Swarming motility: it better be wet. *Curr Biol* **15**: R599-600.

Berg, H.C., and Anderson, R.A. (1973) Bacteria swim by rotating their flagellar filaments. *Nature* **245**: 380-382.

Bernard, C.S., Bordi, C., Termine, E., Filloux, A., and de Bentzmann, S. (2009) Organization and PprB-dependent control of the *Pseudomonas aeruginosa* tad locus, involved in Flp pilus biology. *J Bacteriol* **191**: 1961-1973.

Bhattacharjee, M.K., Kachlany, S.C., Fine, D.H., and Figurski, D.H. (2001) Nonspecific adherence and fibril biogenesis by *Actinobacillus actinomycetemcomitans*: TadA protein is an ATPase. *J Bacteriol* **183**: 5927-5936.

Bhaya, D., Watanabe, N., Ogawa, T., and Grossman, A.R. (1999) The role of an alternative sigma factor in motility and pilus formation in the cyanobacterium *Synechocystis sp*. strain PCC6803. *Proc Natl Acad Sci U S A* **96**: 3188-3193.

Bibikov, S.I., Biran, R., Rudd, K.E., and Parkinson, J.S. (1997) A signal transducer for aerotaxis in Escherichia coli. *J Bacteriol* **179**: 4075-4079.

Biebl, H., and Drews, G. (1969) [The in vivo spectrum as taxonomic characteristic in distribution studies of *Athiorhodaceae*]. *Zentralbl Bakteriol Parasitenkd Infektionskr Hyg* **123**: 425-452.

Bitter, W., Koster, M., Latijnhouwers, M., de Cock, H., and Tommassen, J. (1998) Formation of oligomeric rings by XcpQ and PilQ, which are involved in protein transport across the outer membrane of *Pseudomonas aeruginosa*. *Mol Microbiol* **27**: 209-219.

Blakemore, R.P. (1975) Magnetotactic bacteria. *Science* **190**: 377-379.

Blankenship, R.E. (2002) *Molecular mechanisms of photosynthesis*. Oxford ; Malden, MA: Blackwell Science.

Block, S.M., Segall, J.E., and Berg, H.C. (1982) Impulse responses in bacterial chemotaxis. *Cell* **31**: 215-226.

Bollivar, D.W., Suzuki, J.Y., Beatty, J.T., Dobrowolski, J.M., and Bauer, C.E. (1994) Directed mutational analysis of bacteriochlorophyll a biosynthesis in *Rhodobacter capsulatus*. *J Mol Biol* **237**: 622-640.

Bose, N., Payne, S.M., and Taylor, R.K. (2002) Type 4 pilus biogenesis and type II-mediated protein secretion by *Vibrio cholerae* occur independently of the TonB-facilitated proton motive force. *J Bacteriol* **184**: 2305-2309.

Boyd, A., and Simon, M. (1982) Bacterial chemotaxis. *Annu Rev Physiol* **44**: 501-517.

Boyer, H.W., and Roulland-Dussoix, D. (1969) A complementation analysis of the restriction and modification of DNA in *Escherichia coli*. *J Mol Biol* **41**: 459-472.

Brahamsha, B. (1999) Non-flagellar swimming in marine *Synechococcus*. *J Mol Microbiol Biotechnol* **1**: 59-62.

Braun, M., Kuhnert, P., Nicolet, J., Burnens, A.P., and Frey, J. (1999) Cloning and characterization of two bistructural S-layer-RTX proteins from *Campylobacter rectus*. *J Bacteriol* **181**: 2501-2506.

Braun, T.F., Khubbar, M.K., Saffarini, D.A., and McBride, M.J. (2005) *Flavobacterium johnsoniae* gliding motility genes identified by mariner mutagenesis. *J Bacteriol* **187**: 6943-6952.

Brautigam, E., Fiedler, F., Woitzik, D., Flammann, H.T., and Weckesser, J. (1988) Capsule polysaccharide-protein-peptidoglycan complex in the cell envelope of *Rhodobacter capsulatus*. *Arch Microbiol* **150**: 567- 573.

Brent, R., and Ptashne, M. (1980) The lexA gene product represses its own promoter. *Proc Natl Acad Sci U S A* **77**: 1932-1936.

Bromley, D.B., and Charon, N.W. (1979) Axial filament involvement in the motility of *Leptospira interrogans*. *J Bacteriol* **137**: 1406-1412.

Buggy, J., and Bauer, C.E. (1995) Cloning and characterization of *senC*, a gene involved in both aerobic respiration and photosynthesis gene expression in *Rhodobacter capsulatus*. *J Bacteriol* **177**: 6958-6965.

Burchard, R.P. (1970) Gliding motility mutants of *Myxococcus xanthus*. *J Bacteriol* **104**: 940-947.

Burchard, R.P. (1981) Gliding motility of prokaryotes: ultrastructure, physiology, and genetics. *Annu Rev Microbiol* **35**: 497-529.

Burchard, R.P. (1982) Trail following by gliding bacteria. *J Bacteriol* **152**: 495-501.

Burchard, R.P., Rittschof, D., and Bonaventura, J. (1990) Adhesion and motility of gliding bacteria on substrata with different surface free energies. *Appl Environ Microbiol* **56**: 2529-2534.

Burriesci, M., and Bhaya, D. (2008) Tracking phototactic responses and modeling motility of *Synechocystis sp*. strain PCC6803. *J Photochem Photobiol B* **91**: 77-86.

Burrows, L.L. (2005) Weapons of mass retraction. *Mol Microbiol* **57**: 878-888.

Burrows, L.L. (2008) A nice return on the "stalk" exchange. *Structure* **16**: 19-20.

Cabello, P., Pino, C., Olmo-Mira, M.F., Castillo, F., Roldan, M.D., and Moreno-Vivian, C. (2004) Hydroxylamine assimilation by *Rhodobacter capsulatus* E1F1. Requirement of the *hcp* gene (hybrid cluster protein) located in the nitrate assimilation *nas* gene region for hydroxylamine reduction. *J Biol Chem* **279**: 45485-45494.

Caiazza, N.C., Shanks, R.M., and O'Toole, G.A. (2005) Rhamnolipids modulate swarming motility patterns of *Pseudomonas aeruginosa*. *J Bacteriol* **187**: 7351-7361.

Campbell, R.E., Tour, O., Palmer, A.E., Steinbach, P.A., Baird, G.S., Zacharias, D.A., and Tsien, R.Y. (2002) A monomeric red fluorescent protein. *Proc Natl Acad Sci U S A* **99**: 7877-7882.

Cannon, W., Missailidis, S., Austin, S., Moore, M., Drake, A., and Buck, M. (1996) Purification and activities of the *Rhodobacter capsulatus* RpoN (sigma N) protein. *Mol Microbiol* **21**: 233-245.

Chami, M., Guilvout, I., Gregorini, M., Rémigy, H., Müller, S.A., Valerio, M. et al. (2005) Structural insights into the secretin PulD and its trypsin resistant core. *J Biol Chem* **280**: 37732-37741.

Che, A., Cui, J., and Dinov, I. (2009) SOCR analyses - an instructional Java web-based statistical analysis toolkit. *Journal of Online Learning and Teaching* **5**: 1-19.

Chen, J., Groves, R., Civerolo, E., and Livingston, S. (2007) Surface motility of *Xylella fastidiosa* visualized by oblique illumination. *Can J Microbiol* **53**: 435-439.

Chiang, P., Habash, M., and Burrows, L.L. (2005) Disparate subcellular localization patterns of *Pseudomonas aeruginosa* Type IV pilus ATPases involved in twitching motility. *J Bacteriol* **187**: 829-839.

Chiang, P., Sampaleanu, L.M., Ayers, M., Pahuta, M., Howell, P.L., and Burrows, L.L. (2008) Functional role of conserved residues in the characteristic secretion NTPase motifs of the *Pseudomonas aeruginosa* Type IV pilus motor proteins PilB, PilT and PilU. *Microbiology* **154**: 114-126.

Chilcott, G.S., and Hughes, K.T. (2000) Coupling of flagellar gene expression to flagellar assembly in *Salmonella enterica* serovar *typhimurium* and *Escherichia coli*. *Microbiol Mol Biol Rev* **64**: 694-708.

Choi, J.S., Chung, Y.H., Moon, Y.J., Kim, C., Watanabe, M., Song, P.S. et al. (1999) Photomovement of the gliding cyanobacterium *Synechocystis sp*. PCC 6803. *Photochem Photobiol* **70**: 95-102.

Clausznitzer, D., Oleksiuk, O., Lovdok, L., Sourjik, V., and Endres, R.G. (2010) Chemotactic response and adaptation dynamics in *Escherichia coli*. *PLoS Comput Biol* **6**: e1000784.

Colegrave, G.T. (1983) Agricultural applications of microbial polysaccharides. *Ind Eng Chem Prod Res Dev* **22**: 456-460.

Collins, R.F., Davidsen, L., Derrick, J.P., Ford, R.C., and Tonjum, T. (2001) Analysis of the PilQ secretin from *Neisseria meningitidis* by transmission electron microscopy reveals a dodecameric quaternary structure. *J Bacteriol* **183**: 3825-3832.

Costerton, J.W., Irvin, R.T., and Cheng, K.J. (1981) The bacterial glycocalyx in nature and disease. *Annu Rev Microbiol* **35**: 299-324.

Craig, L., and Li, J. (2008) Type IV pili: paradoxes in form and function. *Curr Opin Struct Biol* **18**: 267-277.

Craig, L., Pique, M.E., and Tainer, J.A. (2004) Type IV pilus structure and bacterial pathogenicity. *Nat Rev Microbiol* **2**: 363-378.

Craig, L., Volkmann, N., Arvai, A.S., Pique, M.E., Yeager, M., Egelman, E.H., and Tainer, J.A. (2006) Type IV pilus structure by cryo-electron microscopy and crystallography: implications for pilus assembly and functions. *Mol Cell* **23**: 651-662.

Craig, L., Taylor, R.K., Pique, M.E., Adair, B.D., Arvai, A.S., Singh, M. et al. (2003) Type IV pilin structure and assembly: X-ray and EM analyses of *Vibrio cholerae* toxin-coregulated pilus and *Pseudomonas aeruginosa* PAK pilin. *Mol Cell* **11**: 1139-1150.

D'Andrea, L.D., and Regan, L. (2003) TPR proteins: the versatile helix. *Trends Biochem Sci* **28**: 655-662.

Dai, G., Ohno, Y., Ikeda, Y., Tamogami, J., Kikukawa, T., Kamo, N., and Iwasa, T. (2010) Photoreaction cycle of phoborhodopsin (sensory rhodopsin II) from *Halobacterium salinarum* expressed in *Escherichia coli*. *Photochem Photobiol*.

Dang, C.V., Niwano, M., Ryu, J., and Taylor, B.L. (1986) Inversion of aerotactic response in *Escherichia coli* deficient in *cheB* protein methylesterase. *J Bacteriol* **166**: 275-280.

Darnton, N.C., Turner, L., Rojevsky, S., and Berg, H.C. (2010) Dynamics of bacterial swarming. *Biophys J* **98**: 2082-2090.

de Bentzmann, S., Aurouze, M., Ball, G., and Filloux, A. (2006) FppA, a novel *Pseudomonas aeruginosa* prepilin peptidase involved in assembly of Type IVb pili. *J Bacteriol* **188**: 4851-4860.

De La Fuente, L., Montanes, E., Meng, Y., Li, Y., Burr, T.J., Hoch, H.C., and Wu, M. (2007) Assessing adhesion forces of Type I and Type IV pili of *Xylella fastidiosa* bacteria by use of a microfluidic flow chamber. *Appl Environ Microbiol* **73**: 2690-2696.

del Campo, A.M., Ballado, T., de la Mora, J., Poggio, S., Camarena, L., and Dreyfus, G. (2007) Chemotactic control of the two flagellar systems of *Rhodobacter sphaeroides* is mediated by different sets of CheY and FliM proteins. *J Bacteriol* **189**: 8397-8401.

DeRosier, D.J. (1995) Spinning tails. *Curr Opin Struct Biol* **5**: 187-193.

Dev, I.K., and Ray, P.H. (1990) Signal peptidases and signal peptide hydrolases. *J Bioenerg Biomembr* **22**: 271-290.

Dodd, D.C., and Eisenstein, B.I. (1982) Antigenic quantitation of Type 1 fimbriae on the surface of *Escherichia coli* cells by an enzyme-linked immunosorbent inhibition assay. *Infect Immun* **38**: 764-773.

Dong, C., Elsen, S., Swem, L.R., and Bauer, C.E. (2002) AerR, a second aerobic repressor of photosynthesis gene expression in *Rhodobacter capsulatus*. *J Bacteriol* **184**: 2805-2814.

Drews, G. (2005) Contributions of Theodor Wilhelm Engelmann on phototaxis, chemotaxis, and photosynthesis. *Photosynth Res* **83**: 25-34.

Du, S., Bird, T.H., and Bauer, C.E. (1998) DNA binding characteristics of RegA. A constitutively active anaerobic activator of photosynthesis gene expression in *Rhodobacter capsulatus*. *J Biol Chem* **273**: 18509-18513.

Durand, E., Michel, G., Voulhoux, R., Kurner, J., Bernadac, A., and Filloux, A. (2005) XcpX controls biogenesis of the *Pseudomonas aeruginosa* XcpT-containing pseudopilus. *J Biol Chem* **280**: 31378-31389.

Dworkin, M., Keller, K.H., and Weisberg, D. (1983) Experimental observations consistent with a surface tension model of gliding motility of *Myxococcus xanthus*. *J Bacteriol* **155**: 1367-1371.

Ehlers, K.M., Samuel, A.D., Berg, H.C., and Montgomery, R. (1996) Do cyanobacteria swim using traveling surface waves? *Proc Natl Acad Sci U S A* **93**: 8340-8343.

Elsen, S., Dischert, W., Colbeau, A., and Bauer, C.E. (2000) Expression of uptake hydrogenase and molybdenum nitrogenase in *Rhodobacter capsulatus* is coregulated by the RegB-RegA two-component regulatory system. *J Bacteriol* **182**: 2831-2837.

Elsen, S., Swem, L.R., Swem, D.L., and Bauer, C.E. (2004) RegB/RegA, a highly conserved redox-responding global two-component regulatory system. *Microbiol Mol Biol Rev* **68**: 263-279.

Emerson, D. (1999) Complex pattern formation by *Pseudomonas* strain KC in response to nitrate and nitrite. *Microbiology* **145 (Pt 3)**: 633-641.

Engelmann, T.W. (1883) Bacterium photometricum. *Ein Beitrag zur vergleichenden Physiologic des Licht- und Farbensinnes* **30**: 95-124.

Entcheva-Dimitrov, P., and Spormann, A.M. (2004) Dynamics and control of biofilms of the oligotrophic bacterium *Caulobacter crescentus*. *J Bacteriol* **186**: 8254-8266.

Fall, R., Kearns, D.B., and Nguyen, T. (2006) A defined medium to investigate sliding motility in a *Bacillus subtilis* flagella-less mutant. *BMC Microbiol* **6**: 31.

Favinger, J., Stadtwald, R., and Gest, H. (1989) *Rhodospirillum centenum*, *sp*. nov., a thermotolerant cyst-forming anoxygenic photosynthetic bacterium. *Antonie Van Leeuwenhoek* **55**: 291-296.

Figurski, D.H., and Helinski, D.R. (1979) Replication of an origin-containing derivative of plasmid RK2 dependent on a plasmid function provided in *trans*. *Proc Natl Acad Sci U S A* **76**: 1648-1652.

Flammann, H.T., Golecki, J.R., and Weekesser, J. (1984) The capsule and slime polysaccharides of the wild type and a phage resistant mutant of *Rhodopseudomonas capsulata* St. Louis. *Arch Microbiol* **139**: 38-43.

Flores, H., Lobaton, E., Mendez-Diez, S., Tlupova, S., and Cortez, R. (2005) A study of bacterial flagellar bundling. *Bull Math Biol* **67**: 137-168.

Fradkov, A.F., Verkhusha, V.V., Staroverov, D.B., Bulina, M.E., Yanushevich, Y.G., Martynov, V.I. et al. (2002) Far-red fluorescent tag for protein labelling. *Biochem J* **368**: 17-21.

Fraser, G.M., and Hughes, C. (1999) Swarming motility. *Curr Opin Microbiol* **2**: 630-635.

Fujinaga, R., Nakazawa, T., and Shirai, M. (2001) Allelic exchange mutagenesis of rpoN encoding RNA-polymerase sigma54 subunit in *Helicobacter pylori*. *J Infect Chemother* **7**: 148-155.

Gari, E., Gibert, I., and Barbe, J. (1992) Spontaneous and reversible high-frequency frameshifts originating a phase transition in the carotenoid biosynthesis pathway of the phototrophic bacterium *Rhodobacter sphaeroides* 2.4.1. *Mol Gen Genet* **232**: 74-80.

Gauden, D.E., and Armitage, J.P. (1995) Electron transport-dependent taxis in *Rhodobacter sphaeroides*. *J Bacteriol* **177**: 5853-5859.

Gerson, D.F., and Scheer, D. (1980) Cell surface energy, contact angles and phase partition. III. Adhesion of bacterial cells to hydrophobic surfaces. *Biochim Biophys Acta* **602**: 506-510.

Gest, H. (1995) Phototaxis and other sensory phenomena in purple photosynthetic bacteria. *FEMS Microbiol Rev* **16**: 287-294.

Gestwicki, J.E., and Kiessling, L.L. (2002) Inter-receptor communication through arrays of bacterial chemoreceptors. *Nature* **415**: 81-84.

Giovannoni, S.J., Schabtach, E., and Castenholz, R.W. (1987) *Isosphaera pallida*, gen. and comb. nov., a gliding, budding eubacterium from hot springs. *Arch Microbiol* **147**: 276-284.

Giuliano, G., Al-Babili, S., and von Lintig, J. (2003) Carotenoid oxygenases: cleave it or leave it. *Trends Plant Sci* **8**: 145-149.

Gluch, M.F., Typke, D., and Baumeister, W. (1995) Motility and thermotactic responses of *Thermotoga maritima*. *J Bacteriol* **177**: 5473-5479.

Gordeliy, V.I., Labahn, J., Moukhametzianov, R., Efremov, R., Granzin, J., Schlesinger, R. et al. (2002) Molecular basis of transmembrane signalling by sensory rhodopsin II-transducer complex. *Nature* **419**: 484-487.

Goy, M.F., Springer, M.S., and Adler, J. (1977) Sensory transduction in *Escherichia coli*: role of a protein methylation reaction in sensory adaptation. *Proc Natl Acad Sci U S A* **74**: 4964-4968.

Grammel, H., Gilles, E.D., and Ghosh, R. (2003) Microaerophilic cooperation of reductive and oxidative pathways allows maximal photosynthetic membrane biosynthesis in *Rhodospirillum rubrum*. *Appl Environ Microbiol* **69**: 6577-6586.

Greer-Phillips, S.E., Alexandre, G., Taylor, B.L., and Zhulin, I.B. (2003) Aer and Tsr guide *Escherichia coli* in spatial gradients of oxidizable substrates. *Microbiology* **149**: 2661-2667.

Haase, E.M., Zmuda, J.L., and Scannapieco, F.A. (1999) Identification and molecular analysis of rough-colony-specific outer membrane proteins of *Actinobacillus actinomycetemcomitans*. *Infect Immun* **76**: 2901-2908.

Hader, D.P. (1987) Photosensory behavior in procaryotes. *Microbiol Rev* **51**: 1-21.

Han, X., Kennan, R.M., Davies, J.K., Reddacliff, L.A., Dhungyel, O.P., Whittington, R.J. et al. (2008) Twitching motility is essential for virulence in *Dichelobacter nodosus*. *J Bacteriol* **190**: 3323-3335.

Hanahan, D. (ed) (1985) *DNA Cloning Volume I. A Practical Approach*. Oxford: IRL Press.

Hanahan, D. (1986) BRL pUC host *E. coli* DH5α competent cells. *Focus* **8**: 9.

Hansen, T.A., and van Gemerden, H. (1972) Sulfide utilization by purple nonsulfur bacteria. *Arch Mikrobiol* **86**: 49-56.

Harayama, S., and Lino, T. (1976) Phototactic response of aerobically cultivated *Rhodospirillum rubrum*. *J Gen Microbiol* **94**: 173-179.

Harshey, R.M. (1994) Bees aren't the only ones: swarming in gram-negative bacteria. *Mol Microbiol* **13**: 389-394.

Harshey, R.M. (2003) Bacterial motility on a surface: many ways to a common goal. *Annu Rev Microbiol* **57**: 249-273.

Harshey, R.M., and Matsuyama, T. (1994) Dimorphic transition in *Escherichia coli* and *Salmonella typhimurium*: surface-induced differentiation into hyperflagellate swarmer cells. *Proc Natl Acad Sci U S A* **91**: 8631-8635.

Hartzell, P.L., and Youderian, P. (1995) Genetics of gliding motility and development in *Myxococcus xanthus*. *Arch Microbiol* **164**: 309-323.

Haselkorn, R., Lapidus, A., Kogan, Y., Vlcek, C., Paces, J., Paces, V. et al. (2001) The *Rhodobacter capsulatus* genome. *Photosynth Res* **70**: 43-52.

Hasselbring, B.M., and Krause, D.C. (2007a) Cytoskeletal protein P41 is required to anchor the terminal organelle of the wall-less prokaryote *Mycoplasma pneumoniae*. *Mol Microbiol* **63**: 44-53.

Hasselbring, B.M., and Krause, D.C. (2007b) Proteins P24 and P41 function in the regulation of terminal-organelle development and gliding motility in *Mycoplasma pneumoniae*. *J Bacteriol* **189**: 7442-7449.

Hauri, D.C., and Ross, J. (1995) A model of excitation and adaptation in bacterial chemotaxis. *Biophys J* **68**: 708-722.

Hazelbauer, G.L., Berg, H.C., and Matsumura, P. (1993) Bacterial motility and signal transduction. *Cell* **73**: 15-22.

Hellingwerf, K.J., Kort, R., and Crielaard, W. (1998) *Negative phototaxis in photosynthetic bacteria*. Cambridge: Cambridge University Press.

Henderson, G.P., and Jensen, G.J. (2006) Three-dimensional structure of *Mycoplasma pneumoniae*'s attachment organelle and a model for its role in gliding motility. *Mol Microbiol* **60**: 376-385.

Hendrixson, D.R., Akerley, B.J., and DiRita, V.J. (2001) Transposon mutagenesis of *Campylobacter jejuni* identifies a bipartite energy taxis system required for motility. *Mol Microbiol* **40**: 214-224.

Henrichsen, J. (1972) Bacterial surface translocation: a survey and a classification. *Bacteriol Rev* **36**: 478-503.

Henrichsen, J. (1975a) The influence of changes in the environment on twitching motility. *Acta Pathol Microbiol Scand B* **83**: 179-186.

Henrichsen, J. (1975b) The occurrence of twitching motility among gram-negative bacteria. *Acta Pathol Microbiol Scand B* **83**: 171-178.

Henrichsen, J. (1983) Twitching motility. *Annu Rev Microbiol* **37**: 81-93.

Henrichsen, J., Froholm, L.O., and Bovre, K. (1972) Studies on bacterial surface translocation. 2. Correlation of twitching motility and fimbriation in colony variants of *Moraxella nonliquefaciens*, *M. bovis*, and *M. kingii*. *Acta Pathol Microbiol Scand B Microbiol Immunol* **80**: 445-452.

Hensel, Z., and Xiao, J. (2009) A mechanism for stochastic decision making by bacteria. *Chembiochem* **10**: 974-976.

Herrero, M., de Lorenzo, V., and Timmis, K.N. (1990) Transposon vectors containing non-antibiotic resistance selection markers for cloning and stable chromosomal insertion of foreign genes in gram-negative bacteria. *J Bacteriol* **172**: 6557-6567.

Herrmann, G., Jayamani, E., Mai, G., and Buckel, W. (2008) Energy conservation via electron-transferring flavoprotein in anaerobic bacteria. *J Bacteriol* **190**: 784-791.

Hill, B.L., and Purcell, A.H. (1995) Acquisition and retention of *Xylella fastidiosa* by an efficient vector, *Graphocephala atropunctata*. *Phytopathology* **85**: 209-212.

Ho, A.S.Y., Mietzner, T.A., Smith, A.J., and Schoolnik, G.K. (1990) The pili of *Aeromonas hydrophila*: identification of an environmentally regulated "mini pilin". *J Exp Med* **172**: 795-806.

Hoang, H.H., Gurich, N., and Gonzalez, J.E. (2008) Regulation of motility by the ExpR/Sin quorum-sensing system in *Sinorhizobium meliloti*. *J Bacteriol* **190**: 861-871.

Hoff, W.D., Dux, P., Hard, K., Devreese, B., Nugteren-Roodzant, I.M., Crielaard, W. et al. (1994) Thiol ester-linked *p*-coumaric acid as a new photoactive prosthetic group in a protein with rhodopsin-like photochemistry. *Biochemistry* **33**: 13959-13962.

Hoiczyk, E. (2000) Gliding motility in cyanobacterial: observations and possible explanations. *Arch Microbiol* **174**: 11-17.

Hoiczyk, E., and Baumeister, W. (1998) The junctional pore complex, a prokaryotic secretion organelle, is the molecular motor underlying gliding motility in cyanobacteria. *Curr Biol* **8**: 1161-1168.

Houwink, A.L., and van Iterson, W. (1950) Electron microscopical observations on bacterial cytology; a study on flagellation. *Biochim Biophys Acta* **5**: 10-44.

Imamoto, Y., Shichida, Y., Yoshizawa, T., Tomioka, H., Takahashi, T., Fujikawa, K. et al. (1991) Photoreaction cycle of phoborhodopsin studied by low-temperature spectrophotometry. *Biochemistry* **30**: 7416-7424.

Imhoff, J.F. (2006) *The Phototrophic Alpha-Proteobacteria*. New York: Springer New York.

Inoue, T., Tanimoto, I., Ohta, H., Kato, K., Murayama, Y., and Fukui, K. (1998) Molecular characterization of low-molecular-weight component protein, Flp, in *Actinobacillus actinomycetemcomitans* fimbriae. *Microbiol Immunol* **42**: 253-258.

Ishimoto, K.S., and Lory, S. (1989) Formation of pilin in *Pseudomonas aeruginosa* requires the alternative sigma factor (RpoN) of RNA polymerase. *Proc Natl Acad Sci U S A* **86**: 1954-1957.

Jacobs, M.A., Alwood, A., Thaipisuttikul, I., Spencer, D., Haugen, E., Ernst, S. et al. (2003) Comprehensive transposon mutant library of *Pseudomonas aeruginosa*. *Proc Natl Acad Sci U S A* **100**: 14339-14344.

Jakovljevic, V., Leonardy, S., Hoppert, M., and Sogaard-Andersen, L. (2008) PilB and PilT are ATPases acting antagonistically in Type IV pilus function in *Myxococcus xanthus*. *J Bacteriol* **190**: 2411-2421.

James, D.H., and Castor, W.M. (2000) Styrene. In *Ullmann's Encyclopedia of Industrial Chemistry*. Weinheim: Wiley-VCH Verlag GmbH & Co. KGaA.

Jaques, S., and McCarter, L.L. (2006) Three new regulators of swarming in *Vibrio parahaemolyticus*. *J Bacteriol* **188**: 2625-2635.

Jarrell, K.F., and McBride, M.J. (2008) The surprisingly diverse ways that prokaryotes move. *Nat Rev Microbiol* **6**: 466-476.

Jenal, U. (2000) Signal transduction mechanisms in *Caulobacter crescentus* development and cell cycle control. *FEMS Microbiol Rev* **24**: 177-191.

Jeziore-Sassoon, Y., Hamblin, P.A., Bootle-Wilbraham, C.A., Poole, P.S., and Armitage, J.P. (1998) Metabolism is required for chemotaxis to sugars in *Rhodobacter sphaeroides*. *Microbiology* **144 (Pt 1)**: 229-239.

Jiang, Z.Y., and Bauer, C.E. (2001) Component of the *Rhodospirillum centenum* photosensory apparatus with structural and functional similarity to methyl-accepting chemotaxis protein chemoreceptors. *J Bacteriol* **183**: 171-177.

Jiang, Z.Y., Gest, H., and Bauer, C.E. (1997) Chemosensory and photosensory perception in purple photosynthetic bacteria utilize common signal transduction components. *J Bacteriol* **179**: 5720-5727.

Jiang, Z.Y., Rushing, B.G., Bai, Y., Gest, H., and Bauer, C.E. (1998) Isolation of *Rhodospirillum centenum* mutants defective in phototactic colony motility by transposon mutagenesis. *J Bacteriol* **180**: 1248-1255.

Johnson, K., Parker, M.L., and Lory, S. (1986) Nucleotide sequence and transcriptional initiation site of two *Pseudomonas aeruginosa* pilin genes. *J Biol Chem* **26**: 15703-15708.

Jones, M.R. (2009) The petite purple photosynthetic powerpack. *Biochem Soc Trans* **37**: 400-407.

Kahn, H.A. (1984) Scanning electron microscopic studies of etched channels. *Int J Appl Radiat Isot* **35**: 611-615.

Kaiser, D. (2000) Bacterial motility: how do pili pull? *Curr Biol* **10**: R777-780.

Kang, K.S., Veeder, G.T., Mirrasoul, P.J., Kaneko, T., and Cottrell, I.W. (1982) Agar-like polysaccharide produced by a *Pseudomonas* species: production and basic properties. *Appl Environ Microbiol* **43**: 1086-1091.

Karkhanis, Y.D. (1983) Heat shock process for the isolatuon of bacterial protein. In *United States Patent*. Office, U.S.P. (ed). USA: Merck & Co., Inc., p. 3.

Kearns, D.B., and Shimkets, L.J. (1998) Chemotaxis in a gliding bacterium. *Proc Natl Acad Sci U S A* **95**: 11957-11962.

Kearns, D.B., Robinson, J., and Shimkets, L.J. (2001) *Pseudomonas aeruginosa* exhibits directed twitching motility up phosphatidylethanolamine gradients. *J Bacteriol* **183**: 763-767.

Khan, S., Spudich, J.L., McCray, J.A., and Trentham, D.R. (1995) Chemotactic signal integration in bacteria. *Proc Natl Acad Sci U S A* **92**: 9757-9761.

Kleinbaum, D.G. (1998) *Applied regression analysis and other multivariable methods*. Pacific Grove: Duxbury Press.

Kohler, T., Alvarez, J.F., and Harayama, S. (1994) Regulation of the *rpoN*, ORF102 and ORF154 genes in *Pseudomonas putida*. *FEMS Microbiol Lett* **115**: 177-184.

Kohler, T., Curty, L.K., Barja, F., van Delden, C., and Pechere, J.C. (2000) Swarming of *Pseudomonas aeruginosa* is dependent on cell-to-cell signaling and requires flagella and pili. *J Bacteriol* **182**: 5990-5996.

Koraimann, G. (2003) Lytic transglycosylases in macromolecular transport systems of Gram-negative bacteria. *Cell Mol Life Sci* **60**: 2371-2388.

Koronakis, E., Hughes, C., Milisav, I., and Koronakis, V. (1995) Protein exporter function and *in vitro* ATPase activity are correlated in ABC-domain mutants of HlyB. *Mol Microbiol* **16**: 87-96.

Krah, M., Marwan, W., Vermeglio, A., and Oesterhelt, D. (1994) Phototaxis of *Halobacterium salinarium* requires a signalling complex of sensory rhodopsin I and its methyl-accepting transducer HtrI. *EMBO J* **13**: 2150-2155.

Kranz, R.G., and Haselkorn, R. (1985) Characterization of *nif* regulatory genes in *Rhodopseudomonas capsulata* using *lac* gene fusions. *Gene* **40**: 203-215.

Krause, D.C., and Balish, M.F. (2001) Structure, function, and assembly of the terminal organelle of *Mycoplasma pneumoniae*. *FEMS Microbiol Lett* **198**: 1-7.

Krinsky, N.I., and Deneke, S.M. (1982) Interaction of oxygen and oxy-radicals with carotenoids. *J Natl Cancer Inst* **69**: 205-210.

Kyndt, J.A., Hurley, J.K., Devreese, B., Meyer, T.E., Cusanovich, M.A., Tollin, G., and Van Beeumen, J.J. (2004) *Rhodobacter capsulatus* photoactive yellow protein: genetic context, spectral and kinetics characterization, and mutagenesis. *Biochemistry* **43**: 1809-1820.

Laemmli, U.K. (1970) Cleavage of structural proteins during the assembly of the head of bacteriophage T4. *Nature* **227**: 680-685.

Lahaye, M., and Rochas, C. (1991) Chemical structure and physio-chemical properties of agar. *Hydrobiologia* **221**: 137-148.

Lang, A.S., and Beatty, J.T. (2002) A bacterial signal transduction system controls genetic exchange and motility. *J Bacteriol* **184**: 913-918.

Larsen, R.A., Wilson, M.M., Guss, A.M., and Metcalf, W.W. (2002) Genetic analysis of pigment biosynthesis in *Xanthobacter autotrophicus* Py2 using a new, highly efficient transposon mutagenesis system that is functional in a wide variety of bacteria. *Arch Microbiol* **178**: 193-201.

LeBrasseur, N. (2002) PilT: a motor on steroids. *J Cell Biol* **159**: 912-913.

Leung, M.M.Y. (2010) CtrA and GtaR: Two systems that regulate the gene transfer agent in *Rhodobacter capsulatus*. In *Microbiology and Immunology*. Vancouver: University of British Columbia, p. 179.

Levy, D., and Requeijo, T. (2008) Stochastic models for phototaxis. *Bull Math Biol* **70**: 1684-1706.

Li, C.M., Brown, I., Mansfield, J., Stevens, C., Boureau, T., Romantschuk, M., and Taira, S. (2002) The Hrp pilus of *Pseudomonas syringae* elongates from its tip and acts as a conduit for translocation of the effector protein HrpZ. *EMBO J* **21**: 1909-1915.

Li, M., and Hazelbauer, G.L. (2005) Adaptational assistance in clusters of bacterial chemoreceptors. *Mol Microbiol* **56**: 1617-1626.

Li, Y., Lux, R., Pelling, A.E., Gimzewski, J.K., and Shi, W. (2005) Analysis of Type IV pilus and its associated motility in *Myxococcus xanthus* using an antibody reactive with native pilin and pili. *Microbiology* **151**: 353-360.

Lilburn, T.G., Prince, R.C., and Beatty, J.T. (1995) Mutation of the Ser2 codon of the light-harvesting B870 alpha polypeptide of *Rhodobacter capsulatus* partially suppresses the *pufX* phenotype. *J Bacteriol* **177**: 4593-4600.

Lindum, P.W., Anthoni, U., Christophersen, C., Eberl, L., Molin, S., and Givskov, M. (1998) N-Acyl-L-homoserine lactone autoinducers control production of an extracellular lipopeptide biosurfactant required for swarming motility of *Serratia liquefaciens* MG1. *J Bacteriol* **180**: 6384-6388.

Liu, J., McBride, M.J., and Subramaniam, S. (2007) Cell surface filaments of the gliding bacterium *Flavobacterium johnsoniae* revealed by cryo-electron tomography. *J Bacteriol* **189**: 7503-7506.

Llewellyn, M., Dutton, R.J., Easter, J., O'Donnol, D., and Gober, J.W. (2005) The conserved *flaF* gene has a critical role in coupling flagellin translation and assembly in *Caulobacter crescentus*. *Mol Microbiol* **57**: 1127-1142.

Lorow, D., and Jessee, J. (1990) Max efficiency DH10B: a host for cloning methylated DNA. *Focus* **12**: 19.

Ma, D., Cook, D.N., O'Brien, D.A., and Hearst, J.E. (1993) Analysis of the promoter and regulatory sequences of an oxygen-regulated *bch* operon in *Rhodobacter capsulatus* by site-directed mutagenesis. *J Bacteriol* **175**: 2037-2045.

Macnab, R.M. (1992) Genetics and biogenesis of bacterial flagella. *Annu Rev Genet* **26**: 131-158.

Macnab, R.M. (2003) How bacteria assemble flagella. *Annu Rev Microbiol* **57**: 77-100.

Macnab, R.M., and Koshland, D.E., Jr. (1972) The gradient-sensing mechanism in bacterial chemotaxis. *Proc Natl Acad Sci U S A* **69**: 2509-2512.

Macnab, R.M., and Aizawa, S. (1984) Bacterial motility and the bacterial flagellar motor. *Annu Rev Biophys Bioeng* **13**: 51-83.

Madigan, M.T., Cox, J.C., and Gest, H. (1980) Physiology of dark fermentative growth of *Rhodopseudomonas capsulata*. *J Bacteriol* **142**: 908-915.

Magariyama, Y., Sugiyama, S., Muramoto, K., Kawagishi, I., Imae, Y., and Kudo, S. (1995) Simultaneous measurement of bacterial flagellar rotation rate and swimming speed. *Biophys J* **69**: 2154-2162.

Manson, M.D. (1992) Bacterial motility and chemotaxis. *Adv Microb Physiol* **33**: 277-346.

Marrs, B. (1974) Genetic recombination in *Rhodopseudomonas capsulata*. *Proc Natl Acad Sci U S A* **71**: 971-973.

Marrs, B. (1981) Mobilization of the genes for photosynthesis from *Rhodopseudomonas capsulata* by a promiscuous plasmid. *J Bacteriol* **146**: 1003-1012.

Martin, A.C., Gould, M., Byles, E., Roberts, M.A.J., and Armitage, J.P. (2006) Two chemosensory operons of *Rhodobacter sphaeroides* are regulated independently by sigma 28 and sigma 54. *J Bacteriol* **188**: 7932-7940.

Martin, P.R., Hobbs, M., Freer, P.D., Jeske, Y., and Mattick, J.S. (1993) Characterization of *pilQ*, a new gene required for the biogenesis of Type 4 fimbriae in *Pseudomonas aeruginosa*. *Mol Microbiol* **9**: 857-868.

Martinez, A., Torello, S., and Kolter, R. (1999) Sliding motility in *Mycobacteria*. *J Bacteriol* **181**: 7331-7338.

Masuda, S., Matsumoto, Y., Nagashima, K.V., Shimada, K., Inoue, K., Bauer, C.E., and Matsuura, K. (1999) Structural and functional analyses of photosynthetic regulatory genes *regA* and *regB* from *Rhodovulum sulfidophilum*, *Roseobacter denitrificans*, and *Rhodobacter capsulatus*. *J Bacteriol* **181**: 4205-4215.

Matsunaga, T. (1991) Applications of bacterial magnets. *Trends Biotechnol* **9**: 91-95.

Matsunaga, T., Nakamura, C., Burgess, J.G., and Sode, K. (1992) Gene transfer in magnetic bacteria: transposon mutagenesis and cloning of genomic DNA fragments required for magnetosome synthesis. *J Bacteriol* **174**: 2748-2753.

Matsuyama, T., Bhasin, A., and Harshey, R.M. (1995) Mutational analysis of flagellum-independent surface spreading of *Serratia marcescens* 274 on a low-agar medium. *J Bacteriol* **177**: 987-991.

Mattick, J.S. (2002) Type IV pili and twitching motility. *Annu Rev Microbiol* **56**: 289-314.

McBride, M.J. (2001) Bacterial gliding motility: multiple mechanisms for cell movement over surfaces. *Annu Rev Microbiol* **55**: 49-75.

McCarren, J., and Brahamsha, B. (2009) Swimming motility mutants of marine *Synechococcus* affected in production and localization of the S-layer protein SwmA. *J Bacteriol* **191**: 1111-1114.

McCarren, J.W. (2005) Microscopic, genetic, and biochemical characterization of non-flagellar swimming motility in marine cyanobacteria. In *Marine Biology*. San Diego: University of California, p. 126.

McCarter, L.L. (2010) Bacterial acrobatics on a surface: swirling packs, collisions, and reversals during swarming. *J Bacteriol* **192**: 3246-3248.

McClain, J., Rollo, D.R., Rushing, B.G., and Bauer, C.E. (2002) *Rhodospirillum centenum* utilizes separate motor and switch components to control lateral and polar flagellum rotation. *J Bacteriol* **184**: 2429-2438.

McMichael, J.C. (1992) Bacterial differentiation within *Moraxella bovis* colonies growing at the interface of the agar medium with the Petri dish. *J Gen Microbiol* **138**: 2687-2695.

Mercer, R.G., Callister, S.J., Lipton, M.S., Pasa-Tolic, L., Strnad, H., Paces, V. et al. (2010) Loss of the response regulator CtrA causes pleiotropic effects on gene expression but does not affect growth phase regulation in *Rhodobacter capsulatus*. *J Bacteriol* **192**: 2701-2710.

Merz, A.J., So, M., and Sheetz, M.P. (2000) Pilus retraction powers bacterial twitching motility. *Nature* **407**: 98-102.

Messing, J. (1983) New M13 vectors for cloning. *Methods Enzymol* **101**: 20-78.

Meyer, R.J., and Shapiro, J.A. (1980) Genetic organization of the broad-host-range IncP-1 plasmid R751. *J Bacteriol* **143**: 1362-1373.

Michaelis, S., and Beckwith, J. (1982) Mechanism of incorporation of cell envelope proteins in *Escherichia coli*. *Annu Rev Microbiol* **36**: 435-465.

Mignot, T., Merlie, J.P., Jr., and Zusman, D.R. (2005) Regulated pole-to-pole oscillations of a bacterial gliding motility protein. *Science* **310**: 855-857.

Mignot, T., Shaevitz, J.W., Hartzell, P.L., and Zusman, D.R. (2007) Evidence that focal adhesion complexes power bacterial gliding motility. *Science* **315**: 853-856.

Minamino, T., and Namba, K. (2004) Self-assembly and Type III protein export of the bacterial flagellum. *J Mol Microbiol Biotechnol* **7**: 5-17.

Minamino, T., Imae, Y., Oosawa, F., Kobayashi, Y., and Oosawa, K. (2003) Effect of intracellular pH on rotational speed of bacterial flagellar motors. *J Bacteriol* **185**: 1190-1194.

Minamino, T., Kazetani, K., Tahara, A., Suzuki, H., Furukawa, Y., Kihara, M., and Namba, K. (2006) Oligomerization of the bacterial flagellar ATPase FliI is controlled by its extreme N-terminal region. *J Mol Biol* **360**: 510-519.

Mironova, O.S., Efremov, R.G., Person, B., Heberle, J., Budyak, I.L., Buldt, G., and Schlesinger, R. (2005) Functional characterization of sensory rhodopsin II from *Halobacterium salinarum* expressed in *Escherichia coli*. *FEBS Lett* **579**: 3147-3151.

Miyata, M. (2008) Centipede and inchworm models to explain *Mycoplasma* gliding. *Trends Microbiol* **16**: 6-12.

Miyata, M., and Uenoyama, A. (2002) Movement on the cell surface of the gliding bacterium, *Mycoplasma mobile*, is limited to its head-like structure. *FEMS Microbiol Lett* **215**: 285-289.

Miyata, M., Yamamoto, H., Shimizu, T., Uenoyama, A., Citti, C., and Rosengarten, R. (2000) Gliding mutants of *Mycoplasma mobile*: relationships between motility and cell morphology, cell adhesion and microcolony formation. *Microbiology* **146 (Pt 6)**: 1311-1320.

Moens, S., and Vanderleyden, J. (1996) Functions of bacterial flagella. *Crit Rev Microbiol* **22**: 67-100.

Mosley, C.S., Suzuki, J.Y., and Bauer, C.E. (1994) Identification and molecular genetic characterization of a sensor kinase responsible for coordinately regulating light harvesting and reaction center gene expression in response to anaerobiosis. *J Bacteriol* **176**: 7566-7573.

Mujumdar, R.B., Ernst, L.A., Mujumdar, S.R., Lewis, C.J., and Waggoner, A.S. (1993) Cyanine dye labeling reagents: sulfoindocyanine succinimidyl esters. *Bioconjug Chem* **4**: 105-111.

Murray, T.S., and Kazmierczak, B.I. (2008) *Pseudomonas aeruginosa* exhibits sliding motility in the absence of Type IV pili and flagella. *J Bacteriol* **190**: 2700-2708.

Nara, T., Kawagishi, I., Nishiyama, S., Homma, M., and Imae, Y. (1996) Modulation of the thermosensing profile of the *Escherichia coli* aspartate receptor Tar by covalent modification of its methyl-accepting sites. *J Biol Chem* **271**: 17932-17936.

Nelson, S.S., Bollampalli, S., and McBride, M.J. (2008) SprB is a cell surface component of the *Flavobacterium johnsoniae* gliding motility machinery. *J Bacteriol* **190**: 2851-2857.

Nelson, S.S., Glocka, P.P., Agarwal, S., Grimm, D.P., and McBride, M.J. (2007) *Flavobacterium johnsoniae* SprA is a cell surface protein involved in gliding motility. *J Bacteriol* **189**: 7145-7150.

Neu, T.R. (1996) Significance of bacterial surface-active compounds in interaction of bacteria with interfaces. *Microbiol Rev* **60**: 151-166.

Niehus, E., Ye, F., Suerbaum, S., and Josenhans, C. (2002) Growth phase-dependent and differential transcriptional control of flagellar genes in *Helicobacter pylori*. *Microbiology* **148**: 3827-3837.

Nonaka, T., Adan-Kubo, J., and Miyata, M. (2010) Triskelion structure of the Gli521 protein, involved in the gliding mechanism of *Mycoplasma mobile*. *J Bacteriol* **192**: 636-642.

Nudleman, E., Wall, D., and Kaiser, D. (2006) Polar assembly of the Type IV pilus secretin in *Myxococcus xanthus*. *Mol Microbiol* **60**: 16-29.

Nultsch, W., and Hader, D.P. (1988) Photomovement in motile microorganisms--II. *Photochem Photobiol* **47**: 837-869.

Nunn, D.N., and Lory, S. (1991) Product of the *Pseudomonas aeruginosa* gene *pilD* is a prepilin leader peptidase. *Proc Natl Acad Sci U S A* **88**: 3281-3285.

O'Neill, A., Oliva, B., Storey, C., Hoyle, A., Fishwick, C., and Chopra, I. (2000) RNA polymerase inhibitors with activity against rifampin-resistant mutants of *Staphylococcus aureus*. *Antimicrob Agents Chemother* **44**: 3163-3166.

O'Toole, G.A., and Kolter, R. (1998) Flagellar and twitching motility are necessary for *Pseudomonas aeruginosa* biofilm development. *Mol Microbiol* **30**: 295-304.

Omar, A.S., Weckesser, J., and Mayer, H. (1983a) Different polysaccharides in the external layers (capsule and slime) of the cell envelope of *Rhodopseudomonas capsulata* Sp11. *Arch Microbiol* **136**: 291-296.

Omar, A.S., Flammann, H.T., Borowiak, D., and Weckesser, J. (1983b) Lipopolysaccharides of two strains of the phototrophic bacterium *Rhodopseudomonas capsulata*. *Arch Microbiol* **134**: 212-216.

Overmann, J., Beatty, J.T., Hall, K.J., Pfennig, N., and Northcote, T.G. (1991) Characterization of a dense, purple sulfur bacterial layer in a meromictic salt lake. *Limnol. Oceanogr.* **36**: 846-859.

Paetzel, M., Karla, A., Strynadka, N.C., and Dalbey, R.E. (2002) Signal petidases. *Chem Rev* **102**: 4549-4580.

Parkinson, J.S. (1993) Signal transduction schemes of bacteria. *Cell* **73**: 857-871.

Pate, J.L., and Chang, L.-Y.E. (1979) Evidence that gliding motility in prokaryotic cells is driven by rotary assemblies in the cell envelopes. *Curr Microbiol* **2**: 59-64.

Pellequer, J.L., Wager-Smith, K.A., Kay, S.A., and Getzoff, E.D. (1998) Photoactive yellow protein: a structural prototype for the three-dimensional fold of the PAS domain superfamily. *Proc Natl Acad Sci U S A* **95**: 5884-5890.

Penfold, R.J., and Pemberton, J.M. (1992) An improved suicide vector for construction of chromosomal insertion mutations in bacteria. *Gene* **118**: 145-146.

Philippe, N., and Wu, L.F. (2010) An MCP-like protein interacts with the MamK cytoskeleton and is involved in magnetotaxis in *Magnetospirillum magneticum* AMB-1. *J Mol Biol* **400**: 309-322.

Pollock, D.D., and Larkin, J.C. (2004) Estimating the degree of saturation in mutant screens. *Genetics* **168**: 489-502.

Porter, S.L., Wadhams, G.H., and Armitage, J.P. (2008) *Rhodobacter sphaeroides*: complexity in chemotactic signalling. *Trends Microbiol* **16**: 251-260.

Pringault, O., and Garcia-Pichel, F. (2004) Hydrotaxis of cyanobacteria in desert crusts. *Microb Ecol* **47**: 366-373.

Proft, T., and Baker, E.N. (2009) Pili in Gram-negative and Gram-positive bacteria - structure, assembly and their role in disease. *Cell Mol Life Sci* **66**: 613-635.

Rader, B.A., Campagna, S.R., Semmelhack, M.F., Bassler, B.L., and Guillemin, K. (2007) The quorum-sensing molecule autoinducer 2 regulates motility and flagellar morphogenesis in *Helicobacter pylori*. *J Bacteriol* **189**: 6109-6117.

Ragatz, L., Jiang, Z.Y., Bauer, C.E., and Gest, H. (1994) Phototactic purple bacteria. *Nature* **370**: 104.

Ragatz, L., Jiang, Z.Y., Bauer, C.E., and Gest, H. (1995) Macroscopic phototactic behavior of the purple photosynthetic bacterium *Rhodospirillum centenum*. *Arch Microbiol* **163**: 1-6.

Rajagopal, S., and Moffat, K. (2003) Crystal structure of a photoactive yellow protein from a sensor histidine kinase: conformational variability and signal transduction. *Proc Natl Acad Sci U S A* **100**: 1649-1654.

Rashid, M.H., and Kornberg, A. (2000) Inorganic polyphosphate is needed for swimming, swarming, and twitching motilities of *Pseudomonas aeruginosa*. *Proc Natl Acad Sci U S A* **97**: 4885-4890.

Rebbapragada, A., Johnson, M.S., Harding, G.P., Zuccarelli, A.J., Fletcher, H.M., Zhulin, I.B., and Taylor, B.L. (1997) The Aer protein and the serine chemoreceptor Tsr independently sense intracellular energy levels and transduce oxygen, redox, and energy signals for *Escherichia coli* behavior. *Proc Natl Acad Sci U S A* **94**: 10541-10546.

Ren, D., Sims, J.J., and Wood, T.K. (2002) Inhibition of biofilm formation and swarming of *Bacillus subtilis* by (5Z)-4-bromo-5-(bromomethylene)-3-butyl-2(5H)-furanone. *Lett Appl Microbiol* **34**: 293-299.

Rhodes, R.G., Nelson, S.S., Pochiraju, S., and McBride, M.J. (2011) *Flavobacterium johnsoniae sprB* is part of an operon spanning the additional gliding motility genes *sprC*, *sprD*, and *sprF*. *J Bacteriol* **193**: 599-610.

Rodriguez, A.M., and Spormann, A.M. (1999) Genetic and molecular analysis of *cglB*, a gene essential for single-cell gliding in *Myxococcus xanthus*. *J Bacteriol* **181**: 4381-4390.

Romagnoli, S., Packer, H.L., and Armitage, J.P. (2002) Tactic responses to oxygen in the phototrophic bacterium *Rhodobacter sphaeroides* WS8N. *J Bacteriol* **184**: 5590-5598.

Rosengarten, R., Klein-Struckmeier, A., and Kirchhoff, H. (1988) Rheotactic behavior of a gliding mycoplasma. *J Bacteriol* **170**: 989-990.

Rudel, T., Scheurerpflug, I., and Meyer, T.F. (1995a) *Neisseria* PilC protein identified as Type-4 pilus tip-located adhesin. *Nature* **373**: 357-359.

Rudel, T., Facius, D., Barten, R., Scheuerpflug, I., Nonnenmacher, E., and Meyer, T.F. (1995b) Role of pili and the phase-variable PilC protein in natural competence for transformation of *Neisseria gonorrhoeae*. *Proc Natl Acad Sci U S A* **92**: 7986-7990.

Rushing, B.G., Jiang, Z.-Y., Gest, H., and Bauer, C.E. (2000) *Photosensory behavior*. New York: Academic Press.

Saeki, K., and Kumagai, H. (1998) The *rnf* gene products in *Rhodobacter capsulatus* play an essential role in nitrogen fixation during anaerobic DMSO-dependent growth in the dark. *Arch Microbiol* **169**: 464-467.

Salama, N.R., Shepherd, B., and Falkow, S. (2004) Global transposon mutagenesis and essential gene analysis of *Helicobacter pylori*. *J Bacteriol* **186**: 7926-7935.

Salit, I.E., Vavougios, J., and Hofmann, T. (1983) Isolation and characterization of *Escherichia coli* pili from diverse clinical sources. *Infect Immun* **42**: 755-762.

Sambrook, J., Fritsch, E.F., and Maniatis, T. (1989) *Molecular cloning: a laboratory manual*. Cold Spring Harbor, NY: Cold Spring Harbor Laboratory Press.

Samuel, A.D., Petersen, J.D., and Reese, T.S. (2001) Envelope structure of *Synechococcus sp*. WH8113, a nonflagellated swimming cyanobacterium. *BMC Microbiol* **1**: 4.

Sato, K., Naito, M., Yukitake, H., Hirakawa, H., Shoji, M., McBride, M.J. et al. (2010) A protein secretion system linked to bacteroidete gliding motility and pathogenesis. *Proc Natl Acad Sci U S A* **107**: 276-281.

Schaefer, A.L., Taylor, T.A., Beatty, J.T., and Greenberg, E.P. (2002) Long-chain acyl-homoserine lactone quorum-sensing regulation of *Rhodobacter capsulatus* gene transfer agent production. *J Bacteriol* **184**: 6515-6521.

Schulze, M., and Rodel, G. (1989) Accumulation of the cytochrome c oxidase subunits I and II in yeast requires a mitochondrial membrane-associated protein, encoded by the nuclear SCO1 gene. *Mol Gen Genet* **216**: 37-43.

Schweinitzer, T., and Josenhans, C. (2010) Bacterial energy taxis: a global strategy? *Arch Microbiol*.

Schweinitzer, T., Mizote, T., Ishikawa, N., Dudnik, A., Inatsu, S., Schreiber, S. et al. (2008) Functional characterization and mutagenesis of the proposed behavioral sensor TlpD of *Helicobacter pylori*. *J Bacteriol* **190**: 3244-3255.

Semmler, A.B., Whitchurch, C.B., and Mattick, J.S. (1999) A re-examination of twitching motility in *Pseudomonas aeruginosa*. *Microbiology* **145 (Pt 10)**: 2863-2873.

Sganga, M.W., and Bauer, C.E. (1992) Regulatory factors controlling photosynthetic reaction center and light-harvesting gene expression in *Rhodobacter capsulatus*. *Cell* **68**: 945-954.

Shaevitz, J.W., Lee, J.Y., and Fletcher, D.A. (2005) Spiroplasma swim by a processive change in body helicity. *Cell* **122**: 941-945.

Shah, D.S., Perehinec, T., Stevens, S.M., Aizawa, S.I., and Sockett, R.E. (2000) The flagellar filament of *Rhodobacter sphaeroides*: pH-induced polymorphic transitions and analysis of the *fliC* gene. *J Bacteriol* **182**: 5218-5224.

Shelswell, K.J., Taylor, T.A., and Beatty, J.T. (2005) Photoresponsive flagellum-independent motility of the purple phototrophic bacterium *Rhodobacter capsulatus*. *J Bacteriol* **187**: 5040-5043.

Shi, B., and Xia, X. (2003) Morphological changes of *Pseudomonas pseudoalcaligenes* in response to temperature selection. *Curr Microbiol* **46**: 120-123.

Shi, W., and Zusman, D.R. (1993) The two motility systems of *Myxococcus xanthus* show different selective advantages on various surfaces. *Proc Natl Acad Sci U S A* **90**: 3378-3382.

Shi, W., Stocker, B.A., and Adler, J. (1996) Effect of the surface composition of motile *Escherichia coli* and motile *Salmonella* species on the direction of galvanotaxis. *J Bacteriol* **178**: 1113-1119.

Shih, Y.L., and Rothfield, L. (2006) The bacterial cytoskeleton. *Microbiol Mol Biol Rev* **70**: 729-754.

Shungu, D., Valiant, M., Tutlane, V., Weingberg, E., Weissberger, B., Koupal, L. et al. (1983) GELRITE as an agar substitue in bacteriological media. *Appl Environ Microbiol* **46**: 840-845.

Simon, R., Priefer, U., and Pühler, A. (1983) A broad host range mobilization system for *in vivo* genetic engineering: transposon mutagenesis in Gram-negative bacteria. *Bio/technology* **1**: 37-45.

Skerker, J.M., and Shapiro, L. (2000) Identification and cell cycle control of a novel pilus system in *Caulobacter crescentus*. *EMBO J* **19**: 3223-3234.

Skerker, J.M., and Berg, H.C. (2001) Direct observation of extension and retraction of Type IV pili. *Proc Natl Acad Sci U S A* **98**: 6901-6904.

Sliusarenko, O., Zusman, D.R., and Oster, G. (2007) The motors powering A-motility in *Myxococcus xanthus* are distributed along the cell body. *J Bacteriol* **189**: 7920-7921.

Smart, J.L., Willett, J.W., and Bauer, C.E. (2004) Regulation of *hem* gene expression in *Rhodobacter capsulatus* by redox and photosystem regulators RegA, CrtJ, FnrL, and AerR. *J Mol Biol* **342**: 1171-1186.

Solioz, M., and Marrs, B. (1977) The gene transfer agent of *Rhodopseudomonas capsulata*. Purification and characterization of its nucleic acid. *Arch Biochem Biophys* **181**: 300-307.

Solioz, M., Yen, H.C., and Marris, B. (1975) Release and uptake of gene transfer agent by *Rhodopseudomonas capsulata*. *J Bacteriol* **123**: 651-657.

Sourjik, V. (2004) Receptor clustering and signal processing in *E. coli* chemotaxis. *Trends Microbiol* **12**: 569-576.

Sourjik, V., Muschler, P., Scharf, B., and Schmitt, R. (2000) VisN and VisR are global regulators of chemotaxis, flagellar, and motility genes in Sinorhizobium (Rhizobium) meliloti. *J Bacteriol* **182**: 782-788.

Sperandio, V., Torres, A.G., and Kaper, J.B. (2002) Quorum sensing *Escherichia coli* regulators B and C (QseBC): a novel two-component regulatory system involved in the regulation of flagella and motility by quorum sensing in *E. coli*. *Mol Microbiol* **43**: 809-821.

Spiro, P.A., Parkinson, J.S., and Othmer, H.G. (1997) A model of excitation and adaptation in bacterial chemotaxis. *Proc Natl Acad Sci U S A* **94**: 7263-7268.

Spormann, A.M. (1999) Gliding motility in bacteria: insights from studies of *Myxococcus xanthus*. *Microbiol Mol Biol Rev* **63**: 621-641.

Spormann, A.M., and Kaiser, A.D. (1995) Gliding movements in *Myxococcus xanthus*. *J Bacteriol* **177**: 5846-5852.

Spormann, A.M., and Kaiser, D. (1999) Gliding mutants of *Myxococcus xanthus* with high reversal frequencies and small displacements. *J Bacteriol* **181**: 2593-2601.

Springer, W.R., and Koshland, D.E., Jr. (1977) Identification of a protein methyltransferase as the *cheR* gene product in the bacterial sensing system. *Proc Natl Acad Sci U S A* **74**: 533-537.

Stamm, M., and Carlowitz, B. (2000) Plastics, properties and testing. In *Ullmann's Encyclopedia of Industrial Chemistry*. Weinheim: Wiley-VCH Verlag GmbH & Co. KGaA.

Stanier, R.Y. (1942) A note on elasticotaxis in *Myxobacteria*. *J Bacteriol* **44**: 405-412.

Stephens, L.J. (2004) *Advanced Statistics Demystified*. New York: McGraw-Hill Professional.

Strom, M.S., and Lory, S. (1987) Mapping of export signals of *Pseudomonas aeruginosa* pilin with alkaline phosphatase fusions. *J Bacteriol* **169**: 3181-3188.

Strom, M.S., and Lory, S. (1992) Kinetics and sequence specificity of processing of prepilin by PilD, the Type IV leader peptidase of *Pseudomonas aeruginosa*. *J Bacteriol* **174**: 7345-7351.

Strom, M.S., and Lory, S. (1993) Structure-function and biogenesis of the Type IV pili. *Annu Rev Microbiol* **47**: 565-596.

Studdert, C.A., and Parkinson, J.S. (2004) Crosslinking snapshots of bacterial chemoreceptor squads. *Proc Natl Acad Sci U S A* **101**: 2117-2122.

Student (1908) The probable error of a mean. *Biometrika* **6**: 1-25.

Sun, H., Zusman, D.R., and Shi, W. (2000) Type IV pilus of *Myxococcus xanthus* is a motility apparatus controlled by the *frz* chemosensory system. *Curr Biol* **10**: 1143-1146.

Suzuki, T., Iino, T., Horiguchi, T., and Yamaguchi, S. (1978) Incomplete flagellar structures in nonflagellate mutants of *Salmonella typhimurium*. *J Bacteriol* **133**: 904-915.

Swem, D.L., and Bauer, C.E. (2002) Coordination of ubiquinol oxidase and cytochrome cbb(3) oxidase expression by multiple regulators in *Rhodobacter capsulatus*. *J Bacteriol* **184**: 2815-2820.

Swem, D.L., Swem, L.R., Setterdahl, A., and Bauer, C.E. (2005) Involvement of SenC in assembly of cytochrome c oxidase in *Rhodobacter capsulatus*. *J Bacteriol* **187**: 8081-8087.

Swem, L.R., Gong, X., Yu, C.A., and Bauer, C.E. (2006) Identification of a ubiquinone-binding site that affects autophosphorylation of the sensor kinase RegB. *J Biol Chem* **281**: 6768-6775.

Swem, L.R., Elsen, S., Bird, T.H., Swem, D.L., Koch, H.G., Myllykallio, H. et al. (2001) The RegB/RegA two-component regulatory system controls synthesis of photosynthesis and respiratory electron transfer components in *Rhodobacter capsulatus*. *J Mol Biol* **309**: 121-138.

Szabó, Z., Stahl, A.O., Albers, S.V., Kissinger, J.C., Driessen, A.J.M., and Pohlschröder, M. (2007) Identification of diverse archaeal croteins with class III signal peptides cleaved by distinct archaeal prepilin peptidases. *J Bacteriol* **189**: 772-778.

Tamayo, R., Pratt, J.T., and Camilli, A. (2007) Roles of cyclic diguanylate in the regulation of bacterial pathogenesis. *Annu Rev Microbiol* **61**: 131-148.

Taylor, B.L., Zhulin, I.B., and Johnson, M.S. (1999) Aerotaxis and other energy-sensing behavior in bacteria. *Annu Rev Microbiol* **53**: 103-128.

Taylor, D.P., Cohen, S.N., Clark, W.G., and Marrs, B.L. (1983) Alignment of genetic and restriction maps of the photosynthesis region of the *Rhodopseudomonas capsulata* chromosome by a conjugation-mediated marker rescue technique. *J Bacteriol* **154**: 580-590.

Terpe, K. (2003) Overview of tag protein fusions: from molecular and biochemical fundamentals to commercial systems. *Appl Microbiol Biotechnol* **60**: 523-533.

Thar, R., and Kuhl, M. (2003) Bacteria are not too small for spatial sensing of chemical gradients: an experimental evidence. *Proc Natl Acad Sci U S A* **100**: 5748-5753.

Thompson, J.D., Higgins, D.G., and Gibson, T.J. (1994) CLUSTAL W: improving the sensitivity of progressive multiple sequence alignment through sequence weighting, position-specific gap penalties and weight matrix choice. *Nucleic Acids Res* **22**: 4673-4680.

Tomich, M., Fine, D.H., and Figurski, D.H. (2006) The TadV protein of *Actinobacillus actinomycetemcomitans* is a novel aspartic acid prepilin peptidase required for maturation of the Flp1 pilin and TadE and TadF pseudopilins. *J Bacteriol* **188**: 6899-6914.

Tomich, M., Planet, P.J., and Figurski, D.H. (2007) The *tad* locus: postcards from the widespread colonization island. *Nat Rev Microbiol* **5**: 363-375.

Totten, P.A., Lara, J.C., and Lory, S. (1990) The *rpoN* gene product of *Pseudomonas aeruginosa* is required for expression of diverse genes, including the flagellin gene. *J Bacteriol* **172**: 389-396.

Trieschmann, M.D., Pattus, F., and Tadros, M.H. (1996) Molecular characterization and organization of porin from *Rhodobacter capsulatus* strain 37B4. *Gene* **183**: 61-68.

Turner, L.R., Lara, J.C., Nunn, D.N., and Lory, S. (1993) Mutations in the consensus ATP-binding sites of XcpR and PilB eliminate extracellular protein secretion and pilus biogenesis in *Pseudomonas aeruginosa*. *J Bacteriol* **175**: 4962-4969.

van der Horst, M.A., and Hellingwerf, K.J. (2004) Photoreceptor proteins, "star actors of modern times": a review of the functional dynamics in the structure of representative members of six different photoreceptor families. *Acc Chem Res* **37**: 13-20.

van Loosdrecht, M.C., Lyklema, J., Norde, W., Schraa, G., and Zehnder, A.J. (1987) The role of bacterial cell wall hydrophobicity in adhesion. *Appl Environ Microbiol* **53**: 1893-1897.

van Loosdrecht, M.C.M., Norde, W., Lyklema, J., and Zehnder, A.J.B. (1990) Hydrophobic and electrostatic parameters in bacterial adhesion. *Aquatic Sciences* **52**: 103-114.

Van Niel, C.B. (1944) The culture, general physiology, and classification of the non-sulfur purple and brown bacteria. *Bacteriol Rev* **8**: 1.

Varga, J.J., Nguyen, V., O'Brien, D.K., Rodgers, K., Walker, R.A., and Melville, S.B. (2006) Type IV pili-dependent gliding motility in the Gram-positive pathogen *Clostridium perfringens* and other *Clostridia*. *Mol Microbiol* **62**: 680-694.

Varshneya, A.K. (1994) *Fundamentals of inorganic glasses : Arun K. Varshneya*. Boston: Academic Press.

Vignais, P.M., Elsen, S., and Colbeau, A. (2005) Transcriptional regulation of the uptake [NiFe]hydrogenase genes in *Rhodobacter capsulatus*. *Biochem Soc Trans* **33**: 28-32.

Viollier, P.H., and Shapiro, L. (2003) A lytic transglycosylase homologue, PleA, is required for the assembly of pili and the flagellum at the *Caulobacter crescentus* cell pole. *Mol Microbiol* **49**: 331-345.

Viollier, P.H., Sternheim, N., and Shapiro, L. (2002) Identification of a localization factor for the polar positioning of bacterial structural and regulatory proteins. *Proc Natl Acad Sci U S A* **99**: 13831-13836.

Vogel, W. (1994) *Glass chemistry*. Berlin ; New York: Springer-Verlag.

Wadhams, G.H., and Armitage, J.P. (2004) Making sense of it all: bacterial chemotaxis. *Nat Rev Mol Cell Biol* **5**: 1024-1037.

Wall, D., and Kaiser, D. (1999) Type IV pili and cell motility. *Mol Microbiol* **32**: 1-10.

Wall, J.D., Weaver, P.F., and Gest, H. (1975) Gene transfer agents, bacteriophages, and bacteriocins of *Rhodopseudomonas capsulata*. *Arch Microbiol* **105**: 217-224.

Wall, J.D., Love, J., and Quinn, S.P. (1984) Spontaneous Nif- mutants of *Rhodopseudomonas capsulata*. *J Bacteriol* **159**: 652-657.

Wang, Y.A. (2002) The Function of OmpA in *Escherichia coli*. *Biochem Biophys Res Commun* **292**: 396-401.

Warren, G.J., Saul, M.W., and Sherratt, D.J. (1979) ColE1 plasmid mobility: essential and conditional functions. *Mol Gen Genet* **170**: 103-107.

Weast, R.C., and Astle, M.J. (eds) (1982) *CRC Handbook of chemistry and physics*. Boca Raton: CRC Press Inc.

Weaver, P.F., Wall, J.D., and Gest, H. (1975) Characterization of *Rhodopseudomonas capsulata*. *Arch Microbiol* **105**: 207-216.

Weckesser, J., Drews, G., and Fromme, I. (1972) Chemical analysis of and degradation studies on the cell wall lipopolysaccharide of *Rhodopseudomonas capsulata*. *J Bacteriol* **109**: 1106-1113.

Whitchurch, C.B., and Mattick, J.S. (1994) Characterization of a gene, *pilU*, required for twitching motility but not phage sensitivity in *Pseudomonas aeruginosa*. *Mol Microbiol* **13**: 1079-1091.

Whitchurch, C.B., Hobbs, M., Livingston, S.P., Krishnapillai, V., and Mattick, J.S. (1991) Characterisation of a *Pseudomonas aeruginosa* twitching motility gene and evidence for a specialised protein export system widespread in eubacteria. *Gene* **101**: 33-44.

White, D.J., and Hartzell, P.L. (2000) AglU, a protein required for gliding motility and spore maturation of *Myxococcus xanthus*, is related to WD-repeat proteins. *Mol Microbiol* **36**: 662-678.

Willett, J., Smart, J.L., and Bauer, C.E. (2007) RegA control of bacteriochlorophyll and carotenoid synthesis in *Rhodobacter capsulatus*. *J Bacteriol* **189**: 7765-7773.

Williams, F.D., and Schwarzhoff, R.H. (1978) Nature of the swarming phenomenon in *Proteus*. *Annu Rev Microbiol* **32**: 101-122.

Willows, R.D., and Kriegel, A.M. (2008) Biosynthesis of bacteriochlorophylls in purple bacteria. In *The purple phototrophic bacteria*. Hunter, C.N., Daldal, F., Thurnauer, M.C., and Beatty, J.T. (eds). Dordrecht: Springer, pp. 57-79.

Wolfe, A.J., Millikan, D.S., Campbell, J.M., and Visick, K.L. (2004) *Vibrio fischeri* sigma 54 controls motility, biofilm formation, luminescence, and colonization. *Appl Environ Microbiol* **70**: 2520-2524.

Wolfe, P.B., Wickner, W., and Goodman, J.M. (1983) Sequence of the leader peptidase gene of *Escherichia coli* and the orientation of leader peptidase in the bacterial envelope. *J Biol Chem* **258**: 12073-12080.

Wolfgang, M., van Putten, J.P.M., Hayes, S.F., Dorward, D., and Koomey, M. (2000) Components and dynamics of fiber formation define a ubiquitous biogenesis pathway for bacterial pili. *EMBO J* **19**: 6408-6418.

Wolgemuth, C., Hoiczyk, E., Kaiser, D., and Oster, G. (2002) How myxobacteria glide. *Curr Biol* **12**: 369-377.

Wolgemuth, C.W., Charon, N.W., Goldstein, S.F., and Goldstein, R.E. (2006) The flagellar cytoskeleton of the spirochetes. *J Mol Microbiol Biotechnol* **11**: 221-227.

Wolkin, R.H., and Pate, J.L. (1984) Translocation of motile cells of the gliding bacterium *Cytophaga johnsonae* depends on a surface component that may be modified by sugars. *J Gen Microbiol* **130**: 2651-2669.

Wong, D.K., Collins, W.J., Harmer, A., Lilburn, T.G., and Beatty, J.T. (1996) Directed mutagenesis of the *Rhodobacter capsulatus puhA* gene and orf 214: pleiotropic effects on photosynthetic reaction center and light-harvesting 1 complexes. *J Bacteriol* **178**: 2334-2342.

Wood, T.K., Gonzalez Barrios, A.F., Herzberg, M., and Lee, J. (2006) Motility influences biofilm architecture in *Escherichia coli*. *Appl Microbiol Biotechnol* **72**: 361-367.

Wu, J., and Newton, A. (1997) Regulation of the *Caulobacter* flagellar gene hierarchy; not just for motility. *Mol Microbiol* **24**: 233-239.

Yang, H., Inokuchi, H., and Adler, J. (1995) Phototaxis away from blue light by an *Escherichia coli* mutant accumulating protoporphyrin IX. *Proc Natl Acad Sci U S A* **92**: 7332-7336.

Yang, R., Bartle, S., Otto, R., Stassinopoulos, A., Rogers, M., Plamann, L., and Hartzell, P. (2004) AglZ is a filament-forming coiled-coil protein required for adventurous gliding motility of *Myxococcus xanthus*. *J Bacteriol* **186**: 6168-6178.

Yanisch-Perron, C., Vieira, J., and Messing, J. (1985) Improved M13 phage cloning vectors and host strains: nucleotide sequences of the M13mp18 and pUC19 vectors. *Gene* **33**: 103-119.

Yen, H.C., and Marrs, B. (1976) Map of genes for carotenoid and bacteriochlorophyll biosynthesis in *Rhodopseudomonas capsulata*. *J Bacteriol* **126**: 619-629.

Yen, H.C., Hu, N.T., and Marrs, B.L. (1979) Characterization of the gene transfer agent made by an overproducer mutant of *Rhodopseudomonas capsulata*. *J Mol Biol* **131**: 157-168.

Yonekawa, H., Hayashi, H., and Parkinson, J.S. (1983) Requirement of the *cheB* function for sensory adaptation in *Escherichia coli*. *J Bacteriol* **156**: 1228-1235.

Yoshihara, S., and Ikeuchi, M. (2004) Phototactic motility in the unicellular cyanobacterium *Synechocystis sp*. PCC 6803. *Photochem Photobiol Sci* **3**: 512-518.

Youderian, P. (1998) Bacterial motility: secretory secrets of gliding bacteria. *Curr Biol* **8**: R408-411.

Youderian, P., Burke, N., White, D.J., and Hartzell, P.L. (2003) Identification of genes required for adventurous gliding motility in *Myxococcus xanthus* with the transposable element mariner. *Mol Microbiol* **49**: 555-570.

Yu, R., and Kaiser, D. (2007) Gliding motility and polarized slime secretion. *Mol Microbiol* **63**: 454-467.

APPENDIX A

The information presented in **APPENDIX A** is provided as supplementary material for sections **3.1.3**, **3.1.4**, **3.2.4**, **3.6.4**, **C.1** and **C.2**. The data summarized in graphical format in section **3** and **APPENDIX C**, are presented fully in tabular format in this appendix.

Table A-1: Average motility values of samples incubated in the glass-medium interstice of medium solidification agent titrations.

Solidifier	Solidifier amount (%)	Average motility distance [(a)] (mm)	P_Z [(b)]	Frequency [(c)]	# Samples
Agar	1.5	29 (18)		0.85	97
Agarose	0. 2	9 (6)	0.000012 *	0.79	24
Agarose	0.5	25 (17)	0.23	0.83	24
Agarose	0.75	29 (17)	0.94	0.92	24
Agarose	1	35 (15)	0.19	0.92	24
Agarose	1.25	33 (16)	0.61	0.96	24
Agarose	1.5	29 (18)	0.83	0.92	24
Gelrite	0.25	25 (12)	0.22	1	24
Gelrite	0.5	9 (10)	0.000028 *	0.58	24
Gelrite	0.75	7 (7)	0.000025 *	0.54	24
Gelrite	1	8 (10)	0.0000059 *	0.63	24
Gelrite	1.25	6 (9)	0.0000025 *	0.54	24
Gelrite	1.5	9 (12)	0.000071 *	0.63	24

(a) Taxis distance as measured from the point of inoculation to farthest point of visible cell growth, with standard deviation in parentheses.

(b) Two-tailed two-independent sample Wilcoxon rank sum test of significant difference compared to 1.5% agar samples. For a >0.95 probability that the movement was different from controls, $P_Z < 0.05$. Asterisks indicate cases where $P_Z < 0.05$.

(c) Frequency of samples exhibiting taxis with a distance greater than 4 mm.

Table A-2: Average motility values of samples incubated in the glass-medium interstice of agar medium volume titrations.

Volume (mL)	Average motility distance [(a)] (mm)	P_Z [(b)]	Frequency [(c)]	# Samples
5	18 (16)	0.11	0.71	24
10	31 (14)	0.054	0.96	24
15	21 (18)	0.0035 *	0.71	24
20	38 (13)		0.96	24
25	32 (18)	0.11	0.83	24

(a) Taxis distance as measured from the point of inoculation to farthest point of visible cell growth, with standard deviation in parentheses.

(b) Two-tailed two-independent sample Wilcoxon rank sum test of significant difference compared to 20 mL agar samples. For a >0.95 probability that the movement was different from controls, $P_Z < 0.05$. Asterisks indicate cases where $P_Z < 0.05$.

(c) Frequency of samples exhibiting taxis with a distance greater than 4 mm.

Table A-3: Average evaporation values of agar medium volume titration samples.

Volume (mL)	Average moisture loss [(a)] (g)	Average relative moisture loss [(b)] (%)	P_Z [(c)]	# Samples
5	0.42 (0.074)	8.5 (1.6)	0.14	10
10	0.44 (0.12)	4.5 (1.2)	0.19	10
15	0.42 (0.094)	2.8 (0.64)	0.26	10
20	0.45 (0.064)	2.3 (0.33)		10
25	0.45 (0.094)	1.8 (0.38)	0.57	10

(a) Moisture lost to evaporation as measured by weight before and after incubation, with standard deviation in parentheses.

(b) Moisture loss relative to initial medium weight, with standard deviation in parentheses.

(c) Two-tailed two-independent sample Wilcoxon rank sum test of significant difference compared to 20 mL agar moisture loss samples. For a >0.95 probability that the movement was different from controls, $P_Z < 0.05$. Asterisks indicate cases where $P_Z < 0.05$.

Table A-4: Average motility values of samples incubated in the glass-agar interstice with various incubation temperatures.

Temperature [(a)] (°C)	Average motility distance [(b)] (mm)	Average angle relative to heat source [(c)] (°)	P_Z [(d)]	# Samples
30	24 (20)	38 (122)		40
32	16 (16)	- 5 (109)	0.36	10
34	20 (19)	- 33 (112)	0.24	10
36	22 (21)	- 63 (95)	0.078	6
40	30 (20)	- 77 (144)	0.14	6

(a) Temperature measured at the point of stab inoculation at the edge of the Petri plate closest to the heat source.

(b) Taxis distance as measured from the point of inoculation to farthest point of visible cell growth, with standard deviation in parentheses.

(c) Taxis direction from the point of inoculation to the farthest point of visible cell growth, with standard deviation in parentheses. 0° indicates movement directly toward the heat source, and $\pm$ 180° indicates movement directly away from the heat.

(d) Two-tailed two-independent sample Wilcoxon rank sum test of significant difference compared to isothermal 30 °C samples. For a >0.95 probability that the movement was different from controls, $P_Z < 0.05$.

Table A-5: *R. capsulatus* proteins identified by peptide sequencing of cell surface protein-enrichment resolved by SDS-PAGE.

Annotation	Predicted function [(a)]	# Peptides [(b)]	Coverage (%)[(c)]	E value [(d)]
RCC00008	flagellar hook-associated protein FlgK	1	4.5	$2e^{-17}$
RCC00018	xylose ABC transporter, xylose-binding protein XylF	1	5	$4e^{-14}$
RCC00045	photosynthetic apparatus regulatory protein RegA	1	6.5	$9e^{-10}$
RCC00046	trans-acting regulatory protein HvrA	1	17	$1e^{-13}$
RCC00118	sigma 54 modulation protein/ribosomal protein S30EA	2	15	$3e^{-12}$
RCC00125	UTP-glucoseNT0-1-phosphate uridylyltransferase	1	4.5	$3e^{-10}$
RCC00127	3'(2'),5'-bisphosphate nucleotidase	1	7	$2e^{-16}$
RCC00158	peptidase, M10 family	3	11	$1e^{-24}$
RCC00178	hemolysin-type calcium-binding repeat family protein	2	2.5	$1e^{-16}$
RCC00228	oxidoreductase, DSBA family	2	8.5	$2e^{-16}$
RCC00259	porin family protein	9	27.5	$5e^{-17}$
RCC00284	polyribonucleotide nucleotidyltransferase	1	3	$2e^{-16}$
RCC00287	50S ribosomal protein L11	2	24.5	$2e^{-16}$
RCC00295	30S ribosomal protein S7	1	9	$2e^{-11}$
RCC00297	translation elongation factor Tu	2	10	$1e^{-16}$
RCC00299	50S ribosomal protein L3	2	11	$3e^{-11}$
RCC00300	50S ribosomal protein L4	1	11	$2e^{-20}$
RCC00304	50S ribosomal protein L22	2	21.5	$5e^{-13}$
RCC00311	50S ribosomal protein L24	2	34.5	$9e^{-19}$
RCC00324	30S ribosomal protein S13	3	28	$4e^{-18}$
RCC00325	30S ribosomal protein S11	1	14	$3e^{-15}$
RCC00327	50S ribosomal protein L17	1	7	$2e^{-8}$
RCC00335	glutamate/aspartate ABC transporter, periplasmic glutamate/aspartate-binding protein BztA	8	24	$3e^{-24}$
RCC00362	50S ribosomal protein L19	1	14.5	$3e^{-15}$
RCC00367	30S ribosomal protein S16	2	23	$9e^{-13}$
RCC00438	serine hydroxymethyltransferase	1	3	$8e^{-10}$
RCC00459	glutathione S-transferase domain protein	1	7	$1e^{-11}$
RCC00484	alanine dehydrogenase	4	18	$4e^{-21}$

Annotation	Predicted function [a]	# Peptides [b]	Coverage (%)[c]	E value [d]
RCC00487	inositol-1-monophosphatase	1	5.5	$5e^{-11}$
RCC00706	oligopeptide ABC transporter, periplasmic oligopeptide-binding protein OppA	1	3.5	$3e^{-15}$
RCC00718	malate dehydrogenase	2	8.5	$5e^{-11}$
RCC00786	basic membrane lipoprotein family	7	36	$2e^{-22}$
RCC00836	cobaltochelatase, CobS subunit	1	5	$7e^{-14}$
RCC00895	glycine betaine/L-proline ABC transporter, periplasmic glycine betaine/L-proline-binding protein ProX	1	8	$1e^{-19}$
RCC01156	UspA domain protein	2	10.5	$1e^{-15}$
RCC01160	cytochrome c oxidase, Cbb3-type, subunit III	1	5	$1e^{-10}$
RCC01240	cytochrome c2	7	29	$3e^{-14}$
RCC01244	polyamine ABC transporter, periplasmic polyamine-binding protein PotD	3	12.5	$1e^{-19}$
RCC01369	ABC transporter, periplasmic substrate-binding protein	3	17.5	$1e^{-21}$
RCC01551	peroxiredoxin	1	11.5	$1e^{-15}$
RCC01591	ferredoxin-NADP reductase	1	5	$3e^{-11}$
RCC01620	aldehyde dehydrogenase (NADP(+))	1	3	$6e^{-13}$
RCC01674	glutamine synthetase	1	3	$3e^{-10}$
RCC01692	conserved hypothetical protein	2	9	$1e^{-07}$
RCC01821	30S ribosomal protein S2	2	9.5	$1e^{-10}$
RCC01852	periplasmic ABC transporter branched-chain amino acid-binding protein LivK	2	10.5	$9e^{-23}$
RCC01940	hemolysin-type calcium-binding repeat family protein	2	17	$1e^{-18}$
RCC02009	50S ribosomal protein L9	3	12	$2e^{-10}$
RCC02010	30S ribosomal protein S18	1	14.5	$3e^{-9}$
RCC02019	ribose ABC transporter, periplasmic ribose-binding protein	1	3.5	$5e^{-9}$
RCC02160	glyceraldehyde-3-phosphate dehydrogenase, type I	3	13	$5e^{-13}$
RCC02208	propanediol utilization protein PduB	6	50	$5e^{-20}$
RCC02211	formate C-acetyltransferase	3	7	$3e^{-17}$
RCC02299	50S ribosomal protein L27	1	19	$1e^{-14}$
RCC02311	superoxide dismutase [Fe]	1	6.5	$6e^{-10}$

Annotation	Predicted function [a]	# Peptides [b]	Coverage (%)[c]	E value [d]
RCC02373	monosaccharide ABC transporter, periplasmic monosaccharide-binding protein	2	13.5	$9e^{-22}$
RCC02478	chaperonin GroL	1	33	$9e^{-14}$
RCC02490	OmpA family protein	2	15	$1e^{-18}$
RCC02501	cytochrome c, class I	1	12.5	$6e^{-22}$
RCC02521	pyrimidine ABC transporter, periplasmic pyrimidine-binding protein	1	4	$1e^{-10}$
RCC02533	light-harvesting protein B-800/850 gamma chain	10	37.5	$5e^{-22}$
RCC02537	cysteine synthase	3	17	$4e^{-17}$
RCC02578	iron(III) ABC transporter, periplasmic iron(III)-compound-binding protein	2	9	$6e^{-15}$
RCC02657	monosaccharide ABC transporter, periplasmic monosaccharide-binding protein	4	20	$1e^{-21}$
RCC02689	dimethyladenosine transferase	1	6	$5e^{-14}$
RCC02787	O-acetylhomoserine aminocarboxypropyltransferase/O-acetylserine sulfhydrylase	1	3	$1e^{-10}$
RCC02959	spermidine/putrescine ABC transporter, periplasmic spermidine/putrescine-binding protein	1	5	$2e^{-15}$
RCC02971	ATP synthase F1, beta subunit	2	6.5	$7e^{-14}$
RCC02972	ATP synthase F1, gamma subunit	2	12	$6e^{-16}$
RCC02973	ATP synthase F1, alpha subunit	1	3	$9e^{-11}$
RCC02979	30S ribosomal protein S4	5	28	$5e^{-14}$
RCC03024	TRAP dicarboxylate transporter, DctP subunit	7	24	$5e^{-18}$
RCC03036	NAD-dependent formate dehydrogenase, beta subunit	2	5	$7e^{-13}$
RCC03050	ribosomal protein L25, Ctc-form	1	7	1e-11
RCC03056	conserved hypothetical protein	1	3	$7e^{-16}$
RCC03129	50S ribosomal protein L28	1	15	$4e^{-11}$
RCC03161	D-amino-acid transaminase	1	5	$2e^{-11}$
RCC03195	OmpA/MotB domain protein	2	20	$1e^{-15}$
RCC03232	basic membrane lipoprotein family	1	5	$6e^{-15}$
RCC03315	pyridoxine 5'-phosphate synthase	1	4.5	$7e^{-9}$
RCC03339	conserved hypothetical protein	1	10	$6e^{-9}$

Annotation	Predicted function [(a)]	# Peptides [(b)]	Coverage (%)[(c)]	E value [(d)]
RCC03416	endoribonuclease L-PSP family protein	2	12	$7e^{-15}$
RCC03534	30S ribosomal protein S20	1	16	$5e^{-11}$

(a) Annotation by automated TIGR website.

(b) Number of peptides from *R. capsulatus* gene product matched to *R. capsulatus* MASCOT database.

(c) Peptide coverage of entire gene product sequence.

(d) Top E-value scores from local pairwise protein domain alignment BLASTp.

Table A-6: Average motility values of wild type strain B10 samples incubated in the glass-agar interstice with filtered directional incident light.

Light (nm)	Sample [(a)]	Average motility distance [(b)] (mm)	Average angle relative to light [(c)] (°)	P_Z [(d)]	# Samples
white	E	31 (15)	-33 (140)		34
	C	36 (15)	-83 (90)	0.46	34
> 350	E	28 (18)	-28 (120)	0.62	34
	C	32 (16)	59 (93)	0.003 *	34
> 900	E	39 (9)	-28 (115)	0.69	34
	C	39 (12)	35 (74)	0.019 *	34
650	E	29 (17)	-14 (118)	0.54	34
(±12.5)	C	32 (16)	45 (132)	0.28	34
700	E	31 (17)	30 (94)	0.03 *	34
(±12.5)	C	34 (15)	9 (70)	0.47	34
750	E	31 (18)	-5 (84)	0.29	34
(±12.5)	C	41 (10)	13 (115)	0.44	34

(a) **E = Experimental exposure; C = Control. Experimental = illuminated during incubation; Control = no illumination during incubation.**

(b) **Taxis distance as measured from the point of inoculation to farthest point of visible cell growth, with standard deviation in parentheses.**

(c) **Taxis direction from the point of inoculation to the farthest point of visible cell growth, with standard deviation in parentheses. 0° indicates movement directly toward the light source, and ± 180° indicates movement directly away from the light.**

(d) **Two-tailed two-independent sample Wilcoxon rank sum test of significant difference compared to white light illuminated control samples. For a >0.95 probability that the movement was different from controls, $P_Z < 0.05$. Asterisks indicate cases where $P_Z < 0.05$.**

Table A-7: Average motility values of *flaA* mutant strain bKSDF samples incubated in the glass-agar interstice with defined emission LED directional incident light.

Light (nm)	Sample [a]	Average motility distance [b] (mm)	Average angle relative to light [c] (°)	P_z (white light / dark) [d]	# Samples
white	E	30 (18)	-9 (66)		61
(430-630)	C	28 (20)	-40 (71)	0.96	25
632	E	33 (17)	28 (107)	0.16	34
(±5)	C	30 (19)	-67 (76)	0.065	18
625	E	35 (17)	18 (97)	0.97	34
(±10)	C	34 (16)	44 (94)	0.36	18
610	E	22 (19)	-27 (67)	0.14	30
(±8)	C	32 (17)	29 (71)	0.25	17
572	E	26 (18)	22 (69)	0.0059 *	35
(±10)	C	30 (18)	-52 (74)	0.036 *	14
525	E	35 (14)	0 (88)	0.71	34
(±10)	C	40 (11)	-48 (47)	0.68	21
490	E	32 (17)	35 (87)	0.00071 *	32
(±15)	C	30 (17)	6 (91)	0.0078 *	16
470	E	14 (16)	27 (102)	0.025 *	50
(±15)	C	22 (22)	-26 (78)	0.049 *	25
450	E	28 (17)	26 (56)	0.0035 *	54
(±15)	C	29 (17)	-15 (71)	0.0049 *	27

Light (nm)	Sample [(a)]	Average motility distance [(b)] (mm)	Average angle relative to light [(c)] (°)	P_Z (white light / dark) [(d)]	# Samples
425	E	31 (16)	39 (62)	0.0000034 *	60
(±10)	C	37 (16)	-22 (66)	0.0000079 *	30
405	E	34 (17)	-8 (83)	0.13	36
(±6)	C	31 (19)	18 (95)	0.65	16
395	E	35 (14)	73 (113)	0.00018 *	36
(±6)	C	35 (15)	27 (83)	0.000012 *	18
385	E	31 (14)	15 (103)	0.026 *	36
(±9)	C	33 (17)	-13 (111)	0.098	18
375	E	32 (17)	36 (82)	0.0027 *	54
(±6)	C	39 (12)	-47 (61)	0.001 *	27
dark	E	31 (15)	46 (77)	0.00033 *	54
	C	41 (10)	-46 (35)	0.00000058 *	27

(a) E = Experimental exposure; C = Control. Experimental = illuminated during incubation; Control = no illumination during incubation.

(b) Taxis distance as measured from the point of inoculation to farthest point of visible cell growth, with standard deviation in parentheses.

(c) Taxis direction from the point of inoculation to the farthest point of visible cell growth, with standard deviation in parentheses. 0° indicates movement directly toward the light source, and ± 180° indicates movement directly away from the light.

(d) Two-tailed two-independent sample Wilcoxon rank sum test of significant difference compared to experimental white light illuminated (top) and control dark test set (bottom) samples. . For a >0.95 probability that the movement was different from controls, $P_Z < 0.05$. Asterisks indicate cases where $P_Z < 0.05$.

Table A-8: Average motility values of *flaA* mutant strain bKSDF and *flaA/pyp* mutant strain bKSDFpyp samples incubated in the glass-agar interstice with defined emission LED directional incident light.

Light (nm)	Sample [(a)]	Average motility distance [(b)] (mm)	Average angle relative to light [(c)] (°)	P_Z (white light / dark) [(d)]	# Samples
white	E bKSDF	25 (19)	4 (100)		30
(430-630)	C bKSDF	36 (15)	21 (38)		14
	E bKSDFpyp	28 (17)	17 (102)	0.76	30
	C bKSDFpyp	28 (18)	29 (62)	1	17
435 [(e)]	E bKSDF	26 (18)	44 (47)		42
(+30, -20)	C bKSDF	39 (12)	0 (80)		21
	E bKSDFpyp	30 (17)	48 (48)	0.59	42
	C bKSDFpyp	19 (19)	-31 (95)	0.023 *	21
375	E bKSDF	24 (17)	4 (80)		18
(±6)	C bKSDF	44 (2)	-26 (26)		9
	E bKSDFpyp	32 (17)	5 (79)	0.85	18
	C bKSDFpyp	15 (22)	-18 (73)	0.75	9
dark	E bKSDF	29 (15)	50 (89)		18
	C bKSDF	44 (4)	-48 (38)		9
	E bKSDFpyp	33 (14)	79 (55)	0.44	18
	C bKSDFpyp	38 (14)	-72 (23)	0.000047 *	9

(a) E = Experimental exposure; C = Control. Experimental = illuminated during incubation; Control = no illumination during incubation.

(b) Taxis distance as measured from the point of inoculation to farthest point of visible cell growth, with standard deviation in parentheses.

(c) Taxis direction from the point of inoculation to the farthest point of visible cell growth, with standard deviation in parentheses. 0° indicates movement directly toward the light source, and ± 180° indicates movement directly away from the light.

(d) Two-tailed two-independent sample Wilcoxon rank sum test of significant difference compared to experimental bKSDF illuminated (top) and control bKSDFpyp dark test set (bottom) samples. . For a >0.95 probability that the movement was different from controls, $P_Z < 0.05$. Asterisks indicate cases where $P_Z < 0.05$.

(e) Average results from LED lamps with emission peaks at 450 nm or 425 nm.

Table A-9: *R. capsulatus* transcripts upregulated >2 fold identified by transcriptome comparison of solid substrate medium-harvested cell total RNA to early stationary phase aqueous medium-harvested cell total RNA.

Annotation	Predicted function [(a)]	Probe spot [(b)]	Fold change [(c)]
RCC03525	flagellin protein	Rc_chrom0706S003622_at	126.7027360
RCC01336	acetone carboxylase, beta subunit	Rc_chrom0706S001373_at	55.4977650
RCC01337	acetone carboxylase, alpha subunit	Rc_chrom0706S001374_at	35.2704600
RCC01338	acetone carboxylase, gamma subunit	Rc_chrom0706S001375_at	16.4949760
RCC00863	50S ribosomal protein L13	Rc_chrom0706S000893_at	15.0579320
RCC00311	50S ribosomal protein L24	Rc_chrom0706S000319_at	14.5279550
RCC01821	30S ribosomal protein S2	Rc_chrom0706S001881_at	12.4090500
RCC02211	formate C-acetyltransferase	Rc_chrom0706S002283_at	12.1668930
RCC02119	methyltransferase, type 12 family	Rc_chrom0706S002184_at	11.7204870
RCC00312	50S ribosomal protein L5	Rc_chrom0706S000320_at	10.7591070
RCP00069	conserved hypothetical protein	Rc_plasm0706S004952_at	10.7546420
RCC00136	alkaline phosphatase	Rc_chrom0706S000140_at	10.7199190
RCC03261	TOBE domain protein	Rc_chrom0706S003355_at	10.4069310
RCC00767	hydrogenase, small subunit	Rc_chrom0706S000792_at	10.4056100
RCC03204	isoleucyl-tRNA synthetase	Rc_chrom0706S003297_at	9.9924170
RCC00310	50S ribosomal protein L14	Rc_chrom0706S000318_at	9.9215000
RCC02212	ThiJ/PfpI family protein	Rc_chrom0706S002284_at	9.4545250
RCC03050	50S ribosomal protein L25	Rc_chrom0706S003140_at	9.3737310
RCC00761	NAD-reducing hydrogenase HoxS, beta subunit	Rc_chrom0706S000785_at	9.3449745
RCC02209	propanediol utilization protein PduA	Rc_chrom0706S002281_at	8.7715890

Annotation	Predicted function [a]	Probe spot [b]	Fold change [c]
RCC01720	nucleoside diphosphate kinase	Rc_chrom0706S001772_at	8.6320095
	intergenic region	Rc_chrom0706S003733_at	8.2649310
RCC02786	hemolysin-type calcium-binding repeat family protein	Rc_chrom0706S002875_at	8.1644840
RCC03503	phosphate ABC transporter, periplasmic phosphate-binding protein	Rc_chrom0706S003600_at	8.1014490
RCC02208	propanediol utilization protein PduB	Rc_chrom0706S002280_at	8.0930720
	intergenic region	Rc_chrom0706S003725_at	7.6003175
RCC03159	hemolysin-type calcium-binding repeat family protein	Rc_chrom0706S003251_at	7.5561543
RCC01125	30S ribosomal protein S1	Rc_chrom0706S001159_at	7.5180445
RCC00327	50S ribosomal protein L17	Rc_chrom0706S000335_at	7.4838220
	intergenic region	Rc_chrom0706S004131_at	7.3592780
RCC00762	hydrogenase maturation factor HowW	Rc_chrom0706S000786_at	6.8351190
RCC01960	polysaccharide export protein Wza	Rc_chrom0706S002024_at	6.8145733
RCC00314	30S ribosomal protein S8	Rc_chrom0706S000322_at	6.7162943
control		AFFX-r2-Bs-phe-3_at	6.7001880
RCC00313	30S ribosomal protein S14	Rc_chrom0706S000321_at	6.6608677
RCC01120	methionine adenosyltransferase	Rc_chrom0706S001153_at	6.5072640
RCC00889	NosL protein	Rc_chrom0706S000920_at	6.4328804
RCC00715	pyridine nucleotide transhydrogenase, alpha subunit	Rc_chrom0706S000734_at	6.4319196
control		AFFX-r2-Bs-lys-M_at	6.3906660
RCC02787	O-acetylhomoserine aminocarboxypropyltransferase/o-acetylserine sulfhydrylase	Rc_chrom0706S002876_at	6.3743590

Annotation	Predicted function [a]	Probe spot [b]	Fold change [c]
RCC01822	translation elongation factor Ts	Rc_chrom0706S001882_at	6.2744727
RCC01940	hemolysin-type calcium-binding repeat family protein	Rc_chrom0706S002002_at	6.2557860
RCC03154	50S ribosomal protein L20	Rc_chrom0706S003246_at	6.2221413
RCC02182	aminotransferase, class III	Rc_chrom0706S002253_at	6.1899004
	intergenic region	Rc_chrom0706S003899_at	6.1215270
RCC03502	phosphate ABC transporter, permease protein PstC	Rc_chrom0706S003599_at	6.0853167
RCC01186	conserved hypothetical protein	Rc_chrom0706S001222_at	6.0610385
RCC00888	conserved hypothetical protein	Rc_chrom0706S000919_at	5.9865870
RCC00890	conserved hypothetical protein	Rc_chrom0706S000921_at	5.9693220
control		AFFX-LysX-5_at	5.9597060
	intergenic region	Rc_chrom0706S004096_at	5.8959055
control		AFFX-r2-Bs-lys-3_at	5.8793200
control		AFFX-LysX-3_at	5.8130746
RCC02118	chloramphenicol acetyltransferase	Rc_chrom0706S002183_at	5.7662663
control		AFFX-PheX-3_at	5.7563340
RCC00864	30S ribosomal protein S9	Rc_chrom0706S000894_at	5.7563033
RCC03376	conserved hypothetical protein	Rc_chrom0706S003472_at	5.6905675
RCC00024	glutaryl-CoA dehydrogenase	Rc_chrom0706S000024_at	5.6567140
control		AFFX-LysX-M_at	5.6478047
RCC00315	50S ribosomal protein L6	Rc_chrom0706S000323_at	5.5595200
RCC02373	monosaccharide ABC transporter, periplasmic monosaccharide-binding protein	Rc_chrom0706S002446_at	5.3869410

Annotation	Predicted function [a]	Probe spot [b]	Fold change [c]
control		AFFX-r2-Bs-lys-5_at	5.3747334
RCC00562	molybdenum ABC transporter, periplasmic molybdenum-binding protein ModA	Rc_chrom0706S000577_at	5.3439703
RCC00326	DNA-directed RNA polymerase, alpha subunit	Rc_chrom0706S000334_at	5.3340090
RCC00309	30S ribosomal protein S17	Rc_chrom0706S000317_at	5.2228530
RCC00321	50S ribosomal protein L15	Rc_chrom0706S000329_at	5.2127400
RCC02207	propanediol utilization protein PduA	Rc_chrom0706S002279_at	5.1378202
control		AFFX-PheX-5_at	5.0563245
RCC02113	ornithine cyclodeaminase	Rc_chrom0706S002177_at	5.0549073
	intergenic region	Rc_chrom0706S004708_at	4.9626527
RCC00636	conserved hypothetical protein	Rc_chrom0706S000654_at	4.9286656
RCC02617	5'-nucleotidase	Rc_chrom0706S002706_at	4.9010690
RCC00420	pyruvate kinase	Rc_chrom0706S000430_at	4.8044010
RCC02008	trigger factor	Rc_chrom0706S002071_at	4.7493630
RCC00316	50S ribosomal protein L18	Rc_chrom0706S000324_at	4.7402077
	intergenic region	Rc_chrom0706S004005_at	4.6987590
RCC00208	argininosuccinate synthase	Rc_chrom0706S000213_at	4.6725955
RCC01589	ErfK/YbiS/YcfS/YnhG family protein	Rc_chrom0706S001635_at	4.6253705
RCC01900	hemolysin-type calcium-binding repeat family protein	Rc_chrom0706S001962_at	4.5856776
RCC02877	monosacharide ABC transporter, periplasmic monosacharide-binding protein	Rc_chrom0706S002973_at	4.5762360
RCC00001	chromosomal replication initiator protein DnaA	Rc_chrom0706S000001_at	4.5540223

Annotation	Predicted function [a]	Probe spot [b]	Fold change [c]
RCC03467	hypothetical protein	Rc_chrom0706S003564_at	4.5405680
RCC02621	sulphate transporter	Rc_chrom0706S002710_at	4.5254360
RCC02979	30S ribosomal protein S4	Rc_chrom0706S003073_at	4.5173900
RCC03155	50S ribosomal protein L35	Rc_chrom0706S003247_at	4.4089940
RCC02149	protein of unknown function DUF1223	Rc_chrom0706S002217_at	4.3533030
RCC03191	hemolysin-type calcium-binding repeat family protein	Rc_chrom0706S003284_at	4.3317676
RCP00075	nitrous-oxide reductase	Rc_plasm0706S004958_at	4.3247150
RCC02981	histidinol-phosphate aminotransferase	Rc_chrom0706S003076_at	4.2746380
RCC00354	peptidase T	Rc_chrom0706S000362_at	4.2676134
RCC00706	oligopeptide ABC transporter, periplasmic oligopeptide-binding protein OppA	Rc_chrom0706S000725_at	4.2605104
RCC00290	50S ribosomal protein L7/L12	Rc_chrom0706S000298_at	4.2437690
RCC03210	transaldolase	Rc_chrom0706S003303_at	4.2199855
RCC01335	GAF modulated sigma54 specific transcriptional regulator, Fis family	Rc_chrom0706S001372_at	4.2190760
RCC00817	L-lactate dehydrogenase	Rc_chrom0706S000844_at	4.1833400
RCC02210	aldehyde-alcohol dehydrogenase 2	Rc_chrom0706S002282_at	4.1448107
RCC00289	50S ribosomal protein L10	Rc_chrom0706S000297_at	4.1405460
control		AFFX-PheX-M_at	4.1388574
RCC01546	AMP-dependent synthetase and ligase family protein	Rc_chrom0706S001591_at	4.1309660
RCC02939	conserved hypothetical protein	Rc_chrom0706S003032_at	4.1080213
RCC00367	30S ribosomal protein S16	Rc_chrom0706S000375_at	3.9865770
RCC02647	bifunctional protein PutA	Rc_chrom0706S002736_at	3.9863636

Annotation	Predicted function [a]	Probe spot [b]	Fold change [c]
	intergenic region	Rc_chrom0706S003736_at	3.9279377
RCC01501	bifunctional UDP-N-acetylglucosamine diphosphorylase/glucosamine-1-phosphate N-acetyltransferase	Rc_chrom0706S001544_at	3.9132016
RCC01715	phosphopyruvate hydratase	Rc_chrom0706S001767_at	3.8998458
RCC01502	phosphoglycolate phosphatase	Rc_chrom0706S001545_at	3.8995829
RCC00317	30S ribosomal protein S5	Rc_chrom0706S000325_at	3.8859909
RCC02816	binfunctional sulfate adenylyltransferase/adenylyl-sulfate kinase	Rc_chrom0706S002908_at	3.8777742
RCC00865	hemolysin-type calcium-binding repeat family protein	Rc_chrom0706S000895_at	3.8393312
RCC00538	methylmalonyl-CoA epimerase	Rc_chrom0706S000551_at	3.8261566
RCC00201	site-specific DNA-methyltransferase (adenine-specific)	Rc_chrom0706S000206_at	3.8036320
RCP00071	nitrous oxide reductase accessory protein NosL	Rc_plasm0706S004954_at	3.7997870
	intergenic region	Rc_chrom0706S003793_at	3.7697847
RCC02671	translation elongation factor P	Rc_chrom0706S002761_at	3.7688677
RCP00062	TRAP transporter solute receptor, TAXI family	Rc_plasm0706S004944_at	3.7661731
RCC01625	uridylate kinase	Rc_chrom0706S001677_at	3.7654686
	intergenic region	Rc_chrom0706S004240_at	3.7471077
RCC00561	molybdenum transport operon repressor MopA	Rc_chrom0706S000576_at	3.7395642
RCC02462	membrane protein, putative	Rc_chrom0706S002542_at	3.7324467
RCP00077	conserved hypothetical protein	Rc_plasm0706S004960_at	3.7308360

Annotation	Predicted function [a]	Probe spot [b]	Fold change [c]
RCC00476	protein of unknown function DUF1013	Rc_chrom0706S000489_at	3.7026017
RCP00068	peptidase, M4 family	Rc_plasm0706S004951_at	3.7007444
RCC00484	alanine dehydrogenase	Rc_chrom0706S000496_at	3.6930783
RCC02288	conserved hypothetical protein	Rc_chrom0706S002361_at	3.6870618
RCC00318	50S ribosomal protein L30	Rc_chrom0706S000326_at	3.6754627
RCC00173	glucose-1-phosphate thymidylyltransferase	Rc_chrom0706S000178_at	3.6471508
RCC00282	aldehyde dehydrogenase family protein	Rc_chrom0706S000289_at	3.6394536
RCC01383	UDP-glucose 6-dehydrogenase	Rc_chrom0706S001421_at	3.6344576
RCC01153	imidazole glycerol phosphate synthase, subunit HisF	Rc_chrom0706S001187_at	3.6172965
RCC01236	transcriptional regulator, GntR family	Rc_chrom0706S001272_at	3.6167417
RCC02754	glutamyl-tRNA(Gln) amidotransferase, C subunit	Rc_chrom0706S002841_at	3.6129997
RCC02114	arginase	Rc_chrom0706S002178_at	3.5968857
RCC00768	hydrogenase, large subunit	Rc_chrom0706S000793_at	3.5854223
RCC00873	transcriptional regulator, XRE family	Rc_chrom0706S000904_at	3.5758812
RCC02116	iron siderophore/cobalamin ABC transporter, ATP-binding protein	Rc_chrom0706S002180_at	3.5691743
RCC01849	protein of unknown function DUF1457	Rc_chrom0706S001910_at	3.5626307
RCC01958	tyrosine-protein kinase Wzc	Rc_chrom0706S002022_at	3.5518140
	intergenic region	Rc_chrom0706S004226_at	3.5255730
RCC02700	lipoprotein, putative	Rc_chrom0706S002791_at	3.5228240
RCC03153	phenylalanyl-tRNA synthetase, alpha subunit	Rc_chrom0706S003245_at	3.5043500
RCC02537	cysteine synthase	Rc_chrom0706S002624_at	3.4850283

Annotation	Predicted function [a]	Probe spot [b]	Fold change [c]
RCC02187	amidohydrolase family protein	Rc_chrom0706S002258_at	3.4825826
RCC02785	conserved hypothetical protein	Rc_chrom0706S002874_at	3.4804146
RCC00526	dimethylglycine dehydrogenase	Rc_chrom0706S000539_at	3.4702742
RCC03491	nucleoside-triphosphatase	Rc_chrom0706S003588_at	3.4603372
RCC03179	acetoacetyl-CoA reductase	Rc_chrom0706S003272_at	3.4535983
	intergenic region	Rc_chrom0706S004388_at	3.4501321
RCC02437	cytochrome P450 family protein	Rc_chrom0706S002514_at	3.4350717
RCC02343	phage conserved hypothetical protein	Rc_chrom0706S002416_at	3.4289236
RCC00077	2,3-bisphosphoglycerate-independent phosphoglycerate mutase	Rc_chrom0706S000079_at	3.4287060
RCC00288	50S ribosomal protein L1	Rc_chrom0706S000296_at	3.4220579
RCC01301	CRISPR-associated protein, Cas5 family, Dvulg subtype	Rc_chrom0706S001335_at	3.4194396
RCC01011	peptidase, S24 family	Rc_chrom0706S001040_at	3.4123447
RCC00624	amino acid ABC transporter, periplasmic amino acid-binding protein	Rc_chrom0706S000642_at	3.3755736
RCC00323	adenylate kinase	Rc_chrom0706S000331_at	3.3668513
RCP00114	plasmid partitioning protein RepA	Rc_plasm0706S005001_at	3.3556616
	intergenic region	Rc_chrom0706S004639_at	3.3495185
	intergenic region	Rc_chrom0706S003738_at	3.3486729
RCC02845	trimethylamine-N-oxide reductase	Rc_chrom0706S002937_at	3.3457742
RCC00438	serine hydroxymethyltransferase	Rc_chrom0706S000449_at	3.3284354
	intergenic region	Rc_chrom0706S003734_at	3.3271960
	intergenic region	Rc_chrom0706S004050_at	3.3089855
RCC00294	30S ribosomal protein S12	Rc_chrom0706S000302_at	3.3072930

Annotation	Predicted function [a]	Probe spot [b]	Fold change [c]
RCC03151	phenylalanyl-tRNA synthetase, beta subunit	Rc_chrom0706S003243_at	3.3065803
	intergenic region	Rc_chrom0706S003968_at	3.2989780
RCC00850	dipeptide ABC transporter, ATP-binding protein DppF	Rc_chrom0706S000879_at	3.2981408
	intergenic region	Rc_chrom0706S004095_at	3.2977352
RCC02405	formyltetrahydrofolate deformylase	Rc_chrom0706S002481_at	3.2808840
RCC00426	conserved hypothetical protein	Rc_chrom0706S000436_at	3.2775630
RCP00046	iron siderophore/cobalamin ABC transporter, periplasmic iron siderophore/cobalamin-binding protein	Rc_plasm0706S004928_at	3.2606082
RCC02186	spermidine/putrescine ABC transporter, periplasmic spermidine/putrescine-binding protein PotF	Rc_chrom0706S002257_at	3.2522023
RCC01241	lipoyltransferase	Rc_chrom0706S001278_at	3.2507343
RCC02476	inorganic pyrophosphatase	Rc_chrom0706S002558_at	3.2489340
RCC03044	lactoylglutathione lyase	Rc_chrom0706S003134_at	3.2303329
RCC00283	conserved hypothetical protein	Rc_chrom0706S000290_at	3.2156494
RCC03108	protein of unknown function DUF305	Rc_chrom0706S003199_at	3.2129190
RCC03095	peptidase, M16 family	Rc_chrom0706S003186_at	3.2029840
RCC00147	translation elongation factor Tu	Rc_chrom0706S000151_at	3.1694200
RCC00369	acetyltransferase, GNAT family	Rc_chrom0706S000377_at	3.1608293
RCC00287	50S ribosomal protein L11	Rc_chrom0706S000295_at	3.1596510
RCC00635	von Willebrand factor type A domain protein	Rc_chrom0706S000653_at	3.1502578
RCC00295	30S ribosomal protein S7	Rc_chrom0706S000303_at	3.1490855

Annotation	Predicted function [a]	Probe spot [b]	Fold change [c]
RCC03096	threonine synthase	Rc_chrom0706S003187_at	3.1348107
RCC00284	polyribonucleotide nucleotidyltransferase	Rc_chrom0706S000291_at	3.1332881
RCC03327	outer membrane lipoprotein carrier protein LolA	Rc_chrom0706S003423_at	3.1144657
RCC00642	peptidoglycan binding domain protein	Rc_chrom0706S000660_at	3.1059766
RCC02973	ATP synthase F1, alpha subunit	Rc_chrom0706S003067_at	3.0998335
RCC00594	ATPase, MoxR family protein	Rc_chrom0706S000611_at	3.0861206
RCC01172	uroporphyrinogen decarboxylase	Rc_chrom0706S001208_at	3.0782948
	intergenic region	Rc_chrom0706S004866_at	3.0691059
control		AFFX-r2-Bs-phe-M_at	3.0417957
RCC00833	acetate kinase	Rc_chrom0706S000861_at	3.0393476
RCC00324	30S ribosomal protein S13	Rc_chrom0706S000332_at	3.0375218
RCC03315	pyridoxine 5'-phosphate synthase	Rc_chrom0706S003411_at	3.0295790
RCC00643	diguanylate cyclase/phosphodiesterase with PAS/PAC sensor	Rc_chrom0706S000661_at	3.0269845
RCC00813	hypothetical protein	Rc_chrom0706S000840_at	3.0262964
RCC02765	branched-chain-amino-acid transaminase	Rc_chrom0706S002853_at	3.0166771
RCC01303	CRISPR-associated protein, Cas2 family	Rc_chrom0706S001337_at	3.0150225
RCC03178	acetyl-CoA acetyltransferase	Rc_chrom0706S003271_at	3.0101435
RCC01543	acetolactate synthase, large subunit	Rc_chrom0706S001587_at	3.0046725
RCC00769	hydrogenase, cytochrome b subunit	Rc_chrom0706S000794_at	2.9981570
RCC01959	protein-tyrosine-phosphatase Wzb	Rc_chrom0706S002023_at	2.9860997
RCC02354	peptidyl-prolyl cis-trans isomerase D	Rc_chrom0706S002427_at	2.9845583

Annotation	Predicted function [a]	Probe spot [b]	Fold change [c]
RCC02185	spermidine/putrescine ABC transporter, permease protein PotI	Rc_chrom0706S002256_at	2.9829273
RCC00308	50S ribosomal protein L29	Rc_chrom0706S000316_at	2.9772970
RCC02502	prephenate dehydratase	Rc_chrom0706S002585_at	2.9767344
RCC00002	DNA polymerase III, beta subunit	Rc_chrom0706S000002_at	2.9760613
RCC01615	methylenetetrahydrofolate reductase family protein	Rc_chrom0706S001666_at	2.9496486
RCC00421	aspartate kinase	Rc_chrom0706S000431_at	2.9494574
RCP00074	nitrous oxide maturation protein NosD	Rc_plasm0706S004957_at	2.9329120
RCC01817	3-hydroxybutyrate dehydrogenase	Rc_chrom0706S001877_at	2.9327028
RCC02152	TM2 domain protein	Rc_chrom0706S002221_at	2.9257572
	intergenic region	Rc_chrom0706S003944_at	2.9215074
RCC01707	fructose-bisphosphate aldolase	Rc_chrom0706S001759_at	2.9195360
RCC00716	pyridine nucleotide transhydrogenase, beta subunit	Rc_chrom0706S000735_at	2.9103007
RCC01851	transcriptional regulator, AraC family	Rc_chrom0706S001912_at	2.9066324
RCC00737	hypothetical protein	Rc_chrom0706S000759_at	2.9058764
RCC02753	glutamyl-tRNA(Gln) amidotransferase, A subunit	Rc_chrom0706S002840_at	2.8988783
RCC02214	acetate kinase	Rc_chrom0706S002286_at	2.8898802
RCC02157	adenylosuccinate lyase	Rc_chrom0706S002226_at	2.8855736
RCC00322	preprotein translocase, SecY subunit	Rc_chrom0706S000330_at	2.8752956
RCP00147	polyols ABC transporter, periplasmic polyols-binding protein	Rc_plasm0706S005034_at	2.8688102
RCC01894	spermidine/putrescine ABC transporter, permease protein PotI	Rc_chrom0706S001955_at	2.8679798

Annotation	Predicted function [a]	Probe spot [b]	Fold change [c]
RCC00368	hydroxyphenylpyruvate synthase	Rc_chrom0706S000376_at	2.8620405
RCC01027	conserved hypothetical protein	Rc_chrom0706S001054_at	2.8611324
RCC00446	phosphopentomutase	Rc_chrom0706S000459_at	2.8590130
RCC00832	phosphate acetyltransferase	Rc_chrom0706S000860_at	2.8586900
RCC01288	hypothetical protein	Rc_chrom0706S001323_at	2.8576810
RCC03031	PspA/IM30 family protein	Rc_chrom0706S003122_at	2.8569934
RCC01291	kinetochore Spc7 domain protein	Rc_chrom0706S001326_at	2.8531320
RCC00045	photosynthetic apparatus regulatory protein RegA	Rc_chrom0706S000045_at	2.8466008
RCC02050	cob(I)yrinic acid a,c-diamide adenosyltransferase	Rc_chrom0706S002116_at	2.8443830
RCC00881	metallophosphoesterase family protein	Rc_chrom0706S000912_at	2.8368533
	unannotated	Rc_chrom0706S001320_at	2.8368420
RCC03235	monosacharide ABC transporter, permease protein	Rc_chrom0706S003329_at	2.8359270
RCC03171	diaminopimelate decarboxylase	Rc_chrom0706S003264_at	2.8354960
RCC00370	signal recognition particle protein	Rc_chrom0706S000378_at	2.8281653
RCC01895	spermidine/putrescine ABC transporter, permease protein PotH	Rc_chrom0706S001956_at	2.8246007
RCC00219	PpiC-type peptidyl-prolyl cis-trans isomerase	Rc_chrom0706S000224_at	2.8206970
RCC01328	conserved hypothetical protein	Rc_chrom0706S001365_at	2.8195338
RCC02296	GTP-binding protein Obg/CgtA	Rc_chrom0706S002369_at	2.8155482
RCC00465	extracellular ligand-binding receptor family protein	Rc_chrom0706S000478_at	2.8121330
RCC03500	phosphate ABC transporter, ATP-binding protein	Rc_chrom0706S003597_at	2.8103230

Annotation	Predicted function [a]	Probe spot [b]	Fold change [c]
RCC00726	dihydrolipoyl dehydrogenase	Rc_chrom0706S000747_at	2.8080428
	intergenic region	Rc_chrom0706S004274_at	2.8013396
RCC00144	electron transfer flavoprotein, beta subunit	Rc_chrom0706S000148_at	2.7920082
RCC01173	hydroxymethylbilane synthase	Rc_chrom0706S001209_at	2.7825840
RCC00297	translation elongation factor Tu	Rc_chrom0706S000305_s_at	2.7801275
RCC00298	30S ribosomal protein S10	Rc_chrom0706S000306_at	2.7757351
control		AFFX-r2-Bs-thr-5_s_at	2.7653108
RCC00512	TPR repeat domain protein	Rc_chrom0706S000524_at	2.7628640
RCC00608	conserved hypothetical protein	Rc_chrom0706S000626_at	2.7622833
RCC01183	imidazoleglycerol-phosphate dehydratase	Rc_chrom0706S001219_at	2.7561867
RCC00293	conserved hypothetical protein	Rc_chrom0706S000301_at	2.7552314
	intergenic region	Rc_chrom0706S003900_at	2.7536410
RCC01184	CsbD family protein	Rc_chrom0706S001220_at	2.7533450
	intergenic region	Rc_chrom0706S003879_at	2.7532742
	intergenic region	Rc_chrom0706S004211_at	2.7469242
	intergenic region	Rc_chrom0706S003732_at	2.7442780
RCC00004	DNA gyrase, B subunit	Rc_chrom0706S000004_at	2.7418447
RCC01869	invasion associated locus B family protein	Rc_chrom0706S001930_at	2.7333212
RCC01423	conserved hypothetical protein	Rc_chrom0706S001460_at	2.7324939
control		AFFX-ThrX-3_at	2.7187142
RCC01363	2-isopropylmalate synthase	Rc_chrom0706S001399_at	2.7116282

Annotation	Predicted function [a]	Probe spot [b]	Fold change [c]
RCC02676	TPR repeat domain protein	Rc_chrom0706S002766_at	2.7074585
RCC01852	branched-chain amino acid ABC transporter, periplasmic branched-chain amino acid-binding protein LivK	Rc_chrom0706S001913_at	2.7021446
RCC01752	alanyl-tRNA synthetase	Rc_chrom0706S001809_at	2.6976435
control		AFFX-r2-Bs-phe-5_at	2.6934402
RCC00846	dipeptide ABC transporter, periplasmic dipeptide-binding protein DppA	Rc_chrom0706S000875_at	2.6911250
RCC00297	translation elongation factor Tu	Rc_chrom0706S000305_at	2.6874697
RCC00296	translation elongation factor G	Rc_chrom0706S000304_at	2.6834223
RCC01705	pyruvate dehydrogenase complex, E1 component, pyruvate dehydrogenase (acetyl-transferring), alpha subunit	Rc_chrom0706S001757_at	2.6797814
	intergenic region	Rc_chrom0706S004345_at	2.6797610
RCC01142	aminomethyltransferase	Rc_chrom0706S001176_at	2.6795830
RCC00708	oligopeptide ABC transporter, ATP-binding protein OppD	Rc_chrom0706S000727_at	2.6758447
RCC02959	spermidine/putrescine ABC transporter, periplasmic spermidine/putrescine-binding protein	Rc_chrom0706S003053_at	2.6744654
RCC00551	glutamate racemase	Rc_chrom0706S000565_at	2.6739137
RCC02778	glutamine amidotransferase, class I	Rc_chrom0706S002867_at	2.6732845
RCC01488	phosphoribosylformylglycinamidine cyclo-ligase	Rc_chrom0706S001531_at	2.6690009
RCP00070	NosX protein	Rc_plasm0706S004953_at	2.6647840
RCC00176	dTDP-glucose 4,6-dehydratase	Rc_chrom0706S000181_at	2.6612860
RCC01632	outer membrane protein assembly factor YaeT	Rc_chrom0706S001684_at	2.6607234

Annotation	Predicted function [a]	Probe spot [b]	Fold change [c]
RCC03234	monosaccharide ABC transporter, permease protein	Rc_chrom0706S003328_at	2.6588228
RCC00147	translation elongation factor Tu	Rc_chrom0706S000151_s_at	2.6565459
RCC02472	glutathione peroxidase	Rc_chrom0706S002553_at	2.6536220
RCC00854	arginyl-tRNA synthetase	Rc_chrom0706S000883_at	2.6534605
RCC02821	phosphoribosylaminoimidazole carboxylase, ATPase subunit	Rc_chrom0706S002913_at	2.6529202
RCC00740	ATP synthase F0, I subunit	Rc_chrom0706S000762_at	2.6505117
RCC02893	cold shock protein CspA	Rc_chrom0706S002989_at	2.6484504
RCC00847	dipeptide ABC transporter, permease protein DppB	Rc_chrom0706S000876_at	2.6456210
RCC03314	membrane protein, putative	Rc_chrom0706S003410_at	2.6381430
RCC02358	anthranilate phosphoribosyltransferase	Rc_chrom0706S002431_at	2.6361175
RCC02464	prolyl-tRNA synthetase	Rc_chrom0706S002545_at	2.6356783
RCC02078	membrane protein, putative	Rc_chrom0706S002146_at	2.6323073
	intergenic region	Rc_chrom0706S004277_at	2.6313748
RCC00335	glutamate/aspartate ABC transporter, periplasmic glutamate/aspartate-binding protein BztA	Rc_chrom0706S000343_at	2.6168370
RCC02022	polyols ABC transporter, periplasmic polyols-binding protein	Rc_chrom0706S002087_at	2.6164790
	intergenic region	Rc_chrom0706S004024_at	2.6103150
RCC00530	conserved hypothetical protein	Rc_chrom0706S000543_at	2.6067490
RCC01049	TonB-dependent siderophore receptor	Rc_chrom0706S001077_at	2.5992985
RCC03233	monosaccharide ABC transporter, ATP-binding protein	Rc_chrom0706S003327_at	2.5950992

Annotation	Predicted function [a]	Probe spot [b]	Fold change [c]
RCC00049	adenosylhomocysteinase	Rc_chrom0706S000050_at	2.5914478
RCC00911	propionyl-CoA carboxylase, alpha subunit	Rc_chrom0706S000943_at	2.5898380
RCC01816	extracellular solute-binding protein, family 5	Rc_chrom0706S001876_at	2.5867686
RCP00073	copper ABC transporter, ATP-binding protein NosF	Rc_plasm0706S004956_at	2.5822206
RCC03239	transcriptional regulator, AsnC/Lrp family	Rc_chrom0706S003333_at	2.5813196
RCC00514	transcription elongation factor GreA	Rc_chrom0706S000526_at	2.5682855
RCC01339	hypothetical protein	Rc_chrom0706S001376_at	2.5613450
RCC00887	protein of unknown function DUF214, permease predicted	Rc_chrom0706S000918_at	2.5605080
RCC03157	pyruvate kinase	Rc_chrom0706S003249_at	2.5602170
RCC00553	N-acetyl-gamma-glutamyl-phosphate reductase	Rc_chrom0706S000567_at	2.5555806
	intergenic region	Rc_chrom0706S004276_at	2.5538816
RCC00851	membrane dipeptidase	Rc_chrom0706S000880_at	2.5536723
RCC03214	protein of unknown function DUF1127	Rc_chrom0706S003308_at	2.5510840
	intergenic region	Rc_chrom0706S004583_at	2.5486846
RCC02677	aspartate aminotransferase	Rc_chrom0706S002767_at	2.5477564
	intergenic region	Rc_chrom0706S003782_at	2.5459190
RCC00281	30S ribosomal protein S15	Rc_chrom0706S000288_at	2.5440094
RCC01549	protein of unknown function DUF583	Rc_chrom0706S001594_at	2.5415268
RCC02553	protein of unknown function DUF1486	Rc_chrom0706S002642_at	2.5375720
RCC01836	NADPH:quinone reductase	Rc_chrom0706S001896_at	2.5354020

Annotation	Predicted function [a]	Probe spot [b]	Fold change [c]
RCC01269	conserved domain protein	Rc_chrom0706S001304_at	2.5325980
RCC01554	major facilitator superfamily MFS_1	Rc_chrom0706S001599_at	2.5222363
RCC02058	nicotinate-nucleotide--dimethylbenzimidazole phosphoribosyltransferase	Rc_chrom0706S002124_at	2.5214195
control		AFFX-r2-Bs-thr-3_s_at	2.5212893
RCC00473	transcriptional regulator, MerR family	Rc_chrom0706S000486_at	2.5207262
RCC00718	malate dehydrogenase	Rc_chrom0706S000737_at	2.5201697
RCC02789	glutathione-regulated potassium-efflux system protein KefC	Rc_chrom0706S002879_at	2.5121925
RCP00003	polar amino acid ABC transporter, periplasmic polar amino acid-binding protein	Rc_plasm0706S004887_at	2.5116910
	intergenic region	Rc_chrom0706S003774_at	2.5102620
	intergenic region	Rc_chrom0706S004312_at	2.5080552
	intergenic region	Rc_chrom0706S004412_at	2.5063605
RCP00044	iron siderophore/cobalamin ABC transporter, ATP-binding protein	Rc_plasm0706S004926_at	2.4989953
control		AFFX-r2-Bs-thr-M_s_at	2.4963372
	intergenic region	Rc_chrom0706S003933_at	2.4961689
RCC02652	RbsD/FucU transport protein family	Rc_chrom0706S002741_at	2.4928808
RCC03232	basic membrane lipoprotein family	Rc_chrom0706S003326_at	2.4882972
RCC02306	LysM domain protein	Rc_chrom0706S002379_at	2.4871528
RCC02201	aldehyde-alcohol dehydrogenase	Rc_chrom0706S002273_at	2.4846582
RCC02711	aspartate-semialdehyde dehydrogenase	Rc_chrom0706S002803_at	2.4846418
	intergenic region	Rc_chrom0706S003901_at	2.4765036

Annotation	Predicted function [a]	Probe spot [b]	Fold change [c]
RCC03236	purine-nucleoside phosphorylase	Rc_chrom0706S003330_at	2.4759192
RCC01147	chaperone CsaA	Rc_chrom0706S001181_at	2.4677691
RCC01324	type I restriction-modification system RcaSBIIIP, R subunit	Rc_chrom0706S001361_at	2.4623518
RCC00143	electron transfer flavoprotein, alpha subunit	Rc_chrom0706S000147_at	2.4576726
RCC01544	tripartite ATP-independent periplasmic transporter, DctQ component	Rc_chrom0706S001588_at	2.4536047
RCC00618	ABC transporter, ATP-binding/permease protein	Rc_chrom0706S000636_at	2.4498900
RCC02184	spermidine/putrescine ABC transporter, permease protein PotH	Rc_chrom0706S002255_at	2.4482355
RCC00044	electron transport protein SenC	Rc_chrom0706S000044_at	2.4479604
control		AFFX-ThrX-M_at	2.4471903
RCC00531	carbamoyl-phosphate synthase, large subunit	Rc_chrom0706S000544_at	2.4450138
RCC00637	conserved hypothetical protein	Rc_chrom0706S000655_at	2.4442155
RCC03342	anaerobic ribonucleoside-triphosphate reductase	Rc_chrom0706S003438_at	2.4432560
RCC02312	conserved hypothetical protein	Rc_chrom0706S002385_at	2.4259424
RCC03408	N-formylglutamate amidohydrolase	Rc_chrom0706S003504_at	2.4234390
RCC01466	glutamate synthase domain protein	Rc_chrom0706S001508_at	2.4176340
RCC01494	methionine gamma-lyase	Rc_chrom0706S001537_at	2.4152420
RCC01711	tyrosyl-tRNA synthetase	Rc_chrom0706S001763_at	2.4137344
RCC01616	conserved hypothetical protein	Rc_chrom0706S001667_at	2.4103827
RCC02060	hemolysin-type calcium-binding repeat family protein	Rc_chrom0706S002126_at	2.4097233

Annotation	Predicted function [a]	Probe spot [b]	Fold change [c]
RCP00043	pseudoazurin	Rc_plasm0706S004925_at	2.4092016
RCC03499	phosphate transport system regulatory protein PhoU	Rc_chrom0706S003596_at	2.4061022
RCC00611	nickel-responsive regulator NikR	Rc_chrom0706S000629_at	2.4041069
RCC00697	conserved hypothetical protein	Rc_chrom0706S000716_at	2.4029598
RCC01724	agmatinase	Rc_chrom0706S001777_at	2.3974843
RCC00129	transcriptional regulator, LacI family	Rc_chrom0706S000132_at	2.3915439
RCC01240	cytochrome c2	Rc_chrom0706S001277_at	2.3895369
RCC02646	protein of unknown function DUF461	Rc_chrom0706S002735_at	2.3894453
RCC01490	ribonuclease D	Rc_chrom0706S001533_at	2.3834033
RCC02618	protein of unknown function DUF952	Rc_chrom0706S002707_at	2.3802884
RCC00169	capsule polysaccharide export protein	Rc_chrom0706S000174_at	2.3774004
RCC00257	leucyl-tRNA synthetase	Rc_chrom0706S000263_at	2.3716695
	intergenic region	Rc_chrom0706S003737_at	2.3707402
RCC02294	signal transduction histidine kinase	Rc_chrom0706S002367_at	2.3681417
RCC02860	protein of unknown function DUF485, transmembrane	Rc_chrom0706S002955_s_at	2.3624425
	intergenic region	Rc_chrom0706S003928_at	2.3603992
	intergenic region	Rc_chrom0706S004049_at	2.3591325
RCC00448	sporulation domain protein	Rc_chrom0706S000461_at	2.3585680
RCC00159	hypothetical protein	Rc_chrom0706S000163_at	2.3546672
RCC01915	inosine-5'-monophosphate dehydrogenase	Rc_chrom0706S001978_at	2.3532700
RCC03498	phosphate regulon transcriptional regulatory protein PhoB	Rc_chrom0706S003595_at	2.3532670

Annotation	Predicted function [a]	Probe spot [b]	Fold change [c]
RCC01028	iron siderophore/cobalamin ABC transporter, periplasmic iron siderophore/cobalamin-binding protein	Rc_chrom0706S001055_at	2.3526914
RCC01402	ABC transporter, substrate-binding protein	Rc_chrom0706S001441_at	2.3522280
RCC00389	conserved hypothetical protein	Rc_chrom0706S000398_at	2.3484495
RCC02518	methyltransferase, type 12 family	Rc_chrom0706S002603_at	2.3477013
RCC01481	UDP-N-acetylmuramoyl-L-alanyl-D-glutamate--2,6-diaminopimelate ligase	Rc_chrom0706S001524_at	2.3470092
RCC02385	protein of unknown function DUF1127	Rc_chrom0706S002460_at	2.3464136
RCC00617	secretion protein, HlyD family	Rc_chrom0706S000635_at	2.3443856
RCC01511	protein of unknown function DUF1311	Rc_chrom0706S001555_at	2.3387175
RCC00305	30S ribosomal protein S3	Rc_chrom0706S000313_at	2.3385720
RCP00004	polar amino acid ABC transporter, ATP-binding protein	Rc_plasm0706S004888_at	2.3366745
control		AFFX-ThrX-5_at	2.3334115
RCC00840	aminopeptidase N	Rc_chrom0706S000869_at	2.3311512
RCC01302	CRISPR-associated protein, Csd1 family	Rc_chrom0706S001336_at	2.3279974
RCC02722	conserved hypothetical protein	Rc_chrom0706S002811_at	2.3234744
RCC02200	conserved hypothetical protein	Rc_chrom0706S002272_at	2.3198488
	intergenic region	Rc_chrom0706S003888_at	2.3186383
RCC01238	carbamoyl-phosphate synthase (glutamine-hydrolyzing), small subunit	Rc_chrom0706S001275_at	2.3143966
RCC01137	6-phosphofructokinase	Rc_chrom0706S001171_at	2.3107033
RCC00299	50S ribosomal protein L3	Rc_chrom0706S000307_at	2.3041720
RCC01124	nitroreductase/dihydropteridine reductase	Rc_chrom0706S001158_at	2.2991815

Annotation	Predicted function [a]	Probe spot [b]	Fold change [c]
	intergenic region	Rc_chrom0706S003727_at	2.2907891
RCC03435	molybdopterin binding domain protein	Rc_chrom0706S003531_at	2.2873027
RCC01126	integration host factor, beta subunit	Rc_chrom0706S001160_at	2.2829750
RCC03492	ribonuclease PH	Rc_chrom0706S003589_at	2.2793214
RCC02439	conserved hypothetical protein	Rc_chrom0706S002516_at	2.2781765
RCC01949	undecaprenyl-phosphate galactosephosphotransferase	Rc_chrom0706S002012_at	2.2770157
RCC03162	mandelate racemase/muconate lactonizing enzyme family protein	Rc_chrom0706S003254_at	2.2749440
RCC01626	ribosome recycling factor	Rc_chrom0706S001678_at	2.2742643
	intergenic region	Rc_chrom0706S004867_at	2.2673385
RCC01243	polyamine ABC transporter, ATP binding protein PotA	Rc_chrom0706S001280_at	2.2651107
RCC00362	50S ribosomal protein L19	Rc_chrom0706S000370_at	2.2644012
RCC01710	peptidyl-prolyl cis-trans isomerase B	Rc_chrom0706S001762_at	2.2603319
RCC00707	oligopeptide ABC transporter, ATP-binding protein OppF	Rc_chrom0706S000726_at	2.2601855
	intergenic region	Rc_chrom0706S004176_at	2.2579396
RCC02181	transcriptional regulator, GntR family	Rc_chrom0706S002252_at	2.2525458
RCC02357	anthranilate synthase component II	Rc_chrom0706S002430_at	2.2523105
	intergenic region	Rc_chrom0706S004728_at	2.2512717
RCC00770	hydrogenase maturation protease HupD	Rc_chrom0706S000795_at	2.2511325
RCC02206	propanediol utilization protein PduL	Rc_chrom0706S002278_at	2.2505991
RCC02468	thioesterase superfamily protein	Rc_chrom0706S002549_at	2.2384770
RCC00167	glycosyl transferase, family 2/group 1	Rc_chrom0706S000172_at	2.2326370

Annotation	Predicted function [a]	Probe spot [b]	Fold change [c]
RCC00549	phosphoribosylformylglycinamidine synthase II	Rc_chrom0706S000563_at	2.2320495
RCC01844	sensor histidine kinase	Rc_chrom0706S001905_at	2.2313445
RCC00300	50S ribosomal protein L4	Rc_chrom0706S000308_at	2.2292657
RCC03207	conserved hypothetical protein	Rc_chrom0706S003300_at	2.2281106
RCC00742	ATP synthase F0, C subunit	Rc_chrom0706S000764_at	2.2278500
RCC03142	RNA modification enzyme, MiaB family	Rc_chrom0706S003234_at	2.2264264
RCC00304	50S ribosomal protein L22	Rc_chrom0706S000312_at	2.2251742
RCC02550	translation initiation factor IF-1	Rc_chrom0706S002639_at	2.2246697
RCP00084	transcriptional regulator, ArsR family	Rc_plasm0706S004968_at	2.2217540
RCC00897	betaine-aldehyde dehydrogenase	Rc_chrom0706S000928_at	2.2213926
RCC00895	glycine betaine/L-proline ABC transporter, periplasmic glycine betaine/L-proline-binding protein ProX	Rc_chrom0706S000926_at	2.2187393
RCC03061	homoserine dehydrogenase	Rc_chrom0706S003152_at	2.2184432
	intergenic region	Rc_chrom0706S004070_at	2.2182488
RCC02384	Mrp/NBP35 family protein	Rc_chrom0706S002458_at	2.2181910
	intergenic region	Rc_chrom0706S004595_at	2.2177951
RCC01935	mannose-1-phosphate guanylyltransferase/mannose-6-phosphate isomerase	Rc_chrom0706S001997_at	2.2166576
RCC01205	glycyl-tRNA synthetase, alpha subunit	Rc_chrom0706S001241_at	2.2161918
RCC02117	methyl-accepting chemotaxis protein	Rc_chrom0706S002181_at	2.2149880
	unannotated	Rc_chrom0706S001774_at	2.2089095
	intergenic region	Rc_chrom0706S003880_at	2.2082045
RCC03357	conserved hypothetical protein	Rc_chrom0706S003454_at	2.2076848

Annotation	Predicted function [a]	Probe spot [b]	Fold change [c]
	intergenic region	Rc_chrom0706S004027_at	2.2074332
RCC02183	spermidine/putrescine ABC transporter, ATP-binding protein PotG	Rc_chrom0706S002254_at	2.2072735
RCC02350	enoyl-[acyl-carrier-protein] reductase (NADH)	Rc_chrom0706S002423_at	2.2069350
RCC00597	conserved hypothetical protein	Rc_chrom0706S000614_at	2.2052490
RCC02604	leucyl/phenylalanyl-tRNA--protein transferase	Rc_chrom0706S002693_at	2.2052193
RCC02587	conserved hypothetical protein	Rc_chrom0706S002675_at	2.2046077
RCC02268	spermidine/putrescine ABC transporter, periplasmic spermidine/putrescine-binding protein PotD	Rc_chrom0706S002341_at	2.2043774
	intergenic region	Rc_chrom0706S004375_at	2.2038107
RCC02213	membrane protein, putative	Rc_chrom0706S002285_at	2.1953325
RCC01570	colicin V production protein	Rc_chrom0706S001615_at	2.1948566
RCC01781	preprotein translocase, YajC subunit	Rc_chrom0706S001840_at	2.1936700
RCC02473	TonB-dependent receptor plug domain protein	Rc_chrom0706S002554_at	2.1924320
RCC02219	molybdate ABC transporter, periplasmic molybdate-binding protein ModA	Rc_chrom0706S002291_at	2.1869433
RCC00361	50S ribosomal protein L31	Rc_chrom0706S000369_at	2.1841116
RCC03101	succinyl-CoA:3-ketoacid-CoA transferase, subunit A	Rc_chrom0706S003192_at	2.1797585
RCC01596	uroporphyrinogen-III C-methyltransferase	Rc_chrom0706S001643_at	2.1771147
RCC00633	ABC transporter, permease protein	Rc_chrom0706S000651_at	2.1771033

Annotation	Predicted function [a]	Probe spot [b]	Fold change [c]
RCC01214	ketol-acid reductoisomerase	Rc_chrom0706S001250_at	2.1770630
RCC03123	GTP-binding protein LepA	Rc_chrom0706S003213_at	2.1767724
RCC02561	UDP-N-acetylglucosamine 1-carboxyvinyltransferase	Rc_chrom0706S002651_at	2.1748219
control		AFFX-DapX-3_at	2.1745043
RCC03490	endoribonuclease, L-PSP family	Rc_chrom0706S003587_at	2.1733532
RCC01540	metallo-beta-lactamase family protein	Rc_chrom0706S001584_at	2.1730860
	intergenic region	Rc_chrom0706S003715_at	2.1723600
RCC01569	amidophosphoribosyltransferase	Rc_chrom0706S001614_at	2.1720865
RCC02079	DNA topoisomerase IV, B subunit	Rc_chrom0706S002147_at	2.1719140
	intergenic region	Rc_chrom0706S003990_at	2.1713943
RCC01500	glutamine--fructose-6-phosphate transaminase (isomerizing)	Rc_chrom0706S001543_at	2.1703699
RCC00413	Succinate-semialdehyde dehydrogenase (NAD(P)(+))	Rc_chrom0706S000423_at	2.1669350
RCC02269	spermidine/putrescine ABC transporter, ATP-binding protein PotA	Rc_chrom0706S002342_at	2.1663048
RCC03127	protein-tyrosine-phosphatase	Rc_chrom0706S003217_at	2.1645070
control		AFFX-r2-Bs-dap-3_at	2.1641965
RCC01714	protein of unknown function DUF985	Rc_chrom0706S001766_at	2.1601617
RCC00532	aspartyl-tRNA synthetase	Rc_chrom0706S000545_at	2.1589198
RCC01776	trimethylamine methyltransferase family protein	Rc_chrom0706S001834_at	2.1579952
RCC02289	two-component response regulator receiver protein	Rc_chrom0706S002362_at	2.1558080
RCC01850	3-deoxy-7-phosphoheptulonate synthase	Rc_chrom0706S001911_at	2.1531162

Annotation	Predicted function [a]	Probe spot [b]	Fold change [c]
RCC00710	hippurate hydrolase	Rc_chrom0706S000729_at	2.1526410
RCC03226	Polysaccharide biosynthesis/export protein family	Rc_chrom0706S003320_at	2.1521714
RCC00741	ATP synthase F0, A subunit	Rc_chrom0706S000763_at	2.1502602
RCC01116	PhoH family protein	Rc_chrom0706S001149_at	2.1469991
RCC02824	oxidoreductase, DSBA family	Rc_chrom0706S002916_at	2.1440833
RCC01286	McrBC restriction endonuclease system, McrB subunit	Rc_chrom0706S001321_at	2.1439500
RCC00122	conserved hypothetical protein	Rc_chrom0706S000124_at	2.1415646
RCC00194	ErfK/YbiS/YcfS/YnhG family protein/Tat domain protein	Rc_chrom0706S000199_at	2.1413722
RCC00638	virulence protein SrfB	Rc_chrom0706S000656_at	2.1410480
RCC02481	conserved hypothetical protein	Rc_chrom0706S002563_at	2.1400335
RCC03501	phosphate ABC transporter, permease protein PstA	Rc_chrom0706S003598_at	2.1395907
RCC03381	3-mercaptopyruvate sulfurtransferase	Rc_chrom0706S003477_at	2.1384144
RCC03295	conserved hypothetical protein	Rc_chrom0706S003390_at	2.1380978
RCC00240	conserved hypothetical protein	Rc_chrom0706S000246_at	2.1375508
RCC00744	ATP synthase F0, B subunit	Rc_chrom0706S000766_at	2.1343430
	intergenic region	Rc_chrom0706S004026_at	2.1334937
RCC00328	autoinducer-binding transcriptional regulator, LuxR family	Rc_chrom0706S000336_at	2.1317300
RCC03109	serine--glyoxylate aminotransferase/alanine--glyoxylate aminotransferase/serine--pyruvate aminotransferase	Rc_chrom0706S003200_at	2.1316075
RCC00955	SMC protein, N-terminal domain	Rc_chrom0706S000986_at	2.1291487

Annotation	Predicted function [a]	Probe spot [b]	Fold change [c]
RCC00774	rubredoxin HupJ	Rc_chrom0706S000799_at	2.1281617
RCC02685	glutathione S-transferase family protein	Rc_chrom0706S002776_at	2.1277628
RCC02483	glycosyl transferase, family 14	Rc_chrom0706S002565_at	2.1276827
RCC02627	penicillin-binding protein 4	Rc_chrom0706S002716_at	2.1273227
RCC02394	L-serine ammonia-lyase	Rc_chrom0706S002469_at	2.1250234
RCC02657	monosacharide ABC transporter, periplasmic monosacharide-binding protein	Rc_chrom0706S002747_at	2.1210616
RCC00903	conserved hypothetical protein	Rc_chrom0706S000934_at	2.1151920
RCC01820	carbohydrate/purine kinase family protein	Rc_chrom0706S001880_at	2.1130586
RCC00325	30S ribosomal protein S11	Rc_chrom0706S000333_at	2.1119742
RCC00641	conserved hypothetical protein	Rc_chrom0706S000659_at	2.1058905
RCC02456	lipoprotein-releasing system transmembrane protein LolE	Rc_chrom0706S002534_at	2.1055120
	intergenic region	Rc_chrom0706S004661_at	2.1010823
	intergenic region	Rc_chrom0706S003915_at	2.1000820
RCC01581	conserved hypothetical protein	Rc_chrom0706S001626_at	2.0976990
RCC02882	antibiotic biosynthesis monooxygenase family protein	Rc_chrom0706S002978_at	2.0960965
RCC00345	inner membrane protein OxaA	Rc_chrom0706S000353_at	2.0960217
RCP00076	nitrous-oxide reductase expression regulator NosR	Rc_plasm0706S004959_at	2.0957127
	intergenic region	Rc_chrom0706S004640_at	2.0939603
RCC02612	transthyretin family protein	Rc_chrom0706S002701_at	2.0913908
RCC02202	protein of unknown function DUF336	Rc_chrom0706S002274_at	2.0891497

Annotation	Predicted function [a]	Probe spot [b]	Fold change [c]
RCC00841	glutamyl-tRNA(Gln) amidotransferase, B subunit	Rc_chrom0706S000870_at	2.0889342
RCC00052	conserved hypothetical protein	Rc_chrom0706S000053_at	2.0860074
	intergenic region	Rc_chrom0706S004790_at	2.0834138
RCC01271	conserved hypothetical protein	Rc_chrom0706S001306_at	2.0793126
RCC01769	beta-glucosidase A	Rc_chrom0706S001826_at	2.0790458
RCC03062	fructose-1,6-bisphosphatase	Rc_chrom0706S003153_at	2.0788260
RCC01314	protein of unknown function DUF262	Rc_chrom0706S001347_at	2.0787792
RCC01867	protein of unknown function DUF853, NPT hydrolase putative	Rc_chrom0706S001928_at	2.0787737
RCC02562	conserved hypothetical protein	Rc_chrom0706S002652_at	2.0779383
RCC02402	protease Do	Rc_chrom0706S002478_at	2.0762854
	intergenic region	Rc_chrom0706S004875_at	2.0751793
RCC00085	3-isopropylmalate dehydrogenase	Rc_chrom0706S000087_at	2.0748870
RCC03175	thiol:disulfide interchange protein DsbE	Rc_chrom0706S003268_at	2.0742056
RCC02955	cysteine synthase	Rc_chrom0706S003049_at	2.0729610
RCC03069	conserved hypothetical protein	Rc_chrom0706S003160_at	2.0720074
RCC02705	leucyl aminopeptidase	Rc_chrom0706S002797_at	2.0716789
	intergenic region	Rc_chrom0706S004257_at	2.0700033
	intergenic region	Rc_chrom0706S003729_at	2.0678294
RCC01203	pyruvate carboxylase	Rc_chrom0706S001239_at	2.0640485
RCC00755	thiamine pyrophosphokinase	Rc_chrom0706S000777_at	2.0611608
RCC00632	conserved hypothetical protein	Rc_chrom0706S000650_at	2.0609646
RCC01547	peptide chain release factor 2	Rc_chrom0706S001592_at	2.0606227
RCC00399	conserved hypothetical protein	Rc_chrom0706S000409_at	2.0582008

Annotation	Predicted function [a]	Probe spot [b]	Fold change [c]
RCC03100	DNA topoisomerase I	Rc_chrom0706S003191_at	2.0570338
RCC01086	glycosyl transferase, family 2/group 1	Rc_chrom0706S001115_at	2.0556066
	intergenic region	Rc_chrom0706S004144_at	2.0543050
RCC00619	ABC transporter, permease protein	Rc_chrom0706S000637_at	2.0534390
RCC02500	ABC transporter, periplasmic substrate-binding protein	Rc_chrom0706S002583_at	2.0488222
RCC00303	30S ribosomal protein S19	Rc_chrom0706S000311_at	2.0467267
RCC00402	conserved hypothetical protein	Rc_chrom0706S000412_at	2.0428758
RCC02679	pyridine nucleotide-disulphide oxidoreductase family protein	Rc_chrom0706S002769_at	2.0394864
RCC01614	methionine synthase, B subunit	Rc_chrom0706S001665_at	2.0385268
RCC02660	monosacharide ABC transporter, permease protein	Rc_chrom0706S002750_at	2.0379176
RCC03242	conserved hypothetical protein	Rc_chrom0706S003336_at	2.0356019
RCC00912	methylmalonyl-CoA mutase	Rc_chrom0706S000944_at	2.0342164
RCC01096	aminobenzoyl-glutamate utilization protein B	Rc_chrom0706S001126_at	2.0307730
RCC00891	conserved hypothetical protein	Rc_chrom0706S000922_at	2.0291934
RCC02487	endonuclease III	Rc_chrom0706S002569_at	2.0281582
RCC02048	cobalamin biosynthesis protein CobW	Rc_chrom0706S002113_at	2.0277052
RCC00872	alcohol dehydrogenase, zinc-binding domain protein	Rc_chrom0706S000902_at	2.0247290
RCC01320	conserved hypothetical protein	Rc_chrom0706S001356_at	2.0225565
	intergenic region	Rc_chrom0706S004299_at	2.0224950
control		AFFX-DapX-M_at	2.0199804
RCC01150	chorismate synthase	Rc_chrom0706S001184_at	2.0193691

Annotation	Predicted function [a]	Probe spot [b]	Fold change [c]
RCC03509	uroporphyrinogen-III synthase	Rc_chrom0706S003606_at	2.0187337
	intergenic region	Rc_chrom0706S003870_at	2.0148423
RCC01179	transglycosylase, Slt family	Rc_chrom0706S001215_at	2.0106470
RCC03184	octaprenyl-diphosphate synthase	Rc_chrom0706S003277_at	2.0101793
RCC02248	oxidoreductase, aldo/keto reductase family	Rc_chrom0706S002321_at	2.0096638
RCC02404	ferredoxin VI	Rc_chrom0706S002480_at	2.0083039
	intergenic region	Rc_chrom0706S004148_at	2.0074625
	intergenic region	Rc_chrom0706S003890_at	2.0043523

(a) Annotation by automated TIGR website.

(b) Affymetrix-designed whole genome expression probe designation.

(c) RNA transcriptional upregulation compared to early stationary phase aqueous culture-harvested cell RNA transcription.

APPENDIX B

The information presented in APPENDIX B is provided as supplementary material for sections **3.6.3**, **3.6.6**, **3.6.8**, **3.6.9** and **C.2**. The data summarized in graphical format in section **3** and **APPENDIX C**, are presented fully in graphical format in this appendix to illustrate the distribution of the data.

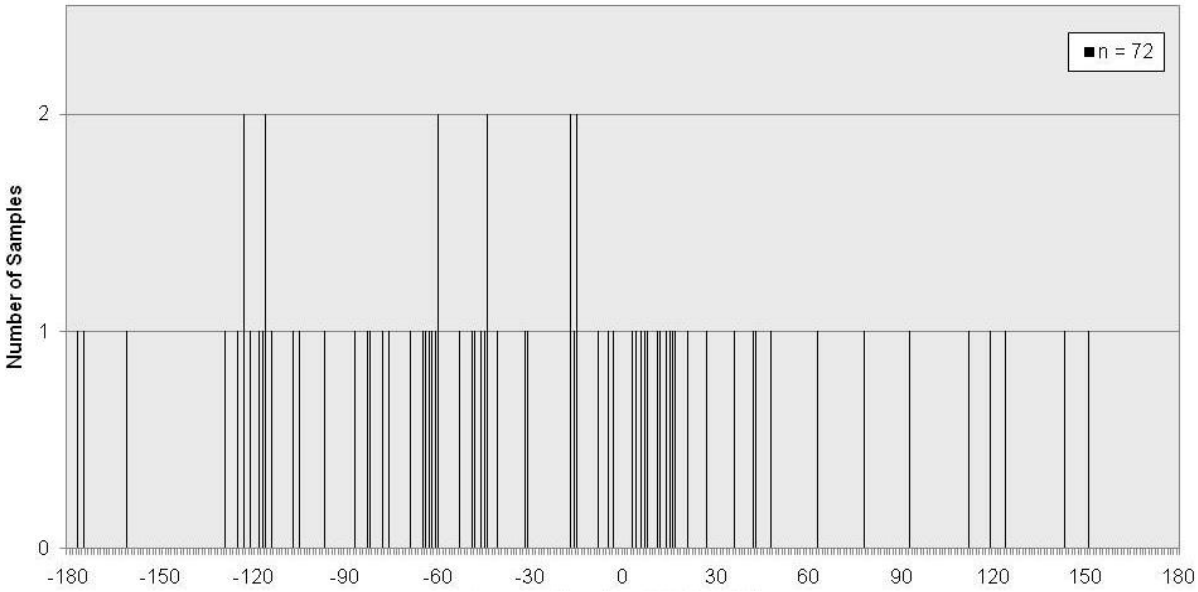

Figure B-1: Graphical representation of the measured angular direction of motility from agar plates with *bchA*/*crtB* mutant cells and incubated in the LED chamber with LED white light. 0° indicates movement directly toward the light source, and ± 180° indicates movement directly away from the light source.

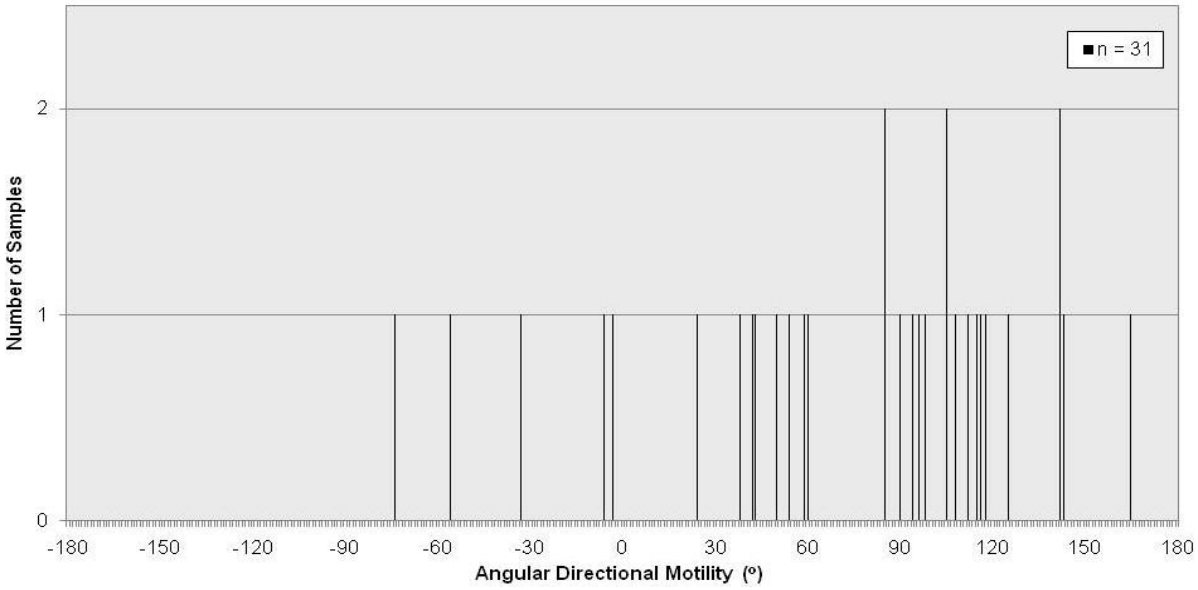

Figure B-2: Graphical representation of the measured angular direction of motility from agar plates with *flaA/gtaI* mutant cells and incubated in the LED chamber with LED white light. 0° indicates movement directly toward the light source, and ± 180° indicates movement directly away from the light source.

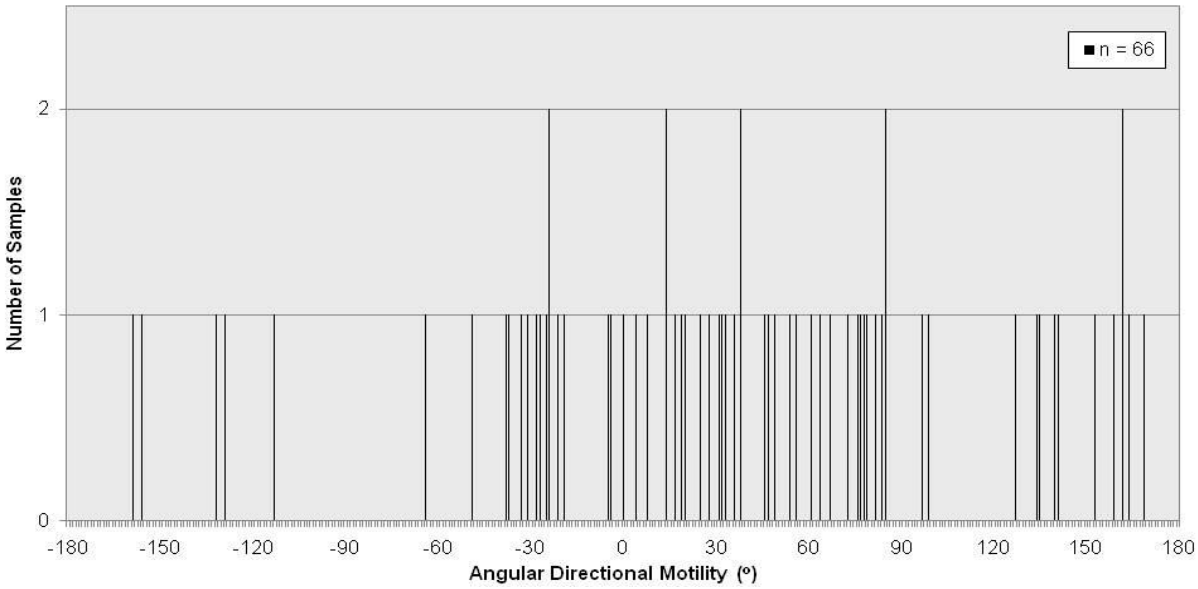

Figure B-3: Graphical representation of the measured angular direction of motility from agar plates with *senC* mutant cells and incubated in the LED chamber with LED white light. 0° indicates movement directly toward the light source, and ± 180° indicates movement directly away from the light source.

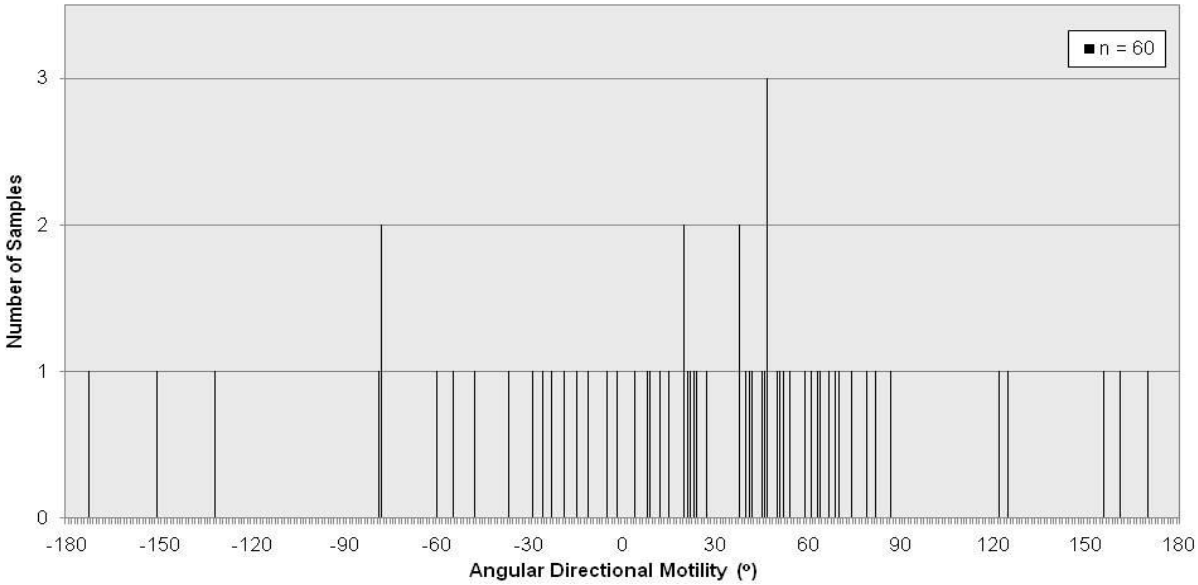

Figure B-4: Graphical representation of the measured angular direction of motility from agar plates with *regA* mutant cells and incubated in the LED chamber with LED white light. 0° indicates movement directly toward the light source, and ± 180° indicates movement directly away from the light source.

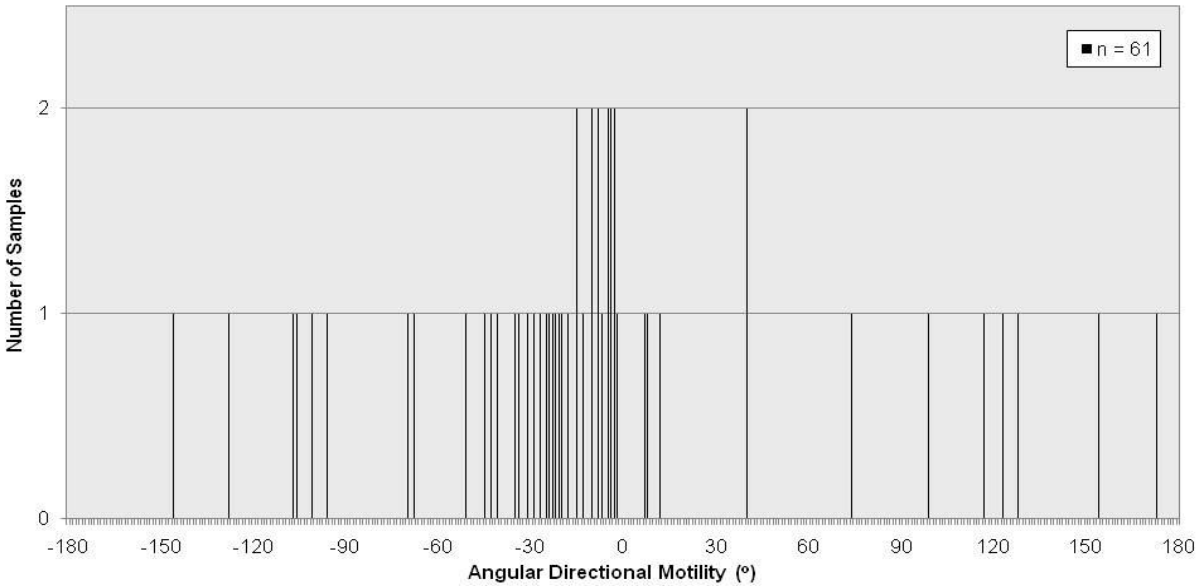

Figure B-5: Graphical representation of the measured angular direction of motility from agar plates with *R. capsulatus* cells and incubated in the LED chamber with LED white light. 0° indicates movement directly toward the light source, and ± 180° indicates movement directly away from the light source.

APPENDIX C

C.1. Photoresponsive motility using optical filters to generate light of defined wavelength ranges

The action spectrum of solid substrate motility of *R. capsulatus* cells was investigated using cut-off and narrow bandpass light filters and tungsten filament lamps. The distribution of movement in response to filtered light was similar for halogen and incandescent lamps (data not shown). An incubation chamber was set up in a 30 °C constant temperature room (see Figure 2-2e) with circular agar plates shielded from room light and illuminated with tungsten filament lamps located 60 cm from a stack of 12 plates. Controls were incubated in a stainless steel container that excluded light, on a level shelf below the illuminated samples. The dark control samples were arranged with a reference mark in a position that corresponded to the direction of the lamps in the illuminated samples (Figure 2-1). Optical filters that transmit light of greater than a particular wavelength (cut-off), or a specific wavelength $\pm$ 12.5 nm (bandpass) were used to generate incident light of wavelengths >900 nm, >350 nm, 750 nm, 700 nm, and 650 nm.

Using the measurement model described in Figure 3-8, and the method described in section **2.17**, statistical analysis was applied to evaluate whether there was a genuine bias in the distribution of angular direction of LED-illuminated bKSDF cell movement when compared to illuminated and dark controls. The average direction of taxis, standard deviations, and P_Z values of tungsten filament - illuminated sample sets were determined (see **APPENDIX A**, Table A-6). The standard deviation provided a means to visualize the clustering of samples, but because the distribution of directional movement in circular plates did not follow a normal curve (see Figure 3-16), the comparison to controls was made using the non-parametric Wilcoxon test that does not rely on the shape of the data distribution. Movement was plotted in Figure C-1 to show the average angle of movement, distribution, and statistical comparison of the data to dark and white light-illuminated controls.

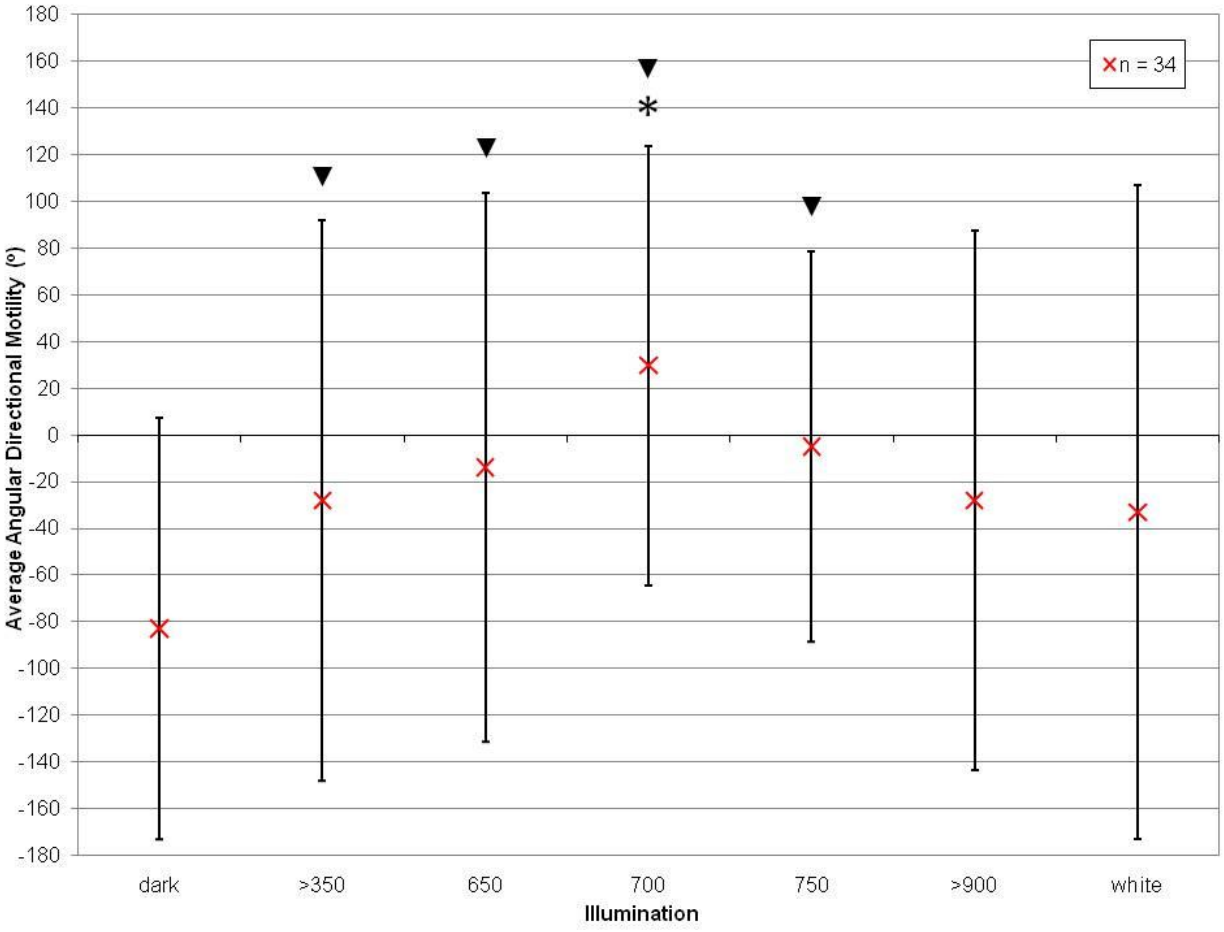

Figure C-1: Graphical representation of the average angular direction of motility in agar plates incubated in the filter chamber with illumination. The vertical axis gives the angle of movement, and the presence/absence of light, and wavelengths, are given on the horizontal axis. 0° indicates movement directly toward the light source, and ± 180° indicates movement directly away from the light. A red "X" represents the average direction of movement. Error bars represent 1 standard deviation. The P_Z value is the probability that a difference from the control value is due to random chance – hence a P_Z value < 0.05 means that the difference is statistically significant. The asterisk indicates where $P_Z < 0.05$ compared to white light tests. Triangles indicate cases where $P_Z < 0.05$ compared to dark tests.

The distribution of directional motility in white light-illuminated tests in the filter chamber was away from the light source (see **APPENDIX C**, Figure C-2), and so the trend did not resemble that of the aquarium chamber tests summarized in Figure 3-16 and Figure 3-18. It appeared that the distance between the light source and the stab-plates may have exacerbated the optical discrepancies of the circular plates. The distance of the stab-plates from the light source in the aquarium chamber was 14

cm from plates, whereas the filter chamber light was 60 cm from plates to reduce heat. Heating was controlled by circulating water around a container holding plates in the aquarium chamber, whereas the filter chamber was set up with temperature controlled by air in a 30°C room (see section **2.2.1**, Figure 2-2).

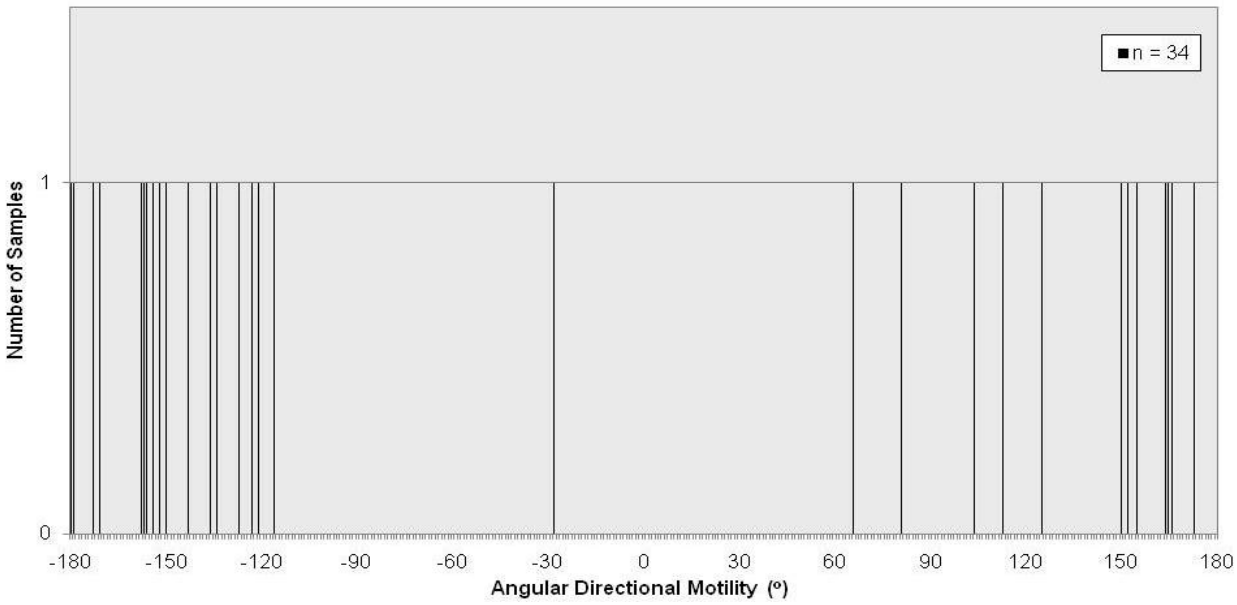

Figure C-2: Graphical representation of the measured angular direction of motility from agar plates with *R. capsulatus* cells and incubated in the filter chamber with incident white light. 0° indicates movement directly toward the light source, and ± 180° indicates movement directly away from the light.

The data obtained by the use of the filter chamber were at odds with some of the data obtained using the aquarium and LED chambers. Furthermore, because the difference in the distribution of the direction of the white light illuminated controls was not statistically significant compared to dark controls, I did not feel that these data could be reliably interpreted.

It could be argued that cells moved away from white light, and that movement in the aquarium chamber was an artefact. However, I believe the movement in the filter chamber was an artefact. Given the similar beahaviour of cells illuminated with white light in both the aquarium and LED chambers (see section **3.2.7** and **0**), and the theory that motile phototrophic cells should travel toward

wavelengths of light that could be used for photosynthesis (Alexandre et al., 2004), it appeared that there were problems associated with the design of the filter chamber.

C.2. Photoresponsive motility induction using light-emitting diodes (LEDs) to generate light of specific wavelength ranges

The action spectrum of solid substrate motility of *R. capsulatus* cells was also investigated using LED lamps with defined emission spectra (Figure C-3). An incubation chamber was set up in a 30 °C constant temperature room (see Figure 2-2c) with agar plates shielded from room light and illuminated with LED lamps located 14 cm from a stack of 12 plates, as in the aquarium chamber. Flagellum-deficient strain bKSDF cells incubated aerobically under directional incident light were compared to control plates incubated in the dark. Controls were incubated in a stainless steel container that excluded light, on the same level shelf and 60 cm to one side of the illuminated plates. The dark control samples were arranged with a reference mark in a position that corresponded to the direction of the lamps, relative to the stack of plates, in the adjacent illuminated chamber (Figure 2-1).

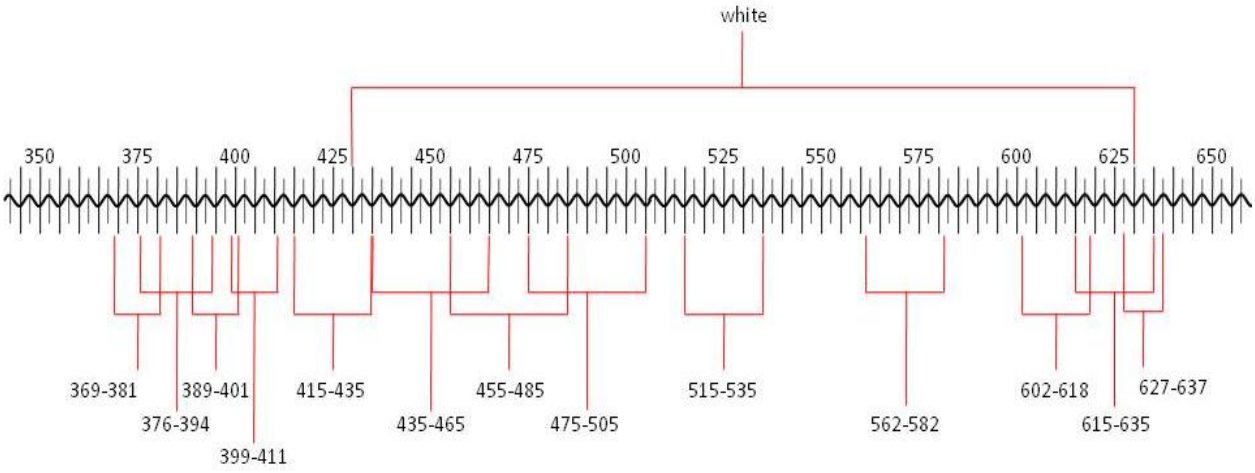

Figure C-3: Spectral region of the visible wavelength tested with LED lamps. 14 LED lamps with defined emission spectra were used to provide coverage over the region from 375 nm to 630 nm. Wavelength ranges correspond to the positions of half-maximal values of the emission peaks.

The LED coverage spanned 369 to 637 nm, in 10 to 30 nm wavelength windows (except for the white light lamps), with four gaps. It is possible that photoresponsive movement responds to wavelengths in these gaps, and this should be investigated if suitable lamps become available.

The relative intensities of the corresponding wavelengths within the white light were not measured, but this action spectrum was concerned with the wavelengths, and not the intensities, that influenced movement.

The distribution of directional motility in white light-illuminated tests in the LED chamber was toward the light source (see **APPENDIX B**, Figure B-5), and so the trend resembled that of the aquarium chamber tests summarized in Figure 3-16 and Figure 3-18.

Using the measurement model described in Figure 3-8, and the method described in section **2.17**, statistical analysis was applied to evaluate whether there was a genuine bias in the distribution of angular direction of LED-illuminated bKSDF cell movement when compared to illuminated and dark controls. The average direction of taxis, standard deviations, and P_Z values of LED-illuminated sample sets were determined (see **APPENDIX A**, Table A-7). The Wilcoxon test was used for the same reasons described in **3.6.3**, and the direction of movement was plotted in Figure C-4 to show the average angle of movement, distribution, and statistical comparison of the data to controls.

The distribution of movement on plates illuminated with 632, 625, 610, 525, and 405 nm wavelengths were not statistically different from white light-illuminated controls. Although this may have appeared to indicate that these wavelengths induced movement toward the light source, the results were not statistically different from dark controls, indicating that movement may not have responded to illumination.

Statistical comparisons of all other illumination wavelength tests showed significant differences from *both* white light illuminated and dark controls. The problem in interpreting these data, as for the wavelengths that did not yield statistically significant differences from the white light and dark controls, was that the direction of movement in white light and dark experiments (supposedly positive and negative controls, respectively) was not significantly different.

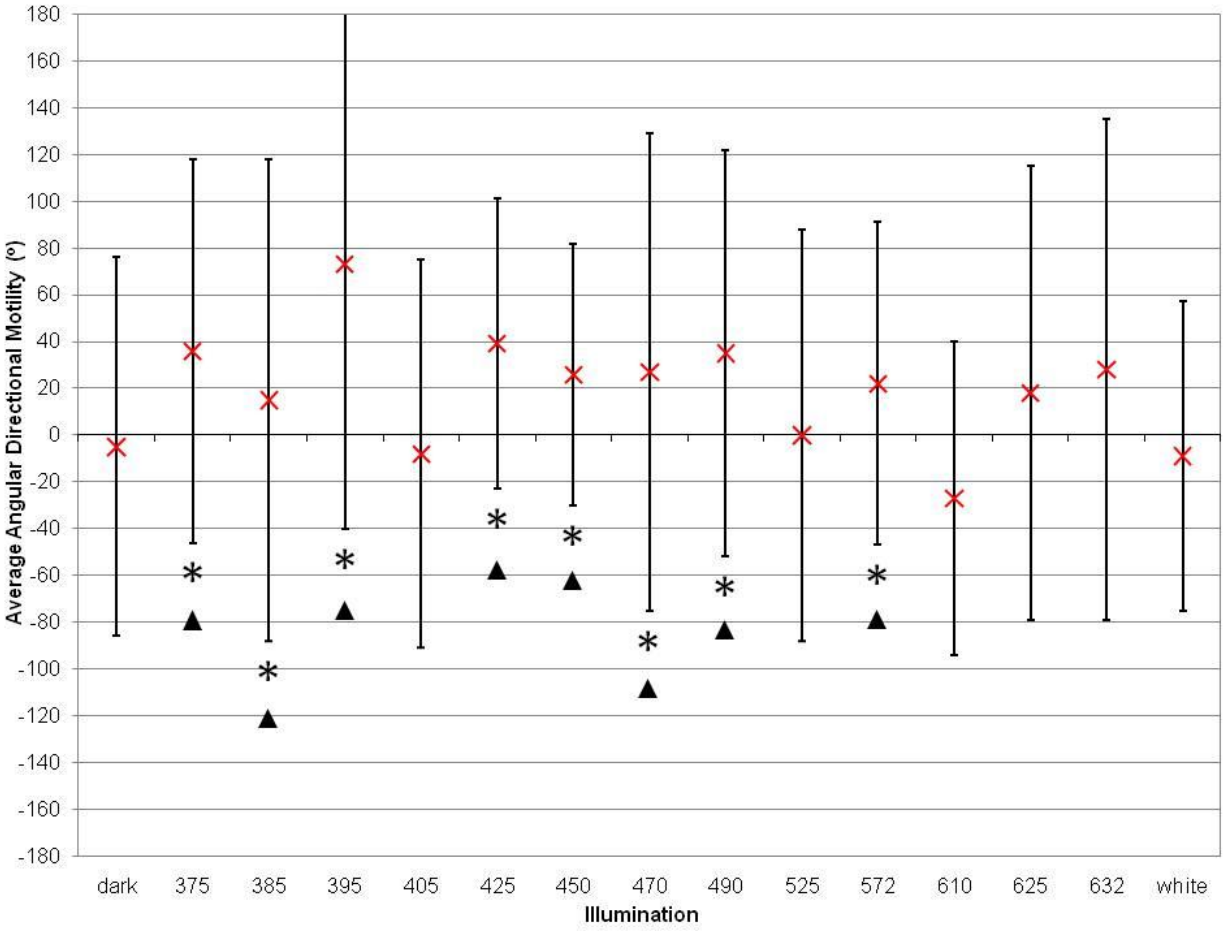

Figure C-4: Graphical representation of the measured angular direction of motility from agar plates with *R. capsulatus* cells and incubated in the LED chamber with illumination. The vertical axis gives the angle of movement, and the presence/absence of light, and wavelengths, are given on the horizontal axis. 0° indicates movement directly toward the light source, and ± 180° indicates movement directly away from the light. A red "X" represents the average direction of movement. Error bars represent 1 standard deviation. The P_Z value is the probability that a difference from the control value is due to random chance – hence a P_Z value < 0.05 means that the difference is statistically significant. Asterisks indicate cases where P_Z < 0.05 compared to white light tests. Triangles indicate cases where P_Z < 0.05 compared to dark tests.

The lack of a truly random trend in the dark control motility, and the large distributions in the directions travelled in all experiments, indicated that cells may have responded to multiple stimuli (see section **3.2.1**). This made it difficult to interpret these data. The relatively tight distribution of the direction of motility and the small angular average of the 450 nm-illuminated tests indicated this may have been a genuine movement toward the light. Conversely, the relatively large angular average and distribution of 395 nm-illuminated tests appeared to be genuinely different from both white light and dark controls, and perhaps may have been a genuine movement away from this wavelength. These preliminary investigations indicated that a complex photoresponsive pathway directed cell movements, and suggested that multiple photoreceptors may have been involved in this biological response.

Circular plates were used for action spectrum experiments in the hopes trends in the distribution of directed movement in response to specific wavelengths would be evident with large sample numbers. Less variability in the distribution of directed movement under white light illumination was observed in square plates (Figure 3-18), but it was found that movement was observed in only ~60% of square plates, as opposed to the ~85% observed in circular plates. The use of square plates may have reduced the variability in the directional distribution of samples for both filtered and LED light tests. Future action spectrum experiments might investigate movement in square plates, with increased sample numbers to compensate for the decreased frequency of movement.